TU Clausthal
Clausthal University of Technology

Thermo-Mechanical Coupling of Transversely Isotropic Materials using High-Order Finite Elements

Doctoral Thesis
(Dissertation)

to be awarded the degree of

Doctor in Mechanical Engineering (Dr.-Ing.)

submitted by

M. Sc. Raad Al-Kinani

from Baghdad
(place of birth)

approved by the Faculty of
Mathematics/Computer Science and Mechanical Engineering,
Clausthal University of Technology

Date of oral examination
25.06.2014

Chairperson of the Board of Examiners
Prof. Dr.-Ing. habil. Gunther Brenner

Chief Reviewer
Prof. Dr.-Ing. habil. Stefan Hartmann

Reviewer
Prof. Dr.-Ing. habil. Stefan Diebels, Universität des Saarlandes

Foreword

The work presented in this thesis was carried out over the last three and a half years at the Institute of Applied Mechanics, Clausthal University of Technology (Institut für Technische Mechanik, Technische Universität Clausthal). The work was funded by the MoHESR/DAAD scholarship program. I would like to thank the DAAD (Deutscher Akademischer Austausch Dienst) and the MoHESR (Ministry of Higher Education and Scientific Research - Iraq) for the financial support of this work.

I would like to express my sincere gratitude to my supervisor Prof. Dr.-Ing. Stefan Hartmann for giving me the opportunity to be a part of his working group. I would like to thank him sincerely for his continuous and unlimited support, and his valuable advices and recommendations.

I would like to thank Prof. Dr.-Ing. Stefan Diebels for agreeing to be the co-examiner of this thesis. I would also like to thank Prof. Dr.-Ing. Gunther Brenner for supporting the applications that I had to submit in order to extend my scholarship.

I want to thank my colleagues at the working group of Solid Mechanics, Torben Netz, Steffen Rothe, Stephan Krämer, Matthias Grafenhorst, Carmen Sguazzo, Maria Angeles Martinez Page, Rose Rogin Gilbert and Susana Rodriguez Porto for creating a supportive and friendly working atmosphere. I am grateful to Torben Netz and Steffen Rothe for allowing me to share their knowledge about finite elements. I am deeply indebted to them for their help regarding numerical implementations. I am particularly thankful to Stephan Krämer and Matthias Grafenhorst for the valuable discussions we had, especially on material parameter identification. I thank Stephan Krämer for the time he spent with me in the laboratory, and I thank my office mate Matthias Grafenhorst for the cooperative and pleasant working atmosphere in the office. My special thanks go to all co-workers of the institute for their help and support in all phases. I want to thank Dipl.-Ing. Sonja Niemeyer for the helpful discussions regarding experimental properties of fiber-reinforced composites.

My hearty gratitude to my closest family, including my mother, my brother and his family and my sisters and their families for their continuous support and encouragement. I would especially like to thank my mother for her patience and her prayers, which are always with me and inspire me.

Clausthal-Zellerfeld, April 2014 Raad Al-Kinani

Abstract

In recent years, constitutive modeling and numerical analysis of the behavior of anisotropic materials, particularly transversely isotropic and orthotropic materials, have attained increasing attention. The attention is mainly due to the wide range of applications of these materials in engineering industries and biomedical technologies. This work aims to develop a constitutive model for transversely isotropic materials undergoing thermo-mechanically coupled finite deformations. The model is based on the idea of multiplicative decomposition of the deformation gradient. Furthermore, the work aims to examine whether the model is able to simulate the behavior of transversely isotropic material under isothermal and thermo-mechanical coupled loadings by performing some numerical experiments based on high-order finite elements.

First of all, a constitutive model for the case of isothermal transversal isotropy is formulated. The proposed model is an extension of the volumetric/isochoric decoupling of the deformation gradient, where the isochoric part is decomposed into two parts, one part containing only the deformation along the preferred direction, while all remaining deformations are included in the other part. This formulation has the advantage that it leads to a clear split of the stress-state, i.e., the stress along the preferred direction is separated from the remaining stresses. Additionally, the proposed model overcomes the obstacle related to the application of volumetric/isochoric decomposition to anisotropy. The formulation is, then, extended to the case of a thermo-mechanically coupled problem, where a thermodynamically consistent constitutive model for transversal isotropy is developed. Moreover, a directionally dependent, i.e., transversely isotropic, heat flux vector is derived, taking the anisotropy in heat conductivity into account.

The proposed model is implemented into a high-order finite element code, in which the p-version finite element method and the high-order diagonally implicit Runge-Kutta (DIRK) methods are used for the spatial and time discretizations, respectively. In p-FEM, the accuracy of the solution is improved by increasing the polynomial degree of the elements, which makes p-FEM more convenient for the analysis of thin structures, like in the case of laminated composites. Thus, computations are carried out in order to investigate the behavior of the proposed model with different numerical examples. To this end, the influence of different factors on the response of transversely isotropic material under isothermal and/or thermo-mechanical loadings is discussed, namely: existence of anisotropy, orientation of the preferred direction, anisotropic thermal expansion and anisotropic heat conductivity. Furthermore, the efficiency of the p-version implementations is demonstrated by comparing them with two different h-version finite element implementations.

Contents

1. Introduction

1.1. Motivation

In physical reality – in order to avoid unexpected and risky failures – it must be verified whether the design requirements of a structure subjected to specific loading conditions are met, based on a careful analysis and prediction of the material behavior under the applied working conditions. However, experimental analysis of material behavior is expensive and time consuming. Consequently, there is a need to find mathematical models to describe the behavior of the material under consideration with a few material parameters that can be obtained from simple experiments. The mathematical models are mostly complicated and can not be solved analytically, due to complexities in materials behavior, such as anisotropy and inhomogeneity. Thus, approximated numerical solutions are developed using, for example, finite element methods. The numerical solutions have to fulfill the requirements of reliability and efficiency, i.e., the errors associated with the approximated solution should be minimized and the computation time should be kept reasonable. One approach within the framework of non-linear Continuum Mechanics, frequently, used in constructing constitutive models is the multiplicative split of the deformation gradient. According to this approach, the deformation gradient is multiplicatively decomposed into specific parts related to specific deformations. This approach is effectively applied in the modeling of various coupled problems, e.g. elastoplasticity, viscoelasticity, viscoplasticity, ... etc. Concerning finite element methods, the superior performance of high-order finite elements over the classical finite element implementation in the analysis of diverse physical problems is evident.

yearsIn recent years, constitutive modeling and numerical analysis of the behavior of anisotropic materials, particularly transversely isotropic and orthotropic materials, attained increasing attention. The motive of this attention is the wide range of applications of these materials in engineering industries and biomedical technologies, see e.g. (Holbery and Houston, 2006) and (Bronzino, 2006). In the case of finite deformation transversal isotropy, the hyperelastic behavior is well investigated and numerous constitutive models are formulated in the literature, see Sec. 1.2. However, according to my knowledge, the thermo-hyperelastic coupled behavior has not been adequately addressed yet. This thesis aims to fill the gap in the modeling of transversal isotropy. Thus, this work is motivated by the interest of mathematical formulation of a constitutive model, using the approach of multiplicative decomposition, and employment of reliable and efficient numerical implementation, based on high-order finite elements, to analyze the behavior of general, slightly compressible transversely isotropic materials undergoing thermo-mechanical coupled finite deformations.

1.2. Literature Review

Finite deformation anisotropy, transversal isotropy and orthotropy in particular, is frequently applied in the constitutive modeling of the behavior of fiber-reinforced elastomers and biological soft tissues. There are numerous publications in the literature dealing with this subject, in which the strain-energy function used for modeling the isotropic hyperelasticity is reinforced with an anisotropic strain-energy function associated to the deformation arising from anisotropy. According to (Helfenstein et al., 2010), this approach was first applied by (Weiss et al., 1996). The behavior of biological joints is investigated by (Almeida and Spilker, 1998), based on modeling the soft tissues as an incompressible transversely isotropic material. (Holzapfel and Ogden, 2010) reviewed and summarized the mathematical models treating the constitutive modeling of the behavior of arteries, drawing on anisotropic soft tissues. A well known constitutive model describing the behavior of arteries was proposed by (Holzapfel et al., 2000). Nevertheless, (Helfenstein et al., 2010) showed that a non-physical effect is associated to the models presented in (Weiss et al., 1996) and (Holzapfel et al., 2000). The active and passive responses of skeletal muscles are characterized by numerous models, e.g. (Odegrad et al., 2008), (Tang et al., 2009) and (Calvo et al., 2010). (Calvo et al., 2009) and (Pena et al., 2011) studied the damage process and softening behavior of vaginal tissues, respectively.

The existence of a solution for boundary-value problems is guaranteed by the property of polyconvexity. The polyconvexity of strain-energy functions for different types of anisotropy was investigated by many authors, see e.g. (Schröder and Neff, 2003), (Steigmann, 2003), (Itskov and Aksel, 2004), (Kambouchev et al., 2006), (Itskov et al., 2006), (Kambouchev et al., 2007) (Schröder et al., 2008) and (Ebbing, 2010), and the references cited therein. Within the framework of the invariants theory, (Schröder and Neff, 2003) formulated a polyconvex constitutive model for the case of transversal isotropy. (Schröder et al., 2005) proposed an anisotropic strain-energy function, which is applicable for modeling soft tissues, and compared the results of the proposed model with two models from the literature. Later on, (Balzani et al., 2006) presented a polyconvex strain-energy function for modeling soft tissues with fewer material parameters than those in (Schröder et al., 2005). Their model is based on the idea of case distinction - applied by (Holzapfel et al., 2000) - in which the anisotropic part of the strain-energy function is set to be zero for shortening deformations along the fiber direction. (Ehret and Itskov, 2007) developed a strain-energy function that is applicable to different types of soft tissues, where scalar weighting factors are used to define so-called *generalized structural tensors* drawing on the structural tensors defined by the fiber orientations.

As mentioned above, in the modeling of anisotropic hyperelasticity, it is common to split the strain-energy function into two parts: one that is described by a classical model of isotropy and another part representing the anisotropy. The anisotropic part of the strain-energy function is frequently assumed to be connected to the stretch in the axis of isotropy only, i.e. considering only one of the two invariants emerged by anisotropy, see (Weiss et al., 1996), (Qiu and Pence, 1997), (Holzapfel et al., 2000), (Markert et al., 2005), (Balzani et al., 2006) (Brown and Smith, 2011) and (Yosibash and Priel, 2011), among others. This approach simplifies the problem and reduces the number of material parameters (Holzapfel et al., 2000). Both the application and the need to develop anisotropic hyper-elasticity relations for engineering purposes can be seen in rubber-

like composite materials. Some manufacturing processes cause the isotropic rubber-like solids to show an anisotropic behavior, such as in the case of calendered plates of filled rubber, see (Diani et al., 2003) and (Diani et al., 2004), for example. These authors proposed a constitutive model, in which the strain-energy function depends on the material directions instead of the principal directions of the deformation gradient tensor. Ciarletta et al. (2011) proposed the definition of a *"novel deformation tensor"* for the modeling of incompressible hyper-elastic fiber-reinforced materials and compared the results of the model with the experimental data of two different fiber-reinforced composites. (Sussman and Bathe, 2009) proposed a model for incompressible isotropic materials based on an additively decomposed free energy in terms of principal logarithmic strains, drawing on spline interpolations of experimental data from tension/compression tests. This approach is extended to the case of incompressible transversal isotropy and used to simulate the behavior of calendered rubber and biological tissues, see (Latorre and Montans, 2012) and (Latorre and Montans, 2013). Cellular materials, such as open-cell foams, show anisotropic behavior on the macroscopic scale, see (Schmitt and Diebels, 2005). This behavior complicates the modeling of these materials. (Diebels et al., 2005) developed a numerical approach to model the behavior of open-cell foams. The approach is based on a second-order homogenization scheme, taking the issue of macroscopic anisotropy into account.

The volumetric/isochoric decomposition of the strain-energy function, which goes back to (Flory, 1961) for the case of isotropy, is commonly used to simulate nearly incompressible isotropic materials, - see, for instance, (Hartmann and Neff, 2003) and the references cited therein. This concept is also applied also in the case of anisotropy, see (Holzapfel et al., 2000), (Rüter and Stein, 2000), (Rubin and Jabareen, 2008), (Guo et al., 2008), (Calvo et al., 2009), (Guo and Caner, 2010) and (Pena et al., 2011). (Lu and Zhang, 2005) used the idea of volumetric/isochoric decomposition of the deformation gradient to propose a constitutive model for transversely isotropic solids. They introduced an alternative approach for constructing physically motivated strain invariants to that used in (Criscione et al., 2001). A further development that follows the concept of multiplicative decomposition serves to divide the deformation gradient into two parts: an uniaxial deformation along the direction of the fibers and another part that is interpreted as a particular shear deformation for modeling incompressible soft tissues, see (Guo et al., 2006, 2007). Later on (Guo et al., 2008) applied a similar concept of multiplicative decomposition to model compressible transversely isotropic materials, assuming an isochoric uniaxial deformation along the direction of anisotropy followed by another two deformations. The model proposed in their treatise shows the disadvantage that *"the iso-choric uniaxial deformation along the preferred direction of the material is associated with a uniaxial stress state, which is not true for general compressible transversely isotropic materials"*, as reported by the authors.

In many applications, hyperelastic materials are subjected to finite deformations combined with an increase or decrease in temperature. Thus, the materials undergo thermo-mechanical coupled finite deformations. Models for this coupled problem within the framework of Continuum Mechanics can also be achieved by following the approach of a multiplicative split, decomposing the deformation gradient tensor into a thermal and a mechanical part. This approach was first presented in the work of (Stojanovic et al., 1964) and (Stojanovic, 1969), and has since contributed significantly to the formulation of thermo-mechanical coupled constitutive models for isotropic materials, see e.g. (Lu and Pister, 1975), (Lion, 2000), (Vujosevic and Lubarda, 2002),

(Lubarda, 2004), (Heimes, 2005), (Hamkar and Hartmann, 2012), (Darijani and Naghdabadi, 2013) and (Yosibash et al., 2014) among others. A comparison between this approach and the classical formulation of finite strain thermoelasticity was carried out by (Vujosevic and Lubarda, 2002). In the classical modeling no decomposition is applied - and the constitutive relations are obtained from the assumed strain-energy function, see (Chadwick, 1974), (Miehe, 1995), (Gurtin et al., 2011) and references cited therein. For the case of anisotropy, (Huang et al., 2011) used experimental data obtained from uniaxial tension tests to propose a strain-energy function for incompressible fiber-reinforced rubber composites. The thermo-elasticity of ideal fiber-reinforced materials, which are assumed to be incompressible and inextensible in the fiber direction, is investigated by (Mićunović, 1982). The literature provide no work that deals with the application of the approach of multiplicative decomposition to the constitutive modeling of general compressible anisotropic materials. The issue is treated in this thesis, under consideration of the thermo-mechanical transversely isotropic problem.

Finite element methods play a central role in Computational Mechanics, providing an efficient approach for analyzing materials behavior by carrying out numerical experiments. Due to the nearly incompressible behavior of biological soft tissues and rubber-like anisotropic materials, the numerical computations require particular elements to overcome volumetric locking phenomena. To this end, the application of high-order finite elements is favorable. This approach makes use of hierarchical shape functions based on the integrated Legendre polynomials. This element formulation goes back to (Babuŝka and Suri, 1992a), see (Düster, 2001) as well. It has been demonstrated that p-version finite element method (p-FEM), with a proper polynomial degree, is locking free in isotropic linear elasticity (Babuŝka and Suri, 1992a), (Babuŝka and Suri, 1992b), and in the analysis of neo-Hookean solids at finite deformations (Heisserer et al., 2008). Furthermore, the p-FEM was efficiently applied in the finite deformation analysis of various physical problems, i.e. hyperelasticity (Düster et al., 2003), (Yosibash et al., 2007) and (Netz et al., 2013a), viscoelasticity (Netz et al., 2013b), thermo-visoelasticity (Netz, 2013) and in the modeling of open-cell foams (Düster et al., 2005). The use of elements with high p-level makes the p-FEM more convenient for the analysis of thin structure problems, such as laminated fiber-reinforced composites (Yosibash and Priel, 2011) and (Al-Kinani et al., 2014). (Yosibash and Priel, 2011) applied p-FEM to simulate the behavior of arteries in term of the model proposed by (Holzapfel et al., 2000), and compared the results to the classical h-version finite element implementation. On the other hand, temporal discretization is required in the analysis of transient problems.[1] Temporal discretization is carried out by integrating the governing equation over time. the application of high-order time integration methods leads to more efficient finite element computations. It has been demonstrated by many authors in the literature that the high-order diagonally implicit Runge-Kutta (DIRK) methods are superior and efficient for performing computations to solve different types of problems, see (Diebels et al., 1999), (Ellsiepen and Hartmann, 2001), (Hartmann, 2002a), (Hartmann, 2006b), (Hartmann and Bier, 2008), (Hartmann et al., 2008) and (Hamkar and Hartmann, 2012). The combination of p-FEM

[1] Transient problems consisting constitutive equations of evolutionary type, such as the problem of thermoelasticity, in which the temperature evolves with time, and the problem of viscoelasticity, in which the internal variables are defined by evolution equations.

with high-order DIRK-methods result in a robust tool, allowing for highly accurate and efficient finite element computations (Netz, 2013).

1.3. Layout of the Thesis

As the motivation of this work and a literature review are presented in this chapter, the theoretical background of the present work, represented by preliminaries of Continuum Mechanics, is introduced in *Chapter two*. Kinematics, the principle of stress and balance relations are outlined in this context. Additionally, the principles of constitutive modeling and representation of isotropic tensor functions are summed up.

The formulation of isothermal hyperelastic constitutive model is presented in *Chapter three*, beginning with the volumetric/isochoric decomposition of the deformation gradient, which is widely applied to modeling nearly incompressible solids. This decomposition is extended by a further decoupling of the isochoric part into two parts, one part describing the deformation in the preferred direction and another part containing all remaining deformations. Consequently, an additively decomposed form of strain-energy function is proposed. Constitutive relations for the stress-state are derived and investigated drawing on some analytical examples. Finally, a short comparison between the proposed and classical approaches is carried out.

In *Chapter four* the formulation is extended to thermo-hyperelastic transversal isotropy, making use of the thermo-mechanical multiplicative decomposition of the deformation gradient. A strain-energy function, taking the temperature effects into consideration, is defined and employed in the dissipation inequality, from which the constitutive relations for the coupled problem are obtained. In order to make the analysis of the problem more comprehensive, a transversely isotropic heat flux vector is derived. The formulation ends with the derivation of the heat conduction equation.

Chapter five deals with the numerical treatment of the problem under consideration. The p-version finite element method is introduced briefly, followed by the formulation of the strong and weak forms of the thermo-mechanically coupled problem. The essential steps of the procedure employed in the numerical solution, which is performed using high-order in space and time computations, are outlined.

Some numerical examples are presented in *Chapter six*, demonstrating the capability of the proposed models to simulate the behavior of transversely isotropic structures under isothermal and thermo-mechanically coupled loading states. The influence of different factors on the response of the examined structures is investigated.

Lastly, in *Chapter seven* the work presented in this thesis is recapped and some notions for future work are proposed.

2. Preliminaries of Continuum Mechanics

Continuum Mechanics is focused on the analysis of the kinematics and material properties of material bodies, denoted by $\mathcal{B}$, which are assumed to be continuous and infinitely sub-dividable into particles represented by $\mathcal{P} \in \mathcal{B}$. There are numerous textbooks dealing with Continuum Mechanics, for example (Truesdell and Noll, 2004), (Eringen, 1980), (Malvern, 1969), (Chadwick, 1999), (Marsden and Hughes, 1994), (Ogden, 1997), (Haupt, 2002), (Holzapfel, 2000), (Hutter and Jöhnk, 2004), (Gurtin et al., 2011) and (Tadmor et al., 2012), among more others. The aim of this chapter is to briefly outline the fundamental relations within the basic fields of Continuum Mechanics, namely kinematics, the concept of stresses, principles of balance relations, principles of constitutive modeling and representation of tensor functions, where these fields represent the background of the present work.

2.1. Kinematics

Kinematics in Continuum Mechanics deals with the description of motion of a continuum. We start with a material body $\mathcal{B}(\mathcal{P})$, which consists of a set of material points $\mathcal{P}$, i.e., $\mathcal{B} = \{ \mathcal{P} \}$, that can be replaced in one-to-one correspondence with a triple of real numbers. The description of the position of all material points (particles) $\mathcal{P} \in \mathcal{B}$ in the Euclidean space $\mathbb{E}^3$ identifies the configuration $\mathcal{K}$ of $\mathcal{B}$. At a fixed (or initial) time, the configuration $\mathcal{K} = \boldsymbol{\mathcal{R}}$ is called the reference configuration, and is defined by the mapping

$$\boldsymbol{\mathcal{R}}\colon \begin{cases} \mathcal{B} & \to \boldsymbol{\mathcal{R}}[\mathcal{B}] \subset \mathbb{E}^3 \\ \mathcal{P} & \mapsto \boldsymbol{\mathcal{R}}(\mathcal{P}) = \boldsymbol{X} \iff \mathcal{P} = \boldsymbol{\mathcal{R}}^{-1}(\boldsymbol{X}). \end{cases} \tag{2.1}$$

After deformation takes place, the material body $\mathcal{B}$ deforms and moves, and at time $t \in \mathbb{R}^+$ it occupies a configuration $\boldsymbol{\chi}_t$ called the current configuration, which is expressed by the mapping

$$\boldsymbol{\chi}_t\colon \begin{cases} \mathcal{B} & \to \boldsymbol{\chi}_t[\mathcal{B}] \subset \mathbb{E}^3 \\ \mathcal{P} & \mapsto \boldsymbol{\chi}_t(\mathcal{P}) = \boldsymbol{x}. \end{cases} \tag{2.2}$$

The vectors $\boldsymbol{X}$ and $\boldsymbol{x}$ describe the material (or Lagrangian) and spatial (or Eulerian) coordinates of the material point $\mathcal{P}$, and they identify its position in the reference configuration $\boldsymbol{\mathcal{R}}$ and current configuration $\boldsymbol{\chi}_t$, respectively, as shown in Fig. 2.1. A motion of a material body $\mathcal{B}$ can be

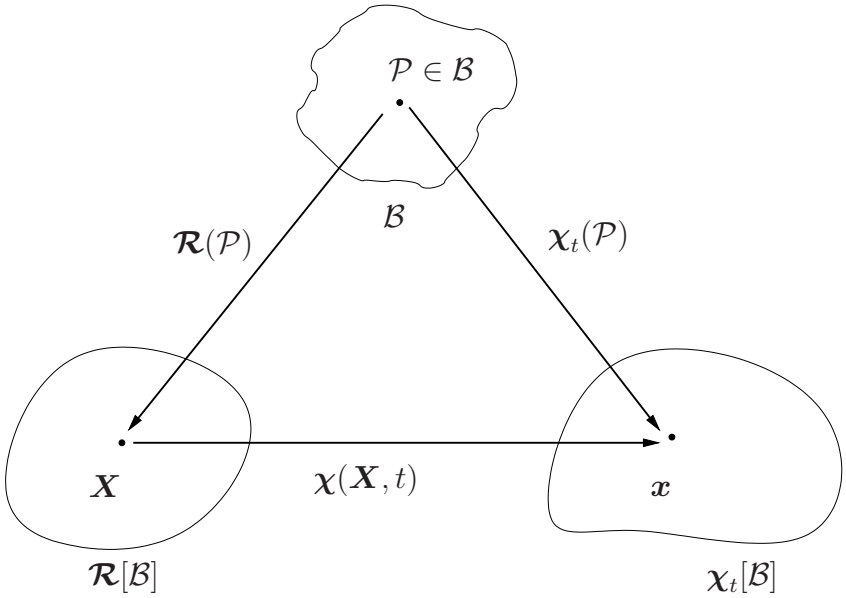

Figure 2.1.: Material and spatial coordinates in the reference and current configurations.

represented by a sequence of mapping by a deformation function $\boldsymbol{\chi}(\,\cdot\,, t)$ which, for each time t, maps $\boldsymbol{\mathcal{R}}$ into $\boldsymbol{\chi}_t$

$$\boldsymbol{x} = \boldsymbol{\chi}(\boldsymbol{X}, t), \tag{2.3}$$

and to ensure that $\boldsymbol{X}$ and $\boldsymbol{x}$ are in one-to-one correspondence, $\boldsymbol{\chi}$ should has an inverse $\boldsymbol{\chi}^{-1}$ at each time t, such that

$$\boldsymbol{X} = \boldsymbol{\chi}^{-1}(\boldsymbol{x}, t). \tag{2.4}$$

The deformation gradient, denoted by the second-order tensor $\mathbf{F}$, which maps the elements of the material body $\mathcal{B}$ from the reference configuration $\boldsymbol{\mathcal{R}}$ to the current configuration $\boldsymbol{\chi}_t$, is defined as the gradient of the motion of the material body $\mathcal{B}$, i.e.,

$$\mathbf{F} = \operatorname{Grad} \boldsymbol{\chi}(\boldsymbol{X}, t) = \frac{\partial \boldsymbol{\chi}(\boldsymbol{X}, t)}{\partial \boldsymbol{X}} \tag{2.5}$$

In order to demonstrate the interpretation of $\mathbf{F}$, consider two smooth curves $\boldsymbol{C}(\xi)$ and $\boldsymbol{c}(\xi)$, which consist of a set of material points and contain points $\boldsymbol{X}$ and $\boldsymbol{x}$, in the reference and current configuration, respectively, as shown in Fig. 2.2, i.e.

$$\xi \longrightarrow \boldsymbol{C}(\xi), \quad \boldsymbol{C}(\xi_0) = \boldsymbol{X} \tag{2.6a}$$

and

$$\xi \longrightarrow \boldsymbol{c}(\xi) = \boldsymbol{\chi}\left(\boldsymbol{C}(\xi), t\right), \quad \boldsymbol{c}(\xi_0) = \boldsymbol{x}. \tag{2.6b}$$

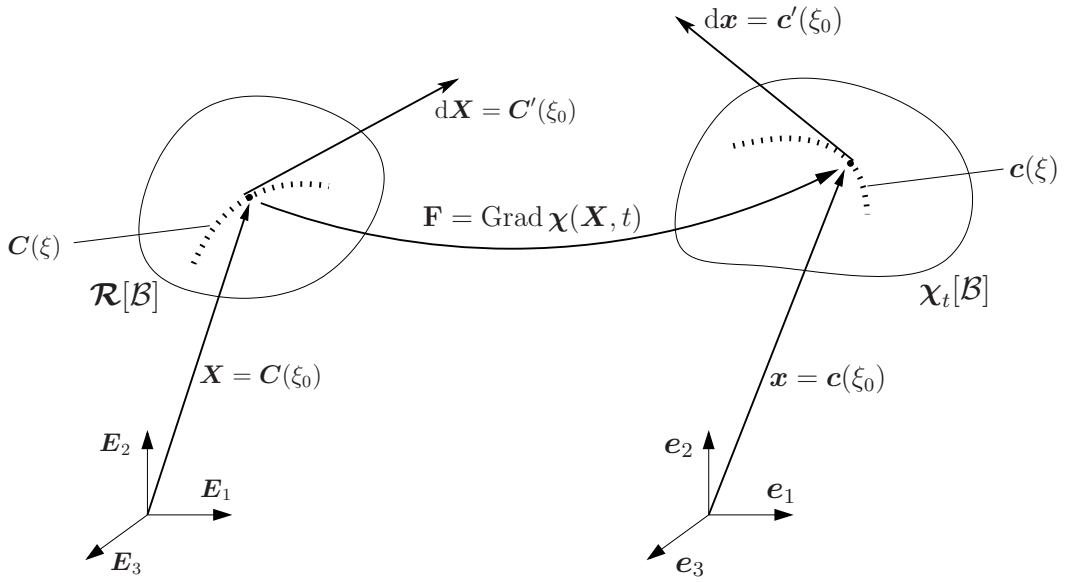

Figure 2.2.: Geometrical interpretation of the deformation gradient tensor $\mathbf{F}$.

The tangent vectors to the smooth curves $\boldsymbol{C}(\xi)$ and $\boldsymbol{c}(\xi)$ at material points $\boldsymbol{X}$ and $\boldsymbol{x}$ read

$$\mathrm{d}\boldsymbol{X} = \frac{\mathrm{d}}{\mathrm{d}\xi}\boldsymbol{C}(\xi)\mathrm{d}\xi|_{\xi=\xi_0} = \boldsymbol{C}(\xi)\mathrm{d}\xi|_{\xi=\xi_0} = \boldsymbol{C}'(\xi_0)\mathrm{d}\xi \tag{2.7a}$$

and

$$\mathrm{d}\boldsymbol{x} = \frac{\mathrm{d}}{\mathrm{d}\xi}\boldsymbol{c}(\xi)\mathrm{d}\xi|_{\xi=\xi_0} = \boldsymbol{c}(\xi)\mathrm{d}\xi|_{\xi=\xi_0} = \boldsymbol{c}'(\xi_0)\mathrm{d}\xi, \tag{2.7b}$$

respectively. Making use of the chain rule, $\boldsymbol{c}'(\xi)$ can be written as

$$\boldsymbol{c}'(\xi) = \mathrm{Grad}\,\boldsymbol{\chi}\,(\boldsymbol{C}(\xi), t)\,\boldsymbol{C}'(\xi), \tag{2.8}$$

which, for $\xi = \xi_0$, follows

$$\underbrace{\boldsymbol{c}'(\xi_0)}_{\mathrm{d}\boldsymbol{x}} = \underbrace{\mathrm{Grad}\,\boldsymbol{\chi}\,(\boldsymbol{C}(\xi_0), t)}_{\mathrm{Grad}\,\boldsymbol{\chi}(\boldsymbol{X},t)}\underbrace{\boldsymbol{C}'(\xi_0)}_{\mathrm{d}\boldsymbol{X}}, \tag{2.9}$$

i.e. a material line element $\mathrm{d}\boldsymbol{X}$ in $\boldsymbol{\mathcal{R}}$ is mapped into a material line element $\mathrm{d}\boldsymbol{x}$ in $\boldsymbol{\chi}_t$ as

$$\mathrm{d}\boldsymbol{x} = \mathbf{F}\mathrm{d}\boldsymbol{X}, \tag{2.10}$$

and since $\mathrm{d}\boldsymbol{X}$ and $\mathrm{d}\boldsymbol{x}$ are in one-to-one correspondence, the inverse of $\mathbf{F}$ must exist, such that

$$\mathbf{F}^{-1} = \mathrm{grad}\,\boldsymbol{\chi}^{-1}(\boldsymbol{x}, t) = \frac{\partial\boldsymbol{\chi}^{-1}(\boldsymbol{x}, t)}{\partial\boldsymbol{x}} = \frac{\partial\boldsymbol{X}}{\partial\boldsymbol{x}}, \tag{2.11}$$

where the existence of such a unique inversion is guaranteed by a non-vanishing of the determinant of $\mathbf{F}$ denoted by J, i.e.

$$J := \det \mathbf{F} \neq 0, \tag{2.12}$$

which is required to be greater than zero, $J > 0$, for all deformations so that the body can not interpenetrate itself. If the displacement vector

$$\boldsymbol{u}(\boldsymbol{X}, t) = \boldsymbol{x} - \boldsymbol{X} = \boldsymbol{\chi}(\boldsymbol{X}, t) - \boldsymbol{X} \tag{2.13}$$

is introduced as shown in Fig 2.3, there follows

$$\mathbf{F} = \operatorname{Grad} \boldsymbol{\chi}(\boldsymbol{X}, t) = \operatorname{Grad}(\boldsymbol{u} + \boldsymbol{X}) = \operatorname{Grad} \boldsymbol{u} + \mathbf{1}, \tag{2.14}$$

where $\mathbf{1}$ is a second-order identity tensor. Furthermore, the transformation of a material surface element $\mathrm{d}\boldsymbol{A} = \mathrm{d}\boldsymbol{X}_1 \times \mathrm{d}\boldsymbol{X}_2$ and a material volume element $\mathrm{d}V = (\mathrm{d}\boldsymbol{X}_1 \times \mathrm{d}\boldsymbol{X}_2) \cdot \mathrm{d}\boldsymbol{X}_3$ defined in the reference configuration to their identical material elements $\mathrm{d}\boldsymbol{a} = \mathrm{d}\boldsymbol{x}_1 \times \mathrm{d}\boldsymbol{x}_2$ and $\mathrm{d}v = (\mathrm{d}\boldsymbol{x}_1 \times \mathrm{d}\boldsymbol{x}_2) \cdot \mathrm{d}\boldsymbol{x}_3$ in the current configuration is given by

$$\begin{aligned} \mathrm{d}\boldsymbol{a} &= \mathrm{d}\boldsymbol{x}_1 \times \mathrm{d}\boldsymbol{x}_2 = \mathbf{F}\mathrm{d}\boldsymbol{X}_1 \times \mathbf{F}\mathrm{d}\boldsymbol{X}_2 = (\det \mathbf{F})\, \mathbf{F}^{-\mathrm{T}}(\mathrm{d}\boldsymbol{X}_1 \times \mathrm{d}\boldsymbol{X}_2) \\ &= (\det \mathbf{F})\, \mathbf{F}^{-\mathrm{T}}\mathrm{d}\boldsymbol{A} = (\operatorname{cof} \mathbf{F})\mathrm{d}\boldsymbol{A}, \end{aligned} \tag{2.15}$$

and

$$\begin{aligned} \mathrm{d}v &= (\mathrm{d}\boldsymbol{x}_1 \times \mathrm{d}\boldsymbol{x}_2) \cdot \mathrm{d}\boldsymbol{x}_3 = (\mathbf{F}\mathrm{d}\boldsymbol{X}_1 \times \mathbf{F}\mathrm{d}\boldsymbol{X}_2) \cdot \mathbf{F}\mathrm{d}\boldsymbol{X}_3 \\ &= \det \mathbf{F}\, [(\mathrm{d}\boldsymbol{X}_1 \times \mathrm{d}\boldsymbol{X}_2) \cdot \mathrm{d}\boldsymbol{X}_3] = (\det \mathbf{F})\, \mathrm{d}V = J\mathrm{d}V, \end{aligned} \tag{2.16}$$

respectively, where $\operatorname{cof}(\bullet)$ is the cofactor of a tensor field $(\bullet)$ and is defined as

$$\operatorname{cof}(\bullet) = \Big(\det(\bullet) \Big) (\bullet)^{-\mathrm{T}} \tag{2.17}$$

The statements in Eqs.(2.16) results from the identity

$$(\mathbf{A}\boldsymbol{a} \times \mathbf{A}\boldsymbol{b}) \cdot \mathbf{A}\boldsymbol{c} = \det \mathbf{A}\, [(\boldsymbol{a} \times \boldsymbol{b}) \cdot \boldsymbol{c}]\,, \tag{2.18}$$

which is valid for any second order tensor $\mathbf{A}$ and vectors $\boldsymbol{a}, \boldsymbol{a}, \boldsymbol{a} \in \mathbb{V}^3$, and it follows the identity

$$\mathbf{A}^{\mathrm{T}}(\mathbf{A}\boldsymbol{a} \times \mathbf{A}\boldsymbol{b}) = \det \mathbf{A}(\boldsymbol{a} \times \boldsymbol{b}), \tag{2.19}$$

which is the base of the statement in Eq.(2.15). The material derivative (partial respectively total time derivative) of the motion of a material line element follows its velocity

$$\boldsymbol{v} = \hat{\boldsymbol{v}}(\boldsymbol{X}, t) = \frac{\partial}{\partial t} \boldsymbol{\chi}(\boldsymbol{X}, t) \tag{2.20a}$$

in material representation, and

$$\boldsymbol{v} = \bar{\boldsymbol{v}}(\boldsymbol{x}, t) = \hat{\boldsymbol{v}} \left(\boldsymbol{\chi}^{-1}(\boldsymbol{x}, t), t \right) \tag{2.20b}$$

in spatial representation, while its acceleration is the material derivative of the velocity, which reads

$$\boldsymbol{a} = \hat{\boldsymbol{a}}(\boldsymbol{X}, t) = \frac{\partial}{\partial t}\hat{\boldsymbol{v}}(\boldsymbol{X}, t) = \frac{\partial^2}{\partial t \partial t}\boldsymbol{\chi}(\boldsymbol{X}, t) \tag{2.21a}$$

and

$$\boldsymbol{a} = \bar{\boldsymbol{a}}(\boldsymbol{x}, t) = \frac{\partial}{\partial t}\bar{\boldsymbol{v}}(\boldsymbol{x}, t) + \big(\operatorname{grad}\bar{\boldsymbol{v}}(\boldsymbol{x}, t)\big)\bar{\boldsymbol{v}}(\boldsymbol{x}, t) \tag{2.21b}$$

in material and spatial representation, respectively, see (Haupt, 2002).

$$\mathbf{L} = \mathbf{L}(\boldsymbol{x}, t) = \operatorname{grad}\bar{\boldsymbol{v}}(\boldsymbol{x}, t) = \dot{\mathbf{F}}\mathbf{F}^{-1} \tag{2.22}$$

is the spatial velocity gradient, which can be additively decomposed into a symmetric part represents the strain-rate tensor $\mathbf{D}$ and a skew symmetric part represents the spin tensor $\mathbf{W}$, i.e,

$$\mathbf{L} = \mathbf{D} + \mathbf{W}, \tag{2.23}$$

with

$$\mathbf{D} = \tfrac{1}{2}\left(\mathbf{L} + \mathbf{L}^{\mathrm{T}}\right) \tag{2.24a}$$

and

$$\mathbf{W} = \tfrac{1}{2}\left(\mathbf{L} - \mathbf{L}^{\mathrm{T}}\right). \tag{2.24b}$$

The time derivatives of material line element $\mathrm{d}\boldsymbol{x}$, material surface element $\mathrm{d}\boldsymbol{a}$ and material volume element $\mathrm{d}v$ are given by the relations[1]

$$[\mathrm{d}\boldsymbol{x}]^{\cdot} = \mathbf{L}\mathrm{d}\boldsymbol{x} \tag{2.25a}$$

$$[\mathrm{d}\boldsymbol{a}]^{\cdot} = \left[(\operatorname{tr}\mathbf{L})\mathbf{1} - \mathbf{L}^{\mathrm{T}}\right]\mathrm{d}\boldsymbol{a} \tag{2.25b}$$

$$[\mathrm{d}v]^{\cdot} = (\operatorname{tr}\mathbf{L})\mathrm{d}v. \tag{2.25c}$$

The deformation gradient tensor $\mathbf{F}$ can be multiplicatively decomposed into two tensors, one of them representing a rotation and the other representing a pure stretch, so

$$\mathbf{F} = \mathbf{R}\mathbf{U} = \mathbf{V}\mathbf{R}, \tag{2.26}$$

where $\mathbf{U}$ and $\mathbf{V}$ are called the right and left stretch tensors, respectively, which are symmetric, positive definite and have the same eigenvalues. $\mathbf{R}$ is a rotation tensor, which is proper orthogonal

$$\mathbf{R}\mathbf{R}^{\mathrm{T}} = \mathbf{R}^{\mathrm{T}}\mathbf{R} = \mathbf{1}, \quad \det\mathbf{R} = +1. \tag{2.27}$$

[1] For proof, see (Haupt, 2002, Theorem 1.5).

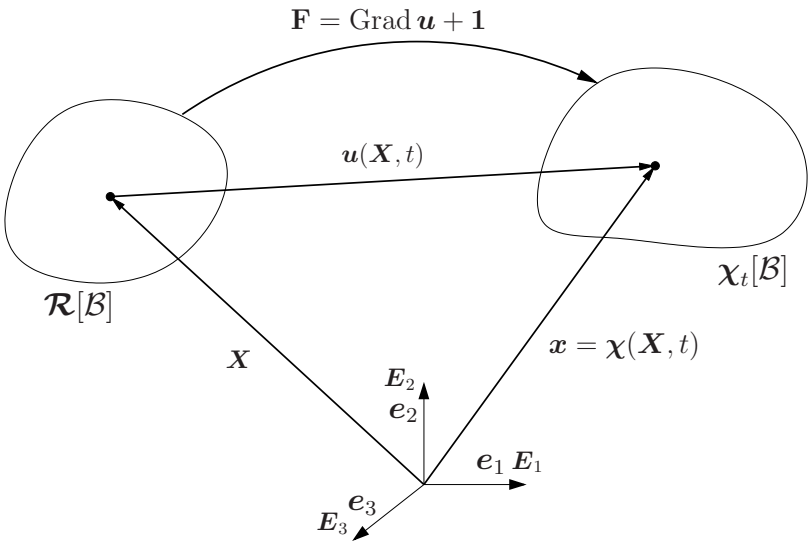

Figure 2.3.: The deformation gradient tensor in term of the displacement vector $\boldsymbol{u}(\boldsymbol{X}, t)$.

The squares of the stretch tensors $\mathbf{U}$ and $\mathbf{V}$ result in the two important tensors, namely, the right Cauchy-Green tensor

$$\mathbf{C} = \mathbf{F}^{\mathrm{T}}\mathbf{F} = \mathbf{U}^2 \tag{2.28a}$$

and the left Cauchy-Green tensor

$$\mathbf{B} = \mathbf{F}\mathbf{F}^{\mathrm{T}} = \mathbf{V}^2. \tag{2.28b}$$

Using $\mathbf{C}$ and $\mathbf{B}$, two strain measures can be defined by

$$\mathbf{E} = \tfrac{1}{2}\left(\mathbf{C} - \mathbf{1}\right) \tag{2.29a}$$

and

$$\mathbf{A} = \tfrac{1}{2}\left(\mathbf{1} - \mathbf{B}^{-1}\right), \tag{2.29b}$$

where $\mathbf{E}$ and $\mathbf{A}$ are called Green strain tensor and Almansi strain tensor, which operate in the reference and current configurations, respectively.

The push-forward and pull-back operators are applied to transform quantities from the reference to the current configuration and from the current to the reference configuration, respectively. Concerning the strain and strain-rate measures, the push-forward $\mathbf{F}^{-\mathrm{T}}(\bullet)\mathbf{F}^{-1}$ and pull-back $\mathbf{F}^{\mathrm{T}}(\bullet)\mathbf{F}$ are applied, where $(\bullet)$ is any strain or strain-rate tensor operating in the reference or current configuration. Thus, $\mathbf{A}$ can be computed by applying the push-forward operator to $\mathbf{E}$

$$\mathbf{A} = \mathbf{F}^{-\mathrm{T}}\mathbf{E}\mathbf{F}^{-1} = \tfrac{1}{2}\left(\mathbf{F}^{-\mathrm{T}}\mathbf{C}\mathbf{F}^{-1} - \mathbf{F}^{-\mathrm{T}}\mathbf{1}\mathbf{F}^{-1}\right) = \tfrac{1}{2}\left(\mathbf{1} - \mathbf{B}^{-1}\right), \tag{2.30a}$$

and similarly, $\mathbf{E}$ can be obtained by applying the pull-back operator to $\mathbf{A}$

$$\mathbf{E} = \mathbf{F}^{\mathrm{T}}\mathbf{A}\mathbf{F} = \tfrac{1}{2}\left(\mathbf{C} - \mathbf{1}\right). \tag{2.30b}$$

2.2. Concept of Stress

The concept of stress-state, which characterizes the surface forces at a material point by a set of traction vectors acting on a set of surfaces passing that point, is described by the Cauchy stress tensor, which can be explained as follows: let $\boldsymbol{x} \in \boldsymbol{\chi}_t$ be a material point on the surface element $\mathrm{d}\boldsymbol{a} = \boldsymbol{n}da$, which has a normal unit vector $\boldsymbol{n}$ passing through $\boldsymbol{x}$, and $\boldsymbol{t}$ representing the traction vector acting on the surface $\mathrm{d}\boldsymbol{a}$. Then, according to Cauchy's theorem, the traction vector $\boldsymbol{t}$ is the mapping of the normal vector $\boldsymbol{n}$ by the stress tensor $\mathbf{T}$, as shown in Fig. 2.4(b), i.e.,

$$\boldsymbol{t}(\boldsymbol{x}, t, \boldsymbol{n}) = \mathbf{T}(\boldsymbol{x}, t)\boldsymbol{n}, \tag{2.31}$$

where $\boldsymbol{t}(\boldsymbol{x}, t, \boldsymbol{n})$ and $\mathbf{T}(\boldsymbol{x}, t)$ are called Cauchy stress vector and Cauchy stress tensor, respectively. Similarly, the relation

$$\boldsymbol{t}_{\mathrm{R}} = \mathbf{T}_{\mathrm{R}}\boldsymbol{n}_{\mathrm{R}}, \tag{2.32}$$

can be introduced, where $\boldsymbol{t}_{\mathrm{R}}$ and $\boldsymbol{n}_{\mathrm{R}}$ has the same meaning as $\boldsymbol{t}$ and $\boldsymbol{n}$, respectively, but they are defined relative to the reference configuration $\boldsymbol{\mathcal{R}}$, as shown in Fig. 2.4(a). $\boldsymbol{t}_{\mathrm{R}}$ and $\mathbf{T}_{\mathrm{R}}$ are called Piola-Kirchhoff stress vector and first Piola-Kirchhoff stress tensor, respectively. Using Eqs.(2.15) and (2.31) and introducing the definition of the body force

$$\boldsymbol{f} = \mathbf{T}\mathrm{d}\boldsymbol{a} = \mathbf{T}_{\mathrm{R}}\mathrm{d}\boldsymbol{A}, \tag{2.33}$$

the first Piola-Kirchhoff stress tensor $\mathbf{T}_{\mathrm{R}}$ can be related to Cauchy stress tensor $\mathbf{T}$

$$\mathbf{T}\mathrm{d}\boldsymbol{a} = \mathbf{T}(J\mathbf{F}^{-\mathrm{T}}\mathrm{d}\boldsymbol{A}) = \underbrace{J\mathbf{T}\mathbf{F}^{-\mathrm{T}}}_{\mathbf{T}_{\mathrm{R}}}\mathrm{d}\boldsymbol{A},$$

i.e. the first Piola-Kirchhoff stress tensor reads

$$\mathbf{T}_{\mathrm{R}} = J\mathbf{T}\mathbf{F}^{-\mathrm{T}}, \tag{2.34}$$

which is a non-symmetric tensor and has the physical interpretation of stress measured relative to the undeformed area $\mathrm{d}\boldsymbol{A} = \boldsymbol{n}_{\mathrm{R}}\mathrm{d}A$. Another convenient stress measure is the second Piola-Kirchhoff stress tensor $\tilde{\mathbf{T}}$, which is defined by the pull-back of the Cauchy stress tensor, i.e.

$$\tilde{\mathbf{T}} = J\mathbf{F}^{-1}\mathbf{T}\mathbf{F}^{-\mathrm{T}}, \tag{2.35}$$

and is related to $\mathbf{T}_{\mathrm{R}}$ by

$$\tilde{\mathbf{T}} = \mathbf{F}^{-1}\mathbf{T}_{\mathrm{R}}. \tag{2.36}$$

In contrast to $\mathbf{T}_{\mathrm{R}}$, $\tilde{\mathbf{T}}$ is a symmetric tensor and has no direct physical interpretation.

The power of internal forces (or the stress power) L_i is defined in the spatial representation as

$$L_i = \int_v \mathbf{T} \cdot \mathbf{L}\,\mathrm{d}v, \tag{2.37}$$

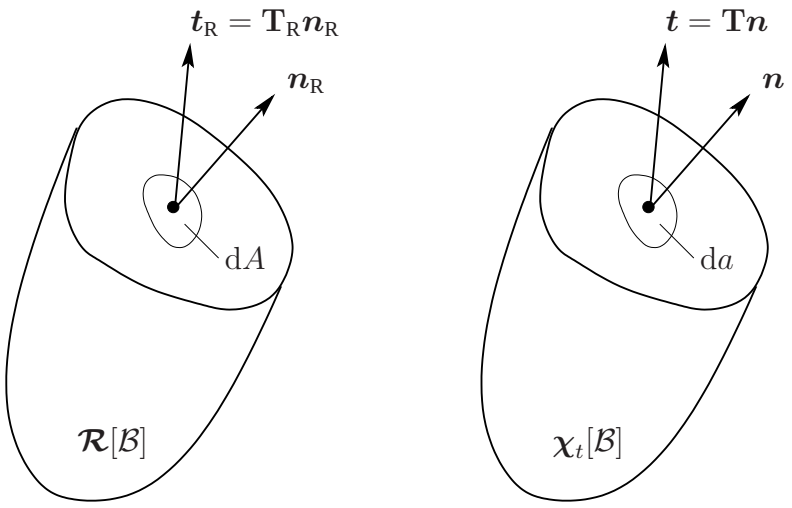

(a) Reference configuration (b) Current configuration

Figure 2.4.: Stress vectors and normal unit vectors in reference configuration (a) and current configuration (b).

where $(\,\cdot\,)$ refers to the dot (or scalar) product. Due to the symmetry of Cauchy stress tensor $\mathbf{T}$, which is a consequence of the balance of angular momentum as explained in Sec. 2.3.2, the stress power can be written as

$$L_i = \int_v \mathbf{T} \cdot \mathbf{D} \mathrm{d}v, \tag{2.38}$$

which indicates that $\mathbf{T}$ and $\mathbf{D}$ are work conjugate variables (or power conjugate). Other pairs of work conjugate are $\mathbf{T}_\mathrm{R}$ with $\dot{\mathbf{F}}$ and $\tilde{\mathbf{T}}$ with $\dot{\mathbf{E}}$, by which the material representation of the stress power is formulated as

$$L_i = \int_V \mathbf{T}_\mathrm{R} \cdot \dot{\mathbf{F}} \mathrm{d}V = \int_V \tilde{\mathbf{T}} \cdot \dot{\mathbf{E}} \mathrm{d}V. \tag{2.39}$$

2.3. Balance Relations

In Continuum Mechanics there are some fundamental principles which are applicable to any kind of material, without concern of its composition and shape. These principles, often called balance relations or balance laws, deal with conservation of mass, balance of linear and angular momentum, conservation of energy and entropy inequality. These principles are explained in the following subsections.

2.3.1. Conservation of Mass

This principle determines that the mass of a body $\mathcal{B}$ remains unchanged during the deformation. This means that the mass of the body in the current configuration $m(\mathcal{B}, t)$ is equal to the mass of

the body in the reference configuration $m(\mathcal{B})$, such that

$$\frac{\mathrm{d}}{\mathrm{d}t} m(\mathcal{B},t) = 0 \Longleftrightarrow m(\mathcal{B},t) = m(\mathcal{B}), \tag{2.40}$$

which leads to

$$\frac{\mathrm{d}}{\mathrm{d}t} m(\mathcal{B},t) = \frac{\mathrm{d}}{\mathrm{d}t} \int\limits_{v} \bar{\varrho}(\boldsymbol{x},t)\,\mathrm{d}v = \frac{\partial}{\partial t} \int\limits_{V} \hat{\varrho}_{\mathrm{R}}(\boldsymbol{X},t)\,\mathrm{d}V = 0, \tag{2.41}$$

where in these representations ϱ and ϱ_{R} are the mass densities of the material body $\mathcal{B}$ in the current and the material configuration, respectively. Furthermore, making use of Eq.(2.16), the relation

$$\varrho_{\mathrm{R}} = \big(\det \mathbf{F}\big)\,\varrho. \tag{2.42}$$

between the mass densities ϱ_{R} and ϱ is valid. Moreover, it follows from Eq.(2.41) that the mass density of the reference configuration is constant in time, i.e.

$$\frac{\partial}{\partial t} \hat{\varrho}_{\mathrm{R}}(\boldsymbol{X},t) = 0 \quad \Longrightarrow \quad \varrho_{\mathrm{R}} = \hat{\varrho}_{\mathrm{R}}(\boldsymbol{X})\,. \tag{2.43}$$

For the spatial representation in (2.41) the calculation of the material time derivative is required, in which the integration is carried out over the volume of the reference configuration,[1] such that

$$\begin{aligned} \frac{\mathrm{d}}{\mathrm{d}t} \int\limits_{v} \bar{\varrho}(\boldsymbol{x},t)\,\mathrm{d}v &= \frac{\partial}{\partial t} \int\limits_{V} \hat{\varrho}(\boldsymbol{X},t) \det \mathbf{F}(\boldsymbol{X},t)\mathrm{d}V \\ &= \int\limits_{V} \big[\dot{\hat{\varrho}}(\boldsymbol{X},t) \det \mathbf{F}\,(\boldsymbol{X},t) + \hat{\varrho}(\boldsymbol{X},t) \det \mathbf{F}(\boldsymbol{X},t)\,\mathrm{tr}(\dot{\mathbf{F}}\mathbf{F}^{-1})\big]\mathrm{d}V. \end{aligned} \tag{2.44}$$

Converting the result in (2.44) back to the current configuration yields

$$\frac{\mathrm{d}}{\mathrm{d}t} \int\limits_{v} \bar{\varrho}(\boldsymbol{x},t)\,\mathrm{d}v = \int\limits_{v} \big[\,\dot{\bar{\varrho}}(\boldsymbol{x},t) + \bar{\varrho}(\boldsymbol{x},t)\,\mathrm{div}\,\bar{\boldsymbol{v}}(\boldsymbol{x},t)\,\big]\mathrm{d}v = 0, \tag{2.45}$$

leading to

$$\dot{\varrho} + \varrho\,\mathrm{div}\,\boldsymbol{v} = 0. \tag{2.46}$$

The result in (2.46) can be written as

$$\frac{\partial \varrho}{\partial t} + \mathrm{div}(\varrho \boldsymbol{v}) = 0, \tag{2.47}$$

where the material time derivative of the density

$$\dot{\varrho}(\boldsymbol{x},t) = \frac{\partial}{\partial \varrho}(\boldsymbol{x},t) + (\mathrm{grad}\,\varrho(\boldsymbol{x},t)) \cdot \boldsymbol{v}(\boldsymbol{x},t)$$

and the product rule

$$(\mathrm{grad}\,\varrho) \cdot \boldsymbol{v} + \varrho\,(\mathrm{div}\,\boldsymbol{v}) = \mathrm{div}\,(\varrho \boldsymbol{v})$$

are inserted.

[1] See (Haupt, 2002, Sec.2.2.2) for more details.

2.3.2. Balance of Linear and Angular Momentum

The linear momentum $\boldsymbol{J}(\mathcal{B},t)$ of a body $\mathcal{B}$ in the current configuration is defined by

$$\boldsymbol{J}(\mathcal{B},t)=\int\limits_{v}\varrho(\boldsymbol{x},t)\,\boldsymbol{v}(\boldsymbol{x},t)\,\mathrm{d}v=\int\limits_{V}\varrho_{\mathrm{R}}(\boldsymbol{X})\,\boldsymbol{v}(\boldsymbol{X},t)\,\mathrm{d}V. \tag{2.48}$$

Assuming a body under the action of a stress vector $\boldsymbol{t}$ on its surface $\mathrm{d}a$ and a body force per unit mass $\boldsymbol{f}\,(\boldsymbol{x},t)$, the external force $\boldsymbol{F}(\mathcal{B},t)$ on the body is

$$\boldsymbol{F}(\mathcal{B},t)=\int\limits_{a}\boldsymbol{t}\,(\boldsymbol{x},t)\,\mathrm{d}a+\int\limits_{v}\varrho\,(\boldsymbol{x},t)\,\boldsymbol{f}\,(\boldsymbol{x},t)\,\mathrm{d}v. \tag{2.49}$$

The balance of linear momentum states that the time derivative of $\boldsymbol{J}(\mathcal{B},t)$ is equal to the external force $\boldsymbol{F}(\mathcal{B},t)$, i.e.

$$\frac{\mathrm{d}}{\mathrm{d}t}\boldsymbol{J}(\mathcal{B},t)=\boldsymbol{F}(\mathcal{B},t), \tag{2.50}$$

leads to

$$\frac{\mathrm{d}}{\mathrm{d}t}\int\limits_{v}\varrho(\boldsymbol{x},t)\boldsymbol{v}(\boldsymbol{x},t)\mathrm{d}v=\int\limits_{a}\boldsymbol{t}\,(\boldsymbol{x},t)\,\mathrm{d}a+\int\limits_{v}\varrho(\boldsymbol{x},t)\boldsymbol{f}(\boldsymbol{x},t)\mathrm{d}v. \tag{2.51}$$

Applying the Cauchy's theorem, i.e. Eq.(2.31), followed by the divergence theorem to the first term of the right-hand side of Eq.(2.51), implies the global form of balance of linear momentum in the spatial representation

$$\int\limits_{v}\left(\varrho\,(\boldsymbol{x},t)\,\frac{\mathrm{d}}{\mathrm{d}t}\boldsymbol{v}\,(\boldsymbol{x},t)-\operatorname{div}\mathbf{T}\,(\boldsymbol{x},t)-\varrho\,(\boldsymbol{x},t)\,\boldsymbol{f}\,(\boldsymbol{x},t)\right)\mathrm{d}v=\mathbf{0}. \tag{2.52}$$

In the same way, the global form of balance of linear momentum can be formulated relative to the reference configuration[1]

$$\int\limits_{V}\left(\varrho_{\mathrm{R}}\,(\boldsymbol{X})\,\frac{\partial}{\partial t}\boldsymbol{v}\,(\boldsymbol{X},t)-\operatorname{Div}\mathbf{T}_{\mathrm{R}}\,(\boldsymbol{X},t)-\varrho_{\mathrm{R}}\,(\boldsymbol{X})\,\boldsymbol{f}\,(\boldsymbol{X},t)\right)\mathrm{d}V=\mathbf{0}. \tag{2.53}$$

Thus, the local forms of balance of linear momentum in spatial respectively material representation read

$$\operatorname{div}\mathbf{T}\,(\boldsymbol{x},t)+\varrho\boldsymbol{f}=\varrho\frac{\mathrm{d}}{\mathrm{d}t}\boldsymbol{v}\,(\boldsymbol{x},t) \tag{2.54a}$$

$$\operatorname{Div}\mathbf{T}_{\mathrm{R}}\,(\boldsymbol{X},t)+\varrho_{\mathrm{R}}\boldsymbol{f}=\varrho_{\mathrm{R}}\frac{\partial}{\partial t}\boldsymbol{v}\,(\boldsymbol{X},t)\,. \tag{2.54b}$$

[1] See (Tadmor et al., 2012, Sec.4.4).

For quasi-static analysis, the local forms of balance of linear momentum in spatial and material representations takes the form

$$\operatorname{div} \mathbf{T}(\boldsymbol{x}, t) + \varrho \boldsymbol{f} = \mathbf{0} \tag{2.55a}$$

and

$$\operatorname{Div} \mathbf{T}_{\mathrm{R}}(\boldsymbol{X}, t) + \varrho_{\mathrm{R}} \boldsymbol{f} = \mathbf{0}, \tag{2.55b}$$

respectively.

The balance of angular momentum (or moment of momentum principle) states that the time derivative of the angular momentum $\boldsymbol{D}_{\mathrm{C}}(\mathcal{B}, t)$ of a body is equal to the external moment $\boldsymbol{M}_{\mathrm{C}}(\mathcal{B}, t)$ of all forces acting on the body. The angular momentum $\boldsymbol{D}_{\mathrm{C}}(\mathcal{B}, t)$ is defined as the moment of the momentum $\boldsymbol{J}(\mathcal{B}, t)$ in Eq.(2.48)

$$\begin{aligned} \boldsymbol{D}_{\mathrm{C}}(\mathcal{B}, t) &= \int_v (\boldsymbol{x} - \boldsymbol{c}) \times \varrho(\boldsymbol{x}, t)\, \boldsymbol{v}(\boldsymbol{x}, t)\, \mathrm{d}v \\ &= \int_V (\boldsymbol{\chi}(\boldsymbol{X}, t) - \boldsymbol{c}) \times \varrho_{\mathrm{R}}(\boldsymbol{X})\, \boldsymbol{v}(\boldsymbol{X}, t)\, \mathrm{d}V, \end{aligned} \tag{2.56}$$

where vector $\boldsymbol{c}$ defines the point in space to which the angular momentum refers, and the moment $\boldsymbol{M}_{\mathrm{C}}(\mathcal{B}, t)$ is the moment of the external force $\boldsymbol{F}(\mathcal{B}, t)$ given in Eq.(2.49)

$$\boldsymbol{M}_{\mathrm{C}}(\mathcal{B}, t) = \int_v (\boldsymbol{x} - \boldsymbol{c}) \times \boldsymbol{t}(\boldsymbol{x}, t)\, \mathrm{d}a + \int_v (\boldsymbol{x} - \boldsymbol{c}) \times \varrho(\boldsymbol{x}, t)\, \boldsymbol{f}(\boldsymbol{x}, t)\, \mathrm{d}v. \tag{2.57}$$

Thus, the mathematical representation of the principle of balance of angular momentum reads

$$\begin{aligned} \frac{\mathrm{d}}{\mathrm{d}t} \int_v (\boldsymbol{x} - \boldsymbol{c}) \times \varrho(\boldsymbol{x}, t)\, \boldsymbol{v}(\boldsymbol{x}, t)\, \varrho \mathrm{d}v &= \int_a (\boldsymbol{x} - \boldsymbol{c}) \times \boldsymbol{t}(\boldsymbol{x}, t)\, \mathrm{d}a \\ &\quad + \int_v (\boldsymbol{x} - \boldsymbol{c}) \times \varrho(\boldsymbol{x}, t)\, \boldsymbol{f}(\boldsymbol{x}, t)\, \mathrm{d}v. \end{aligned} \tag{2.58}$$

Recalling the argument that led to Eq.(2.52), and applying it to Eq.(2.58) yields

$$\begin{aligned} \frac{\mathrm{d}}{\mathrm{d}t} \int_v (\boldsymbol{x} - \boldsymbol{c}) \times \varrho(\boldsymbol{x}, t)\, \boldsymbol{v}(\boldsymbol{x}, t)\, \mathrm{d}v &= \int_v \operatorname{div}\left[(\boldsymbol{x} - \boldsymbol{c}) \times \mathbf{T}(\boldsymbol{x}, t)\right] \mathrm{d}v \\ &\quad + \int_v (\boldsymbol{x} - \boldsymbol{c}) \times \varrho(\boldsymbol{x}, t)\, \boldsymbol{f}(\boldsymbol{x}, t)\, \mathrm{d}v. \end{aligned} \tag{2.59}$$

The result of the first term on the right-hand side reads[1]

$$\operatorname{div}\left[(\boldsymbol{x} - \boldsymbol{c}) \times \mathbf{T}(\boldsymbol{x}, t)\right] = (\boldsymbol{x} - \boldsymbol{c}) \times \operatorname{div} \mathbf{T}(\boldsymbol{x}, t) - T_{ik}\, \boldsymbol{e}_i \times \boldsymbol{e}_k, \tag{2.60}$$

[1] For proof, see (Haupt, 2002, p.99).

with the identity

$$\boldsymbol{e}_p \times \boldsymbol{e}_q = \epsilon_{pqr}\, \boldsymbol{e}_r, \tag{2.61}$$

where the so-called *permutation symbol* ϵ_{pqr} has the property

$$\epsilon_{pqr} = \begin{cases} +1 & \text{if } p,q,r \text{ form an even permutation, } (\epsilon_{123}, \epsilon_{312}, \epsilon_{231}) \\ -1 & \text{if } p,q,r \text{ form an odd permutation, } (\epsilon_{213}, \epsilon_{132}, \epsilon_{321}) \\ 0 & \text{if two indices are equal} \end{cases} \tag{2.62}$$

Using Eq.(2.60) in Eq.(2.59), and performing some rearrangements, lead to

$$\begin{aligned} &\int_v (\boldsymbol{x} - \boldsymbol{c}) \times \left(\varrho\,(\boldsymbol{x},t)\, \frac{\mathrm{d}}{\mathrm{d}t} \boldsymbol{v}\,(\boldsymbol{x},t) - \operatorname{div} \mathbf{T}\,(\boldsymbol{x},t) - \varrho\,(\boldsymbol{x},t)\, \boldsymbol{f}\,(\boldsymbol{x},t) \right) \mathrm{d}v \\ &= \int_v (T_{ij}\, \boldsymbol{e}_i \times \boldsymbol{e}_k)\, \mathrm{d}v. \end{aligned} \tag{2.63}$$

From Eq.(2.52), the term in brackets on the left-hand side of Eq.(2.63) is zero, so

$$\int_v (T_{ik}\, \boldsymbol{e}_i \times \boldsymbol{e}_k)\, \mathrm{d}v = \mathbf{0} \tag{2.64a}$$

leads to

$$T_{ij}\, \boldsymbol{e}_i \times \boldsymbol{e}_k = \mathbf{0}. \tag{2.64b}$$

The component representation of Eq.(2.64b) reads

$$(T_{23} - T_{32})\, \boldsymbol{e}_1 + (T_{31} - T_{13})\, \boldsymbol{e}_2 + (T_{12} - T_{21})\, \boldsymbol{e}_3 = \mathbf{0} \quad \text{or} \quad T_{ik} = T_{ki}, \tag{2.65}$$

which is valid if and only if the Cauchy stress tensor $\mathbf{T}$ is symmetric, i.e.

$$\mathbf{T} = \mathbf{T}^{\mathrm{T}}. \tag{2.66}$$

Thus, the balance of angular momentum implies symmetry of the Cauchy stress tensor. Consequently, this implies that the second Piola-Kirchhoff stress tensor $\tilde{\mathbf{T}}$ is also symmetric, since $\tilde{\mathbf{T}} = J\mathbf{F}^{-1}\mathbf{T}\mathbf{F}^{-\mathrm{T}}$ as given in Eq.(2.35).

2.3.3. Energy Balance

For a continuum subjected to a thermo-mechanical energy transfer, the principle of energy balance determines that the time change of the sum of kinetic energy $K(\mathcal{B},t)$ and the internal energy $E(\mathcal{B},t)$ is equal to the mechanical work $L_e(\mathcal{B},t)$ and the heat supply $Q(\mathcal{B},t)$, i.e.

$$\dot{K}(\mathcal{B},t) + \dot{E}(\mathcal{B},t) = L_e(\mathcal{B},t) + Q(\mathcal{B},t). \tag{2.67}$$

The sum of the kinetic and internal energies is defined by

$$K(\mathcal{B},t)+E(\mathcal{B},t)=\int_v \varrho\left(\tfrac{1}{2}\boldsymbol{v}^2+e\right)\mathrm{d}v, \tag{2.68}$$

where e is called specific internal energy per unit mass. The mechanical work is the work exerted on the body by the surface traction $\boldsymbol{t}$ and the body force $\boldsymbol{f}$

$$L_e(\mathcal{B},t)=\int_a \boldsymbol{t}\cdot\boldsymbol{v}\mathrm{d}a+\int_v \varrho\boldsymbol{f}\cdot\boldsymbol{v}\mathrm{d}v=\int_a \mathbf{T}\boldsymbol{v}\cdot\boldsymbol{n}\mathrm{d}a+\int_v \varrho\boldsymbol{f}\cdot\boldsymbol{v}\mathrm{d}v, \tag{2.69}$$

drawing on Cauchy's theorem. The thermal energy is defined by the heat supply $Q(\mathcal{B},t)$, which is the sum of the heat supplied by the heat flux vector $\boldsymbol{q}(\boldsymbol{x},t)$ across the surface (heat conduction) and the heat supplied by the volume-distributed heat supply $r(\boldsymbol{x},t)$ (heat radiation)

$$Q(\mathcal{B},t)=-\int_a \boldsymbol{q}(\boldsymbol{x},t)\cdot\boldsymbol{n}\mathrm{d}a+\int_v \varrho(\boldsymbol{x},t)r(\boldsymbol{x},t)\mathrm{d}v=\int_a q\mathrm{d}a+\int_v \varrho r\mathrm{d}v, \tag{2.70}$$

with $q=-\boldsymbol{q}\cdot\boldsymbol{n}$, see Fig. 2.5(b).

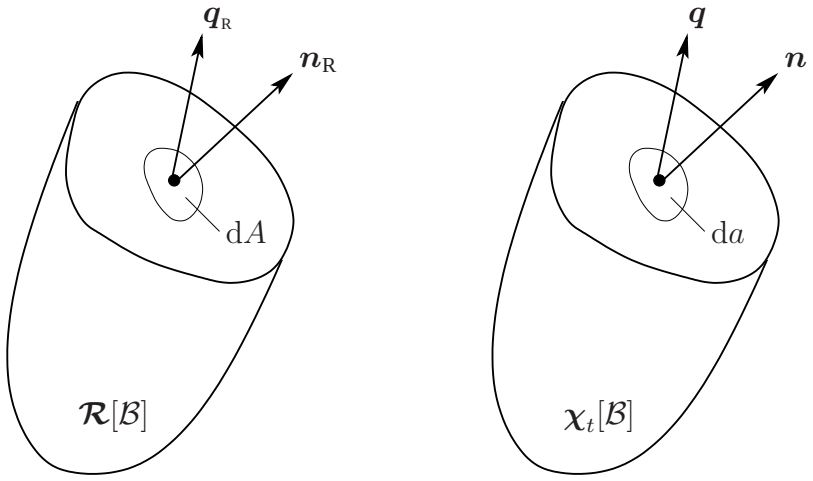

(a) Reference configuration (b) Current configuration

Figure 2.5.: Stress vectors and normal unit vectors in reference configuration (a) and current configuration (b).

A combination of Eqs.(2.67)-(2.70) yields

$$\frac{\mathrm{d}}{\mathrm{d}t}\int_v \varrho\left(\tfrac{1}{2}\boldsymbol{v}^2+e\right)\mathrm{d}v=\int_a\left(\mathbf{T}\boldsymbol{v}\cdot\boldsymbol{n}+q\right)\mathrm{d}a+\int_v \varrho\left(\boldsymbol{f}\cdot\boldsymbol{v}+r\right)\mathrm{d}v. \tag{2.71}$$

Applying the divergence theorem to the first term on the right-hand side and a subsequent rearrangement lead to

$$\frac{\mathrm{d}}{\mathrm{d}t}\int\limits_v \varrho e \mathrm{d}v = \frac{\mathrm{d}}{\mathrm{d}t}\int\limits_v \tfrac{1}{2}\varrho \boldsymbol{v}^2 \mathrm{d}v + \int\limits_v \mathrm{div}\,(\mathbf{T}\boldsymbol{v})\,\mathrm{d}v + \int\limits_v \varrho\,(\boldsymbol{f}\cdot\boldsymbol{v})\,\mathrm{d}v - \int\limits_v \mathrm{div}\,\boldsymbol{q}\mathrm{d}v + \int\limits_v \varrho r \mathrm{d}v. \quad (2.72)$$

Making use of the balance of mechanical energy[1]

$$\int\limits_v \mathbf{T}\cdot\mathbf{D}\mathrm{d}v = -\frac{\mathrm{d}}{\mathrm{d}t}\int\limits_v \tfrac{1}{2}\varrho \boldsymbol{v}^2 \mathrm{d}v + \int\limits_v \mathrm{div}\,(\mathbf{T}\boldsymbol{v})\,\mathrm{d}v + \int\limits_v \varrho\,(\boldsymbol{f}\cdot\boldsymbol{v})\,\mathrm{d}v \quad (2.73)$$

implying the global formulation of energy balance in the spatial representation

$$\frac{\mathrm{d}}{\mathrm{d}t}\int\limits_v \varrho e \mathrm{d}v = -\int\limits_v \mathrm{div}\,\boldsymbol{q}\mathrm{d}v + \int\limits_v \varrho r \mathrm{d}v + \int\limits_v \mathbf{T}\cdot\mathbf{D}\mathrm{d}v. \quad (2.74)$$

The local form of energy balance reads

$$\frac{\mathrm{d}e}{\mathrm{d}t} = -\frac{1}{\varrho}\,\mathrm{div}\,\boldsymbol{q} + r + \frac{1}{\varrho}\mathbf{T}\cdot\mathbf{D} \quad (2.75a)$$

in the spatial representation, and

$$\frac{\mathrm{d}e}{\mathrm{d}t} = -\frac{1}{\varrho_{\mathrm{R}}}\,\mathrm{Div}\,\boldsymbol{q}_{\mathrm{R}} + r + \frac{1}{\varrho_{\mathrm{R}}}\tilde{\mathbf{T}}\cdot\dot{\mathbf{E}} \quad (2.75b)$$

in the material representation, with[2]

$$\boldsymbol{q}_{\mathrm{R}} = (\det\mathbf{F})\,\mathbf{F}^{-1}\boldsymbol{q} \quad (2.76)$$

as the Piola-Kirchhoff heat flux vector, which can be obtained by

$$\boldsymbol{q}\cdot\mathrm{d}\boldsymbol{a} = \boldsymbol{q}\cdot\left((\det\mathbf{F})\mathbf{F}^{-\mathrm{T}}\mathrm{d}\boldsymbol{A}\right) = \underbrace{\left((\det\mathbf{F})\mathbf{F}^{-1}\boldsymbol{q}\right)}_{\boldsymbol{q}_{\mathrm{R}}}\cdot\mathrm{d}\boldsymbol{A} = \boldsymbol{q}_{\mathrm{R}}\cdot\mathrm{d}\boldsymbol{A}, \quad (2.77)$$

drawing on (2.15).

2.3.4. Entropy Inequality

The balance of energy - as demonstrated in the preceding subsection - does not cause a limit concerning the direction of energy transfer. Since the real physical processes are directional, there must be a variable to specify the direction of such process. This variable is the entropy $S(\mathcal{B},t)$, which can be defined as a measure of the energy that cannot be converted to another

[1] See (Haupt, 2002, Sec.2.4.1).
[2] See (Haupt, 2002, p.123).

type of energy or to do work, i.e. a measure of irreversibility of a process.[1] The entropy is expressed as

$$S(\mathcal{B},t)=\int_v \varrho s \mathrm{d}v, \tag{2.78}$$

where s is called specific entropy per unit mass.

Similar to the heat supply in Eq.(2.70), the entropy supply $H(\mathcal{B},t)$ is represented as the sum of the entropy flux vector $\boldsymbol{\Sigma}(\boldsymbol{x},t)$ and the volume-distributed entropy supply $\sigma(\boldsymbol{x},t)$

$$H(\mathcal{B},t)=-\int_a \boldsymbol{\Sigma}(\boldsymbol{x},t)\cdot\boldsymbol{n}\mathrm{d}a+\int_v \varrho(\boldsymbol{x},t)\sigma(\boldsymbol{x},t)\mathrm{d}v=\int_a \Sigma \mathrm{d}a+\int_v \varrho\sigma\mathrm{d}v, \tag{2.79}$$

where $\Sigma=-\boldsymbol{\Sigma}\cdot\boldsymbol{n}$ is the surface-distributed entropy supply.

Moreover, the entropy production is given by

$$\Gamma(\mathcal{B},t)=\int_v \varrho\gamma\mathrm{d}v, \tag{2.80}$$

where γ is called specific entropy production per unit mass. The entropy balance states that the time rate change in an entropy is equal to the sum of the entropy supply and the entropy production

$$\frac{\mathrm{d}}{\mathrm{d}t}S(\mathcal{B},t)=H(\mathcal{B},t)+\Gamma(\mathcal{B},t). \tag{2.81}$$

For any isolated system, the second law of thermodynamics postulates that the entropy production in any process is never negative, i.e. the entropy production is greater than zero for an irreversible process and is equal to zero for a reversible process, but it never less than zero. Thus, the inequality

$$\Gamma(\mathcal{B},t)=\frac{\mathrm{d}}{\mathrm{d}t}S(\mathcal{B},t)-H(\mathcal{B},t)\geq 0 \tag{2.82}$$

holds for any thermodynamical process.

The entropy flux vector $\boldsymbol{\Sigma}$ and entropy supply σ are defined by the heat flux vector $\boldsymbol{q}$ and heat supply r divided by the absolute temperature Θ, respectively,[2]

$$\boldsymbol{\Sigma}=\frac{\boldsymbol{q}}{\Theta}, \tag{2.83a}$$

$$\sigma=\frac{r}{\Theta}. \tag{2.83b}$$

A combination of Eqs.(2.83) and (2.79) leads to

$$H(\mathcal{B},t)=-\int_a \frac{1}{\Theta}\boldsymbol{q}\cdot\boldsymbol{n}\mathrm{d}a+\int_v \frac{1}{\Theta}\varrho r\mathrm{d}v=-\int_v \mathrm{div}\left(\frac{\boldsymbol{q}}{\Theta}\right)\mathrm{d}v+\int_v \frac{1}{\Theta}\varrho r\mathrm{d}v. \tag{2.84}$$

[1] See (Limons, 2013).

[2] See (Haupt, 2002, p.128) and (Hutter and Jöhnk, 2004, p.76).

Using Eqs.(2.78) and (2.84) in the entropy inequality (2.82) yields

$$\Gamma = \int_v \varrho\gamma \mathrm{d}v = \frac{\mathrm{d}}{\mathrm{d}t}\int_v \varrho s \mathrm{d}v + \int_v \left(\frac{1}{\Theta}\operatorname{div}\boldsymbol{q} - \frac{1}{\Theta^2}\operatorname{grad}\Theta\cdot\boldsymbol{q}\right)\mathrm{d}v + \int_v \frac{1}{\Theta}\varrho r \mathrm{d}v \geq 0, \tag{2.85}$$

which represents the global formulation of the most popular form of the second law of thermodynamics, known as the Clausius-Duhem inequality. In the last equation use of

$$\operatorname{div}\left(\frac{\boldsymbol{q}}{\Theta}\right) = \frac{1}{\Theta}\operatorname{div}\boldsymbol{q} - \frac{1}{\Theta^2}\boldsymbol{q}\cdot\operatorname{grad}\Theta \tag{2.86}$$

is made. The local form of the Clausius-Duhem inequality is written as

$$\gamma = \dot{s} + \frac{1}{\varrho\Theta}\operatorname{div}\boldsymbol{q} - \frac{1}{\varrho\Theta^2}\boldsymbol{q}\cdot\operatorname{grad}\Theta - \frac{1}{\Theta}r \geq 0 \tag{2.87a}$$

in the spatial representation, and

$$\gamma = \dot{s} + \frac{1}{\varrho_{\mathrm{R}}\Theta}\operatorname{Div}\boldsymbol{q}_{\mathrm{R}} - \frac{1}{\varrho_{\mathrm{R}}\Theta^2}\boldsymbol{q}_{\mathrm{R}}\cdot\operatorname{Grad}\Theta - \frac{1}{\Theta}r \geq 0 \tag{2.87b}$$

in the material representation.

In view of energy balance Eqs.(2.75a) and (2.75b), the elimination of the local heat supply in Eqs.(2.87a) and (2.87b) implies the alternative representation of Clausius-Duhem inequality in the spatial

$$\delta = \Theta\gamma = -\dot{e} + \Theta\dot{s} + \frac{1}{\varrho}\mathbf{T}\cdot\mathbf{D} - \frac{1}{\varrho\Theta}\boldsymbol{q}\cdot\operatorname{grad}\Theta \geq 0 \tag{2.88a}$$

and material

$$\delta = \Theta\gamma = -\dot{e} + \Theta\dot{s} + \frac{1}{\varrho_{\mathrm{R}}}\tilde{\mathbf{T}}\cdot\dot{\mathbf{E}} - \frac{1}{\varrho_{\mathrm{R}}\Theta}\boldsymbol{q}_{\mathrm{R}}\cdot\operatorname{Grad}\Theta \geq 0 \tag{2.88b}$$

representation, where the term $\delta = \Theta\gamma$ is called the internal dissipation. The inequality $\delta \geq 0$ is called the dissipation inequality.

Defining the Helmholtz free energy (or specific strain-energy per unit mass) Ψ through[1]

$$\Psi := e - \Theta s, \tag{2.89}$$

the Clausius-Duhem inequality can be formulated in the spatial or, respectively, the material representation as

$$\delta = -\dot{\psi} - s\dot{\Theta} + \frac{1}{\varrho}\mathbf{T}\cdot\mathbf{D} - \frac{1}{\varrho\Theta}\boldsymbol{q}\cdot\operatorname{grad}\Theta \geq 0 \tag{2.90a}$$

$$\delta = -\dot{\psi} - s\dot{\Theta} + \frac{1}{\varrho_{\mathrm{R}}}\tilde{\mathbf{T}}\cdot\dot{\mathbf{E}} - \frac{1}{\varrho_{\mathrm{R}}\Theta}\boldsymbol{q}_{\mathrm{R}}\cdot\operatorname{Grad}\Theta \geq 0. \tag{2.90b}$$

[1] See (Gurtin et al., 2011, p.188).

2.4. Principles in Constitutive Modeling

For a material subjected to a specific loading, the mathematical relations, which relate the response (or the behavior) of the material to the applied loading, are called constitutive equations (or constitutive relations). In Continuum Mechanics the constitutive equations are combined with the balance relations, presented in the preceding section, to solve mechanical and thermomechanical problems. The balance relations alone are insufficient to solve such problems, because the number of equations they provide is less than the number of unknowns.

In contrast to balance relations, which hold for all materials, constitutive relations are valid for specific material under consideration. Furthermore, constitutive equations are restricted by some principles, which are necessary to construct these equations appropriately. The principles that are required within the scope of this work are presented in the following.[1]

Principle of Determinism:

For a material body $\mathcal{B}$, the stress state of a material point $\mathcal{P} \in \mathcal{B}$ at time t is determined by the history of the motion of the entire body $\mathcal{B}$.[2] Mathematically

$$\mathbf{T}(\mathcal{P}, t) = \underset{\substack{\mathcal{T} \leq t \\ \mathcal{Q} \in \mathcal{B}}}{\mathfrak{S}} \left[\boldsymbol{\chi}_{\mathcal{T}}(\mathcal{Q}); \mathcal{P}, t \right], \tag{2.91}$$

where the functional $\mathfrak{S}$ combines all the history of the motion $\boldsymbol{\chi}_{\mathcal{T}}$ of all material particles $\mathcal{Q} \in \mathcal{B}$.

Principle of Local Action:

The principle of determinism is restricted by the principle of local action, which states that the response of a material point $\mathcal{P} \in \mathcal{B}$ is determined by the history of motion of the material points in the vicinity of $\mathcal{P}$ and not by the history of motion of the whole material points in the body. According to this restriction, Eq.(2.91) is rewritten as[3]

$$\mathbf{T}(\mathcal{P}, t) = \underset{\substack{\mathcal{T} \leq t \\ \mathcal{Q} \in \mathfrak{U}(\mathcal{P})}}{\mathfrak{S}} \left[\boldsymbol{\chi}_{\mathcal{T}}(\mathcal{Q}); \mathcal{P}, t \right], \tag{2.92}$$

where $\mathfrak{U}(\mathcal{P})$ represents the group of points in the vicinity of $\mathcal{P}$.

2.4.1. Principle of Material Frame-Indifference

This principle, also called objectivity, postulates that the constitutive equations must be invariant under changes of frame of reference. This means that the material response should be uninfluenced by a change of observer.

For a material point $\mathcal{P}$ represented in the spatial representation by vector $\boldsymbol{x}$ at time t, the time-dependent change of frame is given by the transformation $(\boldsymbol{x}, t) = (\boldsymbol{x}^*, t^*)$ defined by[4]

$$\boldsymbol{x}^* = \mathbf{Q}(t)\boldsymbol{x} + \boldsymbol{c}(t), \quad t^* = t - a, \tag{2.93}$$

[1] Further discussion of the fundamental principles restricting constitutive equations can be found in (Tadmor et al., 2012, p.181) and (Eringen, 1980, p.151).

[2] (Truesdell and Noll, 2004, Sec.26) and (Haupt, 2002, p.279).

[3] See (Haupt, 2002, p.281) and (Tadmor et al., 2012, p.182).

[4] See (Haupt, 2002, p.164).

where $\mathbf{Q}(t)$ is an arbitrary proper orthogonal tensor-valued function, see Fig. 2.6, has the properties

$$\mathbf{Q}\mathbf{Q}^{\mathrm{T}} = \mathbf{Q}^{\mathrm{T}}\mathbf{Q} = \mathbf{1}, \quad \det \mathbf{Q} = +1, \tag{2.94}$$

$\boldsymbol{c}(t)$ is an arbitrary vector-valued function, and a is an arbitrary real number.

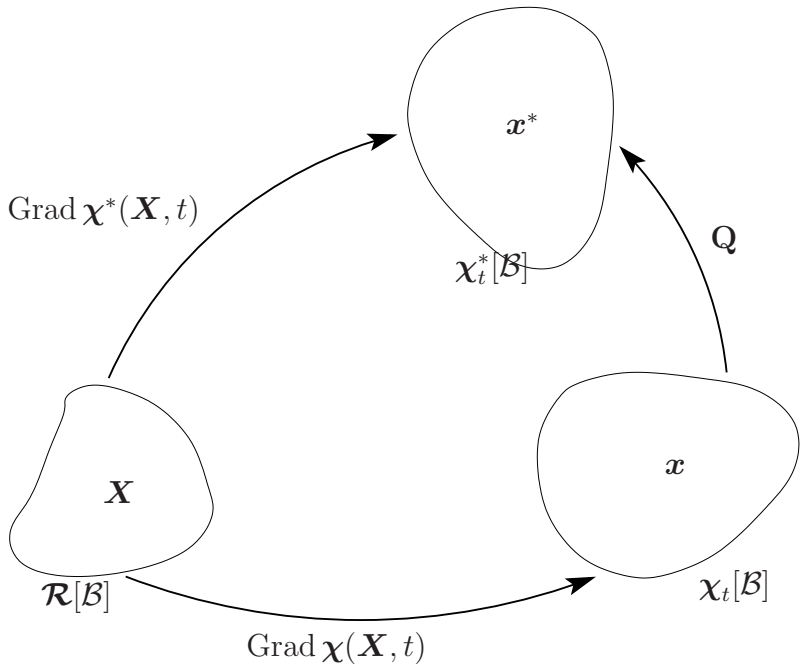

Figure 2.6.: Orthogonal transformation applied to the current configuration, leaving the response unchanged for all observers.

To this end, the deformation gradient tensor $\mathbf{F}$ reads

$$\mathbf{F} = \frac{\partial \boldsymbol{x}}{\partial \boldsymbol{X}} = \frac{\partial \boldsymbol{x}}{\partial \boldsymbol{x}^*}\frac{\partial \boldsymbol{x}^*}{\partial \boldsymbol{X}} = \mathbf{Q}^{-1}\mathbf{F}^*, \tag{2.95}$$

leading to the associated deformation gradient tensor

$$\mathbf{F}^* = \mathbf{Q}\mathbf{F}. \tag{2.96}$$

Thus, by a change of frame of the form Eq.(2.93), a constitutive equation similar to that in Eq.(2.91) can be written by

$$\mathbf{T}^*(\mathcal{P},t) = \underset{\substack{\mathcal{T}\le t^* \\ \mathcal{Q}\in\mathcal{B}}}{\mathfrak{S}}{}^* \left[\boldsymbol{\chi}_{\mathcal{T}}^*(\mathcal{Q});\mathcal{P},t^*\right]. \tag{2.97}$$

According to the principle of material frame-indifference, the constitutive equation Eq.(2.91) should be independent of any change of frame, which means that Eq.(2.91) is equivalent to

Eq.(2.97),[1] i.e. the constitutive equation

$$\mathbf{T}^*(\mathcal{P},t) = \underset{\substack{\mathcal{T}\le t^*\\ \mathcal{Q}\in\mathcal{B}}}{\mathfrak{S}}{}^* \left[\boldsymbol{\chi}_{\mathcal{T}}(\mathcal{Q});\mathcal{P},t^*\right] \tag{2.98}$$

should hold, which implies

$$\mathfrak{S}^* = \mathfrak{S}. \tag{2.99}$$

2.4.2. Principle of Material Symmetry

Another restriction of the constitutive equations is imposed by the principle of material symmetry, which postulates that the material response modeled by the constitutive equations must be invariant under all symmetry transformations. Consider a change of the reference configuration is defined by

$$\boldsymbol{X} \longmapsto \boldsymbol{X}^* = \boldsymbol{\Gamma}(\boldsymbol{X}) \Longleftrightarrow \boldsymbol{X} = \boldsymbol{\chi}\big(\boldsymbol{\Gamma}^{-1}(\boldsymbol{X}^*),t\big), \tag{2.100}$$

leading to

$$\boldsymbol{x} = \boldsymbol{\chi}^*(\boldsymbol{X}^*,t) = \boldsymbol{\chi}\big(\boldsymbol{\Gamma}^{-1}(\boldsymbol{X}^*),t\big). \tag{2.101}$$

Thus, the identity

$$\boldsymbol{\chi}(\boldsymbol{X},t) = \boldsymbol{\chi}^*\big(\boldsymbol{\Gamma}(\boldsymbol{X}),t\big), \tag{2.102}$$

after differentiation, follows[2]

$$\operatorname{Grad}\boldsymbol{\chi}(\boldsymbol{X},t) = \operatorname{Grad}\boldsymbol{\chi}^*(\boldsymbol{X}^*,t)\operatorname{Grad}\boldsymbol{\Gamma}(\boldsymbol{X}). \tag{2.103}$$

Symmetry transformations are defined as a set of orthogonal transformations (rotations), represented by orthogonal tensor $\mathbf{Q}$ with the properties

$$\mathbf{Q}\mathbf{Q}^{\mathrm{T}} = \mathbf{Q}^{\mathrm{T}}\mathbf{Q} = \mathbf{1}, \quad \det\mathbf{Q} = \pm 1, \tag{2.104}$$

that are applied to a reference configuration, occupied by a material body at its undeformed state, and leave the response to deformation unchanged in the current configuration, as shown in Fig. 2.7, so that

$$\boldsymbol{X}^* = \mathbf{Q}\boldsymbol{X}. \tag{2.105}$$

Inserting (2.105) into (2.103), yields

$$\operatorname{Grad}\boldsymbol{\chi}(\boldsymbol{X},t) = \operatorname{Grad}\boldsymbol{\chi}^*(\boldsymbol{X}^*,t)\operatorname{Grad}(\mathbf{Q}\boldsymbol{X}) \Longrightarrow \mathbf{F} = \mathbf{F}^*\mathbf{Q}, \tag{2.106}$$

i.e. a deformation gradient relative to the configuration $\boldsymbol{\mathcal{R}}^*$ can be defined as

$$\mathbf{F}^* = \mathbf{F}\mathbf{Q}^{\mathrm{T}}. \tag{2.107}$$

[1] (Truesdell and Noll, 2004, Sec.26) and (Haupt, 2002, p.279-280).

[2] See (, p.293) HauptBook2002.

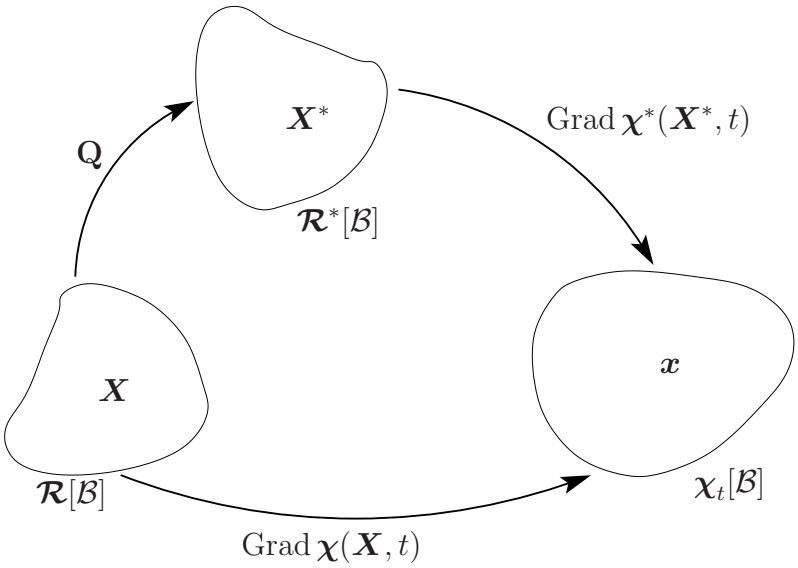

Figure 2.7.: Orthogonal transformation applied to the reference configuration, leaving the response unchanged in the current configuration.

A set of orthogonal tensors forms a symmetry group $\mathcal{G}$ if

$$\begin{cases} \mathbf{Q}_1 \in \mathcal{G} \text{ and } \mathbf{Q}_2 \in \mathcal{G}, & \text{then } \mathbf{Q}_1\mathbf{Q}_2 \in \mathcal{G} \\ \mathbf{Q} \in \mathcal{G}, & \text{then } \mathbf{Q}^{\mathrm{T}} \in \mathcal{G}. \end{cases} \tag{2.108}$$

For an arbitrary second-order tensor $\mathbf{Y}$, a scalar-valued function $\Phi(\mathbf{Y})$ and a tensor-valued function $\mathbf{\Phi}(\mathbf{Y})$ are said to be invariant relative to a symmetry group $\mathcal{G}$ if $\forall \mathbf{Q} \in \mathcal{G}$ provided that they satisfy the conditions

$$\Phi(\mathbf{Y}) = \Phi(\mathbf{Q}\mathbf{Y}\mathbf{Q}^{\mathrm{T}}) \tag{2.109}$$

and

$$\mathbf{Q}\mathbf{\Phi}(\mathbf{Y})\mathbf{Q}^{\mathrm{T}} = \mathbf{\Phi}(\mathbf{Q}\mathbf{Y}\mathbf{Q}^{\mathrm{T}}), \tag{2.110}$$

respectively.[1]

The full orthogonal group $\mathrm{O}(3)$ consists all orthogonal tensors with the properties given in (2.104), while the proper orthogonal group $\mathrm{SO}(3)$ consists of orthogonal tensors with the properties given in (2.94), i.e., the proper orthogonal group is subgroup of the full orthogonal group, $\mathrm{SO}(3) \subset \mathrm{O}(3)$. A material is called isotropic solid if its symmetry group is equal to the full orthogonal group ($\mathcal{G} = \mathrm{O}(3)$), and is called isotropic elastic solid if its symmetry group is equal to the proper orthogonal group ($\mathcal{G} = \mathrm{SO}(3)$). Otherwise, the material is called anisotropic.[2] An anisotropic material which has one preferred direction, defined by a unit vector $\boldsymbol{m}_0$ is called transversely isotropic relative to this preferred direction. The symmetry group of such material

[1] See (Gurtin et al., 2011, Sec.50.1).

[2] See (Ogden, 1997, Sec.4.2.3).

consists of all the rotations about the preferred direction, as well as the reflection that transforms $\boldsymbol{m}_0$ to $-\boldsymbol{m}_0$. In this case, the rotations through an angle $\phi = 2\pi/n$, with $n \in \mathbb{R}$, read

$$\mathbf{Q}^{\phi}_{\boldsymbol{m}_0} = \cos(\phi)\mathbf{1} + \big(1 - \cos(\phi)\big)\boldsymbol{m}_0 \otimes \boldsymbol{m}_0 + \sin(\phi)\overset{3}{\boldsymbol{\epsilon}}\boldsymbol{m}_0, \tag{2.111}$$

where $\overset{3}{\boldsymbol{\epsilon}} = \epsilon_{pqr}\boldsymbol{e}_p \otimes \boldsymbol{e}_q \otimes \boldsymbol{r}$ is given by (2.62). If the material preferred direction is aligned with the x-axis of the Cartesian coordinate system, the rotation matrix takes the form[1]

$$Q^{\phi}_{x} = \begin{bmatrix} 1 & 0 & 0 \\ 0 & \cos(\phi) & -\sin(\phi) \\ 0 & \sin(\phi) & \cos(\phi) \end{bmatrix}. \tag{2.112}$$

2.5. Representation of Isotropic Tensor Functions for Isotropic and Transversely Isotropic Hyperelastic Bodies

In constitutive modeling of isotropic hyperelastic materials, existence of a scalar-valued function $\Psi(\mathbf{E})$ is assumed, such that[2]

$$\frac{1}{\varrho_{\mathrm{R}}}\tilde{\mathbf{T}} = \frac{\partial \Psi(\mathbf{E})}{\partial \mathbf{E}} \tag{2.113}$$

represents the general constitutive equation, where $\Psi(\mathbf{E})$ is the specific strain-energy per unit mass defined in Eq.(2.89). Equivalently, Eq.(2.113) can be written in terms of the right Cauchy-Green tensor

$$\frac{1}{\varrho_{\mathrm{R}}}\tilde{\mathbf{T}} = 2\frac{\partial \Psi(\mathbf{C})}{\partial \mathbf{C}}, \tag{2.114}$$

or

$$\tilde{\mathbf{T}} = 2\frac{\partial \psi(\mathbf{C})}{\partial \mathbf{C}}, \tag{2.115}$$

where the strain-energy function $\psi(\mathbf{C}) = \varrho_{\mathrm{R}}\Psi(\mathbf{C})$ automatically fulfills the restrictions emerged by the principle of material-frame indifference.[3] Furthermore, $\psi(\mathbf{C})$ should be an isotropic tensor function, i.e. it should satisfy the constraint given in Eq.(2.109) emerged by the principle of material symmetry

$$\psi(\mathbf{C}) = \psi(\mathbf{Q}\mathbf{C}\mathbf{Q}^{\mathrm{T}}) \quad \forall\, \mathbf{Q} \in \mathrm{O}(3). \tag{2.116}$$

This constraint is satisfied by representing the strain-energy function $\psi(\mathbf{C})$ in terms of the three basic invariants of $\mathbf{C}$,[4] such that

$$\psi(\mathbf{C}) = \hat{\psi}(\mathrm{I}_1, \mathrm{I}_2, \mathrm{I}_3), \tag{2.117}$$

[1] For a detailed discussion about the symmetry group of transversely isotropic materials see (Ebbing, 2010).
[2] See (Haupt, 2002, Sec.9.2.2).
[3] See (Holzapfel, 2000, p.214-215), P.(214-215).
[4] (Haupt, 2002, Theor.9.6, p.335) for proof.

where

$$\mathrm{I}_1 = \mathrm{tr}\,\mathbf{C} \tag{2.118a}$$
$$\mathrm{I}_2 = \tfrac{1}{2}\left((\mathrm{tr}\,\mathbf{C})^2 - \mathrm{tr}\,\mathbf{C}^2\right) \tag{2.118b}$$
$$\mathrm{I}_3 = \det \mathbf{C}, \tag{2.118c}$$

with $\mathrm{tr}(\bullet)$ as the trace of a tensor field $(\bullet)$. For the case of transversal isotropy, where the material has one preferred direction defined by a unit vector $\boldsymbol{m}_0$, $|\boldsymbol{m}_0| = 1$, in the reference configuration, the strain-energy function is represented in terms of the right Cauchy-Green tensor $\mathbf{C}$ and one additional tensor-valued variable $\mathbf{M}_0$

$$\psi = \psi(\mathbf{C}, \mathbf{M}_0), \tag{2.119}$$

where $\mathbf{M}_0 = \boldsymbol{m}_0 \otimes \boldsymbol{m}_0$ is positive semi-definite tensor, known as the structural tensor denoting the preferred direction of the material with the properties

$$\mathbf{M}_0 = \mathbf{M}_0^T \tag{2.120a}$$
$$\|\mathbf{M}_0\|^2 = 1 \tag{2.120b}$$
$$\mathbf{M}_0 = \mathbf{M}_0^2 = \mathbf{M}_0^3 = \ldots \tag{2.120c}$$
$$\mathrm{tr}\,\mathbf{M}_0 = 1 \tag{2.120d}$$
$$\det \mathbf{M}_0 = \mathrm{adj}\,\mathbf{M}_0 = \mathrm{cof}\,\mathbf{M}_0 = 0, \tag{2.120e}$$

where $(\otimes)$ defines to the dyadic product, and adj is the adjoint of a tensor field

$$\mathrm{adj}(\bullet) = \big(\det(\bullet)\big)(\bullet)^{-1} = \big(\mathrm{cof}(\bullet)\big)^{\mathrm{T}}. \tag{2.121}$$

In this case, the second Piola-Kirchhoff stress tensor reads

$$\tilde{\mathbf{T}} = 2\frac{\partial \psi(\mathbf{C}, \mathbf{M}_0)}{\partial \mathbf{C}}. \tag{2.122}$$

The strain-energy function $\psi(\mathbf{C}, \mathbf{M}_0)$ is the isotropic function of the two tensor-valued variables $\mathbf{C}$ and $\mathbf{M}_0$ if it satisfies the condition

$$\psi(\mathbf{C}, \mathbf{M}_0) = \psi(\mathbf{Q}\mathbf{C}\mathbf{Q}^{\mathrm{T}}, \mathbf{Q}\mathbf{M}_0\mathbf{Q}^{\mathrm{T}}) \quad \forall\, \mathbf{Q} \in \mathrm{O}(3). \tag{2.123}$$

This condition can be satisfied by representing the strain-energy function in terms of a set of invariants including, in addition to the three basic invariants of $\mathbf{C}$ defined in Eq.(2.118), mixed invariants which involve both $\mathbf{C}$ and $\mathbf{M}_0$, see (Spencer, 1984) and (Itskov, 2009). According to (Spencer, 1971), the mixed invariants of two symmetric tensor, in this case $\mathbf{C}$ and $\mathbf{M}_0$, read

$$\mathrm{I}_4 = \mathrm{tr}\,(\mathbf{C}\mathbf{M}_0) \tag{2.124a}$$
$$\mathrm{I}_5 = \mathrm{tr}\left(\mathbf{C}^2\mathbf{M}_0\right) \tag{2.124b}$$
$$\mathrm{I}_6 = \mathrm{tr}\left(\mathbf{C}\mathbf{M}_0^2\right) \tag{2.124c}$$
$$\mathrm{I}_7 = \mathrm{tr}\left(\mathbf{C}^2\mathbf{M}_0^2\right). \tag{2.124d}$$

Due to the property of $\mathbf{M}_0$ given in (2.120), it is obvious that $\mathrm{I}_4 = \mathrm{I}_6$ and $\mathrm{I}_5 = \mathrm{I}_7$. Thus, a set of five invariants $\{\mathrm{I}_1, \mathrm{I}_2, \mathrm{I}_3, \mathrm{I}_4, \mathrm{I}_5\}$ is required, in terms of which the strain-energy function $\psi(\mathbf{C}, \mathbf{M}_0)$ for transversal isotropy is represented

$$\psi(\mathbf{C}, \mathbf{M}_0) = \hat{\psi}(\mathrm{I}_1, \mathrm{I}_2, \mathrm{I}_3, \mathrm{I}_4, \mathrm{I}_5). \tag{2.125}$$

3. Isothermal Transversal Isotropy

As mentioned in Sec. 2.5, the general strain-energy function for transversal isotropic solids, see Eq.(2.125), is represented in terms of the five invariants defined in Eqs.(2.118), (2.124a) and (2.124b). A main issue in constitutive modeling of such problems is how to particularize the general form of the strain-energy function. As pointed out in Chapter 1, there are numerous publications in the literature that address this matter. A common approach is related to the splitting of the general strain-energy function into two parts: an isotropic part, given in Eq.(2.117), and another part connected to the anisotropy, defined in terms of the two invariants in Eqs.(2.124a) and (2.124b), i.e.

$$\hat{\psi}(\mathrm{I}_1, \mathrm{I}_2, \mathrm{I}_3, \mathrm{I}_4, \mathrm{I}_5) = \hat{\psi}^{\mathrm{i}}(\mathrm{I}_1, \mathrm{I}_2, \mathrm{I}_3) + \tilde{\psi}^{\mathrm{t}}(\mathrm{I}_4, \mathrm{I}_5). \tag{3.1}$$

This formulation is motivated by the simple extension of the classical models of isotropy to the case of anisotropy, i.e. by reinforcing the isotropic strain-energy function $\hat{\psi}^{\mathrm{i}}$ with the anisotropic part $\tilde{\psi}^{\mathrm{t}}$.

Another motive to draw on specific forms of strain-energy functions is based on the additive decomposition of the strain-energy function that follows a multiplicative decomposition of the deformation gradient tensor $\mathbf{F}$ into specific deformations, see Chapter 1 for more details. One popular example is the volumetric/isochoric decomposition used in the modeling of nearly-incompressibility (also called weakly-compressibility), the behavior that most solids show at large strain range. In this formulation, originally proposed by (Flory, 1961), the deformation gradient tensor $\mathbf{F}$ is multiplicatively decomposed into a *volumetric part* $\hat{\mathbf{F}}$ and an *isochoric part* $\overline{\mathbf{F}}$, such that

$$\mathbf{F} = \hat{\mathbf{F}}\overline{\mathbf{F}}. \tag{3.2}$$

$\hat{\mathbf{F}}$ and $\overline{\mathbf{F}}$ are connected to volume-changing and volume preserving-deformations, respectively, with the properties

$$\hat{\mathbf{F}} = (\det \mathbf{F})^{1/3}\mathbf{I}, \qquad \det \hat{\mathbf{F}} = \det \mathbf{F} = J, \tag{3.3}$$

$$\overline{\mathbf{F}} = (\det \mathbf{F})^{-1/3}\mathbf{F}, \qquad \det \overline{\mathbf{F}} = 1. \tag{3.4}$$

Consequently, the strain-energy function, in the case of isotropy, is formulated as

$$\psi^{\mathrm{i}}(\mathbf{C}) = U(J) + \overline{\psi}^{\,\mathrm{i}}(\mathrm{I}_{\overline{\mathbf{C}}}, \mathrm{II}_{\overline{\mathbf{C}}}), \tag{3.5}$$

where $U(J)$ and $\overline{\psi}^{\,\mathrm{i}}(\mathrm{I}_{\overline{\mathbf{C}}}, \mathrm{II}_{\overline{\mathbf{C}}})$ represent the volumetric part, defined in terms of the volume-change parameter J - while the isochoric part, represented in terms of the two invariants

$$\mathrm{I}_{\overline{\mathbf{C}}} = \mathrm{tr}\,\overline{\mathbf{C}} \qquad = \mathrm{I}_1\mathrm{I}_3^{-1/3}, \tag{3.6a}$$

$$\mathrm{II}_{\overline{\mathbf{C}}} = \tfrac{1}{2}((\mathrm{tr}\,\overline{\mathbf{C}})^2 - \mathrm{tr}\,\overline{\mathbf{C}}^{\,2}) \qquad = \mathrm{I}_2\mathrm{I}_3^{-2/3}, \tag{3.6b}$$

respectively, with

$$\overline{\mathbf{C}} = \overline{\mathbf{F}}^{\mathrm{T}}\overline{\mathbf{F}} = (\det \mathbf{F})^{-1/3}\mathbf{C} = \mathrm{I}_3^{-1/3}\mathbf{C}, \tag{3.7}$$

is the unimodular right Cauchy-Green tensor. This formulation has the advantage that the resulting stress-state (a) is decomposed into hydrostatic (volume-changing) and deviatoric (volume-preserving) parts and (b) satisfies the condition of a stress-free reference configuration. (Hartmann and Neff, 2003) investigated the problem of near-incompressibility in view of this formulation and showed that a number of proposals in the literature show non-physical behavior in the case of simple tension/compression. To overcome this disadvantage they proposed a new model for the volumetric part $U(J)$ of the strain-energy function, which moreover satisfies the condition (b). The condition (b) is violated if the strain-energy function is formulated as $\psi^{\mathrm{i}}(\mathbf{C}) = U(J) + \hat{\psi}^{\mathrm{i}}(\mathrm{I}_1, \mathrm{I}_2)$. In this case, an additional term should be inserted into the strain-energy function to fulfill this requirement, see e.g. (Simo and Pister, 1984) and (Schröder and Neff, 2003) for isotropic and anisotropic models, respectively. Furthermore, relative to the volumetric/isochoric decomposition, the anisotropic part of the strain-energy function is formulated as $\overline{\psi}^{\,\mathrm{t}}(\bar{\mathrm{I}}_4, \bar{\mathrm{I}}_5)$, i.e. in terms of the two invariants

$$\bar{\mathrm{I}}_4 = \mathrm{tr}\left(\overline{\mathbf{C}}\,\mathbf{M}_0\right) \tag{3.8a}$$

$$\bar{\mathrm{I}}_5 = \mathrm{tr}\left(\overline{\mathbf{C}}^2\,\mathbf{M}_0\right). \tag{3.8b}$$

Thus, the total strain-energy function reads

$$\begin{aligned}\psi(\mathbf{C}, \mathbf{M}_0) &= U(J) + \overline{\psi}(\overline{\mathbf{C}}, \mathbf{M}_0) \\ &= U(J) + \overline{\psi}^{\,\mathrm{i}}(\mathrm{I}_{\overline{\mathbf{C}}}, \mathrm{II}_{\overline{\mathbf{C}}}) + \overline{\psi}^{\,\mathrm{t}}(\bar{\mathrm{I}}_4, \bar{\mathrm{I}}_5),\end{aligned} \tag{3.9}$$

which is frequently applied in the modeling of anisotropy, see e.g. (Weiss et al., 1996), (Holzapfel et al., 2000), (Rüter and Stein, 2000), (Calvo et al., 2009) and (Pena et al., 2011) among several others.

In this work, the idea of multiplicative decomposition of the deformation gradient tensor is used to formulate a constitutive model for transversal isotropic solids. In the first section the idea of the decomposition is presented and the invariants required for the strain-energy function are formulated. In the second section, a specific form of additively decomposed strain-energy function is proposed. Also, a constitutive model for the stress-state is derived - which is then investigated in the third section, based on simple analytical examples that can be used in the material parameter indentification process. Finally, the fourth section compares the proposed model to the classical models following the procedure explained above.

3.1. Multiplicative Decomposition of the Deformation Gradient Tensor

As demonstrated in Sec. 2.4.2, transversely isotropic material is a material that has one preferred direction denoted by a unit vector $\boldsymbol{m}_0$ in the undeformed configuration. The mapping of this unit

vector during the motion of a material body, containing the unit vector, from the undeformed to the deformed configuration, can be explained as follows: let $\mathrm{d}\boldsymbol{X}$, a material line element defined in the reference configuration with a length of Λ_0, be aligned with the preferred direction $\boldsymbol{m}_0$, such that

$$\mathrm{d}\boldsymbol{X} = \Lambda_0 \, \boldsymbol{m}_0. \tag{3.10}$$

During the motion $\boldsymbol{\mathcal{R}} \rightarrow \boldsymbol{\chi}_t$, see Fig. 3.1, $\mathrm{d}\boldsymbol{X}$ is mapped to

$$\mathrm{d}\boldsymbol{x} = \Lambda \, \boldsymbol{m}, \tag{3.11}$$

where Λ and $\boldsymbol{m}$ denote the length and unit vector of the material line element $\mathrm{d}\boldsymbol{x}$. Accordingly, $\boldsymbol{m}$ represents the preferred direction in the current configuration. Recalling Eq.(2.10) and making use of (3.10) and (3.11), yield

$$\Lambda \, \boldsymbol{m} = \Lambda_0 \, \mathbf{F} \boldsymbol{m}_0, \tag{3.12}$$

which can be rewritten as

$$\mathbf{F} \boldsymbol{m}_0 = \lambda_{\mathrm{a}} \boldsymbol{m}, \tag{3.13}$$

where

$$\lambda_{\mathrm{a}} = \frac{\Lambda}{\Lambda_0} \tag{3.14}$$

is the stretch ratio of the material in the preferred direction, and can be defined by taking the scalar product of the vectors in the left- and right-hand side of Eq.(3.12), i.e.

$$\mathbf{F} \boldsymbol{m}_0 \cdot \mathbf{F} \boldsymbol{m}_0 = \lambda_{\mathrm{a}} \boldsymbol{m} \cdot \lambda_{\mathrm{a}} \boldsymbol{m} \Longrightarrow \boldsymbol{m}_0 \cdot \mathbf{F}^{\mathrm{T}} \mathbf{F} \boldsymbol{m}_0 = \lambda_{\mathrm{a}}^2$$

yielding

$$\lambda_{\mathrm{a}} = \sqrt{\boldsymbol{m}_0 \cdot \mathbf{C} \boldsymbol{m}_0} = \sqrt{\mathbf{C} \cdot (\boldsymbol{m}_0 \otimes \boldsymbol{m}_0)} = \sqrt{\mathbf{C} \cdot \mathbf{M}_0}. \tag{3.15}$$

This, leads to the fact that the invariant I_4 defined in Eq.(2.124a) is equal to the square of the stretch in the preferred direction

$$\mathrm{I}_4 = \mathbf{C} \cdot \mathbf{M}_0 = \lambda_{\mathrm{a}}^2. \tag{3.16}$$

If the transversely isotropic material is assumed to be inextensible along the preferred direction, then, the constraint

$$\mathbf{C} \cdot \mathbf{M}_0 - 1 = 0 \tag{3.17}$$

is imposed, i.e. no stretch in the preferred direction can occur. In this case, Eq.(3.13) reads

$$\mathbf{F} \boldsymbol{m}_0 = \boldsymbol{m}. \tag{3.18}$$

This concept led to the idea of splitting the deformation in the preferred direction from the remaining deformations by applying a multiplicative decomposition to the deformation gradient. As a first attempt, the deformation gradient is multiplicatively decomposed into one part constrained to the deformation in the preferred direction and a remaining part, i.e. $\mathbf{F} = \mathbf{F}_{\mathrm{r}} \mathbf{F}_{\mathrm{a}}$. Thus,

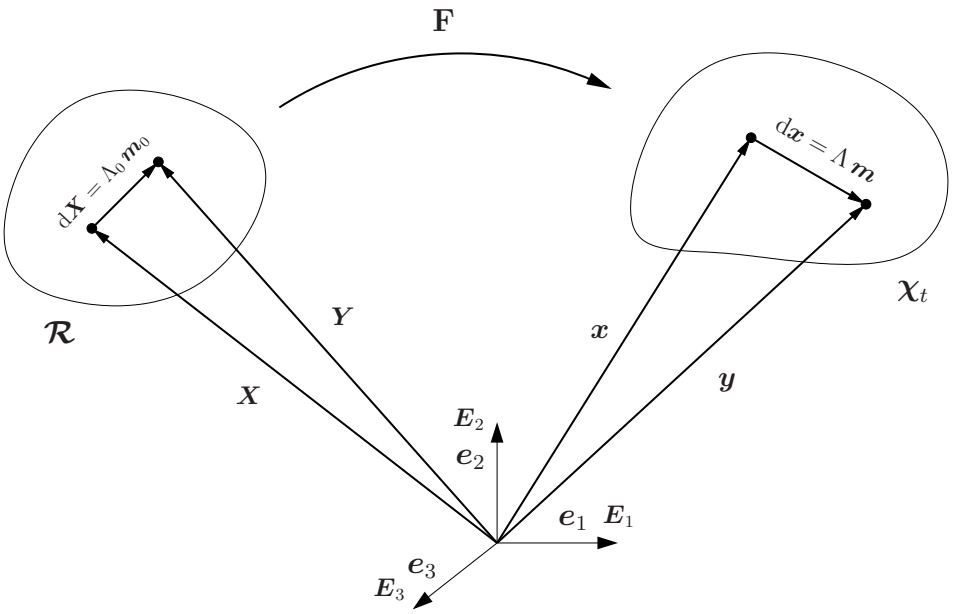

Figure 3.1.: Mapping of a material line element aligned with the preferred direction.

an intermediate configuration is introduced, in which the preferred direction is denoted by a unit vector $\hat{\boldsymbol{m}}$, such that

$$\mathbf{F}_{\mathrm{a}}\boldsymbol{m}_0 = \lambda_{\mathrm{a}}\hat{\boldsymbol{m}} \quad \text{and} \quad \mathbf{F}_{\mathrm{r}}\hat{\boldsymbol{m}} = \boldsymbol{m}. \tag{3.19}$$

This assumption leads to the problem that no deformation in lateral direction occurs in the case of a tensile test along the preferred direction.[1]

The multiplicative decomposition proposed in this work is an extension of the volumetric/isochoric decomposition illustrated above, see Eq.(3.2), where the isochoric part $\overline{\mathbf{F}}$ is further decomposed into two parts, $\mathbf{F}_{\mathrm{a}}$ defines the deformation only in the preferred direction,[2] while $\mathbf{F}_{\mathrm{r}}$ contains the remaining deformations,

$$\overline{\mathbf{F}} = \mathbf{F}_{\mathrm{r}}\mathbf{F}_{\mathrm{a}}. \tag{3.20}$$

Thus, the deformation gradient tensor $\mathbf{F}$ is decomposed into three parts

$$\mathbf{F} = \hat{\mathbf{F}}\overline{\mathbf{F}} = \hat{\mathbf{F}}\mathbf{F}_{\mathrm{r}}\mathbf{F}_{\mathrm{a}} = J^{1/3}\mathbf{F}_{\mathrm{r}}\mathbf{F}_{\mathrm{a}}. \tag{3.21}$$

This decomposition is illustrated in Fig. 3.2. Let $\boldsymbol{m}_0$, $\tilde{\boldsymbol{m}}$ and $\boldsymbol{m}$ be unit vectors representing the preferred direction in $\boldsymbol{\mathcal{R}}$, $\tilde{\mathcal{B}}$ and $\boldsymbol{\chi}_t$, respectively. Thus, the mappings of the preferred direction associated to the motions $\boldsymbol{\mathcal{R}} \to \boldsymbol{\chi}_t$ and $\boldsymbol{\mathcal{R}} \to \tilde{\mathcal{B}}$ read

$$\mathbf{F}\boldsymbol{m}_0 = \lambda_{\mathrm{a}}\boldsymbol{m} \tag{3.22a}$$

$$\overline{\mathbf{F}}\boldsymbol{m}_0 = \overline{\lambda}_{\mathrm{a}}\tilde{\boldsymbol{m}}, \tag{3.22b}$$

[1] This decomposition is discussed in Appendix A.1.

[2] In the subsequent work, the terms *preferred direction* and *fiber direction* are exchangeable, and both refer to the direction of isotropy of transversely isotropic material.

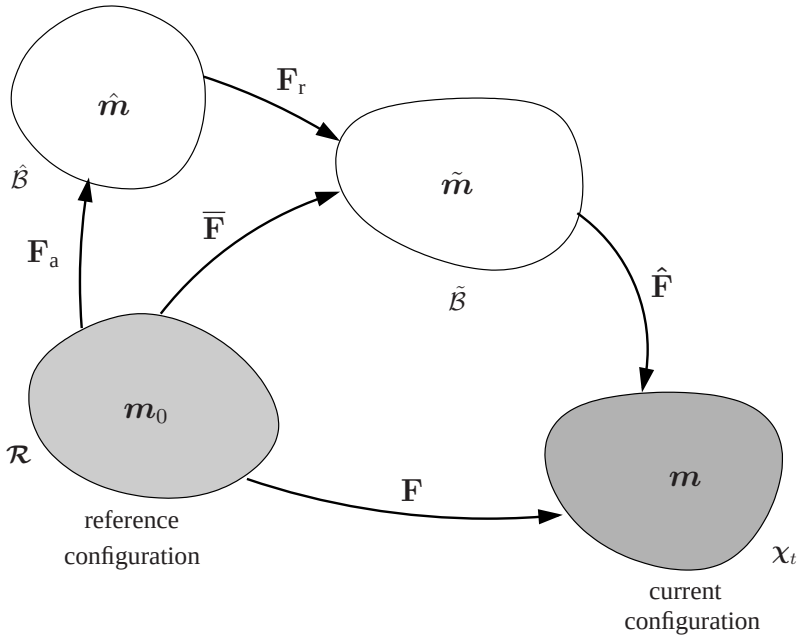

Figure 3.2.: Configurations of the proposed decomposition $\mathbf{F} = \hat{\mathbf{F}}\mathbf{F}_\mathrm{r}\mathbf{F}_\mathrm{a}$.

respectively. Applying a similar procedure there leads to (3.15),

$$\overline{\mathbf{F}}\boldsymbol{m}_0 \cdot \overline{\mathbf{F}}\boldsymbol{m}_0 = \overline{\lambda}_\mathrm{a}\hat{\boldsymbol{m}} \cdot \overline{\lambda}_\mathrm{a}\hat{\boldsymbol{m}} \Longrightarrow \boldsymbol{m}_0 \cdot \overline{\mathbf{F}}^T\overline{\mathbf{F}}\boldsymbol{m}_0 = \overline{\lambda}_\mathrm{a}^2$$

yielding

$$\overline{\lambda}_\mathrm{a} = \sqrt{\boldsymbol{m}_0 \cdot \overline{\mathbf{C}}\boldsymbol{m}_0} = \sqrt{\overline{\mathbf{C}} \cdot (\boldsymbol{m}_0 \otimes \boldsymbol{m}_0)} = \sqrt{\overline{\mathbf{C}} \cdot \mathbf{M}_0}, \tag{3.23}$$

representing the isochoric stretch of the material in the preferred direction. Here, the unimodular right Cauchy-Green tensor $\overline{\mathbf{C}}$ is defined in (3.7), and obviously

$$\overline{\lambda}_\mathrm{a} = J^{-1/3}\lambda_\mathrm{a} \tag{3.24}$$

holds.[1] By applying the proposed decomposition, i.e. Eq.(3.21), a new intermediate configuration $\tilde{\mathcal{B}}$ is obtained. Then, during the motions $\mathcal{R} \to \hat{\mathcal{B}}$ and $\hat{\mathcal{B}} \to \tilde{\mathcal{B}}$ the mappings of the preferred direction read

$$\mathbf{F}_\mathrm{a}\boldsymbol{m}_0 = \overline{\lambda}_\mathrm{a}\hat{\boldsymbol{m}} \tag{3.25a}$$

$$\mathbf{F}_\mathrm{r}\hat{\boldsymbol{m}} = \tilde{\boldsymbol{m}}, \tag{3.25b}$$

respectively, with the unit vector $\tilde{\boldsymbol{m}}$ describing the preferred direction in the intermediate configuration $\tilde{\mathcal{B}}$. Thus, no deformation in the preferred direction occurs during the application of $\mathbf{F}_\mathrm{r}$.

[1] Note that λ_a ($\overline{\lambda}_\mathrm{a}$) represents the total (isochoric) stretch of the bulk material along the fiber direction (the preferred direction) and not the stretch in the fiber itself.

Consequently, analogous to Eq.(3.23), the isochoric stretch along the preferred direction $\overline{\lambda}_{\mathrm{a}}$ can also be defined by

$$\mathbf{F}_{\mathrm{a}}\boldsymbol{m}_0 \cdot \mathbf{F}_{\mathrm{a}}\boldsymbol{m}_0 = \overline{\lambda}_{\mathrm{a}}^2 \hat{\boldsymbol{m}} \cdot \hat{\boldsymbol{m}} \Longrightarrow \boldsymbol{m}_0 \cdot \mathbf{F}_{\mathrm{a}}^T \mathbf{F}_{\mathrm{a}} \boldsymbol{m}_0 = \overline{\lambda}_{\mathrm{a}}^2$$

yielding

$$\overline{\lambda}_{\mathrm{a}} = \sqrt{\boldsymbol{m}_0 \cdot \mathbf{C}_{\mathrm{a}} \boldsymbol{m}_0} = \sqrt{\mathbf{C}_{\mathrm{a}} \cdot (\boldsymbol{m}_0 \otimes \boldsymbol{m}_0)} = \sqrt{\mathbf{C}_{\mathrm{a}} \cdot \mathbf{M}_0}, \tag{3.26}$$

i.e. in combination with (3.23)

$$\mathbf{C}_{\mathrm{a}} \cdot \mathbf{M}_0 = \overline{\mathbf{C}} \cdot \mathbf{M}_0. \tag{3.27}$$

holds.

If Cartesian coordinates in the reference ($\boldsymbol{\mathcal{R}}$) and intermediate ($\hat{\mathcal{B}}$) configurations are assumed, for which $\boldsymbol{m}_0 = \boldsymbol{E}_1$ and $\hat{\boldsymbol{m}} = \hat{\boldsymbol{e}}_1$ hold, then $\mathbf{F}_{\mathrm{a}}$ can be written as

$$\mathbf{F}_{\mathrm{a}} = \overline{\lambda}_{\mathrm{a}}\, \hat{\boldsymbol{e}}_1 \otimes \boldsymbol{E}_1 + \hat{\boldsymbol{e}}_2 \otimes \boldsymbol{E}_2 + \hat{\boldsymbol{e}}_3 \otimes \boldsymbol{E}_3, \tag{3.28}$$

leading to[1]

$$\begin{aligned}
\mathbf{C}_{\mathrm{a}} = \mathbf{F}_{\mathrm{a}}^T \mathbf{F}_{\mathrm{a}} &= \left(\overline{\lambda}_{\mathrm{a}}\, \boldsymbol{E}_1 \otimes \hat{\boldsymbol{e}}_1 + \boldsymbol{E}_2 \otimes \hat{\boldsymbol{e}}_2 + \boldsymbol{E}_3 \otimes \hat{\boldsymbol{e}}_3\right)\left(\overline{\lambda}_{\mathrm{a}}\, \hat{\boldsymbol{e}}_1 \otimes \boldsymbol{E}_1 + \hat{\boldsymbol{e}}_2 \otimes \boldsymbol{E}_2 + \hat{\boldsymbol{e}}_3 \otimes \boldsymbol{E}_3\right) \\
&= \overline{\lambda}_{\mathrm{a}}^2\, \boldsymbol{E}_1 \otimes \boldsymbol{E}_1 + \boldsymbol{E}_2 \otimes \boldsymbol{E}_2 + \boldsymbol{E}_3 \otimes \boldsymbol{E}_3 \\
&= \underbrace{\overline{\lambda}_{\mathrm{a}}^2\, \boldsymbol{E}_1 \otimes \boldsymbol{E}_1 - \boldsymbol{E}_1 \otimes \boldsymbol{E}_1}_{(\overline{\lambda}_{\mathrm{a}}^2 - 1)\boldsymbol{m}_0 \otimes \boldsymbol{m}_0} + \underbrace{\boldsymbol{E}_1 \otimes \boldsymbol{E}_1 + \boldsymbol{E}_2 \otimes \boldsymbol{E}_2 + \boldsymbol{E}_3 \otimes \boldsymbol{E}_3}_{\mathbf{1}} \\
&= (\overline{\lambda}_{\mathrm{a}}^2 - 1)\boldsymbol{m}_0 \otimes \boldsymbol{m}_0 + \mathbf{1} \\
&= (\bar{\mathrm{I}}_4 - 1)\mathbf{M}_0 + \mathbf{1},
\end{aligned} \tag{3.29}$$

where the basis $\hat{\boldsymbol{e}}_1$, $\hat{\boldsymbol{e}}_2$ and $\hat{\boldsymbol{e}}_3$ in $\hat{\mathcal{B}}$ are assumed to be orthogonal, i.e. $\hat{\boldsymbol{e}}_i \cdot \hat{\boldsymbol{e}}_j = \delta_{ij}$ $(i, j = 1, 2, 3)$.

[1] The inverse of $\mathbf{C}_{\mathrm{a}}$ (i.e. $\mathbf{C}_{\mathrm{a}}^{-1}$) is required in the subsequent calculations, and is derived in Appendix A.3.

To this end, the three principal invariants of $\mathbf{C}_{\mathrm{a}}$

$$\begin{aligned}
\mathrm{I}_{\mathbf{C}_{\mathrm{a}}} &= \operatorname{tr}\mathbf{C}_{\mathrm{a}} = \operatorname{tr}\left((\bar{\mathrm{I}}_4-1)\mathbf{M}_0+\mathbf{1}\right) = (\bar{\mathrm{I}}_4-1)\operatorname{tr}\mathbf{M}_0+\operatorname{tr}\mathbf{1} = (\bar{\mathrm{I}}_4-1)+3 \\
&= \bar{\mathrm{I}}_4+2 \qquad (3.30a)\\
\mathrm{II}_{\mathbf{C}_{\mathrm{a}}} &= \tfrac{1}{2}\left((\operatorname{tr}\mathbf{C}_{\mathrm{a}})^2-\operatorname{tr}\mathbf{C}_{\mathrm{a}}^2\right) = \tfrac{1}{2}\left(\mathrm{I}_{\mathbf{C}_{\mathrm{a}}}^2-\operatorname{tr}\left((\bar{\mathrm{I}}_4^2-1)\mathbf{M}_0+\mathbf{1}\right)\right) \\
&= \tfrac{1}{2}\left((\bar{\mathrm{I}}_4+2)^2-(\bar{\mathrm{I}}_4^2-1)\operatorname{tr}\mathbf{M}_0+\operatorname{tr}\mathbf{1}\right) \\
&= \tfrac{1}{2}\left((\bar{\mathrm{I}}_4^2-2\bar{\mathrm{I}}_4+1)-(\bar{\mathrm{I}}_4^2-1)+3\right) \\
&= 2\bar{\mathrm{I}}_4^2+1 \qquad (3.30b)\\
\mathrm{III}_{\mathbf{C}_{\mathrm{a}}} &= \det\mathbf{C}_{\mathrm{a}} = \det\left((\bar{\mathrm{I}}_4-1)\mathbf{M}_0+\mathbf{1}\right) \\
&= \det\left((\bar{\mathrm{I}}_4-1)\mathbf{M}_0\right)+\operatorname{cof}\left((\bar{\mathrm{I}}_4-1)\mathbf{M}_0\right)\cdot\mathbf{1}+(\bar{\mathrm{I}}_4-1)\mathbf{M}_0\cdot\operatorname{cof}(\mathbf{1})+\det(\mathbf{1}) \\
&= (\bar{\mathrm{I}}_4-1)^3\det\mathbf{M}_0+(\bar{\mathrm{I}}_4-1)^2\operatorname{cof}\mathbf{M}_0\cdot\mathbf{1}+(\bar{\mathrm{I}}_4-1)\mathbf{M}_0\cdot\operatorname{cof}\mathbf{1}+\det\mathbf{1} \\
&= (\bar{\mathrm{I}}_4-1)\mathbf{M}_0\cdot\mathbf{1}+1 = (\bar{\mathrm{I}}_4-1)+1 \\
&= \bar{\mathrm{I}}_4 \qquad (3.30c)
\end{aligned}$$

and the three basic invariants of $\mathbf{C}_{\mathrm{a}}$ are

$$\hat{\mathrm{I}}_{\mathbf{C}_{\mathrm{a}}} = \operatorname{tr}\mathbf{C}_{\mathrm{a}} = \bar{\mathrm{I}}_4+2 \qquad (3.31a)$$

$$\hat{\mathrm{II}}_{\mathbf{C}_{\mathrm{a}}} = \operatorname{tr}\mathbf{C}_{\mathrm{a}}^2 = \bar{\mathrm{I}}_4^{\,2}+2 \qquad (3.31b)$$

$$\hat{\mathrm{III}}_{\mathbf{C}_{\mathrm{a}}} = \operatorname{tr}\mathbf{C}_{\mathrm{a}}^3 = \bar{\mathrm{I}}_4^{\,3}+2, \qquad (3.31c)$$

respectively, where use is made of the properties of $\mathbf{M}_0$ given in Eq.(2.120). Obviously,

$$\operatorname{tr}\mathbf{1}=3 \quad \text{and} \quad \det\mathbf{1}=\operatorname{cof}\mathbf{1}=1 \qquad (3.32)$$

and

$$\begin{aligned}
\mathbf{C}_{\mathrm{a}}^2 &= \mathbf{C}_{\mathrm{a}}\mathbf{C}_{\mathrm{a}} = \left((\bar{\mathrm{I}}_4-1)\mathbf{M}_0+\mathbf{1}\right)\left((\bar{\mathrm{I}}_4-1)\mathbf{M}_0+\mathbf{1}\right) \\
&= \left((\bar{\mathrm{I}}_4-1)^2+2(\bar{\mathrm{I}}_4-1)\right)\mathbf{M}_0+\mathbf{1} \\
&= (\bar{\mathrm{I}}_4^2-1)\mathbf{M}_0+\mathbf{1} \\
\mathbf{C}_{\mathrm{a}}^3 &= \mathbf{C}_{\mathrm{a}}^2\mathbf{C}_{\mathrm{a}} = \left((\bar{\mathrm{I}}_4^2-1)\mathbf{M}_0+\mathbf{1}\right)\left((\bar{\mathrm{I}}_4-1)\mathbf{M}_0+\mathbf{1}\right) \\
&= \left((\bar{\mathrm{I}}_4^2-1)(\bar{\mathrm{I}}_4-1)+(\bar{\mathrm{I}}_4^2-1)+(\bar{\mathrm{I}}_4-1)\right)\mathbf{M}_0+\mathbf{1} \\
&= (\bar{\mathrm{I}}_4^3-1)\mathbf{M}_0+\mathbf{1}
\end{aligned}$$

hold. Thus, the invariants of $\mathbf{C}_{\mathrm{a}}$ all depend on the fourth invariant

$$\bar{\mathrm{I}}_4 = \mathbf{C}_{\mathrm{a}}\cdot\mathbf{M}_0 = \overline{\mathbf{C}}\cdot\mathbf{M}_0 = \bar{\lambda}_{\mathrm{a}}^{\,2}. \qquad (3.33)$$

From Eq.(3.21) the remaining deformation represented by $\mathbf{F}_\mathrm{r}$ can be described by

$$\mathbf{F}_\mathrm{r} = J^{-1/3}\mathbf{F}\mathbf{F}_\mathrm{a}^{-1} = \overline{\mathbf{F}}\mathbf{F}_\mathrm{a}^{-1}. \tag{3.34}$$

Thus, the strain measure of the remaining deformation, which operates on the intermediate configuration $\hat{\mathcal{B}}$, can be defined as

$$\mathbf{C}_\mathrm{r} = \mathbf{F}_\mathrm{r}^\mathrm{T}\,\mathbf{F}_\mathrm{r} = \mathbf{F}_\mathrm{a}^{-\mathrm{T}}\,\overline{\mathbf{F}}^\mathrm{T}\,\overline{\mathbf{F}}\,\mathbf{F}_\mathrm{a}^{-1} = \mathbf{F}_\mathrm{a}^{-\mathrm{T}}\,\overline{\mathbf{C}}\,\mathbf{F}_\mathrm{a}^{-1}, \tag{3.35}$$

which represents the push-forward of the unimodular right Cauchy-Green tensor $\overline{\mathbf{C}}$ operating on the reference configuration $\boldsymbol{\mathcal{R}}$. Analogously to Eqs.(3.30) and (3.31), the principal and basic invariants of $\mathbf{C}_\mathrm{r}$ read[1]

$$\mathrm{I}_{\mathbf{C}_\mathrm{r}} = \mathrm{tr}\,\mathbf{C}_\mathrm{r} \qquad = \mathrm{I}_{\overline{\mathbf{C}}} - \bar{\mathrm{I}}_4 + 1 \tag{3.36a}$$

$$\mathrm{II}_{\mathbf{C}_\mathrm{r}} = \tfrac{1}{2}((\mathrm{tr}\,\mathbf{C}_\mathrm{r})^2 - \mathrm{tr}\,\mathbf{C}_\mathrm{r}^2) \qquad = \mathrm{II}_{\overline{\mathbf{C}}} + \mathrm{I}_{\overline{\mathbf{C}}}(1-\bar{\mathrm{I}}_4) + \bar{\mathrm{I}}_5(1-\bar{\mathrm{I}}_4^{-1}) \tag{3.36b}$$

$$\mathrm{III}_{\mathbf{C}_\mathrm{r}} = \det\mathbf{C}_\mathrm{r} \qquad = \bar{\mathrm{I}}_4^{-1}, \tag{3.36c}$$

and

$$\hat{\mathrm{I}}_{\mathbf{C}_\mathrm{r}} = \mathrm{tr}\,\mathbf{C}_\mathrm{r} = \mathrm{I}_{\overline{\mathbf{C}}} - \bar{\mathrm{I}}_4 + 1 \tag{3.37a}$$

$$\hat{\mathrm{II}}_{\mathbf{C}_\mathrm{r}} = \mathrm{tr}\,\mathbf{C}_\mathrm{r}^2 = \mathrm{I}_{\overline{\mathbf{C}}}^2 + \bar{\mathrm{I}}_4^2 - 2(\mathrm{II}_{\overline{\mathbf{C}}} + \bar{\mathrm{I}}_4) + 2(\bar{\mathrm{I}}_4^{-1} - 1)\bar{\mathrm{I}}_5 + 1 \tag{3.37b}$$

$$\begin{aligned}\hat{\mathrm{III}}_{\mathbf{C}_\mathrm{r}} &= \mathrm{tr}\,\mathbf{C}_\mathrm{r}^3 = \mathrm{I}_{\overline{\mathbf{C}}}^3 - \bar{\mathrm{I}}_4^3 + 1 \\ &\quad + 3\left(\bar{\mathrm{I}}_4^2 - \bar{\mathrm{I}}_4 - \mathrm{I}_{\overline{\mathbf{C}}}\mathrm{II}_{\overline{\mathbf{C}}} + 1 + (\bar{\mathrm{I}}_4 + \bar{\mathrm{I}}_4^{-1} - 2)\bar{\mathrm{I}}_5 + (\bar{\mathrm{I}}_4^{-1} - 1)(\mathrm{I}_{\overline{\mathbf{C}}}\bar{\mathrm{I}}_5 - \mathrm{II}_{\overline{\mathbf{C}}}\bar{\mathrm{I}}_4 + 1)\right),\end{aligned} \tag{3.37c}$$

respectively, where $\bar{\mathrm{I}}_5$ is defined in (3.8b). Obviously, the proposed decomposition satisfies the constraint of the isochoric deformation in Eq.(3.4), i.e.

$$\det\overline{\mathbf{F}} = \det(\mathbf{F}_\mathrm{r}\mathbf{F}_\mathrm{a}) = \det\mathbf{F}_\mathrm{r}\det\mathbf{F}_\mathrm{a} = (\det\mathbf{C}_\mathrm{r})^{1/2}(\det\mathbf{C}_\mathrm{a})^{1/2} = \bar{\mathrm{I}}_4^{-1/2}\bar{\mathrm{I}}_4^{1/2} = 1. \tag{3.38}$$

3.2. Strain-Energy Function and Stress-State

Following the multiplicative decomposition of the deformation gradient introduced in the preceding section, the strain-energy function $\psi(\mathbf{C}, \mathbf{M}_0)$ for transversal isotropy, see Sec. 2.5, is additively decomposed into three parts

$$\begin{aligned}\psi(\mathbf{C}, \mathbf{M}_0) = \hat{\psi}(J, \mathbf{C}_\mathrm{a}, \mathbf{C}_\mathrm{r}) &= U(J) + \psi^{\mathrm{isc}}(\mathbf{C}_\mathrm{a}, \mathbf{C}_\mathrm{r}) = \\ &= U(J) + \psi_\mathrm{a}^{\mathrm{isc}}(\mathbf{C}_\mathrm{a}) + \psi_\mathrm{r}^{\mathrm{isc}}(\mathbf{C}_\mathrm{r}),\end{aligned} \tag{3.39}$$

where $U(J)$, $\psi_\mathrm{a}^{\mathrm{isc}}(\mathbf{C}_\mathrm{a})$ and $\psi_\mathrm{r}^{\mathrm{isc}}(\mathbf{C}_\mathrm{r})$ are connected to the volumetric deformation, isochoric deformation along the preferred direction and the remaining isochoric deformation, respectively.

[1] These invariants are calculated in Appendix A.2.

From Eqs.(3.30) and (3.31), it is evident that the invariants of $\mathbf{C}_\mathrm{a}$ are functions of the invariant $\bar{\mathrm{I}}_4$, which is nothing more than the square of $\overline{\lambda}_\mathrm{a}$, see Eq.(3.33). Hence, the strain-energy function $\psi_\mathrm{a}^{\mathrm{isc}}(\mathbf{C}_\mathrm{a})$ originates from the isochoric stretch along the preferred direction $\overline{\lambda}_\mathrm{a}$. Thus, $\psi_\mathrm{a}^{\mathrm{isc}}(\mathbf{C}_\mathrm{a})$ can be assumed as a function of $\bar{\mathrm{I}}_4$ or $\overline{\lambda}_\mathrm{a}$, i.e.

$$\psi_\mathrm{a}^{\mathrm{isc}}(\mathbf{C}_\mathrm{a}) = \hat{v}(\bar{\mathrm{I}}_4) = v(\overline{\lambda}_\mathrm{a}). \tag{3.40}$$

Furthermore, the three basic invariants of $\mathbf{C}_\mathrm{r}$, given in (3.37), serve to represent the strain-energy function $\psi_\mathrm{r}^{\mathrm{isc}}(\mathbf{C}_\mathrm{r})$

$$\psi_\mathrm{r}^{\mathrm{isc}}(\mathbf{C}_\mathrm{r}) = w(\hat{\mathrm{I}}_{\mathbf{C}_\mathrm{r}}, \hat{\mathrm{II}}_{\mathbf{C}_\mathrm{r}}, \hat{\mathrm{III}}_{\mathbf{C}_\mathrm{r}}). \tag{3.41}$$

Accordingly, the strain-energy function in Eq.(3.39) can be rewritten to

$$\begin{aligned}\psi(\mathbf{C}, \mathbf{M}_0) &= U(J) + \hat{v}(\mathrm{I}_4) + w(\hat{\mathrm{I}}_{\mathbf{C}_\mathrm{r}}, \hat{\mathrm{II}}_{\mathbf{C}_\mathrm{r}}, \hat{\mathrm{III}}_{\mathbf{C}_\mathrm{r}}) \\ &= U(J) + v(\overline{\lambda}_\mathrm{a}) + w(\hat{\mathrm{I}}_{\mathbf{C}_\mathrm{r}}, \hat{\mathrm{II}}_{\mathbf{C}_\mathrm{r}}, \hat{\mathrm{III}}_{\mathbf{C}_\mathrm{r}}).\end{aligned} \tag{3.42}$$

Thus, according to the proposed decomposition, $J, \bar{\mathrm{I}}_4, \hat{\mathrm{I}}_{\mathbf{C}_\mathrm{r}}, \hat{\mathrm{II}}_{\mathbf{C}_\mathrm{r}}, \hat{\mathrm{III}}_{\mathbf{C}_\mathrm{r}}$ represents the set of five invariants required to formulate the strain-energy function for transversal isotropy, see Eqs.(3.4), (3.33) and (3.37). In the following, the three parts of $\psi(\mathbf{C}, \mathbf{M}_0)$ in Eq.(3.42) are assumed in terms of moderate stretches. With regard to the modeling idea of fiber reinforced polymers, $v(\overline{\lambda}_\mathrm{a})$ is assumed as a simple non-linear function based on $\overline{\lambda}_\mathrm{a}$, i.e.

$$v(\overline{\lambda}_\mathrm{a}) = \frac{\alpha}{3}(\overline{\lambda}_\mathrm{a}^{\,3} + 3\overline{\lambda}_\mathrm{a}^{\,-1} - 4). \tag{3.43}$$

This form of strain-energy function satisfies the conditions of being zero in the case of no deformation, $v(1) = 0$, and heading towards infinity in the cases of extreme tension $\overline{\lambda}_\mathrm{a} \to \infty$ and extreme compression $\overline{\lambda}_\mathrm{a} \to 0$. To model the behavior of biological materials such as soft tissues, which respond distinctly different to loading along and normal to the fiber direction, an exponential function can be assumed for $v(\overline{\lambda}_\mathrm{a})$, see e.g. (Holzapfel et al., 2000).

Concerning the remaining deformations, in order to simplify the analysis and to reduce the number of material parameters a neo-Hookean model serves as a first ansatz for $\psi_\mathrm{r}^{\mathrm{isc}}(\mathbf{C}_\mathrm{r})$

$$w(\hat{\mathrm{I}}_{\mathbf{C}_\mathrm{r}}) = \frac{\beta}{2}(\hat{\mathrm{I}}_{\mathbf{C}_\mathrm{r}} - 3). \tag{3.44}$$

Due to its physically reasonable behavior, the model proposed in (Hartmann and Neff, 2003) is used to represent the volumetric strain-energy function

$$U(J) = \frac{K}{50}(J^5 + J^{-5} - 2). \tag{3.45}$$

In the case of anisotropy, this ansatz has the disadvantage that it leads to a hydrostatic stress-state if the material is subjected to a hydrostatic deformation, i.e. the material shows only volume changes, which does not reflect the behavior of anisotropic materials, see (Sansour, 2008) and

(Annaidh et al., 2013). To overcome this drawback the modification of the volumetric strain-energy function presented by (Guo et al., 2008) is used as a first ansatz, where the volumetric variable J is coupled with I_4, i.e.

$$\psi^{\text{vol}}(J, \mathrm{I}_4) = U(J)\mathrm{I}_4^{-1/2}. \tag{3.46}$$

A detailed discussion of this proposal is provided in Subsection 3.3.3. To sum up, the concrete form of the strain-energy function $\psi(\mathbf{C}, \mathbf{M}_0)$ reads

$$\begin{aligned}\psi(\mathbf{C}, \mathbf{M}_0) &= \psi^{\text{vol}}(J, \mathrm{I}_4) + v(\overline{\lambda}_{\text{a}}) + w(\hat{\mathrm{I}}_{\mathbf{C}_{\text{r}}}) = \\ &= \frac{K}{50}(J^5 + J^{-5} - 2)\mathrm{I}_4^{-1/2} + \frac{\alpha}{3}(\overline{\lambda}_{\text{a}}^{\,3} + 3\overline{\lambda}_{\text{a}}^{\,-1} - 4) + \frac{\beta}{2}(\hat{\mathrm{I}}_{\mathbf{C}_{\text{r}}} - 3),\end{aligned} \tag{3.47}$$

which consists of three material parameters K, α and β.

By using this strain-energy function, the second Piola-Kirchhoff stress tensor $\tilde{\mathbf{T}}$, see Eq.(2.122), can be obtained[1]

$$\tilde{\mathbf{T}} = 2\frac{\partial \psi(\mathbf{C}, \mathbf{M}_0)}{\partial \mathbf{C}} = \tilde{\mathbf{T}}_{\text{vol}} + \tilde{\mathbf{T}}_{\text{isc}}, \tag{3.48a}$$

where

$$\tilde{\mathbf{T}}_{\text{vol}} = 2\frac{\partial \psi^{\text{vol}}(J, \mathrm{I}_4)}{\partial \mathrm{I}_4}\mathbf{M}_0 + J\frac{\partial \psi^{\text{vol}}(J, \mathrm{I}_4)}{\partial J}\mathbf{C}^{-1} \tag{3.48b}$$

and

$$\tilde{\mathbf{T}}_{\text{isc}} = \left(\left(\overline{\lambda}_{\text{a}}^{-1}v'(\overline{\lambda}_{\text{a}}) + 2(\overline{\mathrm{I}}_4^{-1} - 1)w'(\hat{\mathrm{I}}_{\mathbf{C}_{\text{r}}})\right)\mathbf{M}_0\overline{\mathbf{C}} + 2w'(\hat{\mathrm{I}}_{\mathbf{C}_{\text{r}}})\overline{\mathbf{C}}\right)^{\text{D}}\mathbf{C}^{-1}. \tag{3.48c}$$

Applying the push-forward operation to the second Piola-Kirchhoff stress tensor $\tilde{\mathbf{T}}$ yields the Cauchy stress tensor $\mathbf{T}$, i.e.

$$\mathbf{T} = \frac{1}{J}\mathbf{F}\tilde{\mathbf{T}}\mathbf{F}^{\text{T}} = \mathbf{T}_{\text{vol}} + \mathbf{T}_{\text{isc}}, \tag{3.49a}$$

with

$$\begin{aligned}\mathbf{T}_{\text{vol}} &= \frac{1}{J}\mathbf{F}\tilde{\mathbf{T}}_{\text{vol}}\mathbf{F}^{\text{T}} \\ &= \frac{2}{J}\frac{\partial \psi^{\text{vol}}(J, \mathrm{I}_4)}{\partial \mathrm{I}_4}\underbrace{\mathbf{F}\mathbf{M}_0\mathbf{F}^{\text{T}}}_{\mathrm{I}_4\mathbf{M}} + \frac{\partial \psi^{\text{vol}}(J, \mathrm{I}_4)}{\partial J}\underbrace{\mathbf{F}\mathbf{C}^{-1}\mathbf{F}^{\text{T}}}_{\mathbf{1}} \\ &= \frac{2\mathrm{I}_4}{J}\frac{\partial \psi^{\text{vol}}(J, \mathrm{I}_4)}{\partial \mathrm{I}_4}\mathbf{M} + \frac{\partial \psi^{\text{vol}}(J, \mathrm{I}_4)}{\partial J}\mathbf{I}\end{aligned} \tag{3.49b}$$

[1] A detailed derivation of $\tilde{\mathbf{T}}$ is given in Appendix A.4.

and

$$
\begin{aligned}
\mathbf{T}_{\text{isc}} &= \frac{1}{J}\mathbf{F}\tilde{\mathbf{T}}_{\text{isc}}\mathbf{F}^{\mathrm{T}} \\
&= \frac{1}{J}\mathbf{F}\left(\left(\overline{\lambda}_{\text{a}}^{-1}v'(\overline{\lambda}_{\text{a}}) + 2(\bar{\mathrm{I}}_4^{-1}-1)w'(\hat{\mathrm{I}}_{\mathbf{C}_{\text{r}}})\right)\mathbf{M}_0\overline{\mathbf{C}} + 2w'(\hat{\mathrm{I}}_{\mathbf{C}_{\text{r}}})\overline{\mathbf{C}}\right)^{\mathrm{D}}\mathbf{C}^{-1}\mathbf{F}^{\mathrm{T}} \\
&= \frac{1}{J}\big(J^{-2/3}\left(\overline{\lambda}_{\text{a}}^{-1}v'(\overline{\lambda}_{\text{a}}) + 2(\bar{\mathrm{I}}_4^{-1}-1)w'(\hat{\mathrm{I}}_{\mathbf{C}_{\text{r}}})\right)(\underbrace{\mathbf{F}\mathbf{M}_0\mathbf{F}^{\mathrm{T}}}_{\mathrm{I}_4\mathbf{M}}\underbrace{\mathbf{F}\mathbf{F}^{-1}}_{\mathbf{1}} - \tfrac{1}{3}\mathrm{I}_4\underbrace{\mathbf{F}\mathbf{1}\mathbf{F}^{-1}}_{\mathbf{1}}) \\
&\quad + 2J^{-2/3}w'(\hat{\mathrm{I}}_{\mathbf{C}_{\text{r}}})(\underbrace{\mathbf{F}\mathbf{F}^{\mathrm{T}}}_{\mathbf{B}}\underbrace{\mathbf{F}\mathbf{F}^{-1}}_{\mathbf{1}} - \tfrac{1}{3}\mathrm{I}_1\underbrace{\mathbf{F}\mathbf{1}\mathbf{F}^{-1}}_{\mathbf{1}}) \\
&= \frac{1}{J}\big(\left(\overline{\lambda}_{\text{a}}^{-1}v'(\overline{\lambda}_{\text{a}}) + 2(\bar{\mathrm{I}}_4^{-1}-1)w'(\hat{\mathrm{I}}_{\mathbf{C}_{\text{r}}})\right)\bar{\mathrm{I}}_4(\mathbf{M}-\tfrac{1}{3}\mathbf{1}) + 2w'(\hat{\mathrm{I}}_{\mathbf{C}_{\text{r}}})(\overline{\mathbf{B}}-\tfrac{1}{3}\mathrm{I}_{\overline{\mathbf{B}}}\mathbf{1})\big) \\
&= \frac{1}{J}\big(\left(\overline{\lambda}_{\text{a}}v'(\overline{\lambda}_{\text{a}}) + 2(1-\bar{\mathrm{I}}_4)w'(\hat{\mathrm{I}}_{\mathbf{C}_{\text{r}}})\right)\mathbf{M} + 2w'(\hat{\mathrm{I}}_{\mathbf{C}_{\text{r}}})\overline{\mathbf{B}}\big)^{\mathrm{D}},
\end{aligned}
\tag{3.49c}
$$

where, $\mathbf{M} = \boldsymbol{m}\otimes\boldsymbol{m}$ is the structural tensor defining the direction of isotropy in the current configuration and has the same properties as $\mathbf{M}_0$ given in Eq.(2.120), $\mathbf{M}^{\mathrm{D}} = (\mathbf{M} - (1/3)\mathbf{1})$, and $\overline{\mathbf{B}}$ is the unimodular left Cauchy-Green tensor

$$
\overline{\mathbf{B}} = \overline{\mathbf{F}}\,\overline{\mathbf{F}}^{\mathrm{T}} = J^{-2/3}\mathbf{B}. \tag{3.50}
$$

The superscript D indicates the deviator operator, $(\bullet)^{\mathrm{D}} = (\bullet) - (1/3)\,\mathrm{tr}(\bullet)\mathbf{1}$. The left Cauchy-Green tensor of the remaining part reads

$$
\begin{aligned}
\mathbf{B}_{\text{r}} &= \mathbf{F}_{\text{r}}\,\mathbf{F}_{\text{r}}^{\mathrm{T}} = \overline{\mathbf{F}}\,\mathbf{F}_{\text{a}}^{-1}\,\mathbf{F}_{\text{a}}^{-\mathrm{T}}\,\overline{\mathbf{F}}^{\mathrm{T}} = \overline{\mathbf{F}}\mathbf{C}_{\text{a}}^{-1}\overline{\mathbf{F}}^{\mathrm{T}} \\
&= \overline{\mathbf{F}}\left((\bar{\mathrm{I}}_4^{-1}-1)\mathbf{M}_0 - \mathbf{1}\right)\overline{\mathbf{F}}^{\mathrm{T}} = (\bar{\mathrm{I}}_4^{-1}-1)\underbrace{\overline{\mathbf{F}}\mathbf{M}_0\overline{\mathbf{F}}^{\mathrm{T}}}_{\bar{\mathrm{I}}_4\mathbf{M}} + \underbrace{\overline{\mathbf{F}}\overline{\mathbf{F}}^{\mathrm{T}}}_{\overline{\mathbf{B}}} \\
&= (1-\bar{\mathrm{I}}_4)\mathbf{M} + \overline{\mathbf{B}}
\end{aligned}
\tag{3.51}
$$

Thus, the Cauchy stress tensor reads

$$
\mathbf{T} = \left(\frac{2\mathrm{I}_4}{J}\frac{\partial\psi^{\text{vol}}(J,\mathrm{I}_4)}{\partial\mathrm{I}_4}\mathbf{M} + \frac{\partial\psi^{\text{vol}}(J,\mathrm{I}_4)}{\partial J}\mathbf{I}\right) + \frac{1}{J}\left(\overline{\lambda}_{\text{a}}v'(\overline{\lambda}_{\text{a}})\mathbf{M} + 2w'(\hat{\mathrm{I}}_{\mathbf{C}_{\text{r}}})\mathbf{B}_{\text{r}}\right)^{\mathrm{D}} \tag{3.52}
$$

i.e. leaving a pure hydrostatic and a deviatoric part as well as one part which is connected to the preferred direction resulting from a pure volumetric deformation. Obviously, the idea of decomposition used in the formulation of the present model leads to the stress-state which is decomposed into anisotropic hydrostatic and deviatoric parts, where one term that is connected to the deformation in fiber direction appears in both the volumetric and the isochoric stresses in Eq.(3.52) above. Furthermore, it is evident from Eqs.(3.47), (3.48) and (3.52) that the strain-energy function and stresses in both the reference and the current configurations are zero in the case of no deformation, i.e. $\mathbf{C} = \mathbf{1}$. Hence, the condition of the stress-free undeformed state is automatically satisfied. In the proposed model, only the three material parameters K, α and β need to be identified. This can be achieved by simple experiments, as shown in Section 3.3.1.3

The derivatives of the strain-energy functions included in Eq.(3.52), i.e. $\partial\psi^{\text{vol}}(J,\mathrm{I}_4)/\partial J$, $\partial\psi^{\text{vol}}(J,\mathrm{I}_4)/\partial\mathrm{I}_4$, $v'(\overline{\lambda}_{\mathrm{a}})$ and $w'(\hat{\mathrm{I}}_{\mathbf{C}_{\mathrm{r}}})$ read

$$\frac{\partial\psi^{\text{vol}}(J,\mathrm{I}_4)}{\partial J} = \frac{K}{10}\mathrm{I}_4^{-1/2}(J^4 - J^{-6}) \tag{3.53a}$$

$$\frac{\partial\psi^{\text{vol}}(J,\mathrm{I}_4)}{\partial \mathrm{I}_4} = -\frac{K}{100}\mathrm{I}_4^{-3/2}(J^5 + J^{-5} - 2) \tag{3.53b}$$

$$v'(\overline{\lambda}_{\mathrm{a}}) = \frac{\mathrm{d}v(\overline{\lambda}_{\mathrm{a}})}{\mathrm{d}\overline{\lambda}_{\mathrm{a}}} = \alpha(\overline{\lambda}_{\mathrm{a}}^2 - \overline{\lambda}_{\mathrm{a}}^{-2}) \tag{3.53c}$$

$$w'(\hat{\mathrm{I}}_{\mathbf{C}_{\mathrm{r}}}) = \frac{\mathrm{d}w'(\hat{\mathrm{I}}_{\mathbf{C}_{\mathrm{r}}})}{\mathrm{d}\hat{\mathrm{I}}_{\mathbf{C}_{\mathrm{r}}}} = \frac{\beta}{2}, \tag{3.53d}$$

and substituting these derivatives in Eq.(3.52) yields the concrete form of the Cauchy stress tensor, i.e.

$$\begin{aligned}\mathbf{T} &= \frac{2\mathrm{I}_4}{J}\left(-\frac{K}{100}\mathrm{I}_4^{-3/2}(J^5 + J^{-5} - 2)\right)\mathbf{M} + \frac{K}{10}\mathrm{I}_4^{-1/2}(J^4 - J^{-6})\mathbf{1} \\ &\quad + \frac{1}{J}\left(\left(\alpha\overline{\lambda}_{\mathrm{a}}(\overline{\lambda}_{\mathrm{a}}^2 - \overline{\lambda}_{\mathrm{a}}^{-2}) + \beta(1 - \bar{\mathrm{I}}_4)\right)\mathbf{M} + \beta\overline{\mathbf{B}}\right)^{\mathrm{D}} \\ &= \frac{K}{50J}\mathrm{I}_4^{-1/2}\left(5(J^5 - J^{-5})\mathbf{I} - (J^5 + J^{-5} - 2)\mathbf{M}\right) + \frac{1}{J}\left(\gamma(\overline{\lambda}_{\mathrm{a}})\mathbf{M} + \beta\overline{\mathbf{B}}\right)^{D}\end{aligned} \tag{3.54}$$

with

$$\gamma(\overline{\lambda}_{\mathrm{a}}) := \alpha(\overline{\lambda}_{\mathrm{a}}^{\,3} - \overline{\lambda}_{\mathrm{a}}^{\,-1}) + \beta(1 - \overline{\lambda}_{\mathrm{a}}^{\,2}).$$

The differentiation of the second Piola-Kirchhoff stress tensor given in Eq.(3.48) with respect to the right Cauchy-Green tensor $\mathbf{C}$ gives the tangent operator (or the elasticity tensor)[1]

$$\tilde{\mathcal{C}} := 2\frac{\mathrm{d}\tilde{\mathbf{T}}}{\mathrm{d}\mathbf{C}} = 4\frac{\partial^2\psi(\mathbf{C},\mathbf{M}_0)}{\partial\mathbf{C}\partial\mathbf{C}}, \tag{3.55}$$

which is a symmetric fourth-order tensor representing a measure of stress changes due to change in deformation.

3.3. Analytical Investigation of the Model

The constitutive model (3.52) is investigated by means of simple analytical examples that can be applied for material parameter identification and verification of finite element implementations. To this end, two analytical examples are considered, namely, uniaxial tension/compression and simple shear both along and transverse to the fiber direction, as well as hydrostatic compression.

[1]The tangent operator is required to perform finite elements computations, and is provided in Appendix A.5.

3.3.1. Uniaxial Tension/Compression

In this example, the unixial tension/compression problem of transversely isotropic solid is considered, assuming two loading cases: uniaxial tension along and transverse to the fiber direction. Accordingly, the deformation gradient tensor $\mathbf{F}$ takes the form

$$\mathbf{F} = \begin{bmatrix} \lambda_1 & 0 & 0 \\ 0 & \lambda_2 & 0 \\ 0 & 0 & \lambda_3 \end{bmatrix} \boldsymbol{e}_i \otimes \boldsymbol{E}_j, \qquad i,j = 1,2,3, \tag{3.56}$$

where it is assumed that $\boldsymbol{e}_1$ is the load axis and the stretch λ_1 is prescribed. The Cauchy-Green tensor $\mathbf{B}$ reads

$$\mathbf{B} = \begin{bmatrix} \lambda_1^2 & 0 & 0 \\ 0 & \lambda_2^2 & 0 \\ 0 & 0 & \lambda_3^2 \end{bmatrix} \boldsymbol{e}_i \otimes \boldsymbol{e}_j, \qquad i,j = 1,2,3. \tag{3.57}$$

Eq.(3.50) follows the unimodular right Cauchy-Green tensor

$$\overline{\mathbf{B}} = \frac{1}{J^{2/3}} \begin{bmatrix} \lambda_1^2 & 0 & 0 \\ 0 & \lambda_2^2 & 0 \\ 0 & 0 & \lambda_3^2 \end{bmatrix} \boldsymbol{e}_i \otimes \boldsymbol{e}_j, \quad \Longrightarrow \quad \bar{\lambda}_i = \frac{\lambda_i}{J^{1/3}}, \quad i,j = 1,2,3, \tag{3.58}$$

leading to

$$\mathbf{B}_{\mathrm{r}} = \begin{bmatrix} 1 & 0 & 0 \\ 0 & \bar{\lambda}_2^2 & 0 \\ 0 & 0 & \bar{\lambda}_3^2 \end{bmatrix} \boldsymbol{e}_i \otimes \boldsymbol{e}_j, \tag{3.59}$$

see Eq.(3.51), where

$$J = \det \mathbf{F} = \lambda_1 \lambda_2 \lambda_3. \tag{3.60}$$

Moreover, the components of the Cauchy stress tensor $\mathbf{T}$ are zero - except for the axial stress σ_{11}, i.e. $\mathbf{T} = \sigma_{11} \boldsymbol{e}_1 \otimes \boldsymbol{e}_1$. As there are three unknowns in this case (σ_{11}, λ_2 and λ_3), three equations are required.

3.3.1.1. Uniaxial tension along the fiber direction

In the first case the loading direction is assumed to be parallel to the fiber direction, $\boldsymbol{m}_0 = \boldsymbol{e}_1$, see Fig. 3.3(a). Thus, the stretch λ_1 in the deformation gradient tensor (3.56) represents the stretch in the fiber direction, which is prescribed. From the constitutive model (3.52) the three components of Cauchy stress tensor $\mathbf{T}$ read

$$\sigma_{11} = \frac{1}{J} \left(2\mathrm{I}_4 \frac{\partial \psi^{\mathrm{vol}}(J, \mathrm{I}_4)}{\partial \mathrm{I}_4} + J \frac{\partial \psi^{\mathrm{vol}}(J, \mathrm{I}_4)}{\partial J} \frac{2\bar{\lambda}_1}{3} v'(\bar{\lambda}_1) + \frac{2}{3} w'(\hat{\mathrm{I}}_{\mathbf{C}_{\mathrm{r}}})(2 - \bar{\lambda}_2^2 - \bar{\lambda}_3^2) \right) \tag{3.61a}$$

$$0 = \sigma_{22} = \frac{1}{J} \left(J \frac{\partial \psi^{\mathrm{vol}}(J, \mathrm{I}_4)}{\partial J} - \frac{\bar{\lambda}_1}{3} v'(\bar{\lambda}_1) + \frac{2}{3} w'(\hat{\mathrm{I}}_{\mathbf{C}_{\mathrm{r}}})(1 - 2\bar{\lambda}_2^2 - \bar{\lambda}_3^2) \right) \tag{3.61b}$$

$$0 = \sigma_{33} = \frac{1}{J} \left(J \frac{\partial \psi^{\mathrm{vol}}(J, \mathrm{I}_4)}{\partial J} \right) - \frac{\bar{\lambda}_1}{3} v'(\bar{\lambda}_1) + \frac{2}{3} w'(\hat{\mathrm{I}}_{\mathbf{C}_{\mathrm{r}}})(1 - \bar{\lambda}_2^2 - 2\bar{\lambda}_3^2). \tag{3.61c}$$

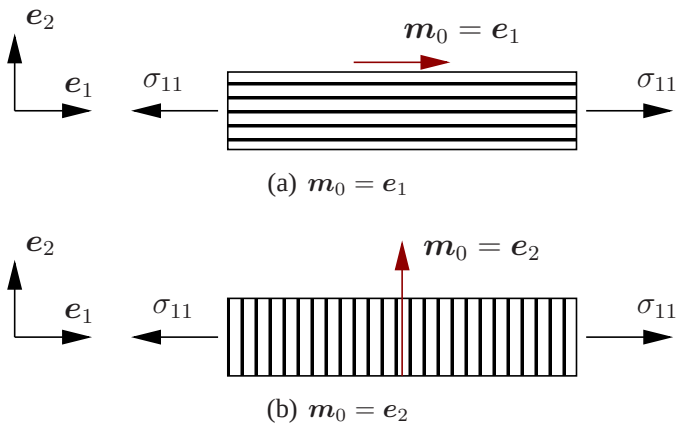

Figure 3.3.: Assumed orientations in uniaxial tensile problems.

Combining Eqs.(3.61b) and (3.61c), gives

$$\lambda_2 = \lambda_3 \tag{3.62a}$$

$$J\frac{\partial \psi^{\text{vol}}(J, \mathrm{I}_4)}{\partial J} = \frac{1}{3}\bar{\lambda}_1\, v'(\bar{\lambda}_1) - \frac{2}{3}w'(\hat{\mathrm{I}}_{\mathbf{C}_\mathrm{r}})(-1 - \bar{\lambda}_3^2 + 2\bar{\lambda}_3^2 1), \tag{3.62b}$$

and by substituting the above equation in (3.61a) the axial stress σ_{11} can be written as

$$\sigma_{11} = \frac{1}{J}\left(\bar{\lambda}_1\, v'(\bar{\lambda}_1) + 2w'(\hat{\mathrm{I}}_{\mathbf{C}_\mathrm{r}})(1 - \bar{\lambda}_2^2) + 2\mathrm{I}_4\frac{\partial \psi^{\text{vol}}(J, \mathrm{I}_4)}{\partial \mathrm{I}_4}\right). \tag{3.63}$$

Furthermore, making use of the derivatives of the strain-energy function in (3.53), we obtain

$$\sigma_{11} = \frac{1}{J}\left(\alpha(\bar{\lambda}_1^3 - \bar{\lambda}_1^{-1}) + \beta(1 - \bar{\lambda}_2^2) - \frac{K}{50\lambda_1}(J^5 + J^{-5} - 2)\right). \tag{3.64}$$

In this case $J = \lambda_1\lambda_2^2$ holds and $\mathrm{I}_4 = \lambda_1^2$ is inserted. For a given axial stretch λ_1, Eqs.(3.63) and (3.62b) represent two equations with two unknown, namely σ_{11} and λ_2.

3.3.1.2. Uniaxial tension normal to the fiber direction

In the next case the fiber direction is aligned to the x_2-axis, $\boldsymbol{m}_0 = \boldsymbol{e}_2$, and the axial stretch is applied normal to the fiber direction, see Fig. 3.3(b). Thus, in the deformation gradient (3.56) λ_1 is known, while λ_2 represents the stretch in the fiber direction and λ_3 is the stretch normal to the loading and fiber directions.

Again, the components of the Cauchy stress tensor can be calculated from the constitutive equation (3.52)

$$\sigma_{11} = \frac{1}{J}\left(J\frac{\partial \psi^{\text{vol}}(J,\mathrm{I}_4)}{\partial J} - \frac{\bar{\lambda}_2}{3}v'(\bar{\lambda}_2) + \frac{2}{3}w'(\hat{\mathrm{I}}_{\mathbf{C}_\mathrm{r}})(2\bar{\lambda}_1^2 - 1 - \bar{\lambda}_3^2)\right) \tag{3.65a}$$

$$0 = \sigma_{22} = \frac{1}{J}\left(\frac{2\bar{\lambda}_2}{3}v'(\bar{\lambda}_2) + \frac{2}{3}w'(\hat{\mathrm{I}}_{\mathbf{C}_\mathrm{r}})(-\bar{\lambda}_1^2 + 2 - \bar{\lambda}_3^2) + 2\mathrm{I}_4\frac{\partial \psi^{\text{vol}}}{\partial \mathrm{I}_4} + J\frac{\partial \psi^{\text{vol}}}{\partial J}\right) \tag{3.65b}$$

$$0 = \sigma_{33} = \frac{1}{J}\left(J\frac{\partial \psi^{\text{vol}}}{\partial J} - \frac{\bar{\lambda}_2}{3}v'(\bar{\lambda}_2) + \frac{2}{3}w'(\hat{\mathrm{I}}_{\mathbf{C}_\mathrm{r}})(-\bar{\lambda}_1^2 - 1 - 2\bar{\lambda}_3^2)\right), \tag{3.65c}$$

representing the three equations required to determine the three unknowns σ_{11}, λ_2 and λ_3. In this context $J = \lambda_1\lambda_2\lambda_3$ holds.

3.3.1.3. Identification of material parameters

In the following, the experimental data provided by (Ciarletta et al., 2011) are used to identify the material parameters K, α and β included in the constitutive model. In their work, (Ciarletta et al., 2011) carried out uniaxial tensile tests on a fiber-reinforced composite, made of soft silicone rubber as a matrix material reinforced with polyamide fibers, along and transverse to the fiber direction. For both cases, the engineering axial stresses P_{11} and the lateral stretches λ_2 are measured, see Fig. 3.4. Thus, four diagrams, i.e. $P_{11} - \lambda_1$ and $\lambda_2 - \lambda_1$ for each loading case, are obtained as shown in Figs. 3.4(a)-3.4(d), where P_{11} is the axial component of the 1st Piola-Kirchhoff stress tensor $\mathbf{T}_\mathrm{R} = J\mathbf{T}\mathbf{F}^{-\mathrm{T}} = P_{ij}\boldsymbol{e}_i \otimes \boldsymbol{e}_j$, see Eq.(2.34), λ_1 is the prescribed axial stretch and λ_2 is the stretch transverse to the loading direction. The material parameter identification process is carried out using a procedure developed by (Krämer et al., 2013), who proposed an iterative procedure to determine the material parameters used in stress algorithms of finite element programs. The stress algorithm developed for the three-dimensional finite element computations can be used directly to identify the material parameters K, α and β. The identification process is carried out with all of the experimental data in Fig. 3.4 together, i.e. with the tensile data where the loading direction is parallel and normal to the fiber direction. The identified material parameters are given in Tab. 3.1. As shown in Figs. 3.4(a)-3.4(d), the predictions of the model show sufficient fitting accuracy to the experimental data. However the predicted λ_2/λ_1-diagram for the case of $\boldsymbol{m}_0 = \boldsymbol{e}_2$, Fig. 3.4(d), could be improved by using a non-linear ansatz for the strain-energy function $w(\hat{\mathrm{I}}_{\mathbf{C}_\mathrm{r}})$, where a linear ansatz is used as first approach, see Eq.(3.44).

Table 3.1.: Identified material parameters.

K (MPa)	α (MPa)	β (MPa)
3.00	0.087	0.054

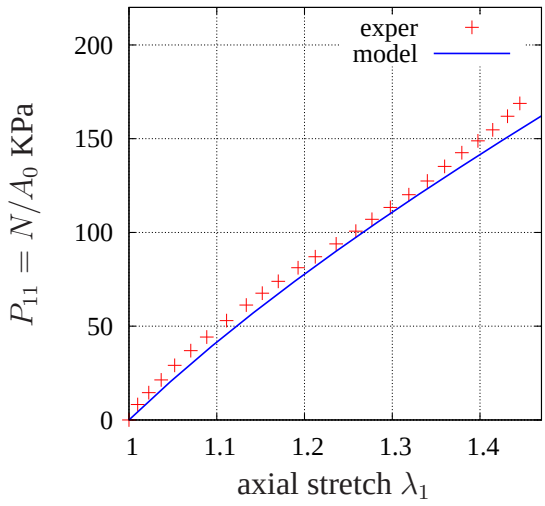

(a) Stress-stretch diagram ($\boldsymbol{m}_0 = \boldsymbol{e}_1$) used for identification

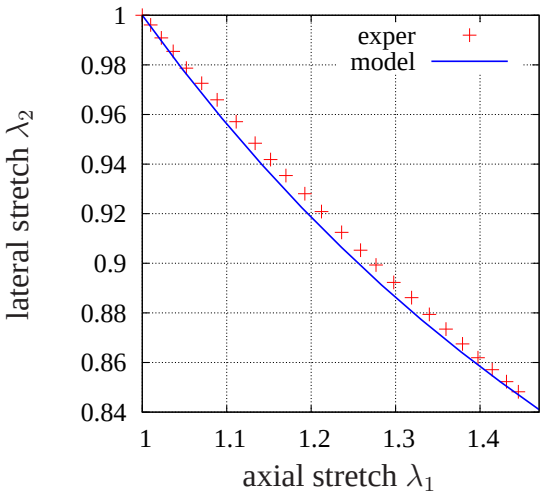

(b) λ_2/λ_1 diagram ($\boldsymbol{m}_0 = \boldsymbol{e}_1$) used for identification

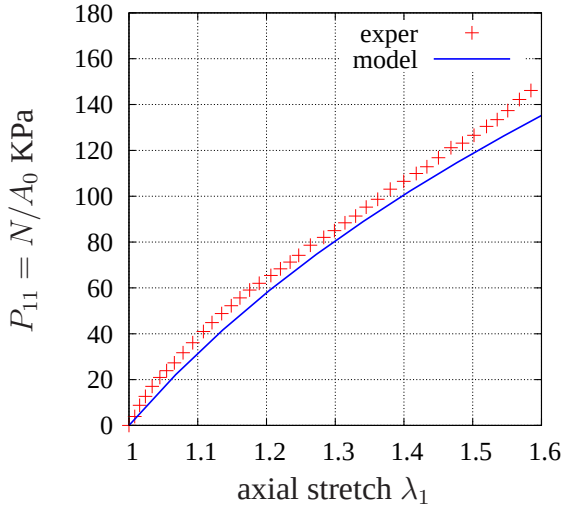

(c) Stress-stretch diagram ($\boldsymbol{m}_0 = \boldsymbol{e}_2$) used for prediction

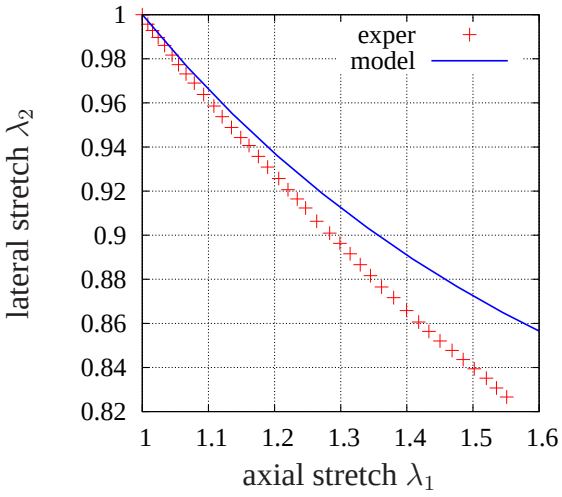

(d) λ_2/λ_1 diagram ($\boldsymbol{m}_0 = \boldsymbol{e}_2$) used for prediction

Figure 3.4.: Identified and predicted results in uniaxial tensile problems using experimental data in (Ciarletta et al., 2011).

3.3.2. Simple Shear

In the case of simple shear, the deformation gradient $\mathbf{F}$ and the left Cauchy-Green tensor $\mathbf{B}$ take the form

$$\mathbf{F} = \begin{bmatrix} 1 & \kappa & 0 \\ 0 & 1 & 0 \\ 0 & 0 & 1 \end{bmatrix} \boldsymbol{e}_i \otimes \boldsymbol{E}_j, \qquad i,j = 1,2,3, \tag{3.66}$$

and

$$\mathbf{B} = \mathbf{F}\mathbf{F}^{\mathrm{T}} = \begin{bmatrix} 1+\kappa^2 & \kappa & 0 \\ \kappa & 1 & 0 \\ 0 & 0 & 1 \end{bmatrix} \boldsymbol{e_i} \otimes \boldsymbol{e_j}, \qquad i,j = 1,2,3, \tag{3.67}$$

respectively, where $J = \det \mathbf{F} = 1$ holds. The consideration of this example is of interest, due to the existence of constitutive models showing non-physical behavior under simple shear, see (Hartmann, 2010). Fig. 3.5 shows the geometry and deformation of two loading cases. In the first case, the fiber is aligned with the x-axis, $\boldsymbol{m}_0 = \boldsymbol{e}_1$, see Fig. 3.5(a), for which the Cauchy stress tensor $\mathbf{T}$ (3.52) is reduced to

$$\mathbf{T} = \beta \mathbf{B}^D, \tag{3.68}$$

and, accordingly, its components read

$$\begin{aligned} \sigma_{xy} &= \beta\kappa \\ \sigma_{xx} &= \frac{2}{3}\beta\kappa^2 \\ \sigma_{yy} &= \sigma_{zz} = -\tfrac{1}{3}\beta\kappa^2. \end{aligned} \tag{3.69}$$

In this case, $\overline{\lambda}_{\mathrm{a}} = 1$ can obviously be calculated.

For the following second case, where the fiber is aligned with y-axis, $\boldsymbol{m}_0 = \boldsymbol{e}_2$, as shown in Fig. 3.5(b), the Cauchy stress tensor $\mathbf{T}$ (3.52) takes the form

$$\mathbf{T} = \left(\alpha((1+\kappa^2)^{3/2} - (1+\kappa^2)^{-1/2}) - \beta\kappa^2\right)\mathbf{M}^D + \beta\mathbf{B}^D, \tag{3.70}$$

which yields the components

$$\begin{aligned} \sigma_{xy} &= \alpha\left(-\frac{\kappa}{\sqrt{(1+\kappa^2)^3}} + \kappa(1+\kappa^2)^{1/2}\right) + \beta\frac{\kappa}{1+\kappa^2} \\ \sigma_{xx} &= \alpha\left(-\frac{\kappa^2}{\sqrt{(1+\kappa^2)^3}} + \kappa^2(1+\kappa^2)^{1/2} - \tfrac{1}{3}(1+\kappa^2)^{3/2} - \frac{1}{3\sqrt{1+\kappa^2}}\right) + \beta\frac{\kappa^2}{1+\kappa^2} \\ \sigma_{yy} &= \alpha\left(-\frac{1}{\sqrt{(1+\kappa^2)^3}} + \frac{1}{3\sqrt{1+\kappa^2}} + (1+\kappa^2)^{1/2} - \tfrac{1}{3}(1+\kappa^2)^{3/2}\right) + \beta\left(\frac{1}{1+\kappa^2} - 1\right) \\ \sigma_{zz} &= -\tfrac{1}{3}\alpha\left(-\frac{1}{\sqrt{1+\kappa^2}} + (1+\kappa^2)^{3/2}\right). \end{aligned} \tag{3.71}$$

Furthermore, $\overline{\lambda}_{\mathrm{a}} = \sqrt{1+\kappa^2}$ holds for this loading case.

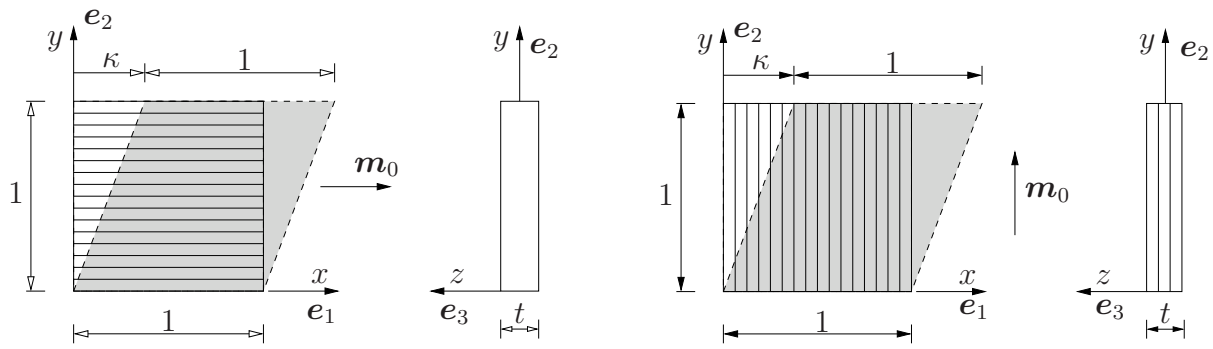

(a) $\boldsymbol{m}_0 = \boldsymbol{e}_1$ (b) $\boldsymbol{m}_0 = \boldsymbol{e}_2$

Figure 3.5.: Assumed orientations in simple shear problem.

3.3.3. Hydrostatic Tension/Compression

In the following, the behavior of the ansatz (3.46) under hydrostatic compression is demonstrated. Thus, the deformation gradient tensor $\mathbf{F}$ takes the form

$$\mathbf{F} = \begin{bmatrix} \lambda & 0 & 0 \\ 0 & \lambda & 0 \\ 0 & 0 & \lambda \end{bmatrix} = \lambda \mathbf{1}, \tag{3.72}$$

which leads to

$$J = \lambda^3 \quad \text{and} \quad \overline{\lambda}_k = \lambda_k J^{-1/3} = 1, \quad k = 1, 2, 3.$$

The left, respectively, unimoduar left Cauchy-Green tensors read

$$\mathbf{B} = \mathbf{F}\,\mathbf{F}^{\mathrm{T}} = \lambda^2\,\mathbf{1} \quad \text{and} \quad \overline{\mathbf{B}} = J^{-2/3}\,\mathbf{B} = \mathbf{1}.$$

In this case, the three components of the Cauchy stress tensor (3.52) read

$$\sigma_{11} = \frac{1}{J}\left(2\mathrm{I}_4 \frac{\partial \psi^{\mathrm{vol}}(J, \mathrm{I}_4)}{\partial \mathrm{I}_4} + J \frac{\partial \psi^{\mathrm{vol}}(J, \mathrm{I}_4)}{\partial J}\right) \tag{3.73a}$$

$$\sigma_{22} = \sigma_{33} = \frac{\partial \psi^{\mathrm{vol}}(J, \mathrm{I}_4)}{\partial J}. \tag{3.73b}$$

This shows that the stress response in the fiber direction is different to the response in the lateral directions, which reflects the behavior of transversely isotropic materials. Using the derivative of ψ^{vol} in Eqs.(3.53a) and (3.53b), the specific expressions of these components can be written as

$$\sigma_{11} = \frac{K}{25\lambda J}(2J^5 - 3J^{-5} + 1) \tag{3.74}$$

$$\sigma_{22} = \sigma_{33} = \frac{K}{10\lambda}(J^4 - J^{-6}), \tag{3.75}$$

which indicates that the material parameter K can be interpreted as the stiffness of volumetric deformation, or in other words, the bulk modulus. As the simplest ansatz is used for Eq.(3.46), this stiffness is identical for all directions. Of course, more general approaches are also possible.

3.4. The Proposed Modeling versus Classical Modeling

As demonstrated at the beginning of this chapter, based on the idea of *volumetric*/*isochoric* split, the classical modeling of the strain-energy function for transversal isotropy is defined by the additively decomposed strain-energy function given in (3.9), i.e.

$$\psi(\mathbf{C},\mathbf{M}_0) = U(J) + \overline{\psi}^{\,\mathrm{t}}(\bar{\mathrm{I}}_4,\bar{\mathrm{I}}_5) + \overline{\psi}^{\,\mathrm{i}}(\mathrm{I}_{\overline{\mathbf{C}}},\mathrm{II}_{\overline{\mathbf{C}}}).$$

In order to simplify the problem, it is common to assume the reduced form of the strain-energy function

$$\psi(\mathbf{C},\mathbf{M}_0) = U(J) + \overline{\psi}^{\,\mathrm{t}}(\bar{\mathrm{I}}_4) + \overline{\psi}^{\,\mathrm{i}}(\mathrm{I}_{\overline{\mathbf{C}}}), \tag{3.76}$$

which leads to constitutive relations for second Piola-Kirchhoff and Cauchy stress tensors to take the forms

$$\tilde{\mathbf{T}} = \tilde{\mathbf{T}}_{\text{vol}} + \tilde{\mathbf{T}}_{\text{isc}} = J\frac{\mathrm{d}U(J)}{\mathrm{d}J}\mathbf{C}^{-1} + 2J^{-2/3}\left(\mathcal{I} - \tfrac{1}{3}\mathbf{C}^{-1}\otimes\mathbf{C}\right)\left(\frac{\mathrm{d}\overline{\psi}^{\,\mathrm{t}}(\bar{\mathrm{I}}_4)}{\mathrm{d}\bar{\mathrm{I}}_4}\mathbf{M}_0 + \frac{\mathrm{d}\overline{\psi}^{\,\mathrm{i}}(\mathrm{I}_{\overline{\mathbf{C}}})}{\mathrm{d}\mathrm{I}_{\overline{\mathbf{C}}}}\mathbf{1}\right) \tag{3.77}$$

and

$$\mathbf{T} = \mathbf{T}_{\text{vol}} + \mathbf{T}_{\text{isc}} = \frac{\mathrm{d}U(J)}{\mathrm{d}J}\mathbf{1} + \frac{2}{J}\left(\bar{\mathrm{I}}_4\frac{\mathrm{d}\overline{\psi}^{\,\mathrm{t}}(\bar{\mathrm{I}}_4)}{\mathrm{d}\bar{\mathrm{I}}_4}\mathbf{M} + \frac{\mathrm{d}\overline{\psi}^{\,\mathrm{i}}(\mathrm{I}_{\overline{\mathbf{C}}})}{\mathrm{d}\mathrm{I}_{\overline{\mathbf{C}}}}\overline{\mathbf{B}}\right)^{\mathrm{D}}, \tag{3.78}$$

respectively, where $\mathcal{I}$ is a fourth-order identity tensor, see e.g. the model proposed in (Holzapfel et al., 2000) for materials with one fiber family. Alternatively, the first term in the parenthesis in (3.78) can be reformulated in terms of the isochoric stretch $\overline{\lambda}_{\mathrm{a}}$

$$\bar{\mathrm{I}}_4\frac{\mathrm{d}\overline{\psi}^{\,\mathrm{t}}(\bar{\mathrm{I}}_4)}{\mathrm{d}\bar{\mathrm{I}}_4} = \overline{\lambda}_{\mathrm{a}}^2\frac{\mathrm{d}\overline{\psi}^{\,\mathrm{t}}(\overline{\lambda}_{\mathrm{a}})}{\mathrm{d}\overline{\lambda}_{\mathrm{a}}}\frac{\mathrm{d}\overline{\lambda}_{\mathrm{a}}}{\mathrm{d}\bar{\mathrm{I}}_4} = \tfrac{1}{2}\overline{\lambda}_{\mathrm{a}}\frac{\mathrm{d}\overline{\psi}^{\,\mathrm{t}}(\overline{\lambda}_{\mathrm{a}})}{\mathrm{d}\overline{\lambda}_{\mathrm{a}}}. \tag{3.79}$$

Thus, the constitutive model in (3.78) can be rewritten to

$$\mathbf{T} = \mathbf{T}_{\text{vol}} + \mathbf{T}_{\text{isc}} = \frac{\mathrm{d}U(J)}{\mathrm{d}J}\mathbf{1} + \frac{1}{J}\left(\overline{\lambda}_{\mathrm{a}}\frac{\mathrm{d}\overline{\psi}^{\,\mathrm{t}}(\overline{\lambda}_{\mathrm{a}})}{\mathrm{d}\overline{\lambda}_{\mathrm{a}}}\mathbf{M} + 2\frac{\mathrm{d}\overline{\psi}^{\,\mathrm{i}}(\mathrm{I}_{\overline{\mathbf{C}}})}{\mathrm{d}\mathrm{I}_{\overline{\mathbf{C}}}}\overline{\mathbf{B}}\right)^{\mathrm{D}}. \tag{3.80}$$

If this constitutive model is now investigated for the example of uniaxial tension, in which the load is applied along the fiber direction, i.e. applying the same procedure given in section 3.3.1.1, the stress components read

$$\begin{aligned}
\sigma_{11} &= \frac{\mathrm{d}U(J)}{\mathrm{d}J} + \frac{1}{3J}\left(2\bar{\lambda}_1\frac{\mathrm{d}\overline{\psi}^{\,\mathrm{t}}(\overline{\lambda}_{\mathrm{a}})}{\mathrm{d}\overline{\lambda}_{\mathrm{a}}} + 2\frac{\mathrm{d}\overline{\psi}^{\,\mathrm{i}}(\mathrm{I}_{\overline{\mathbf{C}}})}{\mathrm{d}\mathrm{I}_{\overline{\mathbf{C}}}}(2\bar{\lambda}_1^2 - \bar{\lambda}_2^2 - \bar{\lambda}_3^2)\right)\\
\sigma_{22} &= \frac{\mathrm{d}U(J)}{\mathrm{d}J} + \frac{1}{3J}\left(-\bar{\lambda}_1\frac{\mathrm{d}\overline{\psi}^{\,\mathrm{t}}(\overline{\lambda}_{\mathrm{a}})}{\mathrm{d}\overline{\lambda}_{\mathrm{a}}} + 2\frac{\mathrm{d}\overline{\psi}^{\,\mathrm{i}}(\mathrm{I}_{\overline{\mathbf{C}}})}{\mathrm{d}\mathrm{I}_{\overline{\mathbf{C}}}}(-\bar{\lambda}_1^2 + 2\bar{\lambda}_2^2 - \bar{\lambda}_3^2)\right)\\
\sigma_{33} &= \frac{\mathrm{d}U(J)}{\mathrm{d}J} + \frac{1}{3J}\left(-\bar{\lambda}_1\frac{\mathrm{d}\overline{\psi}^{\,\mathrm{t}}(\overline{\lambda}_{\mathrm{a}})}{\mathrm{d}\overline{\lambda}_{\mathrm{a}}} + 2\frac{\mathrm{d}\overline{\psi}^{\,\mathrm{i}}(\mathrm{I}_{\overline{\mathbf{C}}})}{\mathrm{d}\mathrm{I}_{\overline{\mathbf{C}}}}(-\bar{\lambda}_1^2 - \bar{\lambda}_2^2 + 2\bar{\lambda}_3^2)\right).
\end{aligned} \tag{3.81}$$

By comparing the stress components in (3.81) with the stress components given in (3.61) as a result of the proposed model, some features can be characterized. Firstly, the split of the isochoric deformation in the fiber direction from the deformation in other directions leads to a clear split of the isochoric stress-state, where, in contrast to stresses in (3.81), the isochoric stretch in the fiber direction $\bar{\lambda}_1$ is associated only with the contribution arising from the anisotropic part of the strain-energy function, while it appears also in the isotropic contribution in (3.81). Secondly, the volumetric stresses in (3.81) are the same in all three stress components, which is unrealistic for transverely isotropic materials, in which the response along the preferred direction differs from the response in all other directions. Also, this drawback can easily be observed when investigating the model in (3.80) under hydrostatic deformation. Here, the deformation gradient takes the form of (3.72), with $J = \lambda^3$, leading to

$$\overline{\mathbf{B}} = J^{-2/3}\,\mathbf{B} = \mathbf{1} \quad \text{and} \quad \overline{\lambda}_{\mathrm{a}} = J^{-1/3}\lambda = 1.$$

In this case, the stress-state given in (3.80) therefore takes the form

$$\mathbf{T} = \mathbf{T}_{\mathrm{vol}} = \frac{\mathrm{d}U(J)}{\mathrm{d}J}\mathbf{1}, \tag{3.82}$$

where

$$\frac{\mathrm{d}\overline{\psi}^{\,\mathrm{t}}(\overline{\lambda}_{\mathrm{a}})}{\mathrm{d}\overline{\lambda}_{\mathrm{a}}}\Big|_{\overline{\lambda}_{\mathrm{a}}=1} = 0$$

is inserted due to the condition of stress-free reference configuration and $\overline{\mathbf{B}}^{\mathrm{D}} = \mathbf{1}^{\mathrm{D}} = \mathbf{0}$. This means that the stress components are the same in all directions. The proposed model takes this effect into consideration, where different volumetric and hydrostatic stresses are obtained along and normal to the preferred direction, see Eqs.(3.61) and (3.73).

4. Temperature-Dependent Transversal Isotropy

In many applications anisotropic materials work at different temperatures above or below the room temperature and are also subjected to thermo-mechanical finite deformations. To this end, it is of interest to model the behavior of anisotropic materials under these conditions, especially when the behavior is strongly affected by changes in temperature, as in the case of fiber reinforced polymers.

In this chapter, a constitutive model for transversely isotropic solids subjected to thermo-mechanical finite deformations is formulated. The formulation is based on the theory of multiplicative decomposition of the deformation gradient tensor into a thermal and a mechanical part. This theory as well as the formulation of the strain-energy function are presented in Sec. 4.1. The thermodynamics consistency of the model is investigated in Sec. 4.2. The derivation of constitutive equations for the stress-state is treated in Sec. 4.3, which is then investigated analytically in Sec. 4.4. In Sec. 4.5 the constitutive equations for the anisotropic heat flux are derived, and finally, the energy equation is formulated in Sec. 4.6.

4.1. Multiplicative Decomposition of Deformation Gradient

The idea of decomposing the total deformation in the case of thermoelasticity into a thermal and an elastic part was first proposed by (Stojanovic et al., 1964) and (Stojanovic, 1969), and later applied by many authors in order to investigate the behavior of isotropic materials, see e.g. (Lu and Pister, 1975), (Lion, 2000), (Vujosevic and Lubarda, 2002), (Lubarda, 2004), (Heimes, 2005), (Hamkar and Hartmann, 2012), (Darijani and Naghdabadi, 2013) and (Yosibash et al., 2014) among others. The literature offers no work that addresses the application of this approach to the general case of anisotropy. This work is based on the idea of formulating a constitutive model for the case of transversely isotropic materials under thermo-mechanical finite deformations. To this end, the development of the constitutive model starts with the multiplicative decomposition of the deformation gradient $\mathbf{F}$ into a thermal part $\mathbf{F}_\Theta$ and a mechanical part $\mathbf{F}_\mathrm{M}$

$$\mathbf{F} = \mathbf{F}_\mathrm{M}\mathbf{F}_\Theta, \tag{4.1}$$

i.e. an intermediate configuration $\hat{\mathcal{B}}$, defined by a fictitious isothermal mechanical unloading, is introduced in addition to the reference and current configurations $\boldsymbol{\mathcal{R}}$ and $\boldsymbol{\chi}_t$, respectively, see Fig. 4.1. Additionally, the mechanical part of the deformation gradient $\mathbf{F}_\mathrm{M}$ is splitted according

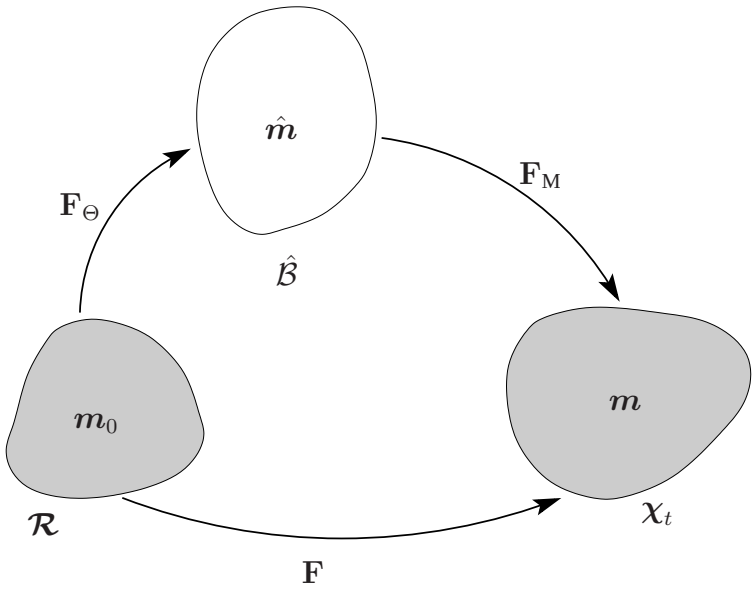

Figure 4.1.: Configurations of the decomposition $\mathbf{F} = \mathbf{F}_\mathrm{M}\mathbf{F}_\Theta$.

to the decomposition in (3.21)

$$\mathbf{F}_\mathrm{M} = \hat{\mathbf{F}}_\mathrm{M}\overline{\mathbf{F}}_\mathrm{M} = \hat{\mathbf{F}}_\mathrm{M}\mathbf{F}^r_\mathrm{M}\mathbf{F}^a_\mathrm{M}. \tag{4.2}$$

Thus, the total deformation gradient $\mathbf{F}$ is decomposed into

$$\mathbf{F} = \hat{\mathbf{F}}_\mathrm{M}\mathbf{F}^r_\mathrm{M}\mathbf{F}^a_\mathrm{M}\mathbf{F}_\Theta, \tag{4.3}$$

as depicted in Fig. 4.2.

Assuming that the fiber direction is represented by the unit vectors $\boldsymbol{m}_0$, $\hat{\boldsymbol{m}}$ and $\boldsymbol{m}$ in the three configurations $\mathcal{R}$, $\hat{\mathcal{B}}$ and $\boldsymbol{\chi}_t$, respectively, as shown in Fig. 4.1, the mapping of these unit vectors according to the decomposition (4.1) can be defined as

$$\mathbf{F}\boldsymbol{m}_0 = \lambda_\mathrm{a}\boldsymbol{m} \tag{4.4a}$$

$$\mathbf{F}_\Theta\boldsymbol{m}_0 = \zeta\hat{\boldsymbol{m}} \tag{4.4b}$$

$$\mathbf{F}_\mathrm{M}\hat{\boldsymbol{m}} = \lambda_\mathrm{M}\boldsymbol{m}, \tag{4.4c}$$

where λ_a, ζ and λ_M are the total, thermal and mechanical stretches of the bulk of transversely isotropic material along the preferred direction, respectively. Furthermore, Eq.(4.4a) can be rewritten in the form

$$\mathbf{F}\boldsymbol{m}_0 = \mathbf{F}_\mathrm{M}\mathbf{F}_\Theta\boldsymbol{m}_0 = \zeta\mathbf{F}_\mathrm{M}\hat{\boldsymbol{m}} = \zeta\lambda_\mathrm{M}\boldsymbol{m}, \tag{4.5}$$

yielding

$$\lambda_\mathrm{a} = \zeta\lambda_\mathrm{M} \tag{4.6a}$$

$$\lambda_\mathrm{M} = \frac{\lambda_\mathrm{a}}{\zeta}, \tag{4.6b}$$

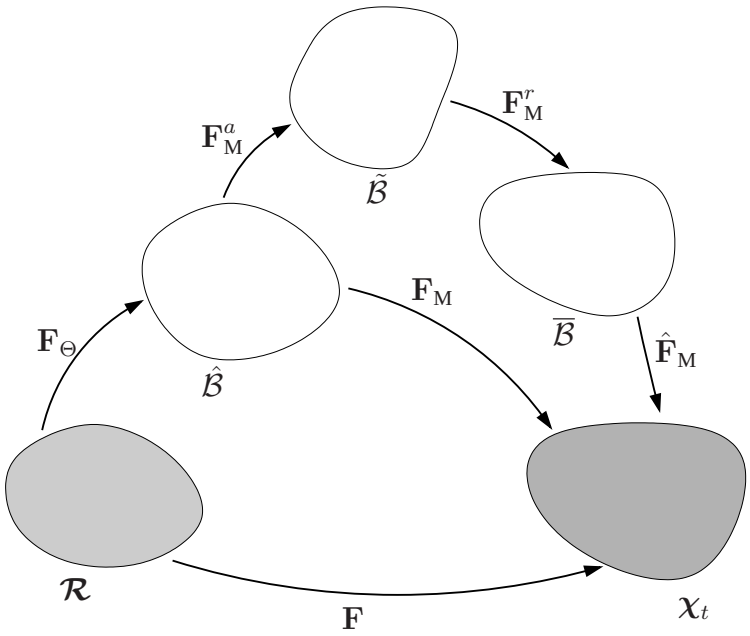

Figure 4.2.: Configurations of the proposed decomposition $\mathbf{F} = \hat{\mathbf{F}}_{\mathrm{M}}\mathbf{F}_{\mathrm{M}}^{r}\mathbf{F}_{\mathrm{M}}^{a}\mathbf{F}_{\Theta}$.

with λ_{a} defined analogously to (3.15)

$$\lambda_{\mathrm{a}} = \sqrt{\mathbf{C} \cdot \mathbf{M}_0}. \tag{4.7}$$

Consider a cube of transversely isotropic material subjected to thermal deformation as shown in Fig. 4.3, and let the preferred direction be aligned to the x_1-axis of the Cartesian coordinate system, i.e., $\boldsymbol{m}_0 = \boldsymbol{E}_1$. During the application of $\mathbf{F}_{\Theta}$ the cube undergoes a volumetric expansion in which the stretch in the directions x_2 and x_3 is equal, denoted by φ, but different from the stretch in the direction of isotropy, represented by ζ. Note that in Fig 4.3 the thermal expansion along the preferred direction is assumed to be larger than the thermal expansion in the other directions. Moreover, the coordinate system before and after the application of $\mathbf{F}_{\Theta}$ remain unchanged, so the unit vectors representing the fiber direction (direction of isotropy) in the reference configuration $\mathcal{R}$ and intermediate configuration $\hat{\mathcal{B}}$, see Fig. 4.1, are equal, i.e. $\boldsymbol{m}_0 = \hat{\boldsymbol{m}}$. Thus, the thermal part of the deformation gradient $\mathbf{F}_{\Theta}$ can be defined by

$$\begin{aligned}
\mathbf{F}_{\Theta} &= \zeta\, \boldsymbol{E}_1 \otimes \boldsymbol{E}_1 + \varphi\, \boldsymbol{E}_2 \otimes \boldsymbol{E}_2 + \varphi\, \boldsymbol{E}_3 \otimes \boldsymbol{E}_3 \\
&= (\zeta - \varphi)\, \underbrace{\boldsymbol{E}_1 \otimes \boldsymbol{E}_1}_{\boldsymbol{m}_0 \otimes \boldsymbol{m}_0} + \varphi\, \underbrace{(\boldsymbol{E}_1 \otimes \boldsymbol{E}_1 + \boldsymbol{E}_2 \otimes \boldsymbol{E}_2 + \boldsymbol{E}_3 \otimes \boldsymbol{E}_3)}_{\mathbf{1}} \\
&= (\zeta - \varphi)\boldsymbol{m}_0 \otimes \boldsymbol{m}_0 + \varphi\mathbf{1} \\
&= (\zeta - \varphi)\mathbf{M}_0 + \varphi\mathbf{1},
\end{aligned} \tag{4.8}$$

where $\mathbf{M}_0 = \boldsymbol{m}_0 \otimes \boldsymbol{m}_0$ is the structural tensor.[1] The thermal stretches ζ and φ are assumed as

[1] Such form of $\mathbf{F}_{\Theta}$ is also mentioned by (Vujosevic and Lubarda, 2002), however the work was restricted to the analysis of isotropic materials.

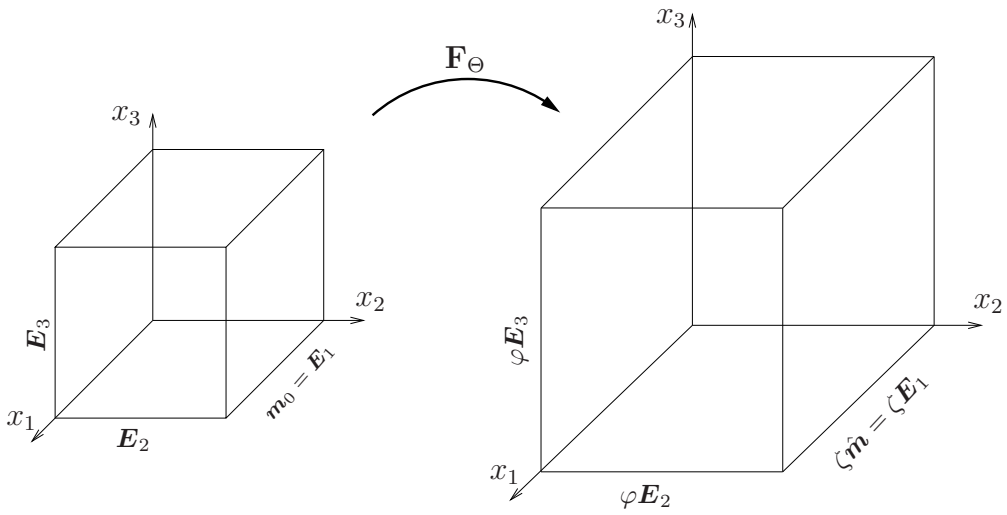

Figure 4.3.: A cube of transversely isotropic material subjected to thermal deformation (expansion). before (left) and after (right) the application of $\mathbf{F}_\Theta$.

linear functions of the temperature

$$\zeta = \hat{\zeta}(\Theta - \Theta_0) = \hat{\zeta}(\vartheta) = 1 + \alpha_a \vartheta, \tag{4.9a}$$
$$\varphi = \hat{\varphi}(\Theta - \Theta_0) = \hat{\varphi}(\vartheta) = 1 + \alpha_n \vartheta, \tag{4.9b}$$

where Θ and Θ_0 define the absolute and the reference temperatures while α_a and α_n represent the thermal expansion coefficients of the material along and normal to the preferred direction, respectively, and $\vartheta = \Theta - \Theta_0$ defines the temperature difference. Note that in the case of no temperature change, i.e., $\vartheta = 0$

$$\zeta = \hat{\zeta}(0) = 1 \tag{4.10a}$$
$$\varphi = \hat{\varphi}(0) = 1 \tag{4.10b}$$

hold.

The determinant of the thermal part of the deformation gradient $\mathbf{F}_\Theta$ represents the change in volume caused by the temperature change, and is given by

$$\begin{aligned} J_\Theta &:= \det \mathbf{F}_\Theta = \det\left((\zeta - \varphi)\mathbf{M}_0 + \varphi\mathbf{1}\right) \\ &= \det\left((\zeta - \varphi)\mathbf{M}_0\right) + \operatorname{cof}\left((\zeta - \varphi)\mathbf{M}_0\right) \cdot (\varphi\mathbf{1}) + (\zeta - \varphi)\mathbf{M}_0 \cdot \operatorname{cof}(\varphi\mathbf{1}) + \det(\varphi\mathbf{1}) \\ &= (\zeta - \varphi)^3 \det \mathbf{M}_0 + \varphi(\zeta - \varphi)^2 \operatorname{cof} \mathbf{M}_0 \cdot \mathbf{1} + \varphi^2(\zeta - \varphi)\mathbf{M}_0 \cdot \operatorname{cof} \mathbf{1} + \varphi^3 \det \mathbf{1} \\ &= \varphi^2(\zeta - \varphi) + \varphi^3 \\ &= \zeta\varphi^2. \end{aligned} \tag{4.11}$$

Drawing on the properties of $\mathbf{M}_0$ and $\mathbf{1}$ in Eqs.(2.120) and (3.32). According to the decomposition in Eq.(4.1), the determinant of the total deformation gradient $\mathbf{F}$ reads

$$J = \det \mathbf{F} = \det \mathbf{F}_{\mathrm{M}} \det \mathbf{F}_\Theta = J_{\mathrm{M}} J_\Theta, \tag{4.12}$$

leading to

$$J_{\mathrm{M}} = \frac{J}{J_\Theta} = \frac{J}{\zeta\varphi^2}, \tag{4.13}$$

where $J_{\mathrm{M}} := \det \mathbf{F}_{\mathrm{M}}$ is the determinant of the mechanical part of the deformation gradient.

Similar to the case of elastoplasticity, in which the deformation gradient is multiplicatively decomposed into an elastic and a plastic part, see (Haupt, 1985), the thermal Green strain tensor measuring the thermal deformations, is defined by a fictive isothermal mechanical unloading

$$\mathbf{E}_\Theta := \lim_{\|\mathbf{F}_{\mathrm{M}}\|\to 0} \mathbf{E} = \tfrac{1}{2}(\mathbf{F}_\Theta^{\mathrm{T}}\mathbf{F}_\Theta - \mathbf{I}) = \tfrac{1}{2}(\mathbf{C}_\Theta - \mathbf{I}), \tag{4.14}$$

where $\mathbf{E}$ is the total Green strain tensor defined in (2.29a) - additively decomposed into a thermal part $\mathbf{E}_\Theta$ and a mechanical part $\mathbf{E}_{\mathrm{M}}$ according to the concept of dual variables, see (Haupt and Tsakmakis, 1989),

$$\mathbf{E} = \mathbf{E}_\Theta + \mathbf{E}_{\mathrm{M}}. \tag{4.15}$$

Inserting the thermal right Cauchy-Green tensor

$$\begin{aligned}\mathbf{C}_\Theta = \mathbf{F}_\Theta^{\mathrm{T}}\mathbf{F}_\Theta &= \left((\zeta-\varphi)\mathbf{M}_0 + \varphi\mathbf{1}\right)^{\mathrm{T}}\left((\zeta-\varphi)\mathbf{M}_0 + \varphi\mathbf{1}\right)\\ &= (\zeta-\varphi)^2\mathbf{M}_0 + 2\varphi(\zeta-\varphi) + \varphi^2\mathbf{1}\\ &= (\zeta^2-\varphi^2)\mathbf{M}_0 + \varphi^2\mathbf{1}\end{aligned} \tag{4.16}$$

in (4.14) yields

$$\mathbf{E}_\Theta = \tfrac{1}{2}\left((\zeta^2-\varphi^2)\mathbf{M}_0 + (\varphi^2-1)\mathbf{1}\right). \tag{4.17}$$

Accordingly, the mechanical Green strain tensor reads

$$\begin{aligned}\mathbf{E}_{\mathrm{M}} = \mathbf{E} - \mathbf{E}_\Theta &= \tfrac{1}{2}(\mathbf{F}^{\mathrm{T}}\mathbf{F} - \mathbf{F}_\Theta^{\mathrm{T}}\mathbf{F}_\Theta) = \tfrac{1}{2}(\mathbf{C} - \mathbf{C}_\Theta)\\ &= \tfrac{1}{2}\left(\mathbf{C} - (\zeta^2-\varphi^2)\mathbf{M}_0 - \varphi^2\mathbf{1}.\right).\end{aligned} \tag{4.18}$$

The strain measures in the intermediate configuration $\hat{\mathcal{B}}$ are obtained by applying the push-forward operator to the strain measures in (4.15)

$$\mathbf{F}_\Theta^{-\mathrm{T}}\mathbf{E}\mathbf{F}_\Theta^{-1} = \mathbf{F}_\Theta^{-\mathrm{T}}(\mathbf{E}_\Theta + \mathbf{E}_{\mathrm{M}})\mathbf{F}_\Theta^{-1}, \tag{4.19}$$

yielding

$$\hat{\boldsymbol{\gamma}} = \hat{\boldsymbol{\gamma}}_\Theta + \hat{\boldsymbol{\gamma}}_{\mathrm{M}}. \tag{4.20}$$

Here, the strain tensors relative to the intermediate configuration are obtained:

$$\begin{aligned}\hat{\boldsymbol{\gamma}} = \mathbf{F}_\Theta^{-\mathrm{T}}\,\mathbf{E}\,\mathbf{F}_\Theta^{-1} &= \tfrac{1}{2}\mathbf{F}_\Theta^{-\mathrm{T}}(\mathbf{F}^{\mathrm{T}}\,\mathbf{F} - \mathbf{1})\mathbf{F}_\Theta^{-1} = \tfrac{1}{2}\mathbf{F}_\Theta^{-\mathrm{T}}\left((\mathbf{F}_{\mathrm{M}}\mathbf{F}_\Theta)^{\mathrm{T}}(\mathbf{F}_{\mathrm{M}}\mathbf{F}_\Theta) - \mathbf{1}\right)\mathbf{F}_\Theta^{-1}\\ &= \tfrac{1}{2}(\underbrace{\mathbf{F}_\Theta^{-\mathrm{T}}\,\mathbf{F}_\Theta^{\mathrm{T}}}_{\mathbf{1}}\,\underbrace{\mathbf{F}_{\mathrm{M}}^{\mathrm{T}}\,\mathbf{F}_{\mathrm{M}}}_{\mathbf{C}_{\mathrm{M}}}\,\underbrace{\mathbf{F}_\Theta\,\mathbf{F}_\Theta^{-1}}_{\mathbf{1}} - \underbrace{\mathbf{F}_\Theta^{-\mathrm{T}}\,\mathbf{1}\,\mathbf{F}_\Theta^{-1}}_{\mathbf{B}_\Theta^{-1}})\\ &= \tfrac{1}{2}(\mathbf{C}_{\mathrm{M}} - \mathbf{B}_\Theta^{-1}) = \tfrac{1}{2}\left(\mathbf{C}_{\mathrm{M}} - (\zeta^{-2}-\varphi^{-2})\mathbf{M}_0 + \varphi^{-2}\mathbf{1}\right),\end{aligned} \tag{4.21a}$$

$$\begin{aligned}\hat{\boldsymbol{\gamma}}_\Theta = \mathbf{F}_\Theta^{-\mathrm{T}}\,\mathbf{E}_\Theta\,\mathbf{F}_\Theta^{-1} &= \tfrac{1}{2}\mathbf{F}_\Theta^{-\mathrm{T}}(\mathbf{F}_\Theta^{\mathrm{T}}\,\mathbf{F}_\Theta - \mathbf{1})\mathbf{F}_\Theta^{-1} = \tfrac{1}{2}(\mathbf{I} - \mathbf{F}_\Theta^{-\mathrm{T}}\mathbf{F}_\Theta^{-1})\\ &= \tfrac{1}{2}(\mathbf{1} - \mathbf{B}_\Theta^{-1}) = \tfrac{1}{2}\left((1-\varphi^{-2})\mathbf{1} - (\zeta^{-2}-\varphi^{-2})\mathbf{M}_0\right),\end{aligned} \tag{4.21b}$$

and

$$\hat{\gamma}_{\mathrm{M}} = \mathbf{F}_{\Theta}^{-\mathrm{T}}\mathbf{E}_{\mathrm{M}}\mathbf{F}_{\Theta}^{-1} = \tfrac{1}{2}\mathbf{F}_{\Theta}^{-\mathrm{T}}(\mathbf{F}^{\mathrm{T}}\,\mathbf{F} - \mathbf{F}_{\Theta}^{\mathrm{T}}\,\mathbf{F}_{\Theta})\mathbf{F}_{\Theta}^{-1} = \tfrac{1}{2}(\mathbf{F}_{\mathrm{M}}^{\mathrm{T}}\mathbf{F}_{\mathrm{M}} - \mathbf{1})$$
$$= \tfrac{1}{2}(\mathbf{C}_{\mathrm{M}} - \mathbf{1}). \tag{4.21c}$$

These strain tensors represent the total, thermal and mechanical strain tensors in the intermediate configuration, respectively, with the mechanical right Cauchy-Green tensor

$$\mathbf{C}_{\mathrm{M}} = \mathbf{F}_{\mathrm{M}}^{\mathrm{T}}\mathbf{F}_{\mathrm{M}} \tag{4.22a}$$

and the thermal left Cauchy-Green tensor

$$\mathbf{B}_{\Theta} = \mathbf{F}_{\Theta}\mathbf{F}_{\Theta}^{\mathrm{T}} = (\zeta^2 - \varphi^2)\mathbf{M}_0 + \varphi^2\mathbf{1}. \tag{4.22b}$$

The inverse of $\mathbf{F}_{\Theta}$ required to calculate $\mathbf{B}_{\Theta}^{-1} = \mathbf{F}_{\Theta}^{-\mathrm{T}}\mathbf{F}_{\Theta}^{-1}$ used in (4.21a) and (4.21b) is calculated by applying the Cayley-Hamilton theory to the deformation gradient tensor $\mathbf{F}_{\Theta}$ in Eq.(4.8).[1] Fig. 4.4 summarizes the strain measures in the reference, intermediate and current configurations. The time derivatives of the strain tensors in Eqs.(4.14),(4.17) and (4.18) yield the total, thermal and mechanical strain-rate tensors in the reference configuration

$$\dot{\mathbf{E}} = \tfrac{1}{2}\dot{\mathbf{C}} = \dot{\mathbf{E}}_{\Theta} + \dot{\mathbf{E}}_{\mathrm{M}}, \tag{4.23a}$$
$$\dot{\mathbf{E}}_{\Theta} = \tfrac{1}{2}\dot{\mathbf{C}}_{\Theta} = \tfrac{1}{2}\left((2\zeta\dot{\zeta} - 2\varphi\dot{\varphi})\mathbf{M}_0 + 2\varphi\dot{\varphi}\mathbf{1}\right) = (\zeta\dot{\zeta} - \varphi\dot{\varphi})\mathbf{M}_0 + \varphi\dot{\varphi}\mathbf{1}$$
$$= ((\zeta\zeta' - \varphi\varphi')\mathbf{M}_0 + \varphi\varphi'\mathbf{1})\,\dot{\Theta}, \tag{4.23b}$$

and

$$\dot{\mathbf{E}}_{\mathrm{M}} = \tfrac{1}{2}(\dot{\mathbf{C}} - \dot{\mathbf{C}}_{\Theta}) = \tfrac{1}{2}\left(\dot{\mathbf{C}} - 2(\zeta\dot{\zeta} - \varphi\dot{\varphi})\mathbf{M}_0 - (2\varphi\dot{\varphi})\mathbf{1}\right)$$
$$= \tfrac{1}{2}\dot{\mathbf{C}} - ((\zeta\zeta' - \varphi\varphi')\mathbf{M}_0 - \varphi\varphi'\mathbf{1})\,\dot{\Theta}, \tag{4.23c}$$

respectively, where

$$\dot{\zeta} = \frac{\mathrm{d}\zeta}{\mathrm{d}t} = \frac{\mathrm{d}\zeta}{\mathrm{d}\Theta}\frac{\mathrm{d}\Theta}{\mathrm{d}t} = \zeta'\dot{\Theta} \tag{4.24a}$$

and

$$\dot{\varphi} = \frac{\mathrm{d}\varphi}{\mathrm{d}t} = \frac{\mathrm{d}\varphi}{\mathrm{d}\Theta}\frac{\mathrm{d}\Theta}{\mathrm{d}t} = \varphi'\dot{\Theta} \tag{4.24b}$$

[1] See Appendix A.6.

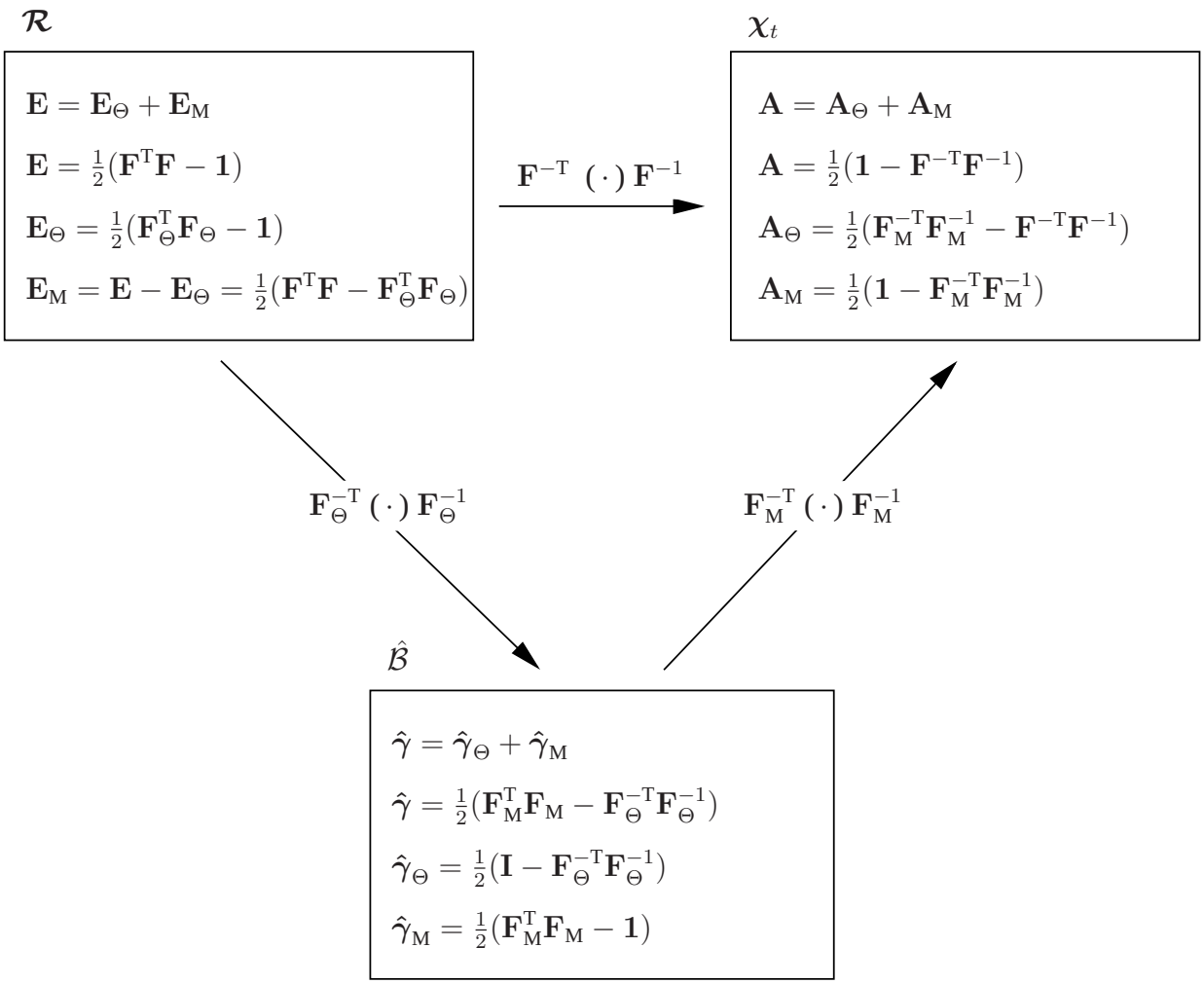

Figure 4.4.: Transformation of the strain measures.

are inserted to represent the time derivative of the thermal stretches. Moreover, the thermal spatial velocity gradient tensor $\mathbf{L}_\Theta$ can be formulated by

$$\begin{aligned}
\mathbf{L}_\Theta = \dot{\mathbf{F}}_\Theta \mathbf{F}_\Theta^{-1} &= \Big((\dot{\zeta} - \dot{\varphi})\mathbf{M}_0 + \dot{\varphi}\mathbf{1}\Big)\left((\zeta^{-1} - \varphi^{-1})\mathbf{M}_0 + \varphi^{-1}\mathbf{1}\right) \\
&= \Big((\dot{\zeta} - \dot{\varphi})(\zeta^{-1} - \varphi^{-1}) + \varphi^{-1}(\dot{\zeta} - \dot{\varphi}) + \dot{\varphi}(\zeta^{-1} - \varphi^{-1})\Big)\,\mathbf{M}_0 + \varphi^{-1}\dot{\varphi}\mathbf{1} \\
&= (\zeta^{-1}\dot{\zeta} - \varphi^{-1}\dot{\varphi})\mathbf{M}_0 + \varphi^{-1}\dot{\varphi}\mathbf{1} \\
&= \left(\left(\frac{\zeta'}{\zeta} - \frac{\varphi'}{\varphi}\right)\mathbf{M}_0 + \frac{\varphi'}{\varphi}\mathbf{1}\right)\dot{\Theta},
\end{aligned} \tag{4.25}$$

where $\mathbf{F}_\Theta^{-1}$ is given in (A.6.4) and

$$\begin{aligned}\dot{\mathbf{F}}_\Theta &= \frac{\mathrm{d}}{\mathrm{d}t}\left((\zeta-\varphi)\mathbf{M}_0+\varphi\mathbf{1}\right) = (\dot\zeta-\dot\varphi)\mathbf{M}_0+\dot\varphi\mathbf{1}\\ &= \left((\zeta'-\varphi')\mathbf{M}_0+\varphi'\mathbf{1}\right)\dot\Theta,\end{aligned} \tag{4.26}$$

which is, in this case, a symmetric tensor, i.e., $\mathbf{L}_\Theta = \mathbf{L}_\Theta^{\mathrm{T}}$. Thus, the thermal strain-rate tensor $\mathbf{D}_\Theta$ and the thermal spin tensor $\mathbf{W}_\Theta$ read

$$\mathbf{D}_\Theta = \tfrac{1}{2}(\mathbf{L}_\Theta+\mathbf{L}_\Theta^{\mathrm{T}}) = \mathbf{L}_\Theta = \left(\left(\frac{\zeta'}{\zeta}-\frac{\varphi'}{\varphi}\right)\mathbf{M}_0+\frac{\varphi'}{\varphi}\mathbf{1}\right)\dot\Theta \tag{4.27a}$$

and

$$\mathbf{W}_\Theta = \tfrac{1}{2}(\mathbf{L}_\Theta-\mathbf{L}_\Theta^{\mathrm{T}}) = \mathbf{0}. \tag{4.27b}$$

By applying the push-forward operation to the quantities in (4.23), the total, thermal, respectively mechanical Oldroyd strain-rate tensors in the intermediate configuration are obtained by

$$\begin{aligned}\overset{\triangle}{\hat{\boldsymbol{\gamma}}} &= \mathbf{F}_\Theta^{-\mathrm{T}}\dot{\mathbf{E}}\mathbf{F}_\Theta^{-1} = \dot{\hat{\boldsymbol{\gamma}}}+\mathbf{L}_\Theta^{\mathrm{T}}\hat{\boldsymbol{\gamma}}+\hat{\boldsymbol{\gamma}}\mathbf{L}_\Theta\\ &= \tfrac{1}{2}\left(\dot{\mathbf{C}}_{\mathrm{M}}+(\dot\zeta\zeta^{-1}-\dot\varphi\varphi^{-1})(\mathbf{C}_{\mathrm{M}}\mathbf{M}_0+\mathbf{M}_0\mathbf{C}_{\mathrm{M}})+2\dot\varphi\varphi^{-1}\mathbf{C}_{\mathrm{M}}\right)\\ &= \tfrac{1}{2}\left(\dot{\mathbf{C}}_{\mathrm{M}}+\left((\frac{\zeta'}{\zeta}-\frac{\varphi'}{\varphi})(\mathbf{C}_{\mathrm{M}}\mathbf{M}_0+\mathbf{M}_0\mathbf{C}_{\mathrm{M}})+2\frac{\varphi'}{\varphi}\mathbf{C}_{\mathrm{M}}\right)\dot\Theta\right)\end{aligned} \tag{4.28a}$$

$$\begin{aligned}\overset{\triangle}{\hat{\boldsymbol{\gamma}}}_\Theta &= \mathbf{F}_\Theta^{-\mathrm{T}}\dot{\mathbf{E}}_\Theta\mathbf{F}_\Theta^{-1} = \dot{\hat{\boldsymbol{\gamma}}}_\Theta+\mathbf{L}_\Theta^{\mathrm{T}}\hat{\boldsymbol{\gamma}}_\Theta+\hat{\boldsymbol{\gamma}}_\Theta\mathbf{L}_\Theta = \mathbf{D}_\Theta\\ &= \left((\frac{\zeta'}{\zeta}-\frac{\varphi'}{\varphi})\mathbf{M}_0+\frac{\varphi'}{\varphi}\mathbf{1}\right)\dot\Theta\end{aligned} \tag{4.28b}$$

$$\begin{aligned}\overset{\triangle}{\hat{\boldsymbol{\gamma}}}_{\mathrm{M}} &= \mathbf{F}_\Theta^{-\mathrm{T}}\dot{\mathbf{E}}_{\mathrm{M}}\mathbf{F}_\Theta^{-1} = \dot{\hat{\boldsymbol{\gamma}}}_{\mathrm{M}}+\mathbf{L}_\Theta^{\mathrm{T}}\hat{\boldsymbol{\gamma}}_{\mathrm{M}}+\hat{\boldsymbol{\gamma}}_{\mathrm{M}}\mathbf{L}_\Theta\\ &= \tfrac{1}{2}\left(\dot{\mathbf{C}}_{\mathrm{M}}+(\dot\zeta\zeta^{-1}-\dot\varphi\varphi^{-1})\mathbf{C}_{\mathrm{M}}\mathbf{M}_0+(\dot\zeta\zeta^{-1}-\dot\varphi\varphi^{-1})\mathbf{M}_0\mathbf{C}_{\mathrm{M}}+2\dot\varphi\varphi^{-1}\mathbf{C}_{\mathrm{M}}\right)\\ &\quad-(\dot\zeta\zeta^{-1}-\dot\varphi\varphi^{-1})\mathbf{M}_0-\dot\varphi\varphi^{-1}\mathbf{1}\\ &= \tfrac{1}{2}\big(\dot{\mathbf{C}}_{\mathrm{M}}+\big((\frac{\zeta'}{\zeta}-\frac{\varphi'}{\varphi})(\mathbf{M}_0\mathbf{C}_{\mathrm{M}}+\mathbf{C}_{\mathrm{M}}\mathbf{M}_0-2\mathbf{M}_0)+2\frac{\varphi'}{\varphi}(\mathbf{C}_{\mathrm{M}}-\mathbf{1})\big)\dot\Theta\big).\end{aligned} \tag{4.28c}$$

Here, the additive decomposition

$$\overset{\triangle}{\hat{\boldsymbol{\gamma}}} = \overset{\triangle}{\hat{\boldsymbol{\gamma}}}_{\mathrm{M}}+\overset{\triangle}{\hat{\boldsymbol{\gamma}}}_\Theta \tag{4.29}$$

holds. Use of

$$\begin{aligned}\dot{\hat{\boldsymbol{\gamma}}} &= \tfrac{1}{2}\frac{\mathrm{d}}{\mathrm{d}t}\left(\left(\mathbf{C}_{\mathrm{M}}-(\zeta^{-2}-\varphi^{-2})\mathbf{M}_0+\varphi^{-2}\mathbf{1}\right)\right)\\ &= \tfrac{1}{2}\left(\dot{\mathbf{C}}_{\mathrm{M}}-(-2\zeta^{-3}\dot\zeta+2\varphi^{-3}\dot\varphi)\mathbf{M}_0-2\varphi^{-3}\dot\varphi\mathbf{1}\right)\\ &= \tfrac{1}{2}\dot{\mathbf{C}}_{\mathrm{M}}+\left((\frac{\zeta'}{\zeta^3}+\frac{\varphi'}{\varphi^3})\mathbf{M}_0-\frac{\varphi'}{\varphi^3}\mathbf{1}\right)\dot\Theta\end{aligned} \tag{4.30}$$

is made in (4.28a) and (4.28c), respectively. The strain-rate measures in the reference, intermediate and current configurations are summarized in Fig. 4.5.

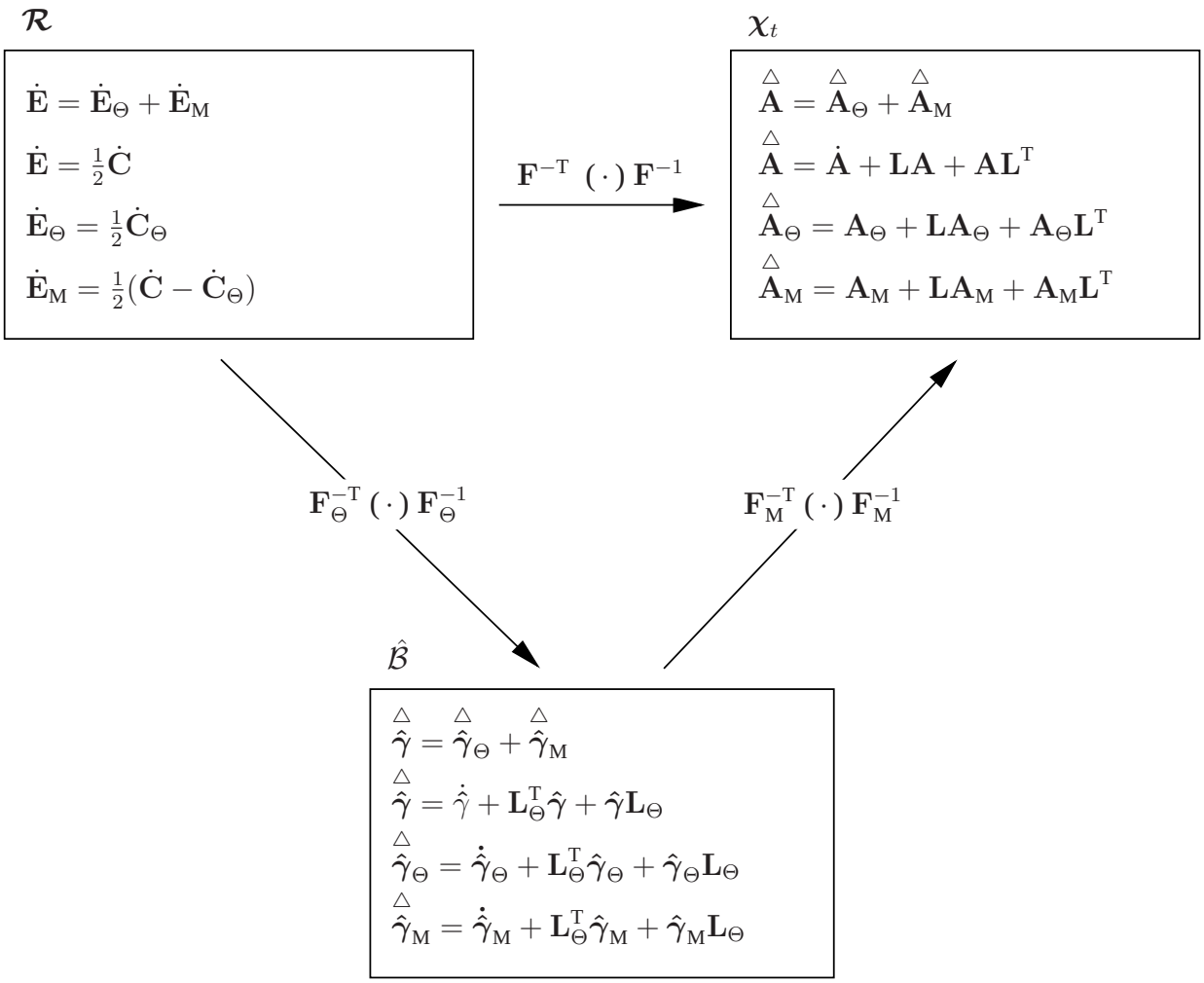

Figure 4.5.: Transformation of the strain-rate measures.

4.2. Thermodynamic Consistency

The specific stress power has to be evaluated leading to

$$p = \tilde{\mathbf{T}} \cdot \dot{\mathbf{E}} = \tilde{\mathbf{T}} \cdot (\mathbf{F}_\Theta^\mathrm{T} \overset{\triangle}{\hat{\boldsymbol{\gamma}}} \mathbf{F}_\Theta) = \mathbf{F}_\Theta \tilde{\mathbf{T}} \mathbf{F}_\Theta^\mathrm{T} \cdot \overset{\triangle}{\hat{\boldsymbol{\gamma}}} = \hat{\mathbf{S}}_\Theta \cdot \overset{\triangle}{\hat{\boldsymbol{\gamma}}}, \tag{4.31}$$

where[1]

$$\hat{\mathbf{S}}_\Theta := \mathbf{F}_\Theta \tilde{\mathbf{T}} \mathbf{F}_\Theta^\mathrm{T} \tag{4.32}$$

[1]The Kirchhoff-type stress $\hat{\mathbf{S}}_\Theta$ is a symmetric second-order tensor, i.e. $\hat{\mathbf{S}}_\Theta^\mathrm{T} = (\mathbf{F}_\Theta \tilde{\mathbf{T}} \mathbf{F}_\Theta^\mathrm{T})^\mathrm{T} = \hat{\mathbf{S}}_\Theta$.

represents a Kirchhoff-type stress tensor relative to the intermediate configuration $\hat{\mathcal{B}}$, defined as the push-forward of the second Piola-Kirchhoff stress tensor $\tilde{\mathbf{T}}$ with the thermal part of the deformation gradient $\mathbf{F}_\Theta$. The Kirchhoff stress tensor $\mathbf{S}$ (also called the weighted Cauchy stress tensor) is defined by

$$\mathbf{S} = \mathbf{F}\tilde{\mathbf{T}}\mathbf{F}^{\mathrm{T}} = J\mathbf{T}, \tag{4.33}$$

with $\mathbf{T}$ as the Cauchy stress tensor.

In view of thermo-mechanical processes the Clausius-Duhem inequality, Eq.(2.90b), has to be fulfilled:

$$-\dot{\psi} - \dot{\Theta}s + \frac{1}{\varrho_{\mathrm{R}}}\tilde{\mathbf{T}} \cdot \dot{\mathbf{E}} - \frac{\boldsymbol{q}_{\mathrm{R}}}{\varrho_{\mathrm{R}}\Theta} \cdot \operatorname{Grad}\Theta = -\dot{\psi} - \dot{\Theta}s + \frac{1}{\varrho_{\mathrm{R}}}\mathbf{S}_\Theta \cdot \overset{\triangle}{\hat{\boldsymbol{\gamma}}} - \frac{\boldsymbol{q}_{\mathrm{R}}}{\varrho_{\mathrm{R}}\Theta} \cdot \operatorname{Grad}\Theta \geq 0, \tag{4.34}$$

where ψ, represents the specific strain-energy function and s is the specific entropy. The idea used in the formulation of the strain-energy function for the case of isothermal transversal isotropy, see Sec. 3.2, is recalled. To this end, the total strain-energy function for thermo-mechanical transversal isotropy is additively decomposed following the multiplicative decomposition of the deformation gradient in (4.1), i.e., into a thermal and a mechanical part. Thus, the total strain-energy function is defined in terms of the mechanical deformation $\mathbf{C}_{\mathrm{M}}$, the fiber orientation $\boldsymbol{m}_0$ (or $\mathbf{M}_0$) and the temperature Θ,[1]

$$\psi(\mathbf{C}_{\mathrm{M}}, \mathbf{M}_0, \Theta) = \psi_{\mathrm{M}}(\mathbf{C}_{\mathrm{M}}, \mathbf{M}_0, \Theta) + \psi_\Theta(\Theta). \tag{4.35}$$

A concrete expression of the thermal part $\psi_\Theta(\Theta)$ is formulated in Sec. 4.6, see Eq.(4.91). Furthermore, the mechanical part $\psi_{\mathrm{M}}(\mathbf{C}_{\mathrm{M}}, \mathbf{M}_0, \Theta)$ is assumed to be linear with respect to the temperature Θ

$$\psi_{\mathrm{M}}(\mathbf{C}_{\mathrm{M}}, \mathbf{M}_0, \Theta) = \frac{\Theta}{\Theta_0}\overline{\psi}_{\mathrm{M}}(\mathbf{C}_{\mathrm{M}}, \mathbf{M}_0). \tag{4.36}$$

Another possibility is to assume temperature dependent material parameters, see e.g. (Johlitz et al., 2010) and (Johlitz et al., 2012) for the case of isotropy. In (4.36), the strain-energy function (3.47) is used to formulate the concrete form of the isothermal mechanical part $\overline{\psi}_{\mathrm{M}}(\mathbf{C}_{\mathrm{M}}, \mathbf{M}_0)$,[2] i.e.

$$\begin{aligned}\overline{\psi}_{\mathrm{M}}(\mathbf{C}_{\mathrm{M}}, \mathbf{M}_0) &= \psi^{\mathrm{vol}}(J_{\mathrm{M}}, \mathrm{I}_{4\mathrm{M}}) + \nu(\overline{\lambda}_{\mathrm{M}}) + \omega(\mathrm{I}^{\mathrm{r}}_{\mathrm{M}}) \\ &= \frac{K}{50}(J_{\mathrm{M}}^5 + J_{\mathrm{M}}^{-5} - 2)(\mathrm{I}_{4\mathrm{M}})^{-1/2} + \frac{\alpha}{3}(\overline{\lambda}_{\mathrm{M}}{}^3 + 3\overline{\lambda}_{\mathrm{M}}{}^{-1} - 4) + \frac{\beta}{2}(\mathrm{I}^{\mathrm{r}}_{\mathrm{M}} - 3),\end{aligned} \tag{4.37}$$

[1] This formulation is analogous to the proposal introduced in (Lion, 2000) and (Heimes, 2005) for the case of isotropic thermoelasticity. In this formulation, the mechanical part of the strain-energy function $\psi(\mathbf{C}_{\mathrm{M}}, \mathbf{M}_0, \Theta)$ is assumed to be a function of the temperature Θ, due to the linear dependency of the stress-state on temperature, which is observed experimentally.

[2] Note that, here, $\mathbf{M}_0$ operates on the same configuration as $\mathbf{C}_{\mathrm{M}}$ does, i.e. on the intermediate configuration $\hat{\mathcal{B}}$, where the unit vectors denoting the fiber orientation in the reference and intermediate configuration are identical, see derivation of Eq.(4.8).

where the two invariants $\mathrm{I}_{4\mathrm{M}}$ and $\mathrm{I}^{\mathrm{r}}_{\mathrm{M}}$ and the isochoric mechanical stretch $\overline{\lambda}_{\mathrm{M}}$ read

$$\mathrm{I}_{4\mathrm{M}} = \mathrm{tr}(\mathbf{C}_{\mathrm{M}}\mathbf{M}_0) = \lambda^2_{\mathrm{M}} \tag{4.38a}$$

$$\mathrm{I}^{\mathrm{r}}_{\mathrm{M}} = \mathrm{tr}\,\mathbf{C}^{\mathrm{r}}_{\mathrm{M}} = \mathrm{tr}\,\overline{\mathbf{C}}_{\mathrm{M}} - \mathrm{tr}(\overline{\mathbf{C}}_{\mathrm{M}}\mathbf{M}_0) + 1 = \bar{\mathrm{I}}_{\mathrm{M}} - \bar{\mathrm{I}}_{4\mathrm{M}} + 1 \tag{4.38b}$$

$$\overline{\lambda}_{\mathrm{M}} = J_{\mathrm{M}}^{-1/3}\lambda_{\mathrm{M}} = \left(\frac{J}{\zeta\varphi^2}\right)^{-1/3}(\lambda_{\mathrm{a}}\zeta) = \left(\frac{\zeta}{\varphi}\right)^{-2/3} J^{-1/3}\lambda_{\mathrm{a}} = \eta^{-2/3}\,\overline{\lambda}_{\mathrm{a}}, \tag{4.38c}$$

with

$$\eta = \frac{\zeta}{\varphi} \tag{4.39}$$

represents the ratio of the thermal stretch along the fiber direction to the thermal stretch in orthogonal directions, and

$$\bar{\mathrm{I}}_{4\mathrm{M}} = \mathrm{tr}(\overline{\mathbf{C}}_{\mathrm{M}}\mathbf{M}_0) = {\overline{\lambda}_{\mathrm{M}}}^2 \tag{4.40a}$$

$$\begin{aligned}\mathrm{I}_{\mathrm{M}} &= \mathrm{tr}\,\mathbf{C}_{\mathrm{M}} = \mathrm{tr}(\mathbf{F}^{\mathrm{T}}_{\mathrm{M}}\mathbf{F}_{\mathrm{M}}) = \mathrm{tr}(\mathbf{F}_\Theta^{-\mathrm{T}}\mathbf{F}^{\mathrm{T}}\mathbf{F}\,\mathbf{F}_\Theta^{-1}) = \mathrm{tr}(\mathbf{C}\mathbf{C}_\Theta^{-1})\\ &= \mathrm{tr}\left(\mathbf{C}\left((\zeta^{-2}-\varphi^{-2})\mathbf{M}_0 + \varphi^{-2}\mathbf{1}\right)\right) = (\zeta^{-2}-\varphi^{-2})\,\mathrm{tr}(\mathbf{C}\mathbf{M}_0) + \varphi^{-2}\,\mathrm{tr}(\mathbf{C})\\ &= (\zeta^{-2}-\varphi^{-2})\mathrm{I}_4 + \varphi^{-2}\mathrm{I}_1\end{aligned} \tag{4.40b}$$

$$\begin{aligned}\bar{\mathrm{I}}_{\mathrm{M}} &= \mathrm{tr}\,\overline{\mathbf{C}}_{\mathrm{M}} = J_{\mathrm{M}}^{-2/3}\,\mathrm{tr}\,\mathbf{C}_{\mathrm{M}} = J_{\mathrm{M}}^{-2/3}\mathrm{I}_{\mathrm{M}} = \left(\frac{J}{\zeta\varphi^2}\right)^{-2/3}\left((\zeta^{-2}-\varphi^{-2})\mathrm{I}_4 + \varphi^{-2}\mathrm{I}_1\right)\\ &= \eta^{2/3}\,(\mathrm{I}_{\overline{\mathbf{C}}} - \bar{\mathrm{I}}_4) + \eta^{-4/3}\,\bar{\mathrm{I}}_4.\end{aligned} \tag{4.40c}$$

Hence, the total strain-energy function reads

$$\psi(\mathbf{C}_{\mathrm{M}}, \mathbf{M}_0, \Theta) = \frac{\Theta}{\Theta_0}\left(\psi^{\mathrm{vol}}(J_{\mathrm{M}}, \mathrm{I}_{4\mathrm{M}}) + \nu(\overline{\lambda}_{\mathrm{M}}) + \omega(\mathrm{I}^{\mathrm{r}}_{\mathrm{M}})\right) + \psi_\Theta(\Theta). \tag{4.41}$$

The material time-derivative of the free energy ψ of Eq.(4.35) reads

$$\begin{aligned}\dot{\psi}(\mathbf{C}_{\mathrm{M}}, \mathbf{M}_0, \Theta) &= \dot{\psi}_{\mathrm{M}}(\mathbf{C}_{\mathrm{M}}, \mathbf{M}_0, \Theta) + \dot{\psi}_\Theta(\Theta)\\ &= \left(\frac{1}{\Theta_0}\overline{\psi}_{\mathrm{M}}(\mathbf{C}_{\mathrm{M}}, \mathbf{M}_0)\right)\dot{\Theta} + \frac{\Theta}{\Theta_0}\frac{\mathrm{d}\overline{\psi}_{\mathrm{M}}(\mathbf{C}_{\mathrm{M}}, \mathbf{M}_0)}{\mathrm{d}\mathbf{C}_{\mathrm{M}}}\cdot\dot{\mathbf{C}}_{\mathrm{M}} + \psi'_\Theta(\Theta)\dot{\Theta},\end{aligned} \tag{4.42}$$

where $\psi'_\Theta(\Theta) = \mathrm{d}\psi_\Theta(\Theta)/\mathrm{d}\Theta$.

From Eq.(4.28a), the time derivative of $\mathbf{C}_{\mathrm{M}}$ reads

$$\dot{\mathbf{C}}_{\mathrm{M}} = 2\overset{\triangle}{\hat{\boldsymbol{\gamma}}} - \left(\left(\frac{\zeta'}{\zeta} - \frac{\varphi'}{\varphi}\right)(\mathbf{C}_{\mathrm{M}}\mathbf{M}_0 + \mathbf{M}_0\mathbf{C}_{\mathrm{M}}) + 2\frac{\varphi'}{\varphi}\mathbf{C}_{\mathrm{M}}\right)\dot{\Theta}, \tag{4.43}$$

by which Eq.(4.42) can be written as

$$\dot{\psi}(\mathbf{C}_{\mathrm{M}},\mathbf{M}_0,\Theta) = 2\frac{\Theta}{\Theta_0}\frac{\mathrm{d}\overline{\psi}_{\mathrm{M}}(\mathbf{C}_{\mathrm{M}},\mathbf{M}_0)}{\mathrm{d}\mathbf{C}_{\mathrm{M}}}\cdot\overset{\triangle}{\hat{\boldsymbol{\gamma}}} + \Bigg[\frac{1}{\Theta_0}\overline{\psi}_{\mathrm{M}}(\mathbf{C}_{\mathrm{M}},\mathbf{M}_0) - \frac{\Theta}{\Theta_0}\frac{\mathrm{d}\overline{\psi}_{\mathrm{M}}(\mathbf{C}_{\mathrm{M}},\mathbf{M}_0)}{\mathrm{d}\mathbf{C}_{\mathrm{M}}}\cdot\left(\left(\frac{\zeta'}{\zeta}-\frac{\varphi'}{\varphi}\right)(\mathbf{C}_{\mathrm{M}}\mathbf{M}_0+\mathbf{M}_0\mathbf{C}_{\mathrm{M}}) + 2\frac{\varphi'}{\varphi}\mathbf{C}_{\mathrm{M}}\right) + \psi'_{\Theta}(\Theta,\mathbf{M}_0)\Bigg]\dot{\Theta}. \tag{4.44}$$

Substituting (4.44) in (4.34) yields,

$$\left(\frac{1}{\varrho_{\mathrm{R}}}\hat{\mathbf{S}}_{\Theta} - 2\frac{\Theta}{\Theta_0}\frac{\mathrm{d}\overline{\psi}_{\mathrm{M}}(\mathbf{C}_{\mathrm{M}},\mathbf{M}_0)}{\mathrm{d}\mathbf{C}_{\mathrm{M}}}\right)\cdot\overset{\triangle}{\hat{\boldsymbol{\gamma}}} + \Bigg(-s - \frac{1}{\Theta_0}\overline{\psi}_{\mathrm{M}}(\mathbf{C}_{\mathrm{M}},\mathbf{M}_0) - \psi'_{\Theta}(\Theta) + \frac{\Theta}{\Theta_0}\frac{\mathrm{d}\overline{\psi}_{\mathrm{M}}(\mathbf{C}_{\mathrm{M}},\mathbf{M}_0)}{\mathrm{d}\mathbf{C}_{\mathrm{M}}}\cdot\left(2\frac{\varphi'}{\varphi}\mathbf{C}_{\mathrm{M}} + \tfrac{1}{2}\left(\frac{\zeta'}{\zeta}-\frac{\varphi'}{\varphi}\right)(\mathbf{C}_{\mathrm{M}}\mathbf{M}_0+\mathbf{M}_0\mathbf{C}_{\mathrm{M}})\right)\Bigg)\dot{\Theta} - \frac{\boldsymbol{q}_{\mathrm{R}}}{\varrho_{\mathrm{R}}\Theta}\cdot\operatorname{Grad}\Theta \geq 0 \tag{4.45}$$

For independent thermal and mechanical processes, a sufficient condition to satisfy the Clausius-Duhem inequality is

$$\hat{\mathbf{S}}_{\Theta} = 2\varrho_{\mathrm{R}}\frac{\Theta}{\Theta_0}\frac{\mathrm{d}\overline{\psi}_{\mathrm{M}}(\mathbf{C}_{\mathrm{M}},\mathbf{M}_0)}{\mathrm{d}\mathbf{C}_{\mathrm{M}}} \tag{4.46}$$

$$s = -\frac{1}{\Theta_0}\overline{\psi}_{\mathrm{M}}(\mathbf{C}_{\mathrm{M}},\mathbf{M}_0) - \psi'_{\Theta}(\Theta,\mathbf{M}_0) + \frac{1}{\varrho_{\mathrm{R}}}\frac{\varphi'}{\varphi}(\hat{\mathbf{S}}_{\Theta}\cdot\mathbf{C}_{\mathrm{M}}) + \frac{1}{\varrho_{\mathrm{R}}}\left(\frac{\zeta'}{\zeta}-\frac{\varphi'}{\varphi}\right)\hat{\mathbf{S}}_{\Theta}\cdot\mathbf{C}_{\mathrm{M}}\mathbf{M}_0$$
$$= -\frac{1}{\Theta_0}\overline{\psi}_{\mathrm{M}}(\mathbf{C}_{\mathrm{M}},\mathbf{M}_0) - \psi'_{\Theta}(\Theta,\mathbf{M}_0) + \frac{1}{\varrho_{\mathrm{R}}}\frac{\varphi'}{\varphi}(\mathbf{C}_{\mathrm{M}}\hat{\mathbf{S}}_{\Theta}\cdot\mathbf{1}) + \frac{1}{\varrho_{\mathrm{R}}}\left(\frac{\zeta'}{\zeta}-\frac{\varphi'}{\varphi}\right)\mathbf{C}_{\mathrm{M}}\hat{\mathbf{S}}_{\Theta}\cdot\mathbf{M}_0 \tag{4.47}$$

$$-\frac{1}{\varrho_{\mathrm{R}}\Theta}\boldsymbol{q}_{\mathrm{R}}\cdot\operatorname{Grad}\Theta \geq 0, \tag{4.48}$$

where $\hat{\mathbf{S}}_{\Theta}\cdot\mathbf{C}_{\mathrm{M}}\mathbf{M}_0 = \hat{\mathbf{S}}_{\Theta}\cdot\mathbf{M}_0\mathbf{C}_{\mathrm{M}}$ is inserted in (4.47) due to the symmetry of these three tensors. We recall Eq.(4.33), i.e. the Kirchhoff stress tensor can be represented as the push-forward of $\hat{\mathbf{S}}_{\Theta}$ by the mechanical deformation gradient,

$$\mathbf{S} = \mathbf{F}\tilde{\mathbf{T}}\mathbf{F}^{\mathrm{T}} = \mathbf{F}_{\mathrm{M}}\underbrace{\mathbf{F}_{\Theta}\tilde{\mathbf{T}}\mathbf{F}_{\Theta}^{\mathrm{T}}}_{\hat{\mathbf{S}}_{\Theta}}\mathbf{F}_{\mathrm{M}}^{\mathrm{T}} = \mathbf{F}_{\mathrm{M}}\hat{\mathbf{S}}_{\Theta}\mathbf{F}_{\mathrm{M}}^{\mathrm{T}}, \tag{4.49}$$

leading to the alternative representation of $\hat{\mathbf{S}}_{\Theta}\cdot\mathbf{C}_{\mathrm{M}}$ in (4.47)

$$\hat{\mathbf{S}}_{\Theta}\cdot\mathbf{C}_{\mathrm{M}} = \hat{\mathbf{S}}_{\Theta}\cdot\mathbf{F}_{\mathrm{M}}^{\mathrm{T}}\mathbf{F}_{\mathrm{M}} = \mathbf{F}_{\mathrm{M}}\hat{\mathbf{S}}_{\Theta}\mathbf{F}_{\mathrm{M}}^{\mathrm{T}}\cdot\mathbf{1} = \mathbf{S}\cdot\mathbf{1} = \operatorname{tr}\mathbf{S}, \tag{4.50}$$

and, subsequently, the specific entropy takes the form

$$s = -\frac{1}{\Theta_0}\overline{\psi}_{\mathrm{M}}(\mathbf{C}_{\mathrm{M}}, \mathbf{M}_0) - \psi'_{\Theta}(\Theta, \mathbf{M}_0) + \frac{1}{\varrho_{\mathrm{R}}}\frac{\varphi'}{\varphi}(\operatorname{tr}\mathbf{S}) + \frac{1}{\varrho_{\mathrm{R}}}\left(\frac{\zeta'}{\zeta} - \frac{\varphi'}{\varphi}\right)\mathbf{C}_{\mathrm{M}}\hat{\mathbf{S}}_{\Theta}\cdot\mathbf{M}_0. \tag{4.51}$$

Note that if $\zeta = \varphi$ the last term in (4.51) vanishes and a similar expression for s in the case of isotropic thermoelasticity is obtained with a strain-energy function depending only on $\mathbf{C}_{\mathrm{M}}$ and Θ, i.e., the material has no preferred direction represented by $\mathbf{M}_0$, see (Hartmann, 2012).

Furthermore, if the Mandel stress[1]

$$\mathbf{P} = \mathbf{C}\tilde{\mathbf{T}} \tag{4.52}$$

is introduced, the dot products in the last two terms in (4.47) can be represented as

$$\hat{\mathbf{S}}_{\Theta}\cdot\mathbf{C}_{\mathrm{M}} = \mathbf{C}_{\mathrm{M}}\hat{\mathbf{S}}_{\Theta}\cdot\mathbf{1} = \mathbf{C}\tilde{\mathbf{T}}\cdot\mathbf{1} = \mathbf{P}\cdot\mathbf{1} = \operatorname{tr}\mathbf{P} \tag{4.53a}$$

and

$$\hat{\mathbf{S}}_{\Theta}\cdot\mathbf{C}_{\mathrm{M}}\mathbf{M}_0 = \mathbf{C}_{\mathrm{M}}\hat{\mathbf{S}}_{\Theta}\cdot\mathbf{M}_0 = \mathbf{C}\tilde{\mathbf{T}}\cdot\mathbf{M}_0 = \mathbf{P}\cdot\mathbf{M}_0, \tag{4.53b}$$

i.e., they represent the trace of Mandel stress and its component in the fiber direction, respectively.[2] Thus, Eq.(4.47) can be rewritten as[3]

$$s = -\frac{1}{\Theta_0}\overline{\psi}_{\mathrm{M}}(\mathbf{C}_{\mathrm{M}}, \mathbf{M}_0) - \psi'_{\Theta}(\Theta, \mathbf{M}_0) + \frac{1}{\varrho_{\mathrm{R}}}\frac{\varphi'}{\varphi}(\mathbf{P}\cdot\mathbf{1}) + \frac{1}{\varrho_{\mathrm{R}}}\left(\frac{\zeta'}{\zeta} - \frac{\varphi'}{\varphi}\right)(\mathbf{P}\cdot\mathbf{M}_0). \tag{4.54}$$

4.3. Constitutive Equations for Stress-State

From (4.32), the second Piola-Kirchhoff stress tensor $\tilde{\mathbf{T}}$ can be defined i.e. it represents the pull-back of the stress tensor $\hat{\mathbf{S}}_{\Theta}$. To this end, the isothermal mechanical strain-energy function in (4.37) has to be differentiated with respect to $\mathbf{C}_{\mathrm{M}}$, leading to

$$\begin{aligned}\frac{\mathrm{d}\overline{\psi}_{\mathrm{M}}(\mathbf{C}_{\mathrm{M}}, \mathbf{M}_0)}{\mathrm{d}\mathbf{C}_{\mathrm{M}}} &= \frac{\mathrm{d}\psi^{\mathrm{vol}}(J_{\mathrm{M}}, \mathrm{I}_{4\mathrm{M}})}{\mathrm{d}\mathbf{C}_{\mathrm{M}}} + \frac{\mathrm{d}\nu(\overline{\lambda}_{\mathrm{M}})}{\mathrm{d}\mathbf{C}_{\mathrm{M}}} + \frac{\mathrm{d}\omega(\mathrm{I}^{\mathrm{r}}_{\mathrm{M}})}{\mathrm{d}\mathbf{C}_{\mathrm{M}}} \\ &= \frac{\partial\psi^{\mathrm{vol}}(J_{\mathrm{M}}, \mathrm{I}_{4\mathrm{M}})}{\partial\mathrm{I}_{4\mathrm{M}}}\mathbf{M}_0 + \tfrac{1}{2}J_{\mathrm{M}}\frac{\partial\psi^{\mathrm{vol}}(J_{\mathrm{M}}, \mathrm{I}_{4\mathrm{M}})}{\partial J_{\mathrm{M}}}\mathbf{C}_{\mathrm{M}}^{-1} \\ &\quad + \left(\left(\tfrac{1}{2}{\overline{\lambda}_{\mathrm{M}}}^{-1}v'(\overline{\lambda}_{\mathrm{M}}) + ({\bar{\mathrm{I}}_{4\mathrm{M}}}^{-1} - 1)w'(\mathrm{I}^{\mathrm{r}}_{\mathrm{M}})\right)\mathbf{M}_0\overline{\mathbf{C}}_{\mathrm{M}} + w'(\mathrm{I}^{\mathrm{r}}_{\mathrm{M}})\overline{\mathbf{C}}_{\mathrm{M}}\right)^{\mathrm{D}}\mathbf{C}_{\mathrm{M}}^{-1},\end{aligned} \tag{4.55}$$

[1] See (Holzapfel, 2000, p.128).

[2] For proof, see Appendix A.7.

[3] Here, the Mandel stress tensor merely serves to unify the representation of the last two terms in the entropy equation.

where $\mathrm{d}\psi^{\mathrm{vol}}(J_{\mathrm{M}}, \mathrm{I}_{4\mathrm{M}})/\mathrm{d}\mathbf{C}_{\mathrm{M}}$, $\mathrm{d}\nu(\overline{\lambda}_{\mathrm{M}})/\mathrm{d}\mathbf{C}_{\mathrm{M}}$ and $\mathrm{d}\omega(\mathrm{I}^{\mathrm{r}}_{\mathrm{M}})/\mathrm{d}\mathbf{C}_{\mathrm{M}}$ are calculated similar to the derivative $\mathrm{d}\psi^{\mathrm{vol}}(J, \mathrm{I}_4)/\mathrm{d}\mathbf{C}$, $\mathrm{d}\nu(\overline{\lambda}_{\mathrm{a}})/\mathrm{d}\mathbf{C}$ and $\mathrm{d}\omega(\mathrm{I}_{\mathbf{C}_{\mathrm{r}}})/\mathrm{d}\mathbf{C}$, see (A.4.1), (A.4.3) and (A.4.7), respectively, with

$$\frac{\partial\psi^{\mathrm{vol}}(J_{\mathrm{M}}, \mathrm{I}_4)}{\partial \mathrm{I}_{4\mathrm{M}}} = -\frac{K}{100}\mathrm{I}_{4\mathrm{M}}^{-3/2}(J_{\mathrm{M}}^5 + J_{\mathrm{M}}^{-5} - 2) \tag{4.56a}$$

$$\frac{\partial\psi^{\mathrm{vol}}(J_{\mathrm{M}}, \mathrm{I}_{4\mathrm{M}})}{\partial J_{\mathrm{M}}} = \frac{K}{10}\mathrm{I}_{4\mathrm{M}}^{-1/2}(J_{\mathrm{M}}^4 - J_{\mathrm{M}}^{-6}) \tag{4.56b}$$

$$v'(\overline{\lambda}_{\mathrm{M}}) = \frac{\mathrm{d}v(\overline{\lambda}_{\mathrm{M}})}{\mathrm{d}\overline{\lambda}_{\mathrm{M}}} = \alpha(\overline{\lambda}_{\mathrm{M}}{}^2 - \overline{\lambda}_{\mathrm{M}}{}^{-2}) \tag{4.56c}$$

$$w'(\mathrm{I}^{\mathrm{r}}_{\mathrm{M}}) = \frac{\mathrm{d}w'(\mathrm{I}^{\mathrm{r}}_{\mathrm{M}})}{\mathrm{d}\mathrm{I}^{\mathrm{r}}_{\mathrm{M}}} = \frac{\beta}{2}. \tag{4.56d}$$

Inserting (4.55) into (4.46) yields the Kirchhoff-type stress tensor $\hat{\mathbf{S}}_\Theta$

$$\hat{\mathbf{S}}_\Theta = \hat{\mathbf{S}}^{\mathrm{vol}}_\Theta + \hat{\mathbf{S}}^{\mathrm{isc}}_\Theta, \tag{4.57}$$

with

$$\hat{\mathbf{S}}^{\mathrm{vol}}_\Theta = \varrho_{\mathrm{R}}\frac{\Theta}{\Theta_0}\left(2\frac{\partial\psi^{\mathrm{vol}}(J_{\mathrm{M}}, \mathrm{I}_{4\mathrm{M}})}{\partial \mathrm{I}_{4\mathrm{M}}}\mathbf{M}_0 + J_{\mathrm{M}}\frac{\partial\psi^{\mathrm{vol}}(J_{\mathrm{M}}, \mathrm{I}_{4\mathrm{M}})}{\partial J_{\mathrm{M}}}\mathbf{C}_{\mathrm{M}}^{-1}\right) \tag{4.58a}$$

and

$$\hat{\mathbf{S}}^{\mathrm{isc}}_\Theta = \varrho_{\mathrm{R}}\frac{\Theta}{\Theta_0}\left(\left(\overline{\lambda}_{\mathrm{M}}{}^{-1}v'(\overline{\lambda}_{\mathrm{M}}) + 2(\overline{\mathrm{I}}_{4\mathrm{M}}{}^{-1} - 1)w'(\mathrm{I}^{\mathrm{r}}_{\mathrm{M}})\right)\mathbf{M}_0\overline{\mathbf{C}}_{\mathrm{M}} + 2w'(\mathrm{I}^{\mathrm{r}}_{\mathrm{M}})\overline{\mathbf{C}}_{\mathrm{M}}\right)^{\mathrm{D}}\mathbf{C}_{\mathrm{M}}^{-1}. \tag{4.58b}$$

Thus, Eqs.(4.32) and (4.57) yield the constitutive equation of the second Piola-Kirchhoff stress

$$\tilde{\mathbf{T}} = \tilde{\mathbf{T}}_{\mathrm{vol}} + \tilde{\mathbf{T}}_{\mathrm{isc}}, \tag{4.59a}$$

where

$$\tilde{\mathbf{T}}_{\mathrm{vol}} = \mathbf{F}_\Theta^{-1}\,\hat{\mathbf{S}}^{\mathrm{vol}}_\Theta\,\mathbf{F}_\Theta^{-\mathrm{T}} = \varrho_{\mathrm{R}}\frac{\Theta}{\Theta_0}\left(\frac{2}{\zeta^2}\frac{\partial\psi^{\mathrm{vol}}(J_{\mathrm{M}}, \mathrm{I}_{4\mathrm{M}})}{\partial \mathrm{I}_{4\mathrm{M}}}\mathbf{M}_0 + \frac{J}{\zeta\varphi^2}\frac{\partial\psi^{\mathrm{vol}}(J_{\mathrm{M}}, \mathrm{I}_{4\mathrm{M}})}{\partial J_{\mathrm{M}}}\mathbf{C}^{-1}\right) \tag{4.59b}$$

and

$$\begin{aligned}\tilde{\mathbf{T}}_{\mathrm{isc}} &= \mathbf{F}_\Theta^{-1}\,\hat{\mathbf{S}}^{\mathrm{isc}}_\Theta\,\mathbf{F}_\Theta^{-\mathrm{T}} \\ &= \varrho_{\mathrm{R}}\eta^{2/3}\frac{\Theta}{\Theta_0}\left(\left(\overline{\mathrm{I}}_4^{-1/2}v'(\overline{\lambda}_{\mathrm{M}}) + 2(\eta^{-2/3}\overline{\mathrm{I}}_4^{-1} - 1)w'(\mathrm{I}^{\mathrm{r}}_{\mathrm{M}})\right)\mathbf{M}_0\overline{\mathbf{C}} + 2w'(\mathrm{I}^{\mathrm{r}}_{\mathrm{M}})\overline{\mathbf{C}}\right)^{\mathrm{D}}\mathbf{C}^{-1},\end{aligned} \tag{4.59c}$$

in which the pull-back operations

$$\mathbf{F}_\Theta^{-1}\,\mathbf{M}_0\,\mathbf{F}_\Theta^{-\mathrm{T}} = \left((\zeta^{-1} - \varphi^{-1})\mathbf{M}_0 + \varphi^{-1}\mathbf{1}\right)\mathbf{M}_0\left((\zeta^{-1} - \varphi^{-1})\mathbf{M}_0 + \varphi^{-1}\mathbf{1}\right) = \frac{1}{\zeta^2}\mathbf{M}_0$$

$$\mathbf{F}_\Theta^{-1}\,\mathbf{C}_{\mathrm{M}}^{-1}\,\mathbf{F}_\Theta^{-\mathrm{T}} = \mathbf{F}_\Theta^{-1}\,(\mathbf{F}_\Theta^{-\mathrm{T}}\,\mathbf{C}\mathbf{F}_\Theta^{-1})^{-1}\,\mathbf{F}_\Theta^{-\mathrm{T}} = \mathbf{F}_\Theta^{-1}\,\mathbf{F}_\Theta\,\mathbf{C}^{-1}\mathbf{F}_\Theta^{\mathrm{T}}\,\mathbf{F}_\Theta^{-\mathrm{T}} = \mathbf{C}^{-1}$$

and

$$\begin{aligned}
\mathbf{F}_{\Theta}^{-1}\,\overline{\mathbf{C}}_{\mathrm{M}}^{\mathrm{D}}\mathbf{C}_{\mathrm{M}}^{-1}\,\mathbf{F}_{\Theta}^{-\mathrm{T}} &= J_{\mathrm{M}}^{-2/3}\,\mathbf{F}_{\Theta}^{-1}\,(\mathbf{1}-\tfrac{1}{3}\mathrm{I}_{\mathrm{M}}\mathbf{C}_{\mathrm{M}}^{-1})\,\mathbf{F}_{\Theta}^{-\mathrm{T}}\\
&= J_{\mathrm{M}}^{-2/3}(\mathbf{F}_{\Theta}^{-1}\,\mathbf{1}\,\mathbf{F}_{\Theta}^{-\mathrm{T}}-\tfrac{1}{3}\mathrm{I}_{\mathrm{M}}\mathbf{F}_{\Theta}^{-1}\,\mathbf{C}_{\mathrm{M}}^{-1}\,\mathbf{F}_{\Theta}^{-\mathrm{T}}) = J_{\mathrm{M}}^{-2/3}(\mathbf{C}_{\Theta}^{-1}-\tfrac{1}{3}\mathrm{I}_{\mathrm{M}}\mathbf{C}^{-1})\\
&= (\frac{J}{\zeta\varphi^2})^{-2/3}\left((\zeta^{-2}-\varphi^{-2})\mathbf{M}_0+\varphi^{-2}\mathbf{1}-\tfrac{1}{3}((\zeta^{-2}-\varphi^{-2})\mathrm{I}_4+\varphi^{-2}\mathrm{I}_1)\mathbf{C}^{-1}\right)\\
&= (\zeta\varphi^2)^{2/3}(\zeta^{-2}-\varphi^{-2})(\mathbf{M}_0\overline{\mathbf{C}}-\tfrac{1}{3}\bar{\mathrm{I}}_4\mathbf{1})\mathbf{C}^{-1}+\frac{(\zeta\varphi^2)^{2/3}}{\varphi^2}(\overline{\mathbf{C}}-\tfrac{1}{3}\mathrm{I}_{\overline{\mathbf{C}}}\mathbf{1})\mathbf{C}^{-1}\\
&= \left((\eta^{-4/3}-\eta^{2/3})(\mathbf{M}_0\overline{\mathbf{C}})+\eta^{2/3}\overline{\mathbf{C}}\right)^{\mathrm{D}}\mathbf{C}^{-1}\\
\mathbf{F}_{\Theta}^{-1}\,(\mathbf{M}_0\overline{\mathbf{C}}_{\mathrm{M}})^{\mathrm{D}}\mathbf{C}_{\mathrm{M}}^{-1}\,\mathbf{F}_{\Theta}^{-\mathrm{T}} &= J_{\mathrm{M}}^{-2/3}\,\mathbf{F}_{\Theta}^{-1}\,(\mathbf{M}_0-\tfrac{1}{3}\mathrm{I}_{4\mathrm{M}}\mathbf{C}_{\mathrm{M}}^{-1})\,\mathbf{F}_{\Theta}^{-\mathrm{T}}\\
&= J_{\mathrm{M}}^{-2/3}(\mathbf{F}_{\Theta}^{-1}\,\mathbf{M}_0\,\mathbf{F}_{\Theta}^{-\mathrm{T}}-\tfrac{1}{3}\mathrm{I}_{4\mathrm{M}}\mathbf{F}_{\Theta}^{-1}\,\mathbf{C}_{\mathrm{M}}^{-1}\,\mathbf{F}_{\Theta}^{-\mathrm{T}})\\
&= J_{\mathrm{M}}^{-2/3}(\frac{1}{\zeta^2}\mathbf{M}_0-\tfrac{1}{3}\mathrm{I}_{4\mathrm{M}}\mathbf{C}^{-1}) = \left(\frac{J}{\zeta\varphi^2}\right)^{-2/3}(\frac{1}{\zeta^2}\mathbf{M}_0-\tfrac{1}{3}\frac{\mathrm{I}_4}{\zeta^2}\mathbf{C}^{-1})\\
&= (\frac{\varphi}{\zeta})^{-4/3}J^{-2/3}(\mathbf{M}_0-\tfrac{1}{3}\mathrm{I}_4\mathbf{C}^{-1}) = (\frac{\varphi}{\zeta})^{-4/3}J^{-2/3}(\mathbf{M}_0\mathbf{C}-\tfrac{1}{3}\mathrm{I}_4\mathbf{1})\mathbf{C}^{-1}\\
&= \eta^{-4/3}(\mathbf{M}_0\overline{\mathbf{C}})^{\mathrm{D}}\mathbf{C}^{-1}
\end{aligned}$$

are used, respectively.

Eqs.(4.52) and (4.59), follow the Mandel stress

$$\begin{aligned}
\mathbf{P} = \varrho_{\mathrm{R}}\frac{\Theta}{\Theta_0}\Big(&\frac{2}{\zeta^2}\frac{\partial\psi^{\mathrm{vol}}(J_{\mathrm{M}},\mathrm{I}_{4\mathrm{M}})}{\partial\mathrm{I}_{4\mathrm{M}}}\mathbf{C}\mathbf{M}_0+\frac{J}{\zeta\varphi^2}\frac{\partial\psi^{\mathrm{vol}}(J_{\mathrm{M}},\mathrm{I}_{4\mathrm{M}})}{\partial J_{\mathrm{M}}}\mathbf{1}\\
&+\left(\bar{\mathrm{I}}_4^{-1/2}v'(\overline{\lambda}_{\mathrm{M}})+2(\eta^{-2/3}\bar{\mathrm{I}}_4^{-1}-1)w'(\mathrm{I}_{\mathrm{M}}^{\mathrm{r}})\overline{\mathbf{C}}\mathbf{M}_0+2w'(\mathrm{I}_{\mathrm{M}}^{\mathrm{r}})\overline{\mathbf{C}}\right)^{\mathrm{D}}\Big)
\end{aligned}\tag{4.60}$$

The Cauchy stress tensor $\mathbf{T}$, defined as the push-forward of the second Piola-Kirchhoff stress tensor $\tilde{\mathbf{T}}$, reads

$$\mathbf{T} = \frac{1}{J}\mathbf{F}\tilde{\mathbf{T}}\mathbf{F}^{\mathrm{T}} = \mathbf{T}_{\mathrm{vol}}+\mathbf{T}_{\mathrm{isc}},\tag{4.61a}$$

where

$$\mathbf{T}_{\mathrm{vol}} = \frac{1}{J}\mathbf{F}\tilde{\mathbf{T}}_{\mathrm{vol}}\mathbf{F}^{\mathrm{T}} = \frac{\varrho_{\mathrm{R}}}{J}\frac{\Theta}{\Theta_0}\Big(2\frac{\mathrm{I}_4}{\zeta^2}\frac{\partial\psi^{\mathrm{vol}}(J_{\mathrm{M}},\mathrm{I}_{4\mathrm{M}})}{\partial\mathrm{I}_{4\mathrm{M}}}\mathbf{M}+\frac{J}{\zeta\varphi^2}\frac{\partial\psi^{\mathrm{vol}}(J_{\mathrm{M}},\mathrm{I}_{4\mathrm{M}})}{\partial J_{\mathrm{M}}}\mathbf{1}\Big)\tag{4.61b}$$

and

$$\begin{aligned}
\mathbf{T}_{\mathrm{isc}} &= \frac{1}{J}\mathbf{F}\tilde{\mathbf{T}}_{\mathrm{isc}}\mathbf{F}^{\mathrm{T}}\\
&= \varrho_{\mathrm{R}}\eta^{2/3}\frac{\Theta}{\Theta_0}\left(\left(\bar{\mathrm{I}}_4^{1/2}v'(\overline{\lambda}_{\mathrm{M}})+2(\eta^{-2/3}-\bar{\mathrm{I}}_4)w'(\mathrm{I}_{\mathrm{M}}^{\mathrm{r}})\right)\mathbf{M}+2w'(\mathrm{I}_{\mathrm{M}}^{\mathrm{r}})\overline{\mathbf{B}}\right)^{\mathrm{D}},
\end{aligned}\tag{4.61c}$$

which can also be represented by

$$\mathbf{T}_{\text{isc}} = \varrho_{\text{R}} \frac{\Theta}{\Theta_0} \left((\overline{\lambda}_{\text{M}} v'(\overline{\lambda}_{\text{M}}) + 2w'(\text{I}^{\text{r}}_{\text{M}})(1 - \bar{\text{I}}_{4\text{M}}))\mathbf{M} + 2w'(\text{I}^{\text{r}}_{\text{M}})\overline{\mathbf{B}}_{\text{M}} \right)^{D} . \tag{4.61d}$$

$\overline{\mathbf{B}}_{\text{M}}$ is the unimodular mechanical left Cauchy-Green tensor[1]

$$\begin{aligned} \overline{\mathbf{B}}_{\text{M}} &= \overline{\lambda}_{\text{M}}{}^{2} \left(1 - \eta^2\right) \mathbf{M} + \eta^{2/3}\, \overline{\mathbf{B}} \\ &= \eta^{2/3} \left(\bar{\text{I}}_4 (\eta^{-2} - 1)\mathbf{M} + \overline{\mathbf{B}} \right) . \end{aligned} \tag{4.62}$$

Note that, in the case of equal stretches, i.e., $\eta = 1$, the above equation yields

$$\overline{\mathbf{B}}_{\text{M}} = \overline{\mathbf{B}}, \tag{4.63}$$

which represents the case of isotropic thermoelasticity, see (Hamkar and Hartmann, 2012) or (Hartmann, 2012).

Substituting the derivatives of the strain-energy functions given in (4.56) in combination with the definitions of λ_{M}, J_{M}, $\overline{\lambda}_{\text{M}}$ and from (4.6b), (4.13) and (4.38c), respectively, in (4.59) and (4.61) yields the concrete forms of second Piola-Kirchhoff stress

$$\begin{aligned} \tilde{\mathbf{T}} =& \varrho_{\text{R}} \frac{\Theta}{\Theta_0} \Big(- \frac{K}{50} \zeta^{-1} \text{I}_4^{-1/2} \left(\left((\frac{J}{\zeta\varphi^2})^5 + (\frac{J}{\zeta\varphi^2})^{-5} - 2 \right) \mathbf{M}_0 + 5\text{I}_4^{-1} \left((\frac{J}{\zeta\varphi^2})^5 - (\frac{J}{\zeta\varphi^2})^{-5} \right) \mathbf{C}^{-1} \right) \\ &+ \left(\alpha(\eta^{-2/3} \bar{\text{I}}_4^{1/2} - \eta^2 \bar{\text{I}}_4^{-3/2}) + \beta(\bar{\text{I}}_4^{-1} - \eta^{2/3}) \right) \mathbf{M}_0 \overline{\mathbf{C}} + \beta \eta^{2/3} \overline{\mathbf{C}} \Big)^{\text{D}} \mathbf{C}^{-1} \end{aligned} \tag{4.64}$$

and the Cauchy stresses

$$\begin{aligned} \mathbf{T} =& \frac{\varrho_{\text{R}}}{J} \frac{\Theta}{\Theta_0} \Big(- \frac{K}{50} \zeta^{-1} \text{I}_4^{-1/2} \left(\left(\left(\frac{J}{\zeta\varphi^2} \right)^5 + \left(\frac{J}{\zeta\varphi^2} \right)^{-5} - 2 \right) \mathbf{M} + 5 \left(\left(\frac{J}{\zeta\varphi^2} \right)^5 - (\frac{J}{\zeta\varphi^2})^{-5} \right) \mathbf{1} \right) \\ &+ \left(\left(\alpha(\eta^{-2/3} \bar{\text{I}}_4^{3/2} - \eta^2 \bar{\text{I}}_4^{-1/2}) + \beta(1 - \eta^{2/3} \bar{\text{I}}_4) \right) \mathbf{M} + \beta \eta^{2/3} \overline{\mathbf{B}} \right)^{\text{D}} \Big), \end{aligned} \tag{4.65}$$

respectively. Five material parameters are included in this model, namely, the three parameters α, β and K of the mechanical subproblem and two additional parameters α_a and α_n, which are included in ζ and φ, respectively, related to the thermal subproblem. For the case of no change in temperature, i.e., $\Theta = \Theta_0$, the thermal stretches read $\zeta(0) = \hat{\zeta}(0) = 1$ and $\varphi(0) = \hat{\varphi}(0) = 1$, and consequently, the above constitutive equation of Cauchy stresses is reduced to the same equation given in (3.54) for isothermal hyperelasticity.

4.4. Investigation of the Model

In the following, the constitutive model in (4.61) is investigated under a simple tension test along and normal to the fiber direction. In this context, the deformation gradient and the unimodular left Cauchy-Green tensor have the same forms given Eqs.(3.56) and (3.58), respectively.

[1] For detailed calculations of Eq.(4.62) see Appendix A.8.

4.4.1. Simple Tension along the Fiber Direction

In this case, the fiber direction $\boldsymbol{m}$ is set to be aligned with x_1-axis of rectangular Cartesian coordinates in the current configuration, i.e. it is parallel to the loading direction. Thus, λ_1 and $\bar{\lambda}_1$ in Eqs.(3.56) and (3.58) represent the total and isochoric stretch ratios in the preferred direction λ_{a} and $\overline{\lambda}_{\mathrm{a}}$, respectively. From Eq.(4.61) , the three components of Cauchy stress tensor $\mathbf{T}$ are:

$$\sigma_{11} = \frac{\varrho_{\mathrm{R}}}{J}\frac{\Theta}{\Theta_0}\big(2\mathrm{I}_{4\mathrm{M}}\frac{\partial \upsilon(J_M,\mathrm{I}_{4\mathrm{M}})}{\partial \mathrm{I}_{4\mathrm{M}}} + J_M\frac{\partial \upsilon(J_M,\mathrm{I}_{4\mathrm{M}})}{\partial J_M} + \frac{2}{3}\overline{\lambda}_{\mathrm{M}}\upsilon'(\overline{\lambda}_{\mathrm{M}}) + \frac{2}{3}\eta^{2/3}w'(\mathrm{I}^{\mathrm{r}}_{\mathrm{M}})(2\eta^{-2/3} - \bar{\lambda}_2^2 - \bar{\lambda}_3^2)\big) \tag{4.66a}$$

$$0 = \sigma_{22} = \frac{\varrho_{\mathrm{R}}}{J}\frac{\Theta}{\Theta_0}\big(J_M\frac{\partial \upsilon(J_M,\mathrm{I}_{4\mathrm{M}})}{\partial J_M} - \frac{1}{3}\overline{\lambda}_{\mathrm{M}}\upsilon'(\overline{\lambda}_{\mathrm{M}}) + \frac{2}{3}\eta^{2/3}w'(\mathrm{I}^{\mathrm{r}}_{\mathrm{M}})(-\eta^{-2/3} + 2\bar{\lambda}_2^2 - \bar{\lambda}_3^2)\big) \tag{4.66b}$$

$$0 = \sigma_{33} = \frac{\varrho_{\mathrm{R}}}{J}\frac{\Theta}{\Theta_0}\big(J_M\frac{\partial \upsilon(J_M,\mathrm{I}_{4\mathrm{M}})}{\partial J_M} - \frac{1}{3}\overline{\lambda}_{\mathrm{M}}\upsilon'(\overline{\lambda}_{\mathrm{M}}) + \frac{2}{3}\eta^{2/3}w'(\mathrm{I}^{\mathrm{r}}_{\mathrm{M}})(-\eta^{-2/3} + 2\bar{\lambda}_3^2 - \bar{\lambda}_2^2)\big) \tag{4.66c}$$

Combining on Eqs.(4.66b) and (4.66c), leads to

$$\lambda_2 = \lambda_3 \tag{4.67a}$$

$$J_M\frac{\partial \upsilon(J_M,\mathrm{I}_{4\mathrm{M}})}{\partial J_M} = \frac{1}{3}\overline{\lambda}_{\mathrm{M}}\upsilon'(\overline{\lambda}_{\mathrm{M}}) - \frac{2}{3}\eta^{2/3}w'(\mathrm{I}^{\mathrm{r}}_{\mathrm{M}})(-\eta^{-2/3} + 2\bar{\lambda}_3^2 - \bar{\lambda}_2^2), \tag{4.67b}$$

and - by substituting the above equation in $(4.66)_1$ the stress component σ_{11} can be written as

$$\begin{aligned}\sigma_{11} &= \frac{\varrho_{\mathrm{R}}}{J}\frac{\Theta}{\Theta_0}\left(2\mathrm{I}_{4\mathrm{M}}\frac{\partial \upsilon(J_M,\mathrm{I}_{4\mathrm{M}})}{\partial \mathrm{I}_{4\mathrm{M}}} + \overline{\lambda}_{\mathrm{M}}\upsilon'(\overline{\lambda}_{\mathrm{M}}) + 2\eta^{2/3}w'(\mathrm{I}^{\mathrm{r}}_{\mathrm{M}})(\eta^{-2/3} - \bar{\lambda}_2^2)\right)\\ &= \frac{\varrho_{\mathrm{R}}}{J}\frac{\Theta}{\Theta_0}\left(2\mathrm{I}_{4\mathrm{M}}\frac{\partial \upsilon(J_M,\mathrm{I}_{4\mathrm{M}})}{\partial \mathrm{I}_{4\mathrm{M}}} + \overline{\lambda}_{\mathrm{M}}\upsilon'(\overline{\lambda}_{\mathrm{M}}) + 2w'(\mathrm{I}^{\mathrm{r}}_{\mathrm{M}})(1 - \eta^{2/3}\bar{\lambda}_2^2)\right).\end{aligned} \tag{4.68}$$

Furthermore, inserting the derivatives of the strain-energy functions, given in (4.56), and the definitions of λ_{M}, J_{M} and $\overline{\lambda}_{\mathrm{M}}$ form (4.6), (4.13) and (4.38c), respectively, into Eqs.$(4.68)_2$ and (4.67b), yield

$$\sigma_{11} = \frac{\varrho_{\mathrm{R}}}{J}\frac{\Theta}{\Theta_0}\left(-\frac{K}{50}\frac{\zeta}{\lambda_1}\left(\left(\frac{J}{\zeta\varphi^2}\right)^5 + \left(\frac{J}{\zeta\varphi^2}\right)^{-5} - 2\right) + \alpha\left(\frac{\bar{\lambda}_1^3}{\eta^2} - \frac{\bar{\lambda}_1^{-1}}{\eta^{-2/3}}\right) + \beta(1 - \eta^{2/3}\bar{\lambda}_2^2)\right) \tag{4.69}$$

and

$$\frac{K}{10}\frac{\zeta}{\lambda_1}\left(\left(\frac{J}{\zeta\varphi^2}\right)^5 + \left(\frac{J}{\zeta\varphi^2}\right)^{-5}\right) = \tfrac{1}{3}\left(\alpha\left(\frac{\bar{\lambda}_1^3}{\eta^2} - \frac{\bar{\lambda}_1^{-1}}{\eta^{-2/3}}\right) + \beta(1 - \eta^{2/3}\bar{\lambda}_2^2)\right) \tag{4.70}$$

representing the two equations required to evaluate the two unknown σ_{11} and λ_2.

4.4.2. Simple Tension Normal to the Fiber Direction

In the second test, the load is assumed to be applied normal to the fiber direction, where the fiber direction $\boldsymbol{m}_0$ is aligned with x_2-axis of rectangular Cartesian coordinates in the current configuration. Consequently, the three components of the stress-state in (4.61) read

$$\sigma_{11} = \frac{\varrho_{\mathrm{R}}}{J}\frac{\Theta}{\Theta_0}\big(J_M\frac{\partial \upsilon(J_M,\mathrm{I}_{4\mathrm{M}})}{\partial J_M}1\frac{1}{3}\overline{\lambda}_{\mathrm{M}}\upsilon'(\overline{\lambda}_{\mathrm{M}}) + \frac{2}{3}\eta^{2/3}w'(\mathrm{I}^{\mathrm{r}}_{\mathrm{M}})(-\eta^{-2/3}+2\bar{\lambda}_1^2-\bar{\lambda}_3^2)\big) \tag{4.71a}$$

$$0 = \sigma_{22} = \frac{\varrho_{\mathrm{R}}}{J}\frac{\Theta}{\Theta_0}\big(2\mathrm{I}_{4\mathrm{M}}\frac{\partial \upsilon(J_M,\mathrm{I}_{4\mathrm{M}})}{\partial \mathrm{I}_{4\mathrm{M}}} + J_M\frac{\partial \upsilon(J_M,\mathrm{I}_{4\mathrm{M}})}{\partial J_M} + \frac{2}{3}\overline{\lambda}_{\mathrm{M}}\upsilon'(\overline{\lambda}_{\mathrm{M}}) + \frac{2}{3}\eta^{2/3}w'(\mathrm{I}^{\mathrm{r}}_{\mathrm{M}})(2\eta^{-2/3}-\bar{\lambda}_1^2-\bar{\lambda}_3^2)\big) \tag{4.71b}$$

$$0 = \sigma_{33} = \frac{\varrho_{\mathrm{R}}}{J}\frac{\Theta}{\Theta_0}\big(J_M\frac{\partial \upsilon(J_M,\mathrm{I}_{4\mathrm{M}})}{\partial J_M} - \frac{1}{3}\overline{\lambda}_{\mathrm{M}}\upsilon'(\overline{\lambda}_{\mathrm{M}}) + \frac{2}{3}\eta^{2/3}w'(\mathrm{I}^{\mathrm{r}}_{\mathrm{M}})(-\eta^{-2/3}-\bar{\lambda}_1^2+2\bar{\lambda}_3^2)\big), \tag{4.71c}$$

i.e. three equations for the three unknowns σ_{11}, λ_2 and λ_3 are obtained.

4.5. Formulation of Transversely Isotropic Heat Flux Vector

In isotropic elasticity, the Cauchy heat flux vector is defined as

$$\boldsymbol{q} = -\kappa\,\mathrm{grad}\,\Theta, \tag{4.72}$$

see (Hamkar and Hartmann, 2012), where the thermal conductivity κ of the material is equal in all directions. For transversely isotropic materials, the thermal conductivity in the direction of isotropy is different to the thermal conductivity in the other orthogonal directions. To this end, the thermal conductivity tensor in spatial description $\boldsymbol{\kappa}_C$ is formulated as

$$\boldsymbol{\kappa}_C = (\kappa_a-\kappa_n)\boldsymbol{m}\otimes\boldsymbol{m} + \kappa_n\mathbf{1} = (\kappa_a-\kappa_n)\mathbf{M} + \kappa_n\mathbf{1}, \tag{4.73}$$

where κ_a and κ_n are the thermal conductivities of the bulk material along and normal to the fiber direction (direction of isotropy). Thus, the Cauchy heat flux vector for transversal isotropy reads

$$\boldsymbol{q} = -\boldsymbol{\kappa}_C\,\mathrm{grad}\,\Theta = -\left((\kappa_a-\kappa_n)\mathbf{M}+\kappa_n\mathbf{1}\right)\mathrm{grad}\,\Theta. \tag{4.74}$$

Making use of the property[1]

$$\mathrm{grad}\,\Theta = \mathbf{F}^{-\mathrm{T}}\,\mathrm{Grad}\,\Theta, \tag{4.75}$$

[1] See (Holzapfel, 2000, p.74).

in the above equation, and substituting the resulting equation into the definition of the Piola-Kirchhoff heat flux vector given in (2.76), yields

$$\boldsymbol{q}_{\mathrm{R}} = -\boldsymbol{\kappa}_R \operatorname{Grad}\Theta = -J\left(\mathrm{I}_4^{-1}(\kappa_a - \kappa_n)\mathbf{M}_0 + \kappa_n \mathbf{C}^{-1}\right)\operatorname{Grad}\Theta, \tag{4.76}$$

with

$$\begin{aligned}\boldsymbol{\kappa}_R = J\mathbf{F}^{-1}\boldsymbol{\kappa}_C\mathbf{F}^{-\mathrm{T}} &= J\mathbf{F}^{-1}\left((\kappa_a - \kappa_n)\mathbf{M} + \kappa_n \mathbf{1}\right)\mathbf{F}^{-\mathrm{T}} \\ &= J\left((\kappa_a - \kappa_n)\underbrace{\mathbf{F}^{-1}\mathbf{M}\mathbf{F}^{-\mathrm{T}}}_{\bar{\mathrm{I}}_4^{-1}\mathbf{M}_0} + \kappa_n \underbrace{\mathbf{F}^{-1}\mathbf{F}^{-\mathrm{T}}}_{\mathbf{C}^{-1}}\right) \\ &= J\left(\mathrm{I}_4^{-1}(\kappa_a - \kappa_n)\mathbf{M}_0 + \kappa_n \mathbf{C}^{-1}\right)\end{aligned} \tag{4.77}$$

represents the thermal conductivity tensor in the material representation, where

$$\mathbf{F}^{-1}\mathbf{M}\mathbf{F}^{-\mathrm{T}} = \mathbf{F}^{-1}(\boldsymbol{m}\otimes\boldsymbol{m})\mathbf{F}^{-\mathrm{T}} = \mathbf{F}^{-1}\boldsymbol{m}\otimes\mathbf{F}^{-1}\boldsymbol{m} = \lambda_{\mathrm{a}}^{-1}\boldsymbol{m}_0\otimes\lambda_{\mathrm{a}}^{-1}\boldsymbol{m}_0 = \bar{\mathrm{I}}_4^{-1}\mathbf{M}_0. \tag{4.78}$$

This formulation satisfies the inequality of the heat conduction in (4.48)

$$-\frac{1}{\Theta}\boldsymbol{q}_{\mathrm{R}}\cdot\operatorname{Grad}\Theta \;\geq 0, \tag{4.79}$$

where the thermal conductivity tensor $\boldsymbol{\kappa}_R$ in Eq.(4.76) is a positive definite tensor for positive thermal conductivities κ_a and κ_n, i.e. for $(\kappa_a, \kappa_n) > 0$.

4.6. Derivation of Heat Conduction Equation

In order to derive the heat conduction equation, the local form of energy balance (2.75b)

$$\dot{e} = -\frac{1}{\varrho_{\mathrm{R}}}\operatorname{Div}\boldsymbol{q}_{\mathrm{R}} + r + \frac{1}{\varrho_{\mathrm{R}}}\tilde{\mathbf{T}}\cdot\dot{\mathbf{E}} \tag{4.80a}$$

is combined with the time derivative of Eq.(2.89)

$$\dot{e} = \dot{\psi} + \dot{\Theta}s + \Theta\dot{\psi}, \tag{4.80b}$$

yielding

$$\dot{\psi} + \dot{\Theta}s + \Theta\dot{\psi} = -\frac{1}{\varrho_{\mathrm{R}}}\operatorname{Div}\boldsymbol{q}_{\mathrm{R}} + r + \frac{1}{\varrho_{\mathrm{R}}}\tilde{\mathbf{T}}\cdot\dot{\mathbf{E}}. \tag{4.81}$$

By substituting the stress power (4.31), the time derivative of the strain-energy function (4.44) and the specific entropy (4.47) with (4.46) into (4.81), we obtain

$$\Theta\dot{s} + \frac{1}{\varrho_{\mathrm{R}}}\operatorname{Div}\boldsymbol{q}_{\mathrm{R}} - r = 0. \tag{4.82}$$

Taking the time derivative of the specific entropy in (4.54) yields

$$\begin{aligned}\dot{s} =& \frac{\mathrm{d}}{\mathrm{d}t}\left(-\frac{1}{\Theta_0}\overline{\psi}_{\mathrm{M}} - \psi'_{\Theta} + \frac{1}{\varrho_{\mathrm{R}}}\frac{\varphi'}{\varphi}(\mathbf{P}\cdot\mathbf{1}) + \frac{1}{\varrho_{\mathrm{R}}}\left(\frac{\zeta'}{\zeta} - \frac{\varphi'}{\varphi}\right)(\mathbf{P}\cdot\mathbf{M}_0)\right)\\ =& -\frac{1}{\Theta_0}\frac{\partial\overline{\psi}_{\mathrm{M}}}{\partial\mathbf{C}}\cdot\dot{\mathbf{C}} - \frac{\mathrm{d}\psi'_{\Theta}}{\mathrm{d}\Theta}\dot{\Theta} + \frac{1}{\varrho_{\mathrm{R}}}\frac{\mathrm{d}}{\mathrm{d}t}\left(\frac{\varphi'}{\varphi}(\mathbf{P}\cdot\mathbf{1}) + \left(\frac{\zeta'}{\zeta} - \frac{\varphi'}{\varphi}\right)(\mathbf{P}\cdot\mathbf{M}_0)\right)\\ =& -\frac{1}{\Theta_0}\left[\frac{\partial\mathbf{C}_{\mathrm{M}}}{\partial\mathbf{C}}\right]^T\frac{\mathrm{d}\overline{\psi}_{\mathrm{M}}}{\mathrm{d}\mathbf{C}_{\mathrm{M}}}\cdot\dot{\mathbf{C}} - \psi''_{\Theta}\dot{\Theta} + \frac{1}{\varrho_{\mathrm{R}}}\frac{\mathrm{d}}{\mathrm{d}t}\left(\frac{\varphi'}{\varphi}(\mathbf{P}\cdot\mathbf{1}) + \left(\frac{\zeta'}{\zeta} - \frac{\varphi'}{\varphi}\right)(\mathbf{P}\cdot\mathbf{M}_0)\right)\\ =& c_{\mathrm{p}}\dot{\Theta} + d, \end{aligned} \tag{4.83}$$

where

$$\begin{aligned}c_{\mathrm{p}} = \frac{\Theta}{\varrho_{\mathrm{R}}}\Big[&-\psi''_{\Theta} + \frac{\varphi'}{\varphi}\frac{\partial(\mathbf{P}\cdot\mathbf{1})}{\partial\Theta} + \left(\frac{\varphi'}{\varphi}\right)^2(\mathbf{P}\cdot\mathbf{1}) + \left(\frac{\zeta'}{\zeta} - \frac{\varphi'}{\varphi}\right)\frac{\partial(\mathbf{P}\cdot\mathbf{M}_0)}{\partial\Theta}\\ &+\left(-\left(\frac{\zeta'}{\zeta}\right)^2 + \left(\frac{\varphi'}{\varphi}\right)^2\right)(\mathbf{P}\cdot\mathbf{M}_0)\Big], \end{aligned} \tag{4.84}$$

is the heat capacity[1] of the material body, and

$$d = \frac{1}{\varrho_{\mathrm{R}}}\left(\frac{1}{\Theta}\tilde{\mathbf{T}} + 2\frac{\varphi'}{\varphi}\frac{\partial(\mathbf{P}\cdot\mathbf{1})}{\partial\mathbf{C}} + 2\left(\frac{\zeta'}{\zeta} - \frac{\varphi'}{\varphi}\right)\frac{\partial(\mathbf{P}\cdot\mathbf{M}_0)}{\partial\mathbf{C}}\right)\cdot\dot{\mathbf{E}}, \tag{4.85}$$

represents the thermoelastic coupling, in which use of

$$\begin{aligned}\frac{1}{\Theta_0}\left[\frac{\partial\mathbf{C}_{\mathrm{M}}}{\partial\mathbf{C}}\right]^T\frac{\mathrm{d}\overline{\psi}_{\mathrm{M}}}{\mathrm{d}\mathbf{C}_{\mathrm{M}}} &= \frac{1}{\Theta_0}\left[\mathbf{F}_{\Theta}^{-1}\otimes\mathbf{F}_{\Theta}^{-1}\right]^{T_{23}}\frac{\mathrm{d}\overline{\psi}_{\mathrm{M}}}{\mathrm{d}\mathbf{C}_{\mathrm{M}}} = \frac{1}{2\varrho_{\mathrm{R}}\Theta}\mathbf{F}_{\Theta}^{-1}\frac{\mathrm{d}\overline{\psi}_{\mathrm{M}}}{\mathrm{d}\mathbf{C}_{\mathrm{M}}}\mathbf{F}_{\Theta}^{-\mathrm{T}}\\ &= \frac{1}{2\varrho_{\mathrm{R}}\Theta}\mathbf{F}_{\Theta}^{-1}\hat{\mathbf{S}}_{\Theta}\mathbf{F}_{\Theta}^{-\mathrm{T}} = \frac{1}{2\varrho_{\mathrm{R}}\Theta}\tilde{\mathbf{T}}\end{aligned} \tag{4.86}$$

is made.

Thus, inserting $\dot{s}$ from (4.83) into the heat conduction equation (4.82) yields the evolution equation of the temperature field

$$c_{\mathrm{p}}\dot{\Theta} = -\frac{1}{\varrho_{\mathrm{R}}}\operatorname{Div}\boldsymbol{q}_{\mathrm{R}} + r + d. \tag{4.87}$$

The specific heat capacity c_{p} can be assumed as a function of the temperature Θ only, see (Holzapfel, 2000).[2] Thus, if the terms in Eq.(4.84) associated to the deformation are ignored, then c_{p} can be approximated in the form

$$c_{\mathrm{p}}(\Theta) \approx \Theta\frac{\mathrm{d}^2\psi_{\Theta}(\Theta)}{\mathrm{d}\Theta\mathrm{d}\Theta}, \tag{4.88}$$

[1] The heat capacity of a material is defined as the amount of energy required to change the temperature of that material by $1^{\circ}\mathrm{C}$, (Halliday et al., 2001, Sec.20.2).

[2] Experimentally, the heat capacity of a composite material is measured for the bulk of the laminate as a function of the temperature alone, i.e. regardless the different phases of the composite, see (Cecen et al., 2009).

leading to the expression of the thermal strain-energy function

$$\psi_\Theta(\Theta) = \int_{\Theta_0}^{\Theta} \int_{\Theta_0}^{\Theta} \frac{1}{\Theta} c_\mathrm{p}(\Theta) \mathrm{d}\Theta. \tag{4.89}$$

According to (Heimes, 2005), for elastomers at temperatures above the glass transition temperature T_g, the specific heat capacity shows a linear dependence on the temperature. In the present work, the proposal for the specific heat capacity

$$c_\mathrm{p} = c_{\mathrm{p}0} \left(1 + c_{\mathrm{pk}}(\Theta - \Theta_0)\right), \tag{4.90}$$

see (Heimes, 2005) is used, where $c_{\mathrm{p}0}$ is the heat capacity at the reference temperature Θ_0. Thus, inserting (4.90) into (4.89) and applying the boundary conditions

$$\psi_\Theta(\Theta_0) = 0 \quad \text{and} \quad \frac{\mathrm{d}\psi_\Theta(\Theta_0)}{\mathrm{d}\Theta} = 0,$$

yield the concrete expression of the thermal strain-energy function

$$\psi_\Theta(\Theta) = \varrho_\mathrm{R} c_{\mathrm{p}0} \left(\left(\Theta - \Theta_0 - \Theta \ln \frac{\Theta}{\Theta_0} \right) (1 - c_{\mathrm{pk}} \Theta_0) - \frac{1}{2} c_{\mathrm{pk}} (\Theta - \Theta_0)^2 \right). \tag{4.91}$$

5. Numerical Solution

This chapter deals with the numerical solution of the boundary value problem (BVP) and the initial-boundary value problem (IBVP) resulting from the combination of the balance relations presented in Chapter 2 with the constitutive relations derived in Chapters 3 and 4 for the case of hyperelasticity and thermo-hyperelasticity, respectively. To this end, the finite element method (FEM), which is a main tool in Computational Mechanics today, is used. The aim of the finite element method is to use weak formulations to find an approximate solution to the BVP and the IBVP. The first section of this Chapter offers a brief introduction to the p-version of the finite element method. The second section deals with the local forms of the problems under consideration. The focus of the third section lies on the formulation of the weak forms required in the finite elements computations, followed by the last section in which the procedure of the numerical solution is presented.

5.1. p-Version Finite Element Method (p-FEM)

As mentioned above, the finite element method uses weak formulations to find an approximate solution to the problem under consideration. The accuracy of the solution is increased by decreasing the size of the elements, i.e. by refining the mesh as in the case of the classical version of the FEM (known as h-version), or by increasing the polynomial degree of the elements with a fixed mesh, as in the p-version of the FEM. For the analysis of large deformation problems, the p-FEM has been demonstrated to be an efficient tool, see (Düster et al., 2003) and (Yosibash et al., 2007). Furthermore, it has been shown that the p-FEM, with an appropriate p-level, is locking free for nearly incompressible problems in isotropic linear elasticity (Babuŝka and Suri, 1992a), (Babuŝka and Suri, 1992b) and for large deformation analyses of neo-Hookean solids (Heisserer et al., 2008). Moreover, the p-FEM is efficiently applied in the finite deformation analysis of various physical problems, e.g. hyperelasticity (Düster et al., 2003), (Yosibash et al., 2007) and (Netz et al., 2013a), viscoelasticity (Netz et al., 2013b) and thermo-visoelasticity (Netz, 2013), in the modeling of open-cell foams (Düster et al., 2005) and in the context of one-dimensional thermo-hyperelasticity (Yosibash et al., 2014). The use of elements with high polynomial degree makes the p-FEM more appropriate for the analysis of thin structure problems such as the laminated composite structures. In (Yosibash and Priel, 2011) and (Al-Kinani et al., 2014), the p-FEM is applied to simulate the behavior of anisotropic structures. By comparing the results with those obtained from the classical h-FEM, they were able to show that the p-FEM is more efficient than the h-FEM for this class of problems.

In this work, the p-FEM is chosen for the spatial discretization of the weak forms formulated in Section 5.3.

5.2. Local Form of IBVP

In this section, the local form of the initial-boundary value problem (IBVP) for the the case of thermo-mechanical coupled problem treated in Chapter 4, is formulated. For the boundary value problem (BVP) derived in Chapter. 3 the local form is obtained by omitting the terms related to the temperature and the heat flux vector. Appropriate initial and boundary conditions are required to solve the IBVP adequately. Since in many situations the inertia has a negligible effect on the analysis of the problem under consideration (Noll, 1995), a quasi-static analysis is considered. Thus, the acceleration term in the balance of momentum is omitted. The initial condition for the displacement field is set to be zero. For the temperature field, the initial condition over the material body $\mathcal{B}$ in the material representation reads

$$\Theta(\boldsymbol{X}, t_{\mathrm{i}}) = \Theta_0(\boldsymbol{X})\,, \qquad \text{for all } \boldsymbol{X} \in \mathcal{B}_R. \tag{5.1}$$

The boundary conditions of displacement (temperature), known as Dirichlet boundary condition, and the stress (heat flux), known as Neumann boundary condition, have to be prescribed on the surface of the material body. To this end, the surface $\partial\mathcal{B}$ of the material body $\mathcal{B}$ is decomposed into two parts: $\partial_{\mathrm{u}}\mathcal{B}$ ($\partial_{\Theta}\,\mathcal{B}$), where the displacement (the temperature) $\boldsymbol{u}$ (Θ) is applied and $\partial_{\mathrm{s}}\mathcal{B}$ ($\partial_{\mathrm{q}}\mathcal{B}$), where the stress vector $\boldsymbol{t}$ (heat flux vector $\boldsymbol{q}_{\mathrm{R}}$) is presented.[1] This decomposition is described in the material representation by

$$\partial\mathcal{B}_R = \overline{\partial_{\mathrm{u}}\mathcal{B}_R \cup \partial_{\mathrm{s}}\mathcal{B}_R}, \qquad \partial_{\mathrm{u}}\mathcal{B}_R \cap \partial_{\mathrm{s}}\mathcal{B}_R = \varnothing, \tag{5.2}$$

$$\mathcal{B}_R = \overline{\partial_{\Theta}\,\mathcal{B}_R \cup \partial_{\mathrm{q}}\mathcal{B}_R}, \qquad \partial_{\Theta}\,\mathcal{B}_R \cap \partial_{\mathrm{q}}\mathcal{B}_R = \varnothing, \tag{5.3}$$

and in the spatial representation by

$$\partial\mathcal{B}_C = \overline{\partial_{\mathrm{u}}\mathcal{B}_C \cup \partial_{\mathrm{s}}\mathcal{B}_C}, \qquad \partial_{\mathrm{u}}\mathcal{B}_C \cap \partial_{\mathrm{s}}\mathcal{B}_C = \varnothing, \tag{5.4}$$

$$\mathcal{B}_C = \overline{\partial_{\Theta}\,\mathcal{B}_C \cup \partial_{\mathrm{q}}\mathcal{B}_C}, \qquad \partial_{\Theta}\,\mathcal{B}_C \cap \partial_{\mathrm{q}}\mathcal{B}_C = \varnothing. \tag{5.5}$$

For the mechanical field, the Dirichlet boundary conditions assign the displacement $\boldsymbol{u}$ over the time interval $[t_{\mathrm{i}}, t_{\mathrm{e}}] \subset \mathbb{R}$ in the reference and current configuration, respectively, i.e.

$$\boldsymbol{u} = \boldsymbol{x} - \boldsymbol{X} = \boldsymbol{\chi}(\boldsymbol{X}, t) - \boldsymbol{X} = \boldsymbol{r}(\boldsymbol{X}, t) \qquad \text{for all } \boldsymbol{X} \in \partial_{\mathrm{u}}\mathcal{B}_R \text{ and } t \in [t_{\mathrm{i}}, t_{\mathrm{e}}]. \tag{5.6}$$

On the other hand, for the thermal field, the Dirichlet boundary conditions in the reference respectively spatial representation read

$$\Theta(\boldsymbol{X}, t) = \bar{\Theta}(\boldsymbol{X}, t) \qquad \text{for all } \boldsymbol{X} \in \partial_{\Theta}\,\mathcal{B}_R \text{ and } t \in [t_{\mathrm{i}}, t_{\mathrm{e}}] \tag{5.7}$$

$$\Theta(\boldsymbol{x}, t) = \bar{\Theta}(\boldsymbol{x}, t) \qquad \text{for all } \boldsymbol{x} \in \partial_{\Theta}\,\mathcal{B}_C \text{ and } t \in [t_{\mathrm{i}}, t_{\mathrm{e}}]. \tag{5.8}$$

The Neumann boundary conditions for the mechanical field, which naturally refer to the current configuration due to the fact that the surface forces act in the current configuration, are defined by prescribing the Cauchy stress vector

$$\boldsymbol{t} = \mathbf{T}\boldsymbol{n} = \bar{\boldsymbol{s}}(\boldsymbol{x}, t) \qquad \text{for all } \boldsymbol{x} \in \partial_{\mathrm{s}}\mathcal{B}_C \text{ and } t \in [t_{\mathrm{i}}, t_{\mathrm{e}}]. \tag{5.9}$$

[1] see (Haupt, 2002, Sec.2.3.5 and Sec.3.4).

Making use of (2.15) and

$$\mathrm{d}a = \sqrt{\mathrm{d}\boldsymbol{a}\cdot\mathrm{d}\boldsymbol{a}} = (\det\mathbf{F})\sqrt{\boldsymbol{n}_{\mathrm{R}}\cdot\mathbf{C}^{-1}\boldsymbol{n}_{\mathrm{R}}}\mathrm{d}A, \tag{5.10}$$

in combination with the definition of the body force $\boldsymbol{f} = \mathbf{T}\mathrm{d}\boldsymbol{a} = \mathbf{T}_{\mathrm{R}}\mathrm{d}\boldsymbol{A}$, see Eq.(2.33), the Neumann boundary condition can be formulated in the reference configuration by

$$\begin{aligned}\boldsymbol{t} &= \frac{1}{(\det\mathbf{F})\sqrt{\boldsymbol{n}_{\mathrm{R}}\cdot\mathbf{F}^{-1}\mathbf{F}^{-\mathrm{T}}\boldsymbol{n}_{\mathrm{R}}}}\mathbf{T}_{\mathrm{R}}\boldsymbol{n}_{\mathrm{R}} \\ &= \hat{\boldsymbol{s}}(\boldsymbol{X},t) = \bar{\boldsymbol{s}}(\boldsymbol{\chi}(\boldsymbol{X},t),t) \qquad \text{for all } \boldsymbol{X}\in\partial_{\mathrm{s}}\mathcal{B}_R \text{ and } t\in\ [t_{\mathrm{i}},t_{\mathrm{e}}].\end{aligned} \tag{5.11}$$

Here, the Cauchy stress vector $\boldsymbol{t}$ is deformation dependent.

For the thermal field, the Neumann boundary condition prescribes the heat flux q in the spatial representation as

$$q = -\boldsymbol{q}\cdot\boldsymbol{n} = \bar{f}_{\mathrm{q}}(\boldsymbol{x},t) \qquad \text{for all } \boldsymbol{x}\in\partial_{\mathrm{q}}\mathcal{B}_C \text{ and } t\in\ [t_{\mathrm{i}},t_{\mathrm{e}}], \tag{5.12}$$

which can also be formulated in the material representation as

$$\begin{aligned}q &= -\frac{1}{(\det\mathbf{F})\sqrt{\boldsymbol{n}_{\mathrm{R}}\cdot\mathbf{C}^{-1}\boldsymbol{n}_{\mathrm{R}}}}\boldsymbol{q}_{\mathrm{R}}\cdot\boldsymbol{n}_{\mathrm{R}} \\ &= \hat{f}_{\mathrm{q}}(\boldsymbol{X},t) = \bar{f}_{\mathrm{q}}(\boldsymbol{\chi}(\boldsymbol{X},t),t) \qquad \text{for all } \boldsymbol{X}\in\partial_{\mathrm{q}}\mathcal{B}_R \text{ and } t\in\ [t_{\mathrm{i}},t_{\mathrm{e}}],\end{aligned} \tag{5.13}$$

based on a similar argument to the one that led to Eq.(5.11). In Eq.(5.13), $\boldsymbol{q}_{\mathrm{R}}$ is the Lagrange (or Piola-Kirchhoff) heat flux vector and is related to $\boldsymbol{q}$ by Eq.(2.76). Tabs. 5.1 and 5.2 summarize the strong forms of the BVP and IBVP, respectively. As mentioned before, the strong forms can not be solved analytically. Instead, the FEM is used to find approximate solutions by using the weak forms that are formulated in the next section.

5.3. Weak Form of the IBVP

In the finite element method, the weak form is used to find an approximate solution to the BVP or IBVP. Unlike the strong form, which fulfills the equations point-wise, the weak form fulfills the equations in an average sense. In the following, the weak form of the IBVP given in Tab. 5.2 is formulated. The weak form of the BVP given in Tab. 5.1 can be formulated by ignoring the thermal field in the following formulation and taking only the terms related to the mechanical field into consideration.

The weak form of the IBVP is formulated by multiplying the strong form of the balance equations, i.e. balance of momentum and the heat conduction equation, by a test (or weighting) function and integrate over the body domain. Thus, the approximate solution of the IBVP is to find the trial functions

$$\boldsymbol{\mathcal{S}}_{u,t} =: \{\, \boldsymbol{u}(\,\cdot\,,t) \mid \boldsymbol{u}\,(\boldsymbol{X},t) = \bar{\boldsymbol{u}}(\boldsymbol{X},t) \text{ for all } \boldsymbol{X}\in\partial_{\mathrm{u}}\mathcal{B}_R \,\} \tag{5.14}$$

Table 5.1.: Strong form of the BVP.

Given the boundary conditions

$$\begin{aligned} \boldsymbol{u}(\boldsymbol{X},t) &= \bar{\boldsymbol{u}}(\boldsymbol{X},t) \qquad \text{for all } \boldsymbol{X} \in \partial_{\mathrm{u}}\mathcal{B}_R \text{ and } t \in [t_{\mathrm{i}}, t_{\mathrm{e}}], \\ \boldsymbol{t}_{\mathrm{R}}(\boldsymbol{X},t) &= \bar{\boldsymbol{t}}_R(\boldsymbol{X},\mathbf{F},t) \quad \text{for all } \boldsymbol{X} \in \partial_{\mathrm{s}}\mathcal{B}_R \text{ and } t \in [t_{\mathrm{i}}, t_{\mathrm{e}}], \end{aligned}$$

find $(\boldsymbol{u})$on$\mathcal{B}_R \times [t_{\mathrm{i}}, t_{\mathrm{e}}]$ such that

$$\mathbf{0} = \operatorname{Div}\mathbf{T}_{\mathrm{R}} + \varrho_{\mathrm{R}}\boldsymbol{f} \quad \text{on } \mathcal{B}_R \times [t_{\mathrm{i}}, t_{\mathrm{e}}],$$

with the constitutive relation

$$\tilde{\mathbf{T}} = \mathbf{h}\left(\mathbf{C}, \mathbf{M}_0\right),$$

where $\mathbf{T}_{\mathrm{R}} = \mathbf{F}\,\tilde{\mathbf{T}}$.

and

$$\mathcal{S}_{\theta,t} =: \left\{ \Theta(\,\cdot\,,t) \;\middle|\; \Theta(\boldsymbol{X},t) = \bar{\Theta}(\boldsymbol{X},t) \text{ for all } \boldsymbol{X} \in \partial_{\Theta}\mathcal{B}_R \right\} \tag{5.15}$$

for the displacement and the temperature, respectively, that satisfy the Dirichlet boundary conditions. The test functions must vanish where the Dirichlet boundary conditions are prescribed. For the displacement and for the temperature fields, respectively, they are defined as

$$\boldsymbol{\mathcal{V}}_u =: \left\{ \delta\boldsymbol{u} \colon \mathcal{B}_R \to \mathbb{R}^3 \;\middle|\; \delta\boldsymbol{u}\left(\boldsymbol{X}\right) = \mathbf{0} \text{ for all } \boldsymbol{X} \in \partial_{\mathrm{u}}\mathcal{B}_R \right\} \tag{5.16}$$

$$\mathcal{V}_\theta =: \left\{ \delta\Theta \colon \mathcal{B}_R \to \mathbb{R} \mid \delta\Theta(\boldsymbol{X}) = 0 \text{ for all } \boldsymbol{X} \in \partial_{\Theta}\mathcal{B}_R \right\}. \tag{5.17}$$

There is no need to enforce the Neumann boundary conditions explicitly where the weak form satisfies them automatically.[1]

5.3.1. Weak Form of the Balance of Momentum

In material representation, the quasi-static formulation of the weak form of the balance of momentum starts by multiplying the strong form given in Eq. (2.55b) with the test function defined in Eq. (5.16), i.e., with the virtual displacement $\delta\boldsymbol{u}$, and integrating over the domain $\mathcal{B}_R$, such that

$$\int_{\mathcal{B}_R} \left(\operatorname{Div}\mathbf{T}_{\mathrm{R}} + \varrho_{\mathrm{R}}\boldsymbol{f}\right) \cdot \delta\boldsymbol{u}\,\mathrm{d}V = \int_{\mathcal{B}_R} \operatorname{Div}\mathbf{T}_{\mathrm{R}} \cdot \delta\boldsymbol{u}\,\mathrm{d}V + \int_{\mathcal{B}_R} \varrho_{\mathrm{R}}\boldsymbol{f} \cdot \delta\boldsymbol{u}\,\mathrm{d}V = 0, \tag{5.18}$$

[1] See (Quint, 2012, p.87) and (Hamkar, 2013, p.64).

Table 5.2.: Strong form of the IBVP.

Given the initial conditions

$$\Theta(\boldsymbol{X}, t_{\mathrm{i}}) = \theta_{\mathrm{i}}(\boldsymbol{X}), \quad \text{for all} \boldsymbol{X} \in \mathcal{B}_R,$$

and the boundary conditions

$$\begin{aligned}
\boldsymbol{u}(\boldsymbol{X}, t) &= \boldsymbol{r}(\boldsymbol{X}, t) && \text{for all } \boldsymbol{X} \in \partial_{\mathrm{u}}\mathcal{B}_R \text{ and } t \in [t_{\mathrm{i}}, t_{\mathrm{e}}], \\
\boldsymbol{t}_{\mathrm{R}}(\boldsymbol{X}, t) &= \boldsymbol{s}(\boldsymbol{X}, \mathbf{F}, t) && \text{for all } \boldsymbol{X} \in \partial_{\mathrm{s}}\mathcal{B}_R \text{ and } t \in [t_{\mathrm{i}}, t_{\mathrm{e}}], \\
\Theta(\boldsymbol{X}, t) &= \hat{T}(\boldsymbol{X}, t) && \text{for all } \boldsymbol{X} \in \partial_{\Theta}\mathcal{B}_R \text{ and } t \in [t_{\mathrm{i}}, t_{\mathrm{e}}] \\
q(\boldsymbol{X}, t) &= \hat{f}_{\mathrm{q}}(\boldsymbol{X}, t) && \text{for all } \boldsymbol{X} \in \partial_{\mathrm{s}}\mathcal{B}_R \text{ and } t \in [t_{\mathrm{i}}, t_{\mathrm{e}}],
\end{aligned}$$

find $(\boldsymbol{u}, \Theta)\colon \mathcal{B}_R \times [t_{\mathrm{i}}, t_{\mathrm{e}}] \to \mathbb{R}^3 \times \mathbb{R}$ such that

$$\begin{aligned}
\mathbf{0} &= \operatorname{Div} \mathbf{T}_{\mathrm{R}} + \varrho_{\mathrm{R}} \boldsymbol{f} && \text{on } \mathcal{B}_R \times [t_{\mathrm{i}}, t_{\mathrm{e}}], \\
c_{\mathrm{p}} \dot{\Theta} &= -\frac{1}{\varrho_{\mathrm{R}}} \operatorname{Div} \boldsymbol{q}_{\mathrm{R}} + r + d && \text{on } \mathcal{B}_R \times [t_{\mathrm{i}}, t_{\mathrm{e}}],
\end{aligned}$$

with the constitutive relations

$$\begin{aligned}
\tilde{\mathbf{T}} &= \mathbf{h}\left(\mathbf{C}, \mathbf{M}_0, \Theta\right), \\
\boldsymbol{q}_{\mathrm{R}} &= -\boldsymbol{\kappa}_R \operatorname{Grad} \Theta.
\end{aligned}$$

which follows

$$\int_{\mathcal{B}_R} \operatorname{Div}\left(\mathbf{T}_{\mathrm{R}}^T \delta\boldsymbol{u}\right) \mathrm{d}V - \int_{\mathcal{B}_R} \mathbf{T}_{\mathrm{R}} \cdot \operatorname{Grad} \delta\boldsymbol{u} \mathrm{d}V + \int_{\mathcal{B}_R} \varrho_{\mathrm{R}} \boldsymbol{f} \cdot \delta\boldsymbol{u} \mathrm{d}V = 0, \tag{5.19}$$

where use of the identity

$$(\operatorname{Div} \mathbf{T}_{\mathrm{R}}) \cdot \delta\boldsymbol{u} = \operatorname{Div}\left(\mathbf{T}_{\mathrm{R}}^{\mathrm{T}} \delta\boldsymbol{u}\right) - \mathbf{T}_{\mathrm{R}} \cdot \operatorname{Grad} \delta\boldsymbol{u}, \tag{5.20}$$

is made. Applying the divergence-theorem to the first term in Eq. (5.19)

$$\int_{\mathcal{B}_R} \operatorname{Div}\left(\mathbf{T}_{\mathrm{R}}^{\mathrm{T}} \delta\boldsymbol{u}\right) \mathrm{d}V = \int_{\partial\mathcal{B}_R} \mathbf{T}_{\mathrm{R}}^{\mathrm{T}} \delta\boldsymbol{u} \cdot \boldsymbol{n}_{\mathrm{R}} \mathrm{d}A = \int_{\partial\mathcal{B}_R} \mathbf{T}_{\mathrm{R}}^{\mathrm{T}} \boldsymbol{n}_{\mathrm{R}} \cdot \delta\boldsymbol{u} \mathrm{d}A, \tag{5.21}$$

yields

$$\int_{\partial\mathcal{B}_R} \mathbf{T}_{\mathrm{R}}^{\mathrm{T}} \boldsymbol{n}_{\mathrm{R}} \cdot \delta\boldsymbol{u} \mathrm{d}A - \int_{\mathcal{B}_R} \mathbf{T}_{\mathrm{R}} \cdot \operatorname{Grad} \delta\boldsymbol{u} \mathrm{d}V + \int_{\mathcal{B}_R} \varrho_{\mathrm{R}} \boldsymbol{f} \cdot \delta\boldsymbol{u} \mathrm{d}V = 0. \tag{5.22}$$

Furthermore, making use of Eqs. (2.32) and (2.35), i.e., $\boldsymbol{t}_{\mathrm{R}} = \mathbf{T}_{\mathrm{R}}\boldsymbol{n}_{\mathrm{R}}$ and $\mathbf{T}_{\mathrm{R}} = \mathbf{F}\tilde{\mathbf{T}}$, and some rearrangements lead to

$$\int_{\partial\mathcal{B}_R} \boldsymbol{t}_{\mathrm{R}} \cdot \delta\boldsymbol{u}\mathrm{d}A - \int_{\mathcal{B}_R} \tilde{\mathbf{T}} \cdot \mathbf{F}^{\mathrm{T}} \operatorname{Grad}\delta\boldsymbol{u}\mathrm{d}V + \int_{\mathcal{B}_R} \varrho_{\mathrm{R}}\boldsymbol{f} \cdot \delta\boldsymbol{u}\mathrm{d}V = 0. \tag{5.23}$$

Since $\tilde{\mathbf{T}}$ is a symmetric tensor, then

$$\tilde{\mathbf{T}} \cdot \mathbf{F}^{\mathrm{T}} \operatorname{Grad}\delta\boldsymbol{u} = \tilde{\mathbf{T}} \cdot \tfrac{1}{2}\left(\mathbf{F}^{\mathrm{T}} \operatorname{Grad}\delta\boldsymbol{u} + \operatorname{Grad}^{\mathrm{T}}\delta\boldsymbol{u}\ \mathbf{F}\right) = \tilde{\mathbf{T}} \cdot \delta\mathbf{E}. \tag{5.24}$$

Thus, the weak form of the balance of momentum in the material representation reads

$$\int_{\mathcal{B}_R} \tilde{\mathbf{T}} \cdot \delta\mathbf{E}\mathrm{d}V = \int_{\partial\mathcal{B}_R} \boldsymbol{t}_{\mathrm{R}} \cdot \delta\boldsymbol{u}\mathrm{d}A + \int_{\partial\mathcal{B}_R} \varrho_{\mathrm{R}}\boldsymbol{f} \cdot \delta\boldsymbol{u}\mathrm{d}V \tag{5.25}$$

and can be identically formulated in the spatial representation as

$$\int_{\mathcal{B}_C} \mathbf{T} \cdot \operatorname{grad}\delta\boldsymbol{u}\mathrm{d}v = \int_{\partial\mathcal{B}_C} \boldsymbol{t} \cdot \delta\boldsymbol{u}\mathrm{d}a + \int_{\mathcal{B}_C} \varrho\boldsymbol{f} \cdot \delta\boldsymbol{u}\mathrm{d}v. \tag{5.26}$$

Table 5.3.: Weak form of the BVP.

Given the boundary conditions

$$\begin{aligned} \boldsymbol{u}(\boldsymbol{X},t) &= \boldsymbol{r}(\boldsymbol{X},t) \qquad \text{for all } \boldsymbol{X} \in \partial_{\mathrm{u}}\mathcal{B}_R \text{ and } t \in [t_{\mathrm{i}}, t_{\mathrm{e}}], \\ \boldsymbol{t}_{\mathrm{R}}(\boldsymbol{X},t) &= \boldsymbol{s}(\boldsymbol{X},\mathbf{F},t) \quad \text{for all } \boldsymbol{X} \in \partial_{\mathrm{s}}\mathcal{B}_R \text{ and } t \in [t_{\mathrm{i}}, t_{\mathrm{e}}], \end{aligned}$$

find $\boldsymbol{u} \in \boldsymbol{\mathcal{S}}_{u,t}$ such that for any $t \in [t_{\mathrm{i}}, t_{\mathrm{e}}]$

$$\int_{\mathcal{B}_R} \tilde{\mathbf{T}} \cdot \delta\mathbf{E}\mathrm{d}V - \int_{\partial\mathcal{B}_R} \boldsymbol{s} \cdot \delta\boldsymbol{u}\mathrm{d}A + \int_{\partial\mathcal{B}_R} \varrho_{\mathrm{R}}\boldsymbol{f} \cdot \delta\boldsymbol{u}\mathrm{d}V = 0, \quad \text{for all} \delta\boldsymbol{u} \in \boldsymbol{\mathcal{V}}_u,$$

with the constitutive relations

$$\tilde{\mathbf{T}} = \mathbf{h}\left(\mathbf{C}, \mathbf{M}_0\right).$$

5.3.2. Weak Form of the Heat Conduction Equation

To formulate the weak form of the heat conduction equation, an analogous procedure to that used in the preceding Sec. 5.3.1 is applied, where the strong form of the heat conduction equation Eq. (4.87) is multiplied by the virtual temperature $\delta\Theta$ defined in Eq. (5.17) and integrated over the domain $\mathcal{B}_R$ as

$$\int_{\mathcal{B}_R} c_{\mathrm{p}}\dot{\Theta}\delta\Theta \mathrm{d}V = -\int_{\mathcal{B}_R} \frac{1}{\varrho_{\mathrm{R}}} \left(\mathrm{Div}\, \boldsymbol{q}_{\mathrm{R}}\right) \delta\Theta \mathrm{d}V + \int_{\mathcal{B}_R} (r+d)\delta\Theta \mathrm{d}V. \tag{5.27}$$

Making use of the equality

$$\mathrm{Div}\left(\boldsymbol{q}_{\mathrm{R}}\delta\Theta\right) = \boldsymbol{q}_{\mathrm{R}} \cdot \mathrm{Grad}\, \delta\Theta + \delta\Theta \left(\mathrm{Div}\, \boldsymbol{q}_{\mathrm{R}}\right), \tag{5.28}$$

then, the first term in the right-hand side of Eq. (5.27) can be written as

$$\int_{\mathcal{B}_R} \frac{1}{\varrho_{\mathrm{R}}} \left(\mathrm{Div}\, \boldsymbol{q}_{\mathrm{R}}\right) \delta\Theta \mathrm{d}V = -\int_{\mathcal{B}_R} \frac{1}{\varrho_{\mathrm{R}}} \mathrm{Div}\left(\boldsymbol{q}_{\mathrm{R}}\delta\Theta\right) \mathrm{d}V + \int_{\mathcal{B}_R} \frac{1}{\varrho_{\mathrm{R}}} \boldsymbol{q}_{\mathrm{R}} \cdot \mathrm{Grad}\, \delta\Theta \mathrm{d}V. \tag{5.29}$$

Furthermore, applying the divergence-theorem to the first term in the right-hand side of Eq. (5.29) and substituting the resulting equation in Eq. (5.27) with some rearrangements yields the material representation of the weak form of the heat conduction equation

$$\int_{\mathcal{B}_R} \varrho_{\mathrm{R}} c_{\mathrm{p}}\dot{\Theta}\delta\Theta \mathrm{d}V - \int_{\mathcal{B}_R} \boldsymbol{q}_{\mathrm{R}} \cdot \mathrm{Grad}\, \delta\Theta \mathrm{d}V = -\int_{\partial\mathcal{B}_R} \boldsymbol{q}_{\mathrm{R}} \cdot \boldsymbol{n}_{\mathrm{R}}\delta\Theta \mathrm{d}A + \int_{\mathcal{B}_R} \varrho_{\mathrm{R}}(r+d)\delta\Theta \mathrm{d}V. \tag{5.30}$$

The spatial representation of the weak form of the heat conduction equation reads

$$\int_{\mathcal{B}_C} \varrho c_{\mathrm{p}}\dot{\Theta}\delta\Theta \mathrm{d}v - \int_{\mathcal{B}_C} \boldsymbol{q} \cdot \mathrm{grad}\, \delta\Theta \mathrm{d}v = -\int_{\partial\mathcal{B}_C} \boldsymbol{q} \cdot \boldsymbol{n}\delta\Theta \mathrm{d}a + \int_{\mathcal{B}_C} \varrho(r+d)\delta\Theta \mathrm{d}v. \tag{5.31}$$

Tabs. 5.3 and 5.4 summarize the weak forms of the BVP and IBVP, respectively.

5.4. Numerical Solution using TASA-FEM

The weak forms of the BVP and the IBVP, given in Tabs. 5.3 and 5.4, respectively, are solved numerically using the in-house finite elements code TASA-FEM, see (Hartmann, 2006a), which is able to perform high-order in space and high-order in time computations. Here, the two step solution procedure is considered: the spatial discretization is carried out first, followed by the time disdretization, see (Hartmann and Rothe, 2013).

The p-version finite element method (p-FEM) is used for the spatial discretization of the weak forms using hierarchic shape functions based on integrated Legendre polynomials are utilized.

Table 5.4.: Weak form of the IBVP.

Given the initial conditions

$$\Theta(\boldsymbol{X}, t_{\mathrm{i}}) = \theta_{\mathrm{i}}(\boldsymbol{X}), \quad \text{for all} \boldsymbol{X} \in \mathcal{B}_R,$$

and the boundary conditions

$$\begin{aligned}
\boldsymbol{u}(\boldsymbol{X}, t) &= \boldsymbol{r}(\boldsymbol{X}, t) && \text{for all } \boldsymbol{X} \in \partial_{\mathrm{u}}\mathcal{B}_R \text{ and } t \in [t_{\mathrm{i}}, t_{\mathrm{e}}], \\
\boldsymbol{t}_{\mathrm{R}}(\boldsymbol{X}, t) &= \boldsymbol{s}(\boldsymbol{X}, \mathbf{F}, t) && \text{for all } \boldsymbol{X} \in \partial_{\mathrm{s}}\mathcal{B}_R \text{ and } t \in [t_{\mathrm{i}}, t_{\mathrm{e}}], \\
\Theta(\boldsymbol{X}, t) &= \hat{T}(\boldsymbol{X}, t) && \text{for all } \boldsymbol{X} \in \partial_{\Theta}\mathcal{B}_R \text{ and } t \in [t_{\mathrm{i}}, t_{\mathrm{e}}] \\
q(\boldsymbol{X}, t) &= \hat{f}_{\mathrm{q}}(\boldsymbol{X}, t) && \text{for all } \boldsymbol{X} \in \partial_{\mathrm{s}}\mathcal{B}_R \text{ and } t \in [t_{\mathrm{i}}, t_{\mathrm{e}}],
\end{aligned}$$

find $\boldsymbol{u} \in \boldsymbol{\mathcal{S}}_{u,t}$ and $\Theta \in \mathcal{S}_{\theta,t}$ such that for any $t \in [t_{\mathrm{i}}, t_{\mathrm{e}}]$

$$\begin{aligned}
\pi_{\mathrm{u}}\big(\boldsymbol{u}, \Theta, \delta\boldsymbol{u}\big) = \int_{\mathcal{B}_R} \tilde{\mathbf{T}} \cdot \delta\mathbf{E} \mathrm{d}V \; &- \int_{\partial\mathcal{B}_R} \boldsymbol{s} \cdot \delta\boldsymbol{u} \mathrm{d}A \\
&+ \int_{\mathcal{B}_R} \varrho_{\mathrm{R}} \boldsymbol{f} \cdot \delta\boldsymbol{u} \mathrm{d}V = 0, \quad \text{for all} \delta\boldsymbol{u} \in \boldsymbol{\mathcal{V}}_u,
\end{aligned}$$

$$\begin{aligned}
\pi_{\Theta}(\boldsymbol{u}, \Theta, \delta\Theta) &= \int_{\mathcal{B}_R} \varrho_{\mathrm{R}}(c_{\mathrm{p}}\dot{\Theta} - r + d)\delta\Theta \mathrm{d}V \\
&- \int_{\mathcal{B}_R} \boldsymbol{q}_{\mathrm{R}} \cdot \operatorname{Grad} \delta\Theta \mathrm{d}V + \int_{\partial\mathcal{B}_R} q\delta\Theta \mathrm{d}A = 0, \quad \text{for all} \delta\Theta \in \mathcal{V}_\theta,
\end{aligned}$$

with the constitutive relations

$$\begin{aligned}
\tilde{\mathbf{T}} &= \mathbf{h}\left(\mathbf{C}, \mathbf{M}_0, \Theta\right) \\
\boldsymbol{q}_{\mathrm{R}} &= -\boldsymbol{\kappa}_R \operatorname{Grad} \Theta.
\end{aligned}$$

To this end, shape functions N_j are defined to approximate the unknown quantities for the mechanical field (i.e. displacement and virtual displacement) as

$$\boldsymbol{u}^h(\mathbf{x}, t) = \boldsymbol{N}_{\mathrm{ad}}(\mathbf{x})\boldsymbol{u}_{\mathrm{a}}(t) = \boldsymbol{N}_{\mathrm{d}}(\mathbf{x})\,\boldsymbol{u}(t) + \overline{\boldsymbol{N}}_{\mathrm{d}}(\mathbf{x})\,\overline{\boldsymbol{u}}(t), \tag{5.32}$$

$$\delta\boldsymbol{u}^h(\mathbf{x}) = \boldsymbol{N}_{\mathrm{d}}(\mathbf{x})\,\delta\boldsymbol{u}, \tag{5.33}$$

and for the thermal field (i.e. temperature and virtual temperature) as

$$\Theta^h(\mathbf{x},t) = \boldsymbol{N}_{\mathrm{a}\Theta}^{\mathrm{T}}(\mathbf{x})\boldsymbol{\Theta}_{\mathrm{a}}(t) = \boldsymbol{N}_{\Theta}^{\mathrm{T}}(\mathbf{x})\boldsymbol{\Theta}(t) + \overline{\boldsymbol{N}}_{\Theta}^{\mathrm{T}}(\mathbf{x})\overline{\boldsymbol{\Theta}}(t) \tag{5.34}$$

$$\delta\Theta^h(\mathbf{x},t) = \boldsymbol{N}_{\Theta}^{\mathrm{T}}(\mathbf{x})\delta\boldsymbol{\Theta}, \tag{5.35}$$

where $\boldsymbol{u}_{\mathrm{a}}$ and $\boldsymbol{\Theta}_{\mathrm{a}}$ contain all coefficients of the displacement and temperature fields, respectively, and each of them is splitted into two parts, $\boldsymbol{u}$, $\overline{\boldsymbol{u}}$ contain the unknown respectively prescribed displacement coefficients, while the unknown and prescribed coefficients of the temperature are contained in $\boldsymbol{\Theta}$ and $\overline{\boldsymbol{\Theta}}$. For detailed discussions of the hierarchic shape functions, see (Szabo and Babuska, 1991), (Düster, 2001) and (Zienkiewicz et al., 2005). Applying the spatial discretization to the weak forms of BVP and IBVP will result in a system of algebraic equations and differential-algebraic equations (DAE), respectively.[1] For the IBVP, the DAE-system reads[2]

$$\boldsymbol{0} = \boldsymbol{g}\left(\boldsymbol{u}(t),\boldsymbol{\Theta}(t),t\right) \tag{5.36a}$$

$$\boldsymbol{C}_{\mathrm{p}}(\boldsymbol{\Theta},t)\dot{\boldsymbol{\Theta}}(t) = \boldsymbol{r}\left(\boldsymbol{u}(t),\dot{\boldsymbol{u}}(t),\boldsymbol{\Theta}(t),t\right) \tag{5.36b}$$

with the initial conditions

$$\boldsymbol{u}(t_0) = \boldsymbol{0} \quad \text{and} \quad \boldsymbol{\Theta}(t_0) = \boldsymbol{\Theta}_0, \tag{5.37}$$

where Eqs.(5.36a) and (5.36b) representing the matrix forms of the spatially discretized weak forms of the balance of linear momentum and heat conduction equation given in Tab. 5.4, respectively. Making use of the ϵ-embedding method,[3] the DAE-system in (5.36) can be regularized as

$$\epsilon\dot{\boldsymbol{u}}(t) = \boldsymbol{g}\left(\boldsymbol{u}(t),\boldsymbol{\Theta}(t),t\right) \tag{5.38a}$$

$$\boldsymbol{C}_{\mathrm{p}}(\boldsymbol{\Theta}(t),t)\dot{\boldsymbol{\Theta}}(t) = \boldsymbol{r}\left(\boldsymbol{u}(t),\dot{\boldsymbol{u}}(t),\boldsymbol{\Theta}(t),t\right), \tag{5.38b}$$

where the algebraic equation (5.36a) is replaced by the ordinary differential equation (ODE)

$$\epsilon\dot{\boldsymbol{u}}(t) = \boldsymbol{g}\left(\boldsymbol{u}(t),\boldsymbol{\Theta}(t),t\right), \tag{5.39}$$

which depends on the small parameter $0 < \epsilon \ll 1$.

Several numerical methods are available for solving a system of equations of the form (5.38), see e.g. (Brenan et al., 1996), (Hairer and Wanner, 2002), (Kunkel and Mehrmann, 2006) and (Rothe et al., 2012). The simplest method is the backward (implicit) Euler method, in which the derivative of the differential equation at the current time step t_{n+1} is approximated by a backward variation, i.e. making use of the solution at the previous time step t, see (Gear, 1971), (Petzold,

[1] Spatial discretization of a weak form of IBVP using p-FEM is presented in details by (Netz, 2013), where the problem of thermo-viscoelasticity is considered.

[2] See also (Hamkar and Hartmann, 2012), (Hamkar, 2013), (Netz, 2013) and (Hartmann and Rothe, 2013).

[3] See (Hairer and Wanner, 2002, p.374).

1982) and (Hairer et al., 2008) among more others. Thus, applying the backward Euler method to the system of equations in (5.38) yields

$$\epsilon \frac{\boldsymbol{u}_{n+1} - \boldsymbol{u}_n}{\Delta t} = \boldsymbol{g}\left(\boldsymbol{u}_{n+1}, \boldsymbol{\Theta}_{n+1}, t_{n+1}\right) \tag{5.40a}$$

$$\boldsymbol{C}_{\mathrm{p}}(\boldsymbol{\Theta}_{n+1}, t_{n+1}) \frac{\boldsymbol{\Theta}_{n+1} - \boldsymbol{\Theta}_n}{\Delta t} = \boldsymbol{r}\left(\boldsymbol{u}_{n+1}, \frac{\boldsymbol{u}_{n+1} - \boldsymbol{u}_n}{\Delta t}, \boldsymbol{\Theta}_{n+1}, t_{n+1}\right), \tag{5.40b}$$

with $\boldsymbol{u}_{n+1}(\boldsymbol{\Theta}_{n+1})$ and $\boldsymbol{u}_n(\boldsymbol{\Theta}_n)$ as the column matrices of the unknown displacement (temperature) coefficients at time step t_{n+1} and t_n, respectively, and $\Delta t = t_{n+1} - t_n$ is the step size. For $\epsilon \to 0$ the system of equations in (5.40a) is reduced to

$$\boldsymbol{0} = \boldsymbol{g}\left(\boldsymbol{u}_{n+1}, \boldsymbol{\Theta}_{n+1}, t_{n+1}\right) \tag{5.41}$$

Thus, applying the temporal discretization to the DAE-system results in a system of non-linear equations

$$\left\{ \begin{array}{c} \boldsymbol{G}_{\mathrm{u}}(\boldsymbol{u}_{n+1}, \boldsymbol{\Theta}_{n+1}) \\ \boldsymbol{G}_{\Theta}\left(\boldsymbol{u}_{n+1}, \boldsymbol{\Theta}_{n+1}\right) \end{array} \right\} = \boldsymbol{0}, \tag{5.42}$$

where

$$\boldsymbol{G}_{\mathrm{u}}(\boldsymbol{u}_{n+1}, \boldsymbol{\Theta}_{n+1}) \equiv \boldsymbol{g}\left(\boldsymbol{u}_{n+1}, \boldsymbol{\Theta}_{n+1}, t_{n+1}\right)$$

and

$$\boldsymbol{G}_{\Theta}\left(\boldsymbol{u}_{n+1}, \boldsymbol{\Theta}_{n+1}\right) \equiv \boldsymbol{C}_{\mathrm{p}}(\boldsymbol{\Theta}_{n+1}, t_{n+1}) \frac{\boldsymbol{\Theta}_{n+1} - \boldsymbol{\Theta}_n}{\Delta t} - \boldsymbol{r}\left(\boldsymbol{u}_{n+1}, \frac{\boldsymbol{u}_{n+1} - \boldsymbol{u}_n}{\Delta t}, \boldsymbol{\Theta}_{n+1}, t_{n+1}\right).$$

By introducing the vector of unknowns

$$\boldsymbol{y}_{n+1} = \left\{ \begin{array}{c} \boldsymbol{u}_{n+1} \\ \boldsymbol{\Theta}_{n+1} \end{array} \right\} \tag{5.44}$$

the system of non-linear equations in (5.42) can be represented by

$$\boldsymbol{G}(\boldsymbol{y}_{n+1}) = \boldsymbol{0}. \tag{5.45}$$

For the time discretization of this system of equations, the in-house finite elements code TASA-FEM makes use of time-adaptive high-order diagonally implicit Runge-Kutta (DIRK) methods. It has been shown that time-adaptive high-order DIRK methods are efficient for performing computations to solve different types of problems, see (Diebels et al., 1999), (Ellsiepen and Hartmann, 2001), (Hartmann, 2002a), (Hartmann, 2006b), (Hartmann and Bier, 2008), (Hartmann et al., 2008) and (Hamkar and Hartmann, 2012). In the DIRK methods, the time domain is divided into N time-steps, and each time-step n is divided into s stages. A system of non-linear equations of the form (5.45) has to be solved at each stage i, see (Alexander, 1977), (Hartmann, 2001), (Ellsiepen and Hartmann, 2001), (Quint, 2012) and (Netz, 2013). The system

of non-linear equations is solved using the Newton-Raphson method (NRM), see (Deuflhard, 2006). To this end, a system of the form (5.45) is expanded to the form of a Taylor series

$$\boldsymbol{G}(\boldsymbol{y}) = \boldsymbol{G}(\boldsymbol{y}_0) + \frac{\mathrm{d}\boldsymbol{G}(\boldsymbol{y})}{\mathrm{d}\boldsymbol{y}}\Big|_{\boldsymbol{y}=\boldsymbol{y}_0} \{\boldsymbol{y} - \boldsymbol{y}_0\} + \dots \tag{5.46}$$

The root of the above equation is approximated by neglecting the high-order terms, i.e.

$$\boldsymbol{G}(\boldsymbol{y}) \approx \boldsymbol{G}(\boldsymbol{y}_0) + \frac{\mathrm{d}\boldsymbol{G}(\boldsymbol{y})}{\mathrm{d}\boldsymbol{y}}\Big|_{\boldsymbol{y}=\boldsymbol{y}_0} \{\boldsymbol{y} - \boldsymbol{y}_0\}, \tag{5.47}$$

where $\boldsymbol{y}_0$ represents the starting value of the unknown $\boldsymbol{y}$. This equation is solved in an iterative manner to find the increment $\Delta\boldsymbol{y} = \boldsymbol{y}^{m+1} - \boldsymbol{y}^m$ that makes $\boldsymbol{G}(\boldsymbol{y}^m)$ vanish

$$\frac{\mathrm{d}\boldsymbol{G}(\boldsymbol{y})}{\mathrm{d}\boldsymbol{y}}\Big|_{\boldsymbol{y}=\boldsymbol{y}^m} \Delta\boldsymbol{y} = -\boldsymbol{G}(\boldsymbol{y}^m), \tag{5.48}$$

with the iteration index m. The iteration process of solving the system of linear equations (5.48) is continued until the value of $\Delta\boldsymbol{y}$ is obtained, at which the error associated to the approximate solution is less than the prescribed tolerance. For the application of NRM in non-linear finite elements analysis see (Hartmann, 2004) or (Hartmann, 2005) and references cited therein.

6. Numerical Examples

This Chapter focuses on illustrating the capability of the two constitutive models formulated in Chapters 3 and 4 to model transversely isotropic fiber-reinforced composites. Due to its applicability and efficiency in the context of hyperelasticity, see Sect. 5.1, the p-version finite elements based on integrated Legendre-polynomials is used in the numerical simulations. The computations are carried out using the in-house finite elements code TASA-FEM, see Sect. 5.4. The first section of this Chapter includes two numerical examples, which demonstrate the behavior of the hyperelastic model presented in Chapter 3. In the first example, Cook's membrane problem subjected to a shear load is considered in order to show the influence of the anisotropy on the behavior of the structure. Furthermore, in order to show the efficiency and accuracy of the p-version finite elements, a comparison between the classical h-version finite elements and p-version finite elements is carried out. The influence of the fiber orientation on the material response is investigated in the second example, where the simple tension problem is considered.

The behavior of the thermal-hyperelastic constitutive model, formulated in Chapter 4, is depicted by another example, in order to examine the the problem of a perforated plate subjected to thermal and thermo-mechanical coupled deformations. In this context, the influence of the anisotropic thermal expansion, anisotropic thermal conductivity and different fiber orientations on the thermal and thermo-mechanical responses of the composite material is studied.

6.1. Isothermal Analysis

In the numerical computations included in this section, the material parameters given in Tab. 3.1 are employed. Several of the following results are published in (Al-Kinani et al., 2012) and (Al-Kinani et al., 2014).

6.1.1. Cook's Membrane

In order to show the effects that anisotropy exerts on the behavior of structures, the example of Cook's membrane subjected to a shear deformation in vertical direction is considered. Fig. 6.1 shows the geometry and boundary conditions of the problem, as well as the p-mesh. The Cook's membrane is fixed on the left-hand side. The displacement u_y is applied on the right-hand side in vertical direction, linearly increases up to $8\mathrm{mm}$. The thickness of the cantilever is set to $1\mathrm{mm}$. Three elements are used - with $0.1\mathrm{mm}$, $0.8\mathrm{mm}$ and $0.1\mathrm{mm}$ in the thickness direction - and the structure is discretized into 42 p-elements. In addition, the direction of isotropy (fiber direction) is defined by $\boldsymbol{m}_0 = 1/\sqrt{3}(\boldsymbol{e}_x + \boldsymbol{e}_y + \boldsymbol{e}_z)$. The first computation is done using a polynomial degree

of 8. As shown in Fig. 6.2, a strongly pronounced out-of-plane bending deformation occurs due to the existence of anisotropy.

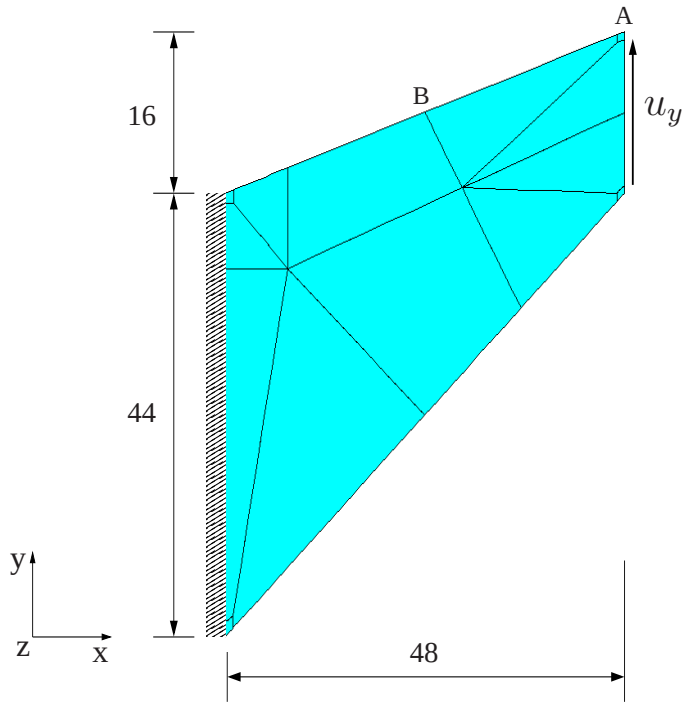

Figure 6.1.: Geometry, boundary conditions and p-mesh of Cook's membrane used in the finite element investigation (measures in mm, depth = $1\mathrm{mm}$).

The same example is investigated by means of an h-FEM implementation, where an initial discretization, see Fig. 6.3 has $20 \times 20 \times 5$ eight-noded hexahedral elements ($n_{ex} \times n_{ey} \times n_{ez}$ defines n_{ex} elements horizontally, n_{ey} elements vertically and n_{ez} elements in thickness direction). As shown in Fig. 6.4, an out-of-plane deformation similar to that observed by (Schröder and Neff, 2003) is obtained, which differs from the S-shaped out-of-plane deformation resulting from the p-FEM computation in Fig. 6.2. Applying a much finer discretization like that shown in Fig. 6.6(d), in which the cantilever is discretized using $75 \times 75 \times 5$ elements, leads to an S-shaped out-of-plane bending deformation. This demonstrates that structures made of anisotropic composites are very sensitive to the discretization used in the finite element computations, as depicted in Fig. 6.5(b). In the following, the mesh and p-level sensitivity are therefore investigated in more details. In order to show this effect, h-version finite element computations are applied making use of eight-noded linear elements and twenty-noded quadratic elements with four different discretizations which are shown in Fig. 6.6. Tab. 6.1 shows the number of degree of freedom of the h-version discretization. Moreover, p-version finite element computations are performed using a polynomial degree from one to ten, i.e., $p = 1, 2, \ldots, 10$.[1] The number of degrees of freedom (DOF) for the p-version discretizations is given in Tab. 6.2. The results of both h-version and p-

[1]The displacements of nodes A and B in Fig 6.1 are given in Appendix A.9 for some p-FEM computations.

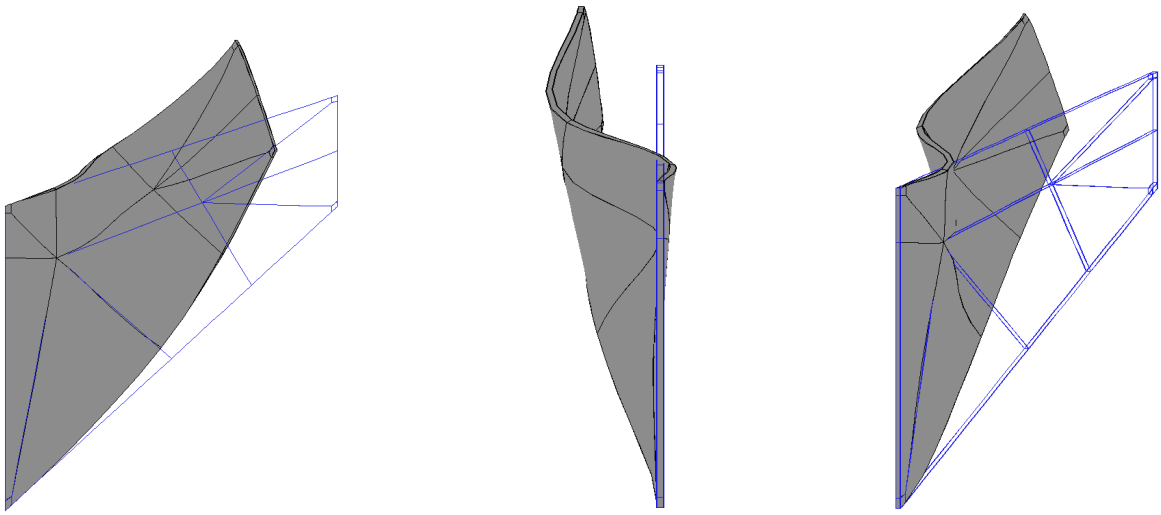

(a) $x-y$ view of the deformed configuration for $u_y = 8\text{mm}$.

(b) $y-z$ view of the deformed configuration for $u_y = 8\text{mm}$.

(c) 3D view of the deformed configuration for $u_y = 8\text{mm}$.

Figure 6.2.: Deformed vs. original views of the tapered cantilever used in p-FEM computations with $p = 8$ and $\boldsymbol{m}_0 = 1/\sqrt{3}(\boldsymbol{e}_x + \boldsymbol{e}_y + \boldsymbol{e}_z)$.

Table 6.1.: Number of degrees of freedom of the h-version discretizations.

mesh	1	2	3	4
discretization	$30 \times 20 \times 5$	$45 \times 30 \times 5$	$60 \times 40 \times 5$	$75 \times 50 \times 5$
8-noded elements	11718	25668	45018	69768
20-noded elements	43983	97008	170733	265158

version computations are compared with a high resolution reference solution, which is obtained by using a fine p-mesh consisting of 208 p-elements and a polynomial degree of 11, yielding 142896 degrees of freedom, as shown in Fig. 6.7(a). The background grid shown in Fig. 6.7(b) is used to evaluate the results of both the reference solution and the h-version and p-version computations for the error investigation. The relative errors in displacements, respectively, stresses are computed by

$$\epsilon_u \,\% = \sqrt{\frac{\sum_{k=1}^{3n_{\text{evp}}} (u_k - u_{\text{ex}k})^2}{\sum_{k=1}^{3n_{\text{evp}}} (u_{\text{ex}k})^2}} \times 100 \tag{6.1a}$$

and

$$\epsilon_T \,\% = \sqrt{\frac{\sum_{k=1}^{6n_{\text{evp}}} (t_k - t_{\text{ex}k})^2}{\sum_{k=1}^{6n_{\text{evp}}} (t_{\text{ex}k})^2}} \times 100 \tag{6.1b}$$

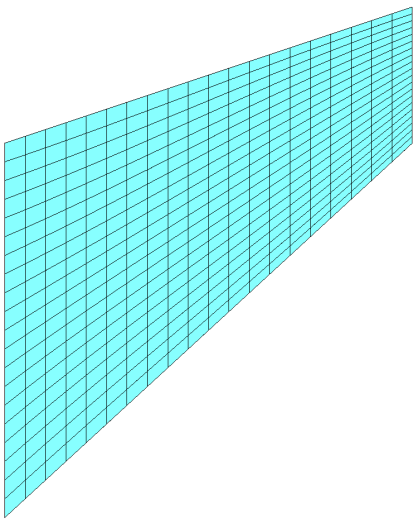

Figure 6.3.: $20 \times 20 \times 5$ eight-noded hexahedral elements used in the h-FEM investigation.

Table 6.2.: Number of degrees of freedom of p-version discretizations for the mesh in Fig. 6.1.

p-level	1	2	3	4	5	6	7	8	9	10
no. of DOF	288	948	1608	2769	4431	6720	9762	113683	18609	24666

where u_k and $u_{\text{ex}k}$, $k = 1, 2, 3$, are the components of displacements of a discretization under investigation and the reference solution, respectively, both evaluated at the background grid of Fig. 6.7(b). Identically, t_k and $t_{\text{ex}k}$, $k = 1, \ldots, 6$, symbolize the components of Cauchy stresses (Voigt-notation). n_{evp} is the number of evaluation points of the background grid. The displacements and stresses of the small elements at the corners of the cantilever are not taken into consideration in the error measurements, in order to exclude the non-physical results near the singularities.

The results of the relative error in displacements and stresses are plotted versus the number of unknowns as shown in Fig. 6.8. It is evident that the p-version discretizations show a faster convergence to the reference solution than the h-version formulations. Moreover, it overcomes locking effects known in bending dominated structures and nearly-incompressible media, see (Yosibash et al., 2014) and (Heisserer et al., 2008). This is also clearly shown by the slope: in comparison to the p-version, the convergence of the stresses in the h-element quadratic formulation are very large.

Since not only the error vs. DOF diagrams are of interest, Figs. 6.9 show the error versus the CPU-time. As an example of the results, Tab. 6.3 shows the values of the errors and CPU-time at specific points, namely $p = 8$ and 18750 quadratic elements of the p-FEM and h-FEM computations, respectively. It can be observed that higher errors in displacements and stresses are associated with a relatively high polynomial degree ($p = 8$). This indicates that the original p-mesh in Fig. 6.1 should be finer. Thus, this issue is also investigated by refining the p-mesh shown in Fig. 6.1 as shown in Fig. 6.10, i.e. the number of p-elements is increased from 42

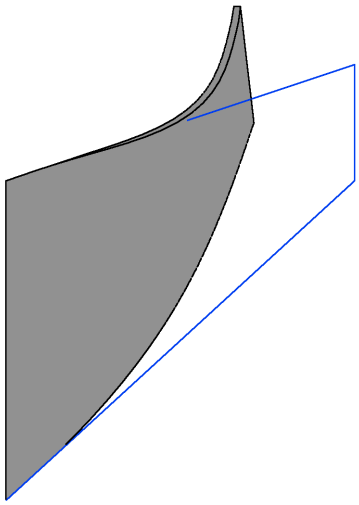

(a) $x-y$ view of the deformed configuration for $u_y = 8\text{mm}$.

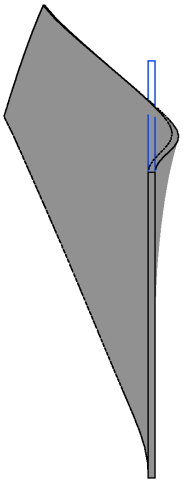

(b) $y - z$ view of the deformed configuration for $u_y = 8\text{mm}$.

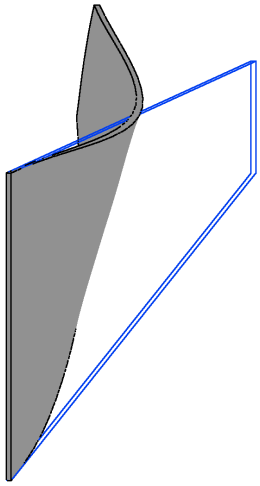

(c) 3D view of the deformed configuration for $u_y = 8\text{mm}$.

Figure 6.4.: Deformed vs. original views of the tapered cantilever used in h-FEM computation with the mesh shown in Fig. 6.3.

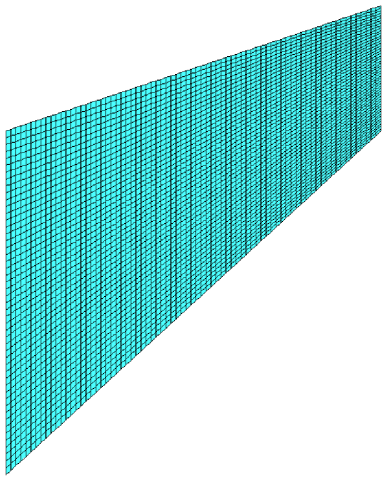

(a) $75 \times 75 \times 5$ eight-noded hexahedral elements

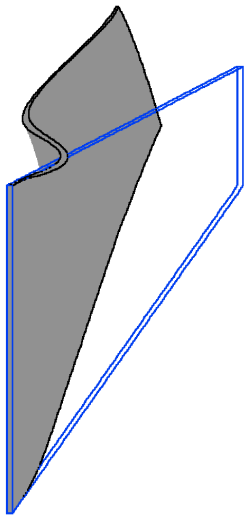

(b) 3D view of the deformed configuration for $u_y = 8\text{mm}$ with $75 \times 75 \times 5$ disretization

Figure 6.5.: Tapered cantilever with fine discretization used in h-FEM computation.

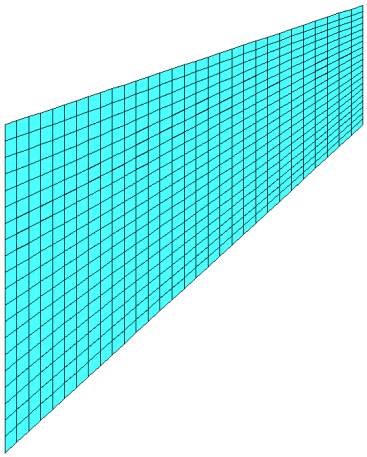

(a) $30 \times 20 \times 5$ eight-noded hexahedral elements

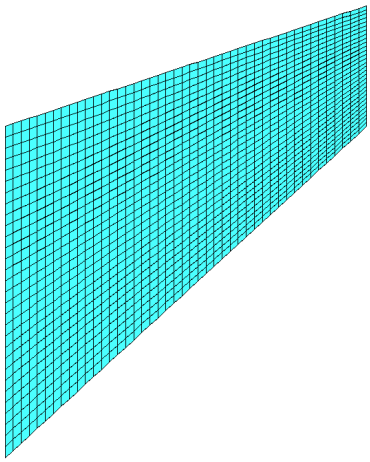

(b) $45 \times 30 \times 5$ eight-noded hexahedral elements

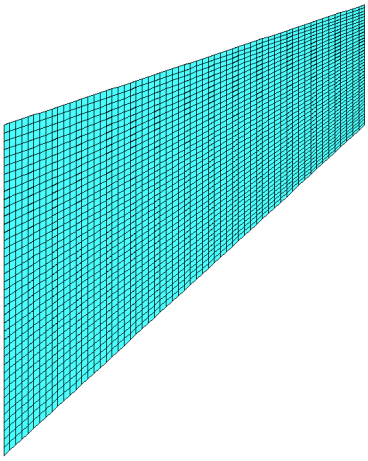

(c) $60 \times 40 \times 5$ eight-noded hexahedral elements

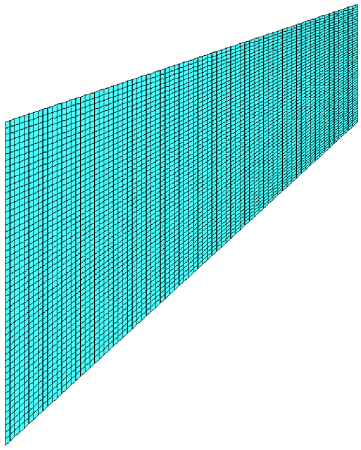

(d) $75 \times 50 \times 5$ eight-noded hexahedral elements

Figure 6.6.: Discretizations of the tapered cantilever used in h-FEM computations.

in the original mesh to 72 in the new one. To this end, p-version finite elements computations are carried out with the new p-mesh using five polynomials degrees, namely, $p = 4, 5, 7, 8, 10$. The errors in displacements and stresses are calculated using Eqs.(6.1a) and (6.1b), respectively. The results are plotted versus the number of unkowns and compared to the original p-version computations for the same polynomial degrees, as depicted in Fig. 6.11. It is evident that the errors in displacements and stresses are reduced to a certain degree. Furthermore, the efficiency of the p-FEM computations is increased in comparison to the h-FEM implementations, as shown in Tab. 6.4. Thus, a p-version using a polynomial degree of 8 saves about 23% of the computation time with a better accuracy than the h-version with 18750 twenty-noded quadratic elements. However, according to the error measure used in Eq.(6.1b) the error in stresses is still relatively high, where a minimum error in stresses of about 12% is obtained for $p = 10$, see Fig. 6.11.

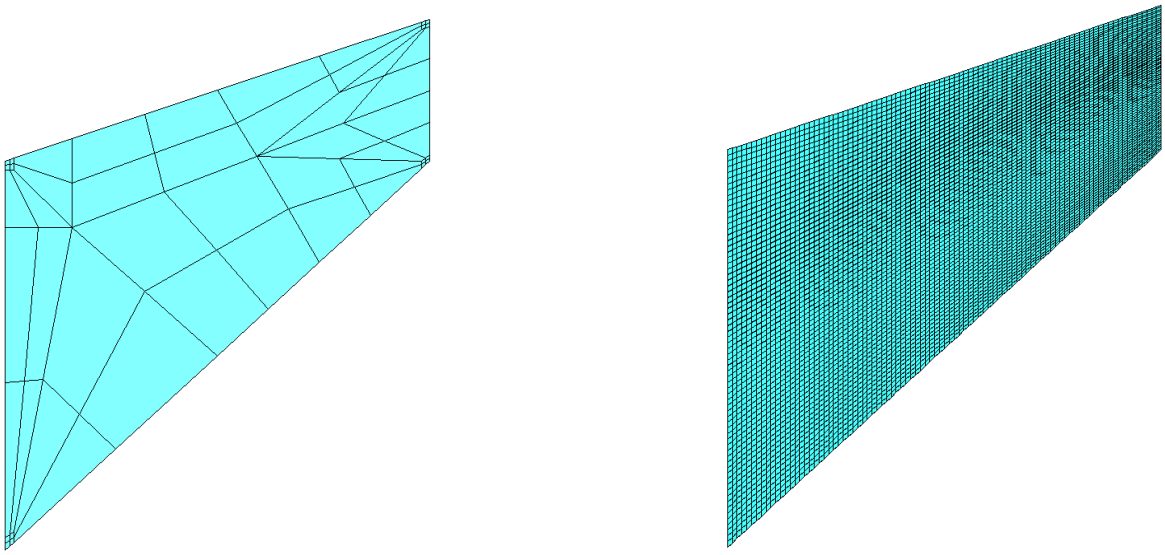

(a) Reference solution with 208 elements and $p = 11$

(b) Evaluation grid with $n_{\text{evp}} = 38766$

Figure 6.7.: Mesh for the reference solution and the evaluation grid.

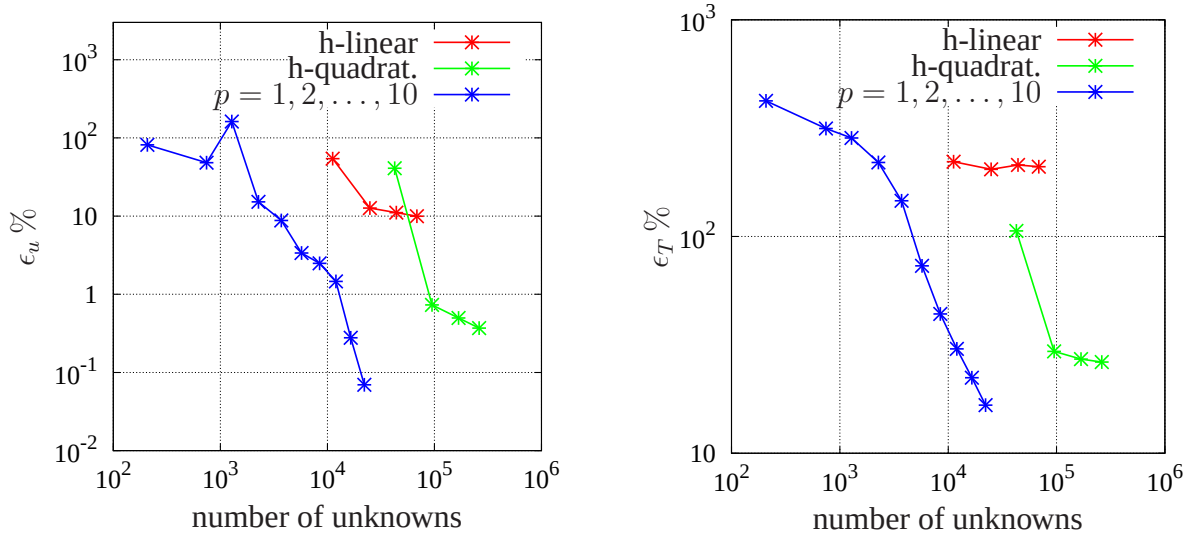

(a) Percentage relative error in displacements

(b) Percentage relative error in stresses

Figure 6.8.: Error versus number of unknowns.

Nevertheless, the application of another error measure leads to different results. If the root mean square error (RMSE) - which is a useful measure of accuracy, see (Hyndman and Koehler, 2006) - is used, the error in stresses for $p = 10$ is reduced to 0.045%. For the notations used in Eq.(6.1b)

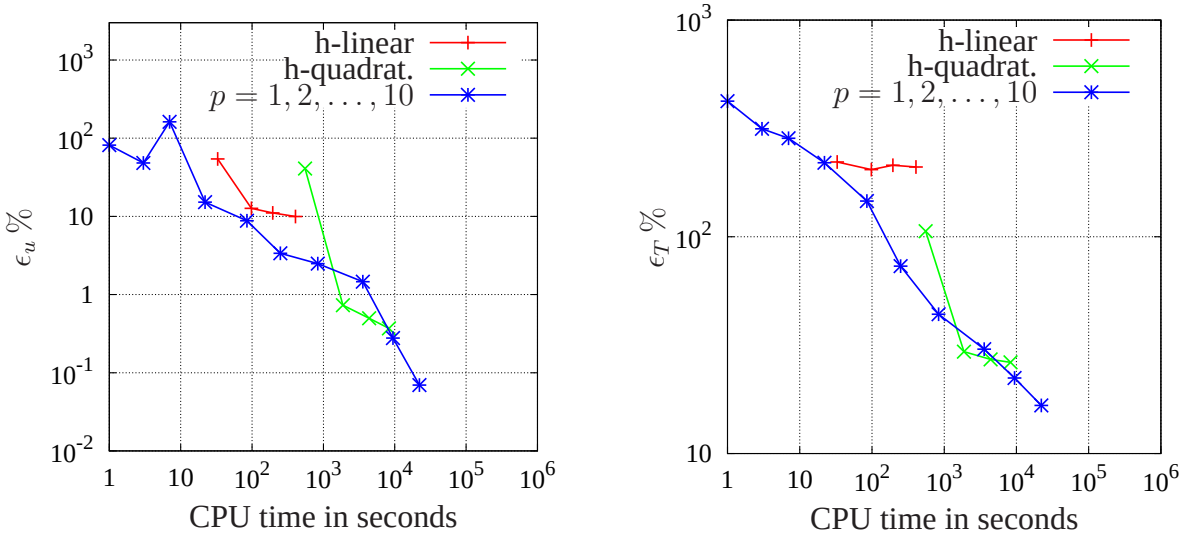

(a) Percentage relative error in displacements

(b) Percentage relative error in stresses

Figure 6.9.: Error versus CPU-time.

Table 6.3.: p-FEM with $p = 8$ vs. h-FEM with 18750 quadratic elements.

	p-FEM (p=8)	h-FEM (18750 quadrat.)
ϵ_u %	1.460	0.369
ϵ_T %	30.305	26.353
CPU-time (sec.)	3574	8282

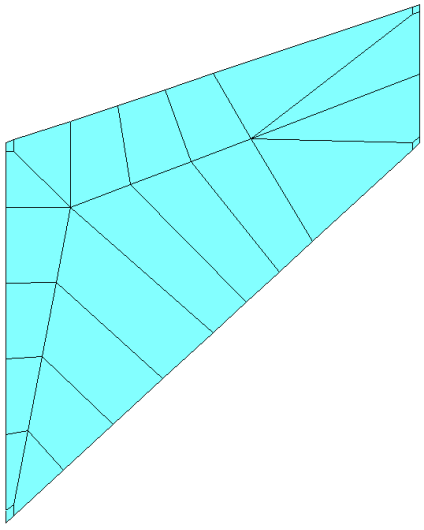

Figure 6.10.: Refined p-mesh with 72 p-elements.

the percentage RMSE in the stresses read

$$\text{RMSE}_T\,\% = \sqrt{\frac{\sum_{k=1}^{6n_{\text{evp}}} (t_k - t_{\text{ex}k})^2}{6\,n_{\text{evp}}}} \times 100, \tag{6.2}$$

The comparison between different error measures is beyond the scope of this thesis, as the purpose of comparing different finite element implementations has been achieved.

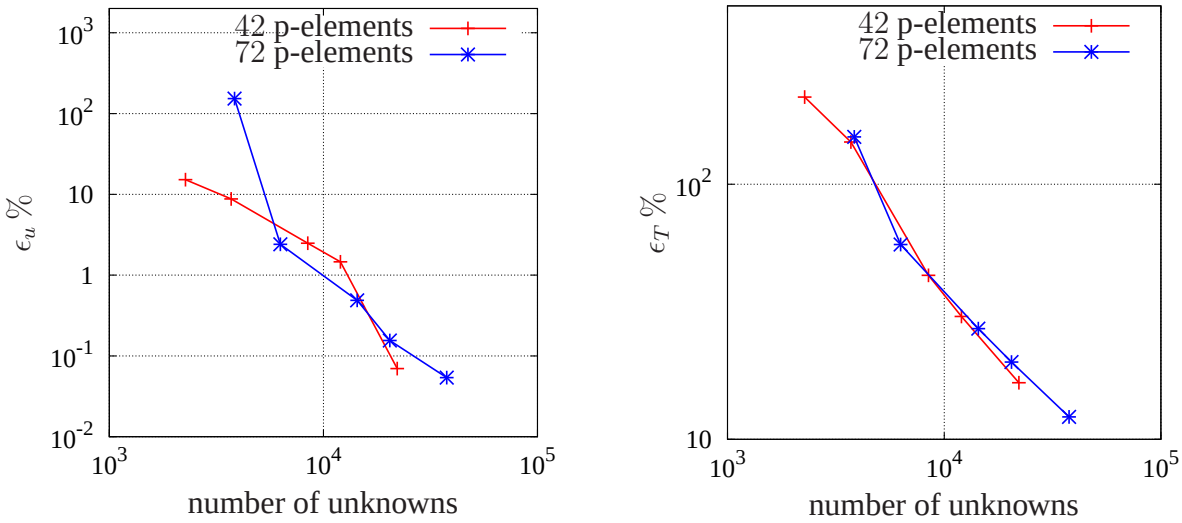

(a) Percentage relative error in displacements

(b) Percentage relative error in stresses

Figure 6.11.: Error versus number of unknowns ($p = 4, 5, 7, 8, 10$).

Table 6.4.: New p-FEM with $p = 8$ vs. h-FEM with 18750 quadratic elements.

	p-FEM ($p = 8$)	h-FEM (18750 quadrat.)
$\epsilon_u\,\%$	0.155	0.369
$\epsilon_T\,\%$	20.080	26.353
CPU-time (sec.)	6409	8282

6.1.2. Bone-Like Specimen under Simple Tension

In this example, the influence of the fiber orientation exerted on the behavior of the anisotropic structures is investigated. Thus, a bone-like specimen, as commonly used in experiments, is subjected to simple tension. Fig. 6.12 shows the geometry of the model.

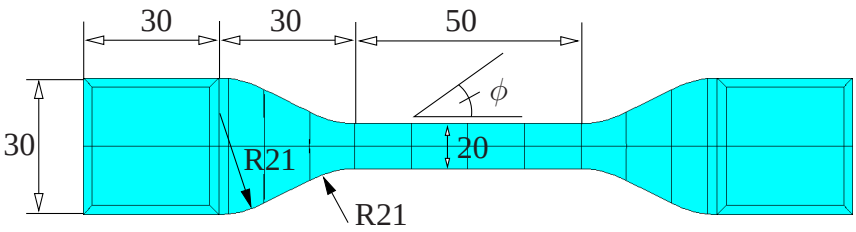

Figure 6.12.: Geometry of specimen (measures in mm, depth $= 8\mathrm{mm}$).

The bone-like specimen is discretized using a fine p-mesh consisting of 120 p-elements, see Fig. 6.13(a), and a polynomial degree $p = 8$ is employed. Two loading paths are applied, as depicted in Fig. 6.13. At the beginning, a displacement boundary condition is applied in z-direction, and increased linearly in time up to a maximum value of $\overline{u}_{z\max} = 0.8\,\mathrm{mm}$. This displacement is applied to the red colored part of the specimen. This loading condition is intended to simulate the clamping process of the specimen in the clamps of the testing machine, where the planes at $z = 0$ are fixed and only the surfaces at $z = 8$ are moved. In the second step, a displacement in x-direction is linearly applied up to a maximum of $\overline{u}_{x\max} = 100\,\mathrm{mm}$, while the displacement boundary conditions in z-direction are kept constant. This loading step describes the axial loading process of the specimen in the testing machine. The computations are performed with three

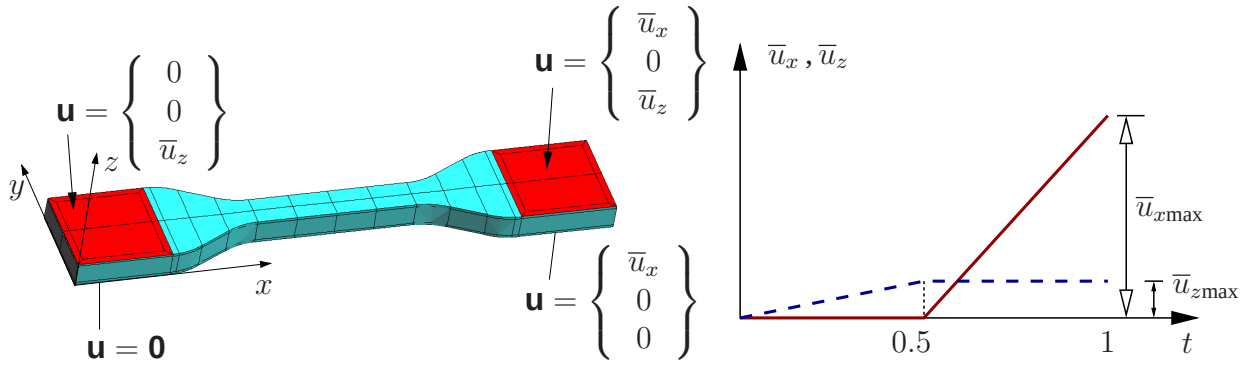

(a) p-FEM mesh with p-level 8

(b) Load functions

Figure 6.13.: Mesh and boundary conditions.

different fiber orientations, i.e., $0°$, $45°$ and $90°$ relative to the loading direction, and the results are presented in Figs. 6.15 and 6.14.

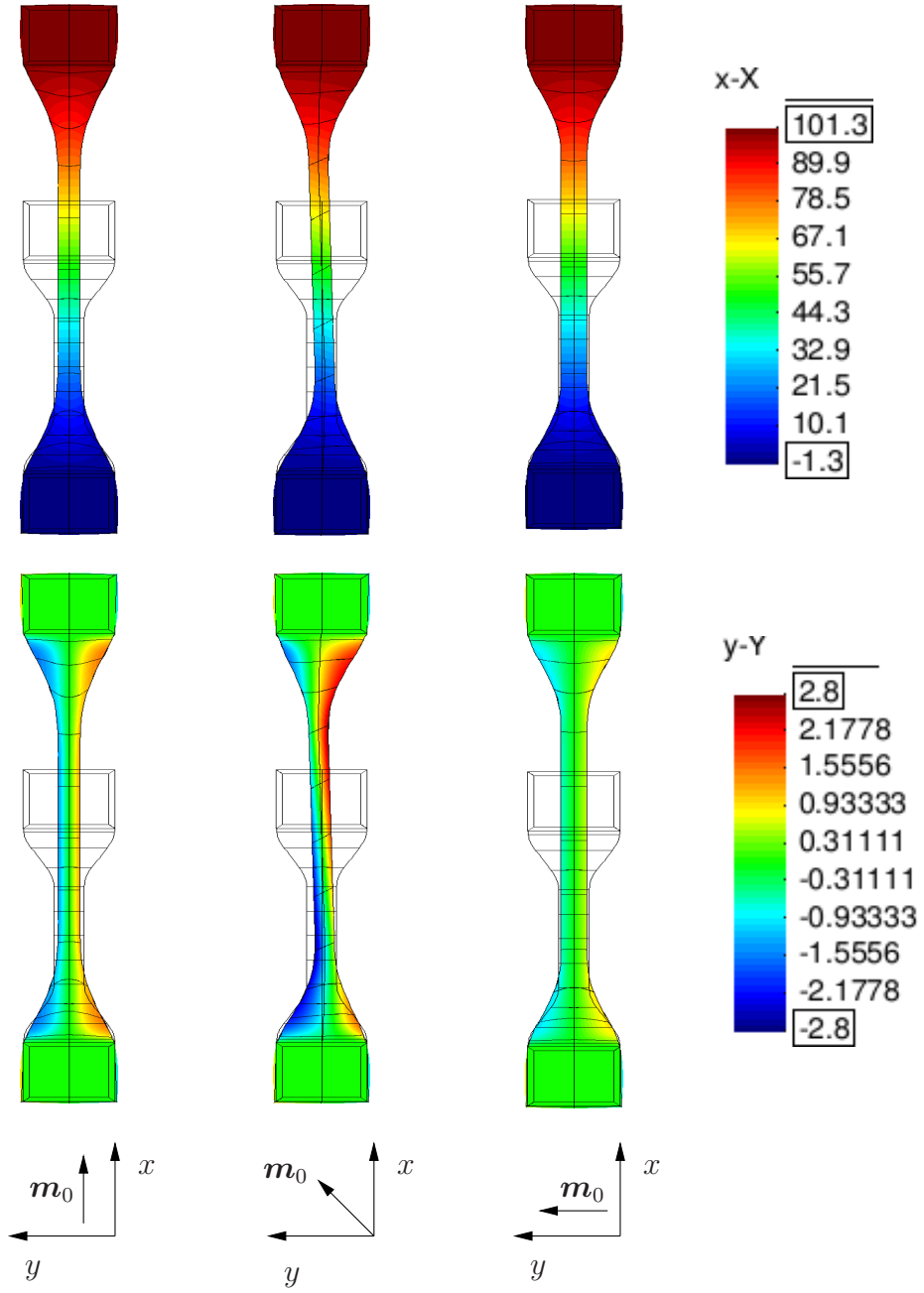

Figure 6.14.: Displacement field (in mm) in x-direction (top) and y-direction (bottom) for different fiber orientations.

The first column of Fig. 6.14 shows the displacement fields $u_x(x, y, 8)$ and $u_y(x, y, 8)$ where the fiber direction coincides with the x-direction, $\boldsymbol{m}_0 = \boldsymbol{e}_x$, $\phi = 0°$. If the fibers are oriented in y-direction $\boldsymbol{m}_0 = \boldsymbol{e}_y$, $\phi = 90°$, as depicted in the third column of Fig. 6.14, we observe a similar deformation to the case of $\phi = 0°$. If the fibers are oriented at an angle of $\phi = 45°$ in the xy-plane, the specimen undergoes an S-shaped deformation in y-direction as shown in Fig. 6.15,

which is a well-known effect.

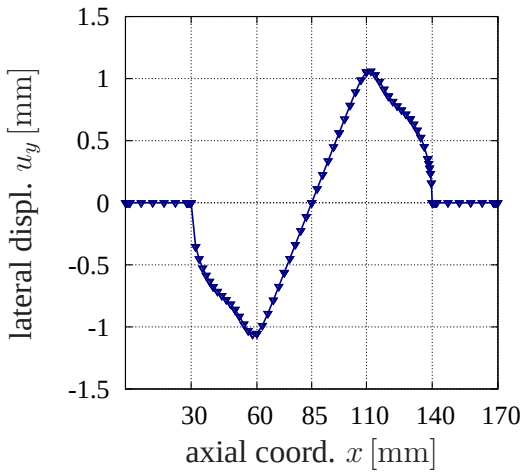

Figure 6.15.: Displacement $u_y(x, 15, 8)$ (top surface) for $\phi = 45°$.

6.2. Temperature-Dependent Analysis

In the following, the focus lies on investigating the capability of the constitutive model formulated in Chapter 4 to simulate the behavior of composite structures under thermal and thermo-mechanically coupled loadings. In addition to the material parameters of the mechanical subproblem given in Tab. 3.1, the material parameters of the thermal subproblem are required too. Tab. 6.5 summarizes the thermal material parameters, which are obtained based on the thermal properties of the two phases of the composites under consideration, i.e. polyamide fiber reinforced silicon rubber, see (Mark, 2007). The example of a perforated plate is considered here,

Table 6.5.: Thermal material parameters.

κ_a W/(m K)	κ_n W/(m K)	α_a K^{-1}	α_n K^{-1}	c_{d0} J/(Kg K)	c_{dk} K^{-1}	Θ_0 K	ϱ_R Kg/m^3
0.4	0.2	4.53e-04	9.06e-04	1.591e+03	1.037e-03	293.15	975

in order to study the influence of anisotropic material properties on the behavior of composite materials subjected to thermal deformations due to changes in temperature as well as thermo-mechanical deformations. Thus, the model of a plate with a hole is generated with the geometry and p-mesh shown in Fig. 6.16. 108 p-elements are used to discretize the plate, where three

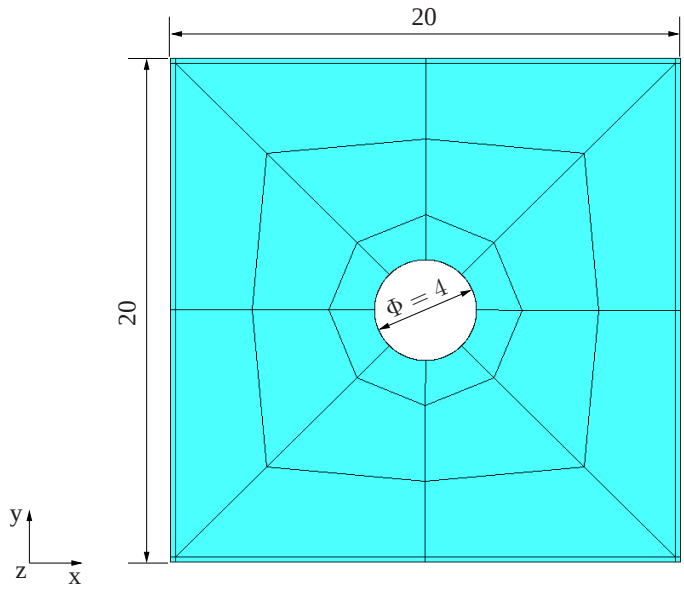

Figure 6.16.: Geometry and p-mesh of the perforated plate (measures in mm, thickness $= 1\mathrm{mm}$).

elements are assumed in thickness direction. Firstly, the plate is assumed to be under thermal deformations caused by a change in temperature in an adiabatic process. The displacement and temperature boundary conditions are illustrated in Figs. 6.17 and 6.18, respectively. The boundary conditions are applied to the red colored sides of the plate, where the plate is fixed at the two faces. Then, the temperature is increased linearly with time from $20°\mathrm{C}(293.15\mathrm{K})$ to $50°\mathrm{C}(323.15\mathrm{K})$, as depicted in Fig. 6.18(b). The computations are carried out using a p-level of 8. The second-order time discretization scheme (Ellsiepen's method) is applied, see (Ellsiepen and Hartmann, 2001).

6.2.1. Anisotropic Thermal Expansion

The thermal stretches ζ and φ used in Eq.(4.8) to define the thermal part of the deformation gradient tensor $\mathbf{F}_\Theta$ are represented in terms of the thermal expansion coefficients along (α_a) and normal to (α_n) the preferred direction, respectively, see Eq.(4.9). In order to examine the effect of changing the thermal expansion coefficients on the response of the composite structures, computations with different ratios of (α_a/α_n) are carried out. Fig. 6.19 shows the case of a composite with isotropic thermal coefficients, i.e. $(\alpha_a/\alpha_n) = 1$, in which the thermal stretches in x- and y- axes are equal, i.e $(u_x/u_y) = 1$. If the ratio (α_a/α_n) is not identity, an anisotropic behavior of the plate is observed, where different thermal stretches in the x- and y-axes are obtained. The displacement ratio u_x/u_y changes linearly with the ratio (α_a/α_n) as a result of the linear functions assumed in Eq.(4.9).

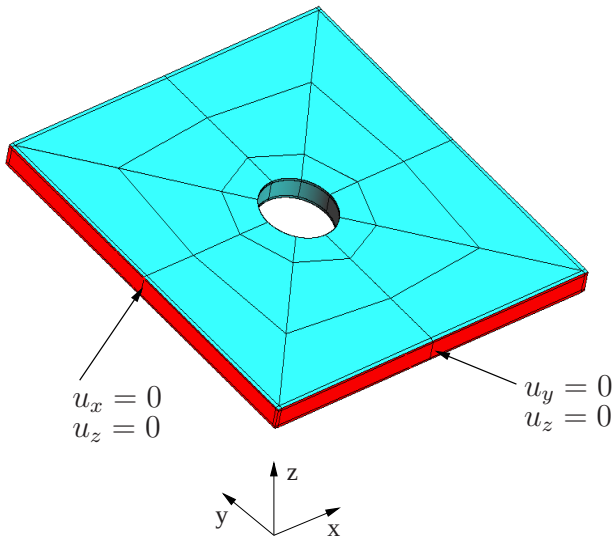

Figure 6.17.: Displacement boundary conditions.

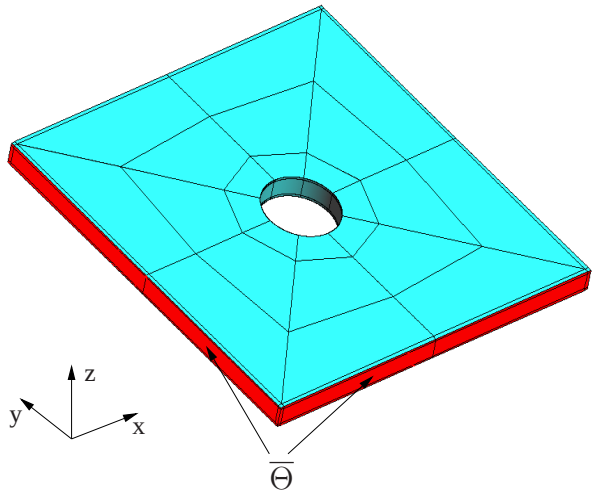

(a) Temperature boundary conditions

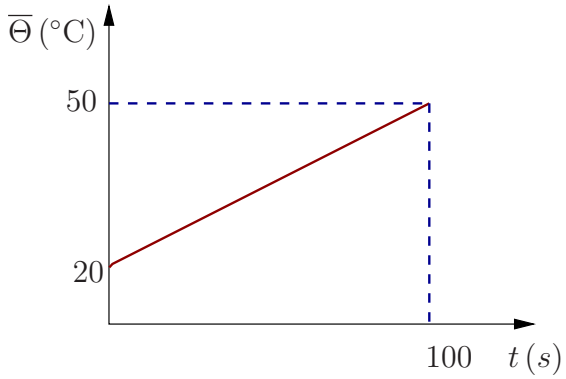

(b) Temperature load function

Figure 6.18.: Temperature boundary conditions and load function.

6.2.2. Anisotropic Thermal Conductivity

In the formulation of the anisotropic heat flux vector, see Eq.(4.74), two thermal conductivities κ_a and κ_n are assumed, representing the thermal conductivity of the composite material along and normal to the preferred direction. The influence of the anisotropic thermal conductivity is investigated by changing the parameter $\kappa_r = \kappa_n/\kappa_a$, denoting the ratio of thermal conductivity normal to the preferred direction to the thermal conductivity along the preferred direction. The computations are performed with five different ratios of thermal conductivity, namely, $\kappa_r = 0.1, 0.25, 0.5, 0.75, 1$. The fiber is set to be aligned with the x-axis, i.e. $\boldsymbol{m}_0 = \boldsymbol{e}_x$. The

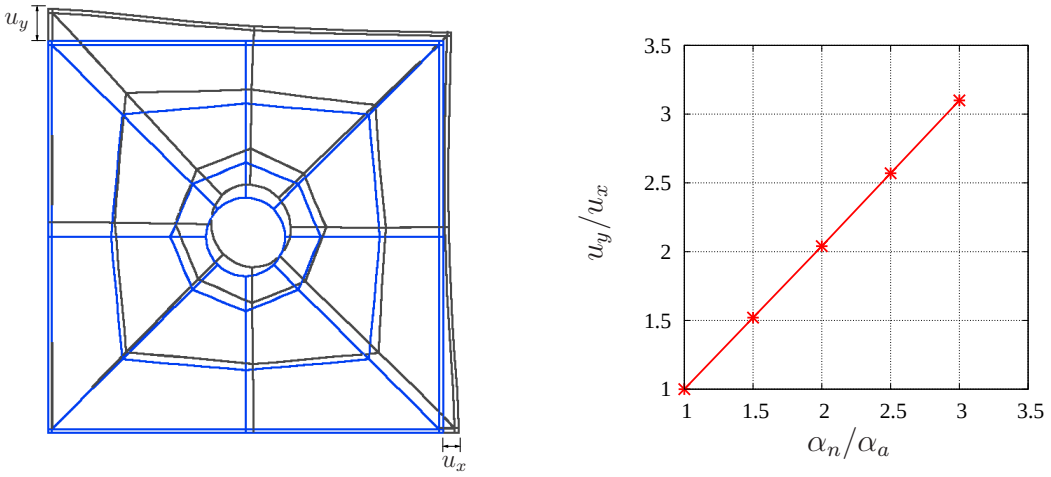

(a) $\alpha_n/\alpha_a = 2.0$

(b) Displacement ratio vs. thermal expansion ratio

Figure 6.19.: Effect of anisotropic thermal expansion on the displacement field (original in blue and deformed in gray, fiber oriented in x-axis).

results are shown in Fig. 6.20. It is evident that the change in thermal conductivity has a big influence on the material response. In contrast to the symmetric temperature field along the fiber direction, which is obtained for the case of $\kappa_r = 1$ as depicted in Fig. 6.20(e), non-symmetric temperature fields are observed for the other ratios, see Fig. 6.20(a)- 6.20(b). This effect can be shown more clearly by comparing the temperatures at nodes A and B for different ratios of thermal conductivity - as shown in Fig. 6.21(a). Thus, the percentage relative difference in the measurements resulting from neglecting the anisotropic thermal conductivity, i.e., when $\kappa_r = 1.0$ is considered, is calculated by

$$\epsilon_\Theta\% = \frac{\Theta_{\text{iso}} - \Theta_{\text{aniso}}}{\Theta_{\text{aniso}}} \times 100. \tag{6.3}$$

Θ_{iso} is the temperature for the case of $\kappa = 1.0$ and Θ_{aniso} represents the temperature for the cases of $\kappa_r = 0.1, 0.25, 0.5, 0.75$. The percentage error $\epsilon_\Theta\%$ versus the ratio of thermal conductivity κ_r is plotted in Fig. 6.21(b). For the case $\kappa_r = 0.1$, nodes A and B show differences in temperatures of about 42% and about 31%, respectively - while the difference is only about 6% at both nodes if the anisotropy of the thermal conductivity is reduced to 0.75%. This proves that it is of significant importance to consider anisotropic thermal conductivity when analyzing the thermal behavior of anisotropic materials, especially if the ratio of thermal conductivity shows a high value of anisotropy, as in the case of metal fiber-reinforced polymers.

6.2.3. Fiber Orientation

In this section, two sets of computations are performed in order to show the influence of the fiber orientation on the temperature and displacement fields. Concerning the first set of computations,

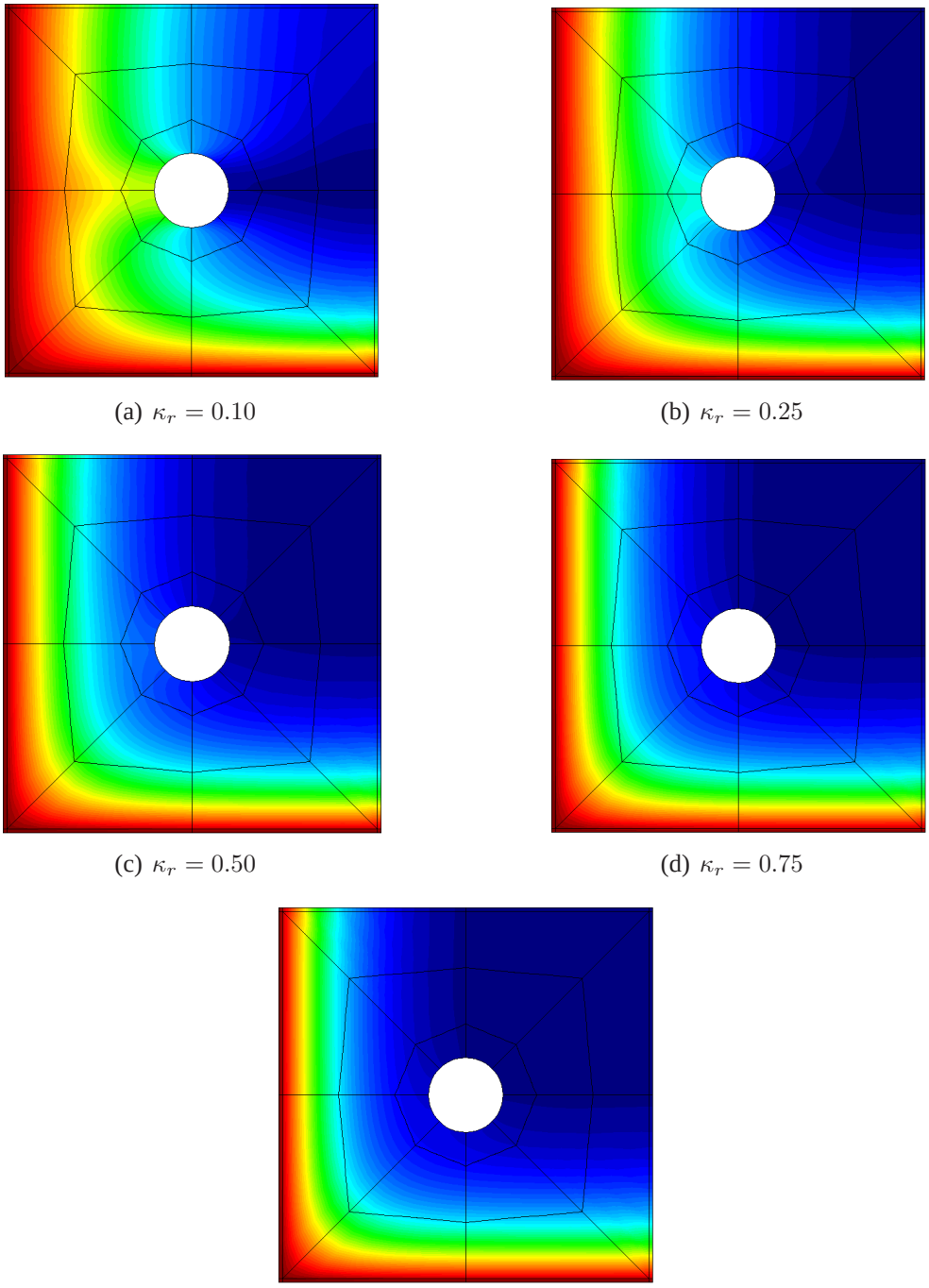

(a) $\kappa_r = 0.10$ (b) $\kappa_r = 0.25$

(c) $\kappa_r = 0.50$ (d) $\kappa_r = 0.75$

(e) $\kappa_r = 1.00$

Figure 6.20.: Effect of anisotropic thermal conductivity on the temperature field (fiber oriented in x-axis $\boldsymbol{m}_0 = \boldsymbol{e}_x$).

the perforated plate is subjected to the same boundary conditions that have been considered so far, see Figs. 6.17 and 6.18, in which the plate undergoes thermal deformations caused by tem-

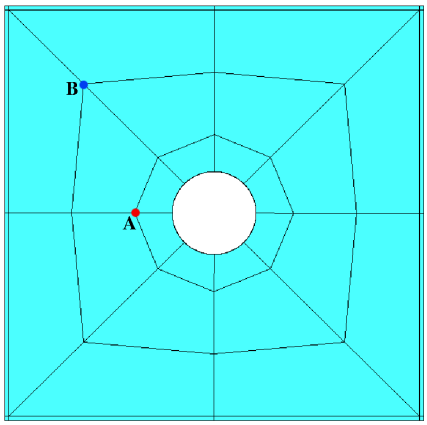

(a) Positions of nodes A and B where the temperature measurements are compared

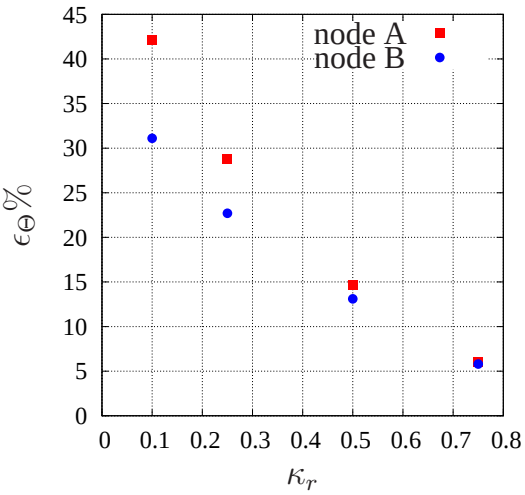

(b) Percentage relative difference in temperature measurements $\epsilon_\Theta\%$ vs. ratio of thermal conductivity κ_r

Figure 6.21.: Effect of neglecting the anisotropy in thermal conductivity on the resulting temperature measurements.

perature increase. To this end, computations are carried out with two different fiber orientations: the fibers are oriented in the direction of the x-axis and with an angle of $45°$ relative to the coordinate system of Fig 6.16. The ratio of thermal conductivity κ_r is set to be 0.1. Fig. 6.22 illustrates the results of these computations, where the temperature field is depicted for the three fiber orientations. As expected, fibers aligned $45°$ to the (x, y)-plane show a symmetric temperature distribution along the fiber orientation, as shown in Fig. 6.22(b), due to the fact that the fiber is aligned with the axis of symmetry of the applied boundary conditions. If the fibers are aligned with the x–axes, a fully non-symmetric temperature distribution is to be observed, see Figs. 6.22(a).

In the second computation the perforated plate in Fig. 6.16 is assumed to be subjected to thermo-mechanical coupled deformations. The temperature boundary conditions are kept as given in Fig. 6.18. The displacement boundary conditions are shown in Fig. 6.23(a), where the plate is fixed at the two red colored sides and a biaxial tension is applied on the other two sides. The plate is pulled with a displacement of 10mm in both x and y directions ($\overline{u}_x = \overline{u}_y = 10\text{mm}$). The displacement is increased linearly with time, as shown in Fiq. 6.23(b). Two cases are considered, in which the fiber is assumed to be oriented along the x-axes. Fig. 6.24 shows the undeformed and the deformed shape of the plate, where the circular hole of the perforated plate is deformed into an elliptical hole because of the preferred direction. Furthermore, the elliptical hole is rotated following the fiber orientation, so that the major axis of the ellipse is aligned with the preferred (fiber) direction. The stress components S_{xx} and S_{yy} for this fiber orientation $\boldsymbol{m}_0 = \boldsymbol{e}_x$ are depicted in Fig. 6.25. However, the same elongation is applied along x- and y-axes of the plate. Due to the anisotropy, different stress components S_{xx} and S_{yy} are obtained.

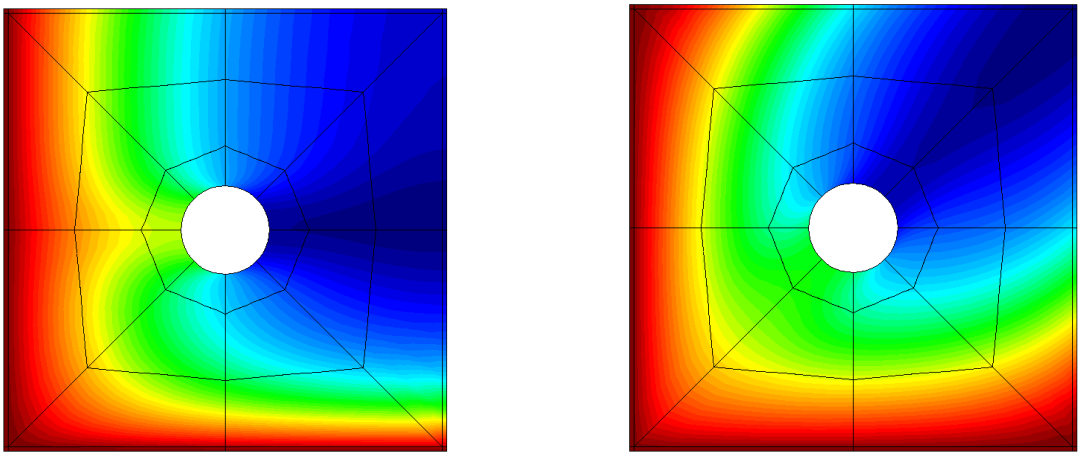

(a) Fiber oriented in x-axis ($\boldsymbol{m}_0 = \boldsymbol{e}_x$)

(b) Fiber with an angle of $45°$ ($\boldsymbol{m}_0 = (\boldsymbol{e}_x + \boldsymbol{e}_y)/\sqrt{2}$)

Figure 6.22.: Effect of fiber orientation on the temperature field.

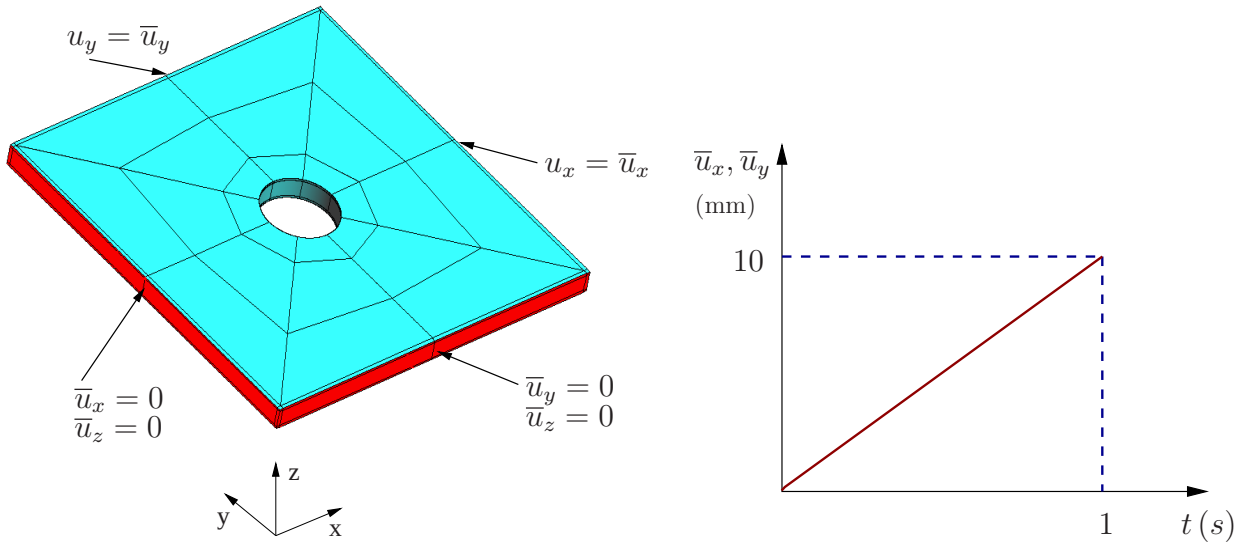

(a) Displacement boundary conditions

(b) Displacement load function

Figure 6.23.: Displacement boundary conditions and loading function.

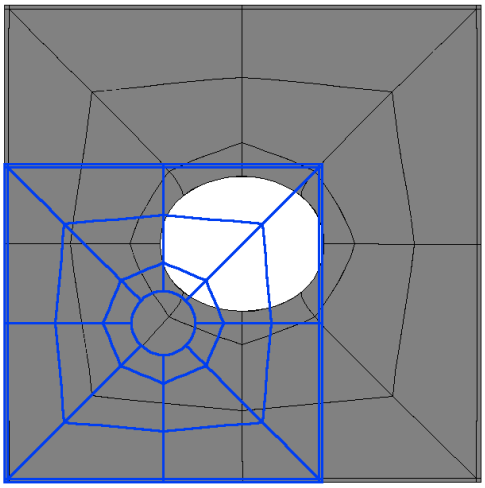

(a) Fiber oriented in x-axis ($\boldsymbol{m}_0 = \boldsymbol{e}_x$)

Figure 6.24.: Deformed vs. original shape of the perforated plate.

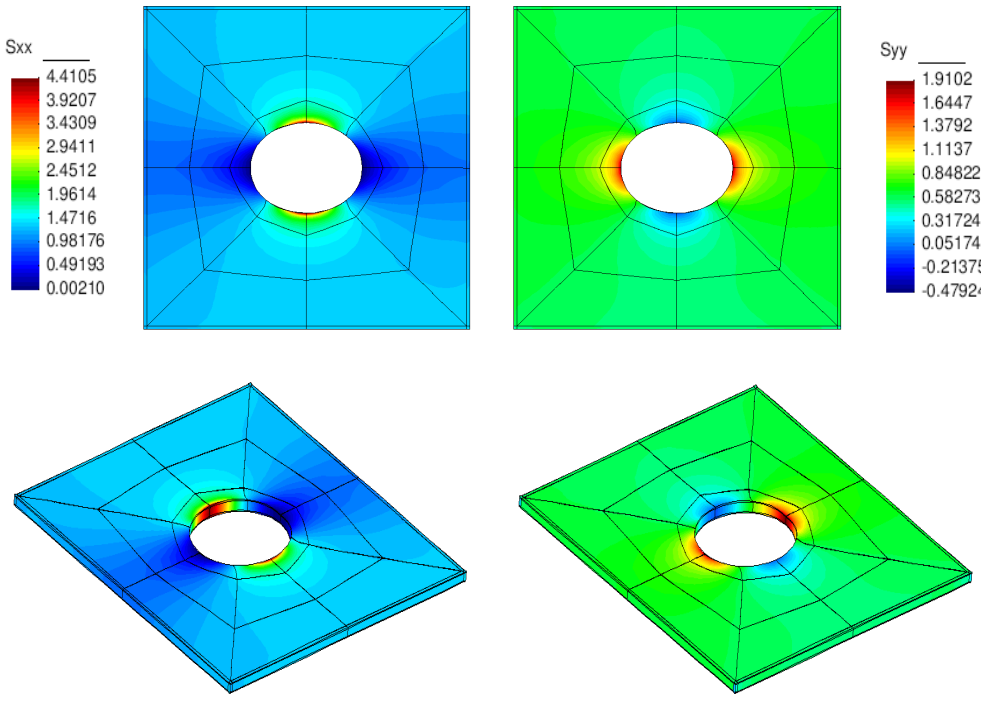

Figure 6.25.: Stress components S_{xx} (left) and S_{yy} (right) in (x, y)-plane (top) and 3D-view (bottom) with fiber oriented in x-axis ($\boldsymbol{m}_0 = \boldsymbol{e}_x$).

7. Conclusion and Outlook

In recent years, constitutive modeling and numerical simulation of the behavior of anisotropic materials, particularly transversal isotropic and orthotropic materials, have attained increasing attention. This is due to the wide range of applications of anisotropic materials in both industrial and scientific areas of application, such as in fiber-reinforced composites and bio-mechanical systems technology.

The aim of this thesis is to develop a new constitutive model describing the behavior of transversely isotropic materials under both mechanical and thermo-mechanical coupled loadings and to use the developed model to perform numerical simulations using high-order finite elements.

First of all, for the isothermal case, a new constitutive model is formulated based on the multiplicative decomposition of the deformation gradient tensor. The model is an extension of the volumetric/isochoric decomposition, where the isochoric deformation gradient is further decomposed into two parts: one part describing the deformation in the preferred direction (fiber direction) and another part that contains the remaining deformations. The proposed model fulfills the condition of a stress-free undeformed state, and has advantages over the classical modeling given in Sec. 3.4: firstly, it leads to a clear split of the stress-state in the preferred direction from the remaining stresses; secondly, it overcomes the drawback of applying the volumetric/isochoric decoupling to the case of anisotropy. The proposed model includes only three material parameters, which can easily be obtained from simple experiments.

The model is then extended to the case of thermo-mechanical transversal isotropy, drawing on the multiplicative split of the deformation gradient tensor into thermal and mechanical parts. The thermal part is formulated as a volumetric tensor with a transversely isotropic structure, taking into consideration the distinct thermal stretches, defined in terms of thermal expansion coefficients, along and normal to the preferred direction. The thermo-mechanical model fulfills thermodynamical consistency. Thus, thermo-mechanically coupled constitutive equations for the stress-state and specific entropy are derived. The heat flux vector is normally assumed by scalar parameter times the temperature gradient, i.e., the thermal conductivities of anisotropic materials are assumed to be the same in all directions, see for example (Zhang, 2010). This issue is also investigated in this thesis, where a transversely isotropic heat flux vector is formulated by considering different thermal conductivities along and normal to the direction of isotropy.

Moreover, the boundary value problem (BVP) and the initial-boundary value problem (IBVP) resulting from the isothermal and thermo-mechanical coupled problems, respectively, are solved numerically by means of high-order finite elements. To this end, numerical computations are carried out using the in-house finite element program TASA-FEM, which is capable of performing high-order computations in space and time. Due to its efficiency in the analysis of large deformation problems and the possibility of using elements with high polynomials, which is a necessary feature to analyze thin structures such as composite laminates, the p-version finite el-

ement method is used here. The capability of the proposed constitutive model to simulate the behavior of transversely isotropic materials under isothermal, thermal and thermo-mechanical loading cases is demonstrated by different numerical examples. The influence of the existence of a preferred direction on the behavior of structures made of transversely isotropic composite materials is addressed by considering the example of Cook's membrane subjected to isothermal shear deformation. In contrast to the case of isotropy, in which the structure undergoes only in-plane deformations, a strongly apparent out-of-plane deformation is observed, caused by the anisotropy. For comparison purposes, the same example is investigated using h-version finite elements. In this case, it is found that if the mesh is not fine enough, an out-of-plane deformation similar to that observed by (Schröder and Neff, 2003) will be obtained, which is different from the S-shaped out-of-plane deformation obtained from more accurate computations. This shows that care must be taken when performing finite elements computations for anisotropic structures in order to investigate the mesh and p-level sensitivity of the results. This finding leads to a comparison between the p-FEM with different p-levels and the h-FEM, based on eight-noded linear and twenty-noded quadratic elements with different discretizations. The relative errors in displacements and stresses are compared, proving the faster convergence of the p-FEM variant in comparison with the convergence of h-FEM. However, a large CPU time and high p-level are required for the p-FEM computations to reach the required accuracy, which indicates the need to refine the p-mesh. In doing so, more efficient p-FEM results were obtained, see Fig. 6.11.
The simulations of the thermo-mechanical behavior of a perforated plate made of transversely isotropic composite show the pronounced influence of the anisotropic thermal properties of the composite (namely, anisotropic thermal expansion and heat conductivity) on the response of the plate under thermal loading, where both the displacement and temperature fields are strongly affected by changing these parameters. The advantage of counting anisotropic heat conductivity is established by computing the error in the temperature measure at specific nodes that arises from neglecting the anisotropy in thermal conductivity. An error of about 42% is observed for a ratio of 10% thermal conductivity, i.e., thermal conductivity normal to the preferred direction is equal to 10% of the thermal conductivity along the preferred direction. The error is reduced to 6% for a ratio of 75% thermal conductivity. Thus, according to the considered example, the anisotropic thermal conductivity should be taken into consideratio for materials with a ratio of thermal conductivity up to 75%. Above this value, it can be ignored above this value. It should be emphasized that this holds for applications in which a small difference in temperature has a negligible effect on the material behavior. Otherwise, anisotropic thermal conductivity has to be taken into account, regardless if it is of a small or a high ratio. Additionally, the effect of the orientation of the preferred direction (fiber direction) is evident in all loading cases, i.e. isothermal, thermal as well as thermo-mechanical coupled loadings, where the displacement, the temperature and the stress fields are all affected according to the orientation of the preferred direction, as depicted in Sections 6.1.2 and 6.2.3.

The work presented in this thesis provides various possibilities of extension. In fiber reinforced composites, one factor that influences the behavior of the material is the fiber volume fraction, which measures the amount of fiber contained in the composite. Thus, a possible extension could be to formulate fiber contents dependent material parameters by adapting the material parameters included in the proposed model to experimental data, obtained from simple experi-

ments - uniaxial tension, for example, carried out for a composite with different fiber contents. Another item could be the extension of the model to consider the viscous effect, i.e., to formulate a thermo-visco-hyperelastic model for transversal isotropy. Moreover, the idea of the multiplicative decomposition of the deformation gradient tensor used in this work could be applied to model the behavior of materials reinforced with two fiber families, such as for arterial tissues, in which the elastin matrix is reinforced by two collagen fibers.

A. Appendix

A.1. Other Forms of Decomposition

During the development of the theory, several investigations were carried out that led to multiplicative decompositions with some essential drawbacks. These are summarized in the following.

A.1.1. First Investigation

Basically, the first idea of decomposition is to multiplicatively decompose the deformation gradient $\mathbf{F}$ into two parts. One part, $\mathbf{F}_\mathrm{a}$ describes the deformation only along the fiber direction, while the other part contains the remaining deformation denoted by $\mathbf{F}_\mathrm{r}$,

$$\mathbf{F} = \mathbf{F}_\mathrm{r}\mathbf{F}_\mathrm{a} \tag{A.1.1}$$

This decomposition leads to the problem that there is no deformation in the remaining part, irrespective of the deformation in the fiber direction. This can be explained as follows: the two parts of the deformation gradient tensor are defined by

$$\mathbf{F}_\mathrm{a} = \lambda_\mathrm{a}\,\hat{\boldsymbol{e}}_1 \otimes \boldsymbol{E}_1 + \hat{\boldsymbol{e}}_2 \otimes \boldsymbol{E}_2 + \hat{\boldsymbol{e}}_3 \otimes \boldsymbol{E}_3 \tag{A.1.2}$$

$$\mathbf{F}_\mathrm{r} = \mathbf{F}\mathbf{F}_\mathrm{a}^{-1}. \tag{A.1.3}$$

This leads to the following tensors

$$\begin{aligned}
\mathbf{C}_\mathrm{a} &= (\lambda_\mathrm{a}\,\boldsymbol{E}_1 \otimes \hat{\boldsymbol{e}}_1 + \boldsymbol{E}_2 \otimes \hat{\boldsymbol{e}}_2 + \boldsymbol{E}_3 \otimes \hat{\boldsymbol{e}}_3)\,(\lambda_\mathrm{a}\,\hat{\boldsymbol{e}}_1 \otimes \boldsymbol{E}_1 + \hat{\boldsymbol{e}}_2 \otimes \boldsymbol{E}_2 + \hat{\boldsymbol{e}}_3 \otimes \boldsymbol{E}_3) \\
&= \lambda_\mathrm{a}\,\boldsymbol{E}_1 \otimes \boldsymbol{E}_1 + \boldsymbol{E}_2 \otimes \boldsymbol{E}_2 + \boldsymbol{E}_3 \otimes \boldsymbol{E}_3 \\
&= \underbrace{\lambda_\mathrm{a}^2\,\boldsymbol{E}_1 \otimes \boldsymbol{E}_1 - \boldsymbol{E}_1 \otimes \boldsymbol{E}_1}_{(\lambda_\mathrm{a}^2-1)\boldsymbol{E}_1\otimes\boldsymbol{E}_1} + \underbrace{\boldsymbol{E}_1 \otimes \boldsymbol{E}_1 + \boldsymbol{E}_2 \otimes \boldsymbol{E}_2 + \boldsymbol{E}_3 \otimes \boldsymbol{E}_3}_{\mathbf{1}} \\
&= (\lambda_\mathrm{a}^2 - 1)\boldsymbol{m}_0 \otimes \boldsymbol{m}_0 + \mathbf{I} && \text{(A.1.4)} \\
&= (\mathrm{I}_4 - 1)\mathbf{M}_0 + \mathbf{I}, && \text{(A.1.5)}
\end{aligned}$$

and

$$\mathbf{C}_\mathrm{r} = \mathbf{F}_\mathrm{r}^\mathrm{T}\mathbf{F}_\mathrm{r} = \mathbf{F}_\mathrm{a}^{-\mathrm{T}}\,\mathbf{F}^\mathrm{T}\,\mathbf{F}\mathbf{F}_\mathrm{a}^{-1} = \mathbf{F}_\mathrm{a}^{-\mathrm{T}}\,\mathbf{C}\,\mathbf{F}_\mathrm{a}^{-1}, \tag{A.1.6}$$

where $\boldsymbol{m}_0 = \boldsymbol{E}_1$ is assumed in (A.1.4). Thus, the three principal invariants of $\mathbf{C}_\mathrm{a}$ and $\mathbf{C}_\mathrm{r}$ are

$$\begin{aligned}
\mathrm{I}_{\mathbf{C}_\mathrm{a}} &= \operatorname{tr}\mathbf{C}_\mathrm{a} = \mathrm{I}_4 + 2 \\
\mathrm{II}_{\mathbf{C}_\mathrm{a}} &= \tfrac{1}{2}\left((\operatorname{tr}\mathbf{C}_\mathrm{a})^2 - \operatorname{tr}\mathbf{C}_\mathrm{a}^2\right) = 2\mathrm{I}_4 + 1 \\
\mathrm{III}_{\mathbf{C}_\mathrm{a}} &= \det\mathbf{C}_\mathrm{a} = \mathrm{I}_4
\end{aligned} \tag{A.1.7}$$

and

$$\begin{aligned}
\mathrm{I}_{\mathbf{C}_\mathrm{r}} &= \operatorname{tr}\mathbf{C}_\mathrm{r} = \mathrm{I}_1 - \mathrm{I}_4 + 1 \\
\mathrm{II}_{\mathbf{C}_\mathrm{r}} &= \tfrac{1}{2}\left((\operatorname{tr}\mathbf{C}_\mathrm{r})^2 - \operatorname{tr}\mathbf{C}_\mathrm{r}^2\right) = \mathrm{I}_2 - (\mathrm{I}_4 - 1)\mathrm{I}_1 - (\mathrm{I}_4^{-1} - 1)\mathrm{I}_5 \\
\mathrm{III}_{\mathbf{C}_\mathrm{r}} &= \det\mathbf{C}_\mathrm{r} = \mathrm{I}_3\mathrm{I}_4^{-1},
\end{aligned} \tag{A.1.8}$$

Similar to the final formulation in Section 3.2, a strain-energy function $\psi(\mathbf{C}, \mathbf{M}_0)$ is assumed, which can be additively split into two parts

$$\psi(\mathbf{C}, \mathbf{M}_0) = \psi_\mathrm{a}(\mathbf{C}_\mathrm{a}) + \psi_\mathrm{r}(\mathbf{C}_\mathrm{r}), \tag{A.1.9}$$

where $\psi_\mathrm{a}(\mathbf{C}_\mathrm{a})$ represents the strain-energy depending on the deformation along the preferred direction only, and it can be assumed to be a function of I_4 since the three principal invariants of $\mathbf{C}_\mathrm{a}$ are functions of I_4. $\psi_\mathrm{r}(\mathbf{C}_\mathrm{r})$ represents the remaining part of the strain-energy caused by the deformation in the matrix material, which is regarded as a nearly incompressible isotropic material, i.e.,

$$\begin{aligned}
\psi(\mathbf{C}, \mathbf{M}_0) &= \psi_\mathrm{a}(\mathrm{I}_4) + \psi_\mathrm{r}(J_\mathrm{r}, \mathrm{I}_{\overline{\mathbf{C}}_\mathrm{r}}) \\
&= \psi_\mathrm{a}(\mathrm{I}_4) + U(J_\mathrm{r}) + w_\mathrm{r}(\mathrm{I}_{\overline{\mathbf{C}}_\mathrm{r}}),
\end{aligned} \tag{A.1.10}$$

where

$$J_\mathrm{r} = \det\mathbf{F}_\mathrm{r} = \mathrm{III}_{\mathbf{C}_\mathrm{r}}^{1/2} \quad \text{and} \quad \mathrm{I}_{\overline{\mathbf{C}}_\mathrm{r}} = J_\mathrm{r}^{-2/3}\mathrm{I}_{\mathbf{C}_\mathrm{r}}.$$

The 2nd Piola-Kirchhoff tensor results from the direct computation of

$$\begin{aligned}
\tilde{\mathbf{T}} &= 2\frac{\partial\psi(\mathbf{C}, \mathbf{M}_0)}{\partial\mathbf{C}} \\
&= 2\left(\frac{\mathrm{d}\psi_\mathrm{a}(\mathrm{I}_4)}{\mathrm{d}\mathrm{I}_4}\frac{\mathrm{d}\mathrm{I}_4}{\mathrm{d}\mathbf{C}} + \left[\frac{\partial\mathbf{C}_\mathrm{r}}{\partial\mathbf{C}}\right]^\mathrm{T}\left(\frac{\mathrm{d}U(J_\mathrm{r})}{\mathrm{d}\mathbf{C}_\mathrm{r}} + \frac{\partial w_\mathrm{r}(\mathrm{I}_{\overline{\mathbf{C}}_\mathrm{r}})}{\partial\mathbf{C}_\mathrm{r}}\right)\right) \\
&= 2\frac{\mathrm{d}\psi_\mathrm{a}(\mathrm{I}_4)}{\mathrm{d}\mathrm{I}_4}\mathbf{M}_0 + J_\mathrm{r}\frac{\mathrm{d}U(J_\mathrm{r})}{\mathrm{d}J_\mathrm{r}}\mathbf{C}^{-1} + 2J_\mathrm{r}^{-2/3}\frac{\mathrm{d}w_\mathrm{r}(\mathrm{I}_{\overline{\mathbf{C}}_\mathrm{r}})}{\mathrm{d}\mathrm{I}_{\overline{\mathbf{C}}_\mathrm{r}}}(\mathbf{C}_\mathrm{a}^{-1} - \tfrac{1}{3}\mathrm{I}_{\mathbf{C}_\mathrm{r}}\mathbf{C}^{-1}),
\end{aligned} \tag{A.1.11}$$

where use of the derivatives

$$\begin{aligned}
\frac{\mathrm{d}\mathrm{I}_4}{\mathrm{d}\mathbf{C}} &= \mathbf{M}_0 \\
\frac{\mathrm{d}U(J_\mathrm{r})}{\mathrm{d}\mathbf{C}_\mathrm{r}} &= \frac{\mathrm{d}U(J_\mathrm{r})}{\mathrm{d}J_\mathrm{r}}\frac{\mathrm{d}J_\mathrm{r}}{\mathrm{d}\mathbf{C}_\mathrm{r}} = \tfrac{1}{2}J_\mathrm{r}\frac{\mathrm{d}U(J_\mathrm{r})}{\mathrm{d}J_\mathrm{r}}\mathbf{C}_\mathrm{r}^{-1} \\
\frac{\partial w_\mathrm{r}(\mathrm{I}_{\overline{\mathbf{C}}_\mathrm{r}})}{\partial\mathbf{C}_\mathrm{r}} &= \frac{\partial w_\mathrm{r}(\mathrm{I}_{\overline{\mathbf{C}}_\mathrm{r}})}{\partial\mathrm{I}_{\overline{\mathbf{C}}_\mathrm{r}}}\left[\frac{\mathrm{d}\overline{\mathbf{C}_\mathrm{r}}}{\mathrm{d}\mathbf{C}_\mathrm{r}}\right]^\mathrm{T}\frac{\partial\mathrm{I}_{\overline{\mathbf{C}}_\mathrm{r}}}{\partial\overline{\mathbf{C}_\mathrm{r}}} = J_\mathrm{r}^{-2/3}\frac{\partial w_\mathrm{r}(\mathrm{I}_{\overline{\mathbf{C}}_\mathrm{r}})}{\partial\mathrm{I}_{\overline{\mathbf{C}}_\mathrm{r}}}(\mathbf{1} - \tfrac{1}{3}\mathrm{I}_{\mathbf{C}_\mathrm{r}}\mathbf{C}_\mathrm{r}^{-1}) \\
\left[\frac{\partial\mathbf{C}_\mathrm{r}}{\partial\mathbf{C}}\right]^\mathrm{T} &= \left[\left[\mathbf{F}_\mathrm{a}^{-\mathrm{T}} \otimes \mathbf{F}_\mathrm{a}^{-\mathrm{T}}\right]^{T_{23}}\right]^\mathrm{T} = \left[\mathbf{F}_\mathrm{a}^{-1} \otimes \mathbf{F}_\mathrm{a}^{-1}\right]^{T_{23}},
\end{aligned}$$

is made. Thus, the Cauchy stress tensor $\mathbf{T}$ reads

$$\mathbf{T} = \frac{1}{J}\mathbf{F}\tilde{\mathbf{T}}\mathbf{F}^{\mathrm{T}} = \frac{1}{J}\left(2\mathrm{I}_4\frac{\partial\psi_{\mathrm{a}}(\mathrm{I}_4)}{\partial\mathrm{I}_4}\mathbf{M} + J_{\mathrm{r}}\frac{\partial U_{\mathrm{r}}(J_r)}{\partial J_r}\mathbf{I} + 2\frac{\partial w_{\mathrm{r}}(\mathrm{I}_{\mathbf{C}_{\mathrm{r}}})}{\partial\mathrm{I}_{\mathbf{C}_{\mathrm{r}}}}\overline{\mathbf{B}}_{\mathrm{r}}^{D}\right) \tag{A.1.12}$$

This constitutive model is investigated for the case of simple tension along the fiber direction, $\boldsymbol{m}_0 = \boldsymbol{E}_1$, where a similar procedure to that in 3.3.1 is applied. To this end, the stress boundary conditions $\sigma_{22} = \sigma_{33} = 0$ lead to $\lambda_2 = \lambda_3$. Let $\lambda_q := \lambda_2 = \lambda_3$ and make use of $U_{\mathrm{r}}(J_{\mathrm{r}})$ and $w_{\mathrm{r}}(\mathrm{I}_{\overline{\mathbf{C}}_{\mathrm{r}}})$

$$U_{\mathrm{r}}(J_{\mathrm{r}}) = \frac{K}{50}(J_{\mathrm{r}}^5 + J_{\mathrm{r}}^{-5} - 2) \tag{A.1.13}$$

$$w_{\mathrm{r}}(\mathrm{I}_{\overline{\mathbf{C}}_{\mathrm{r}}}) = c_{10}(\mathrm{I}_{\overline{\mathbf{C}}_{\mathrm{r}}} - 3), \tag{A.1.14}$$

then the components of the Cauchy-stresses $\mathbf{T}$ in the lateral directions can be written as

$$0 = \sigma_{22} = \sigma_{33} = \frac{K}{20}(\lambda_q^{10} - \lambda_q^{-10}) + \tfrac{1}{3}c_{10}(\lambda_q^{2/3} - \lambda_q^{-4/3}) = 0 \tag{A.1.15}$$

Since this equation is only satisfied for $\lambda_q = 1$, it follows that there is no deformation in lateral direction.

A.1.2. Second Investigation

In this investigation, the same decomposition is studied as in Section A.1.1, $\mathbf{F}_{\mathrm{a}}$ being the isochoric uniaxial tension along the fiber direction, i.e.

$$\mathbf{F}_{\mathrm{a}} = \lambda_{\mathrm{a}}\hat{\boldsymbol{e}}_1 \otimes \boldsymbol{E}_1 + \lambda_{\mathrm{a}}^{-1/2}\hat{\boldsymbol{e}}_2 \otimes \boldsymbol{E}_2 + \lambda_{\mathrm{a}}^{-1/2}\hat{\boldsymbol{e}}_3 \otimes \boldsymbol{E}_3. \tag{A.1.16}$$

Thus, $\mathbf{C}_{\mathrm{a}}$ reads

$$\begin{aligned}
\mathbf{C}_{\mathrm{a}} &= \mathbf{F}_{\mathrm{a}}^{\mathrm{T}}\mathbf{F}_{\mathrm{a}} \\
&= (\lambda_{\mathrm{a}}\boldsymbol{E}_1 \otimes \hat{\boldsymbol{e}}_1 + \lambda_{\mathrm{a}}^{-1/2}\boldsymbol{E}_2 \otimes \hat{\boldsymbol{e}}_2 + \lambda_{\mathrm{a}}^{-1/2}\boldsymbol{E}_3 \otimes \hat{\boldsymbol{e}}_3)(\lambda_{\mathrm{a}}\hat{\boldsymbol{e}}_1 \otimes \boldsymbol{E}_1 + \lambda_{\mathrm{a}}^{-1/2}\hat{\boldsymbol{e}}_2 \otimes \boldsymbol{E}_2 + \lambda_{\mathrm{a}}^{-1/2}\hat{\boldsymbol{e}}_3 \otimes \boldsymbol{E}_3) \\
&= \lambda_{\mathrm{a}}^2\boldsymbol{E}_1 \otimes \boldsymbol{E}_1 + \lambda_{\mathrm{a}}^{-1}\boldsymbol{E}_2 \otimes \boldsymbol{E}_2 + \lambda_{\mathrm{a}}^{-1}\boldsymbol{E}_3 \otimes \boldsymbol{E}_3 \\
&= \lambda_{\mathrm{a}}^{-1}(\underbrace{\lambda_{\mathrm{a}}^3\boldsymbol{E}_1 \otimes \boldsymbol{E}_1 - \boldsymbol{E}_1 \otimes \boldsymbol{E}_1}_{(\lambda_{\mathrm{a}}^3-1)\boldsymbol{E}_1\otimes\boldsymbol{E}_1} + \underbrace{\boldsymbol{E}_1 \otimes \boldsymbol{E}_1 + \boldsymbol{E}_2 \otimes \boldsymbol{E}_2 + \boldsymbol{E}_3 \otimes \boldsymbol{E}_3}_{\mathbf{1}}) \\
&= \lambda_{\mathrm{a}}^{-1}\left((\lambda_{\mathrm{a}}^3 - 1)\mathbf{M}_0 + \mathbf{I}\right) \qquad \text{(A.1.17)} \\
&= \mathrm{I}_4^{-1/2}\left((\mathrm{I}_4^{3/2} - 1)\mathbf{M}_0 + \mathbf{I}\right), \qquad \text{(A.1.18)}
\end{aligned}$$

while $\mathbf{F}_{\mathrm{r}}$ and $\mathbf{C}_{\mathrm{r}}$ have the same definition as in the first investigation, see (A.1.3) and (A.1.6). The three principal invariants of $\mathbf{C}_{\mathrm{a}}$ and $\mathbf{C}_{\mathrm{r}}$ are

$$\begin{aligned}
\mathrm{I}_{\mathbf{C}_{\mathrm{a}}} &= \mathrm{I}_4 + 2\mathrm{I}_4 \\
\mathrm{II}_{\mathbf{C}_{\mathrm{a}}} &= 3\mathrm{I}_4^{-1} + 2\mathrm{I}_4^{1/2} \qquad \text{(A.1.19)} \\
\mathrm{III}_{\mathbf{C}_{\mathrm{a}}} &= 1,
\end{aligned}$$

and

$$\begin{aligned} \mathrm{I}_{\mathbf{C}_\mathrm{r}} &= (\mathrm{I}_1 - \mathrm{I}_4)\mathrm{I}_4^{1/2} + 1 \\ \mathrm{II}_{\mathbf{C}_\mathrm{r}} &= \mathrm{I}_2\mathrm{I}_4 - (\mathrm{I}_4^2 - \mathrm{I}_4^{1/2})\mathrm{I}_1 - (\mathrm{I}_4 - \mathrm{I}_4^{-1/2})\mathrm{I}_5 \\ \mathrm{III}_{\mathbf{C}_\mathrm{r}} &= \mathrm{I}_3. \end{aligned} \tag{A.1.20}$$

By using the same additively decomposed strain-energy function as before, the same constitutive model as in (A.1.12) is obtained. When the resulting model is investigated with the help of Eqs.(A.1.13) and (A.1.14), the components of $\mathbf{T}$ in the lateral directions read

$$0 = \sigma_{22} = \sigma_{33} = \frac{K}{20}\left((\lambda_1\lambda_q^2)^5 - (\lambda_1\lambda_q^2)^{-5}\right) + \tfrac{1}{3}c_{10}(\lambda_1\lambda_q^2)^{1/3}\left(1 - (\lambda_1\lambda_q^2)^{-1}\right), \tag{A.1.21}$$

with $\lambda_q = \lambda_1^{-1/2}$. From this equation, it becomes clear that the deformation is always isochoric for a uniaxial tensile problem. In other words, it is not possible to model a material with a Poisson-ratio less than 0.5.

A.1.3. Third Investigation

By way of a further trial to overcome the problem mentioned above, a modification of $\mathbf{F}_\mathrm{a}$ is employed to describe an equi-biaxial deformation on the transverse directions in addition to the iso-choric uniaxial deformation along the fiber direction

$$\mathbf{F}_\mathrm{a} = \lambda_\mathrm{a}\hat{\boldsymbol{e}}_1 \otimes \boldsymbol{E}_1 + \left(\frac{J}{\lambda_\mathrm{a}}\right)^{1/2}\hat{\boldsymbol{e}}_2 \otimes \boldsymbol{E}_2 + \left(\frac{J}{\lambda_\mathrm{a}}\right)^{1/2}\hat{\boldsymbol{e}}_3 \otimes \boldsymbol{E}_3, \tag{A.1.22}$$

implying

$$\mathbf{C}_\mathrm{a} = \frac{J}{\lambda_\mathrm{a}}\left(\left(\frac{\lambda_\mathrm{a}^3}{J}\right)\mathbf{M}_0 + \mathbf{I}\right) \tag{A.1.23}$$

$$= \frac{J}{\mathrm{I}_4^{1/2}}\left(\left(\frac{\mathrm{I}_4^{3/2}}{J}\right)\mathbf{M}_0 + \mathbf{I}\right). \tag{A.1.24}$$

Again, $\mathbf{F}_\mathrm{r}$ and $\mathbf{C}_\mathrm{r}$ have the same definitions as before. The three principal invariants of $\mathbf{C}_\mathrm{a}$ and $\mathbf{C}_\mathrm{r}$ read

$$\begin{aligned} \mathrm{I}_{\mathbf{C}_\mathrm{a}} &= \mathrm{I}_4 + 2\left(\frac{\mathrm{I}_3}{\mathrm{I}_4}\right)^{1/2} \\ \mathrm{II}_{\mathbf{C}_\mathrm{a}} &= \frac{\mathrm{I}_3}{\mathrm{I}_4} + 2(\mathrm{I}_3\mathrm{I}_4)^{1/2} \\ \mathrm{III}_{\mathbf{C}_\mathrm{a}} &= \mathrm{I}_3 \end{aligned} \tag{A.1.25}$$

and

$$\begin{aligned}
\mathrm{I}_{\mathbf{C}_\mathrm{r}} &= \left(\frac{\mathrm{I}_4}{\mathrm{I}_3}\right)^{1/2}\mathrm{I}_1 - \left(\frac{\mathrm{I}_4^3}{\mathrm{I}_3}\right)^{1/2} + 1 \\
\mathrm{II}_{\mathbf{C}_\mathrm{r}} &= \mathrm{I}_2 + \left(1 - \left(\frac{\mathrm{I}_4^3}{\mathrm{I}_3}\right)^{1/2}\right)\left(\frac{\mathrm{I}_4}{\mathrm{I}_3}\right)\mathrm{I}_1 + \left(1 - \left(\frac{\mathrm{I}_3}{\mathrm{I}_4^3}\right)^{1/2}\right)\left(\frac{\mathrm{I}_4}{\mathrm{I}_3}\right)\mathrm{I}_5 \\
\mathrm{III}_{\mathbf{C}_\mathrm{r}} &= 1
\end{aligned} \tag{A.1.26}$$

In this case, the total volume change in the material is included in $\mathbf{F}_\mathrm{a}$. Using a form of additively decomposed strain-energy function

$$\psi(\mathbf{C}, \mathbf{M}_0) = \psi_\mathrm{a}(\mathrm{I}_4, J) + w_\mathrm{r}(\mathrm{I}_{\mathbf{C}_\mathrm{r}}), \tag{A.1.27}$$

with,

$$\begin{aligned}
\psi_\mathrm{a}(\mathrm{I}_4, J) &= v(\mathrm{I}_4) + \frac{K}{50}(J^5 + J^{-5} - 2) \\
w_\mathrm{r}(\mathrm{I}_{\mathbf{C}_\mathrm{r}}) &= c_{10}(\mathrm{I}_{\mathbf{C}_\mathrm{r}} - 3)^2
\end{aligned}$$

a constitutive model of the form

$$\mathbf{T} = \frac{2}{J}\left(\mathrm{I}_4\frac{\partial\psi_\mathrm{a}(\mathrm{I}_4, J)}{\partial \mathrm{I}_4}\mathbf{M} + \tfrac{1}{2}J\frac{\partial\psi_\mathrm{a}(\mathrm{I}_4, J)}{\partial J}\mathbf{I} + \frac{\partial w_\mathrm{r}(\mathrm{I}_{\mathbf{C}_\mathrm{r}})}{\partial \mathrm{I}_{\mathbf{C}_\mathrm{r}}}\mathbf{B}_\mathrm{r}\right). \tag{A.1.28}$$

is obtained. This model is again studied for the uniaxial tensile problem leading to the equation

$$0 = \sigma_{22} = \sigma_{33} = \frac{K}{20}(J^5 - J^{-5}) \tag{A.1.29}$$

for the lateral direction. This produces the result that

$$\lambda_q = \lambda_1^{-1/2},$$

which means that the material always behaves as an incompressible material. The same result is reported by Guo et al. (2008), who assumed the same form of the deformation gradient and also mentioned this type of problem. Again, based on this assumption, it is not possible to model the behavior of a material with a Poisson-ratio different to an incompressible material.

A.2. Invariants of C_r

The tensor $\mathbf{C}_\mathrm{r}$ is defined in (3.35) as the push-forward of the unimodular right Cauchy-Green tensor $\overline{\mathbf{C}}$, i.e.,

$$\mathbf{C}_\mathrm{r} = \mathbf{F}_\mathrm{a}^{-\mathrm{T}}\,\overline{\mathbf{C}}\,\mathbf{F}_\mathrm{a}^{-1}.$$

Thus, the three principal invariants of $\mathbf{C}_\mathrm{r}$ are calculated

$$
\begin{aligned}
\mathrm{I}_{\mathbf{C}_\mathrm{r}} &= \operatorname{tr}\mathbf{C}_\mathrm{r} = \operatorname{tr}(\mathbf{F}_\mathrm{a}^{-\mathrm{T}}\,\overline{\mathbf{C}}\,\mathbf{F}_\mathrm{a}^{-1}) = \operatorname{tr}(\overline{\mathbf{C}}\,\mathbf{F}_\mathrm{a}^{-1}\,\mathbf{F}_\mathrm{a}^{-\mathrm{T}}) = \operatorname{tr}(\overline{\mathbf{C}}\,\mathbf{C}_\Theta^{-1}) \\
&= \operatorname{tr}\left(\overline{\mathbf{C}}\left((\bar{\mathrm{I}}_4^{-1}-1)\mathbf{M}_0+\mathbf{1}\right)\right) = (\bar{\mathrm{I}}_4^{-1}-1)\operatorname{tr}(\overline{\mathbf{C}}\mathbf{M}_0) + \operatorname{tr}\overline{\mathbf{C}} = (\bar{\mathrm{I}}_4^{-1}-1)\bar{\mathrm{I}}_4 + \mathrm{I}_{\overline{\mathbf{C}}} \\
&= \mathrm{I}_{\overline{\mathbf{C}}} - \bar{\mathrm{I}}_4 + 1 \\
\mathrm{II}_{\mathbf{C}_\mathrm{r}} &= \tfrac{1}{2}\left((\operatorname{tr}\mathbf{C}_\mathrm{r})^2 - \operatorname{tr}\mathbf{C}_\mathrm{r}^2\right) \\
&= \tfrac{1}{2}\left((\mathrm{I}_{\overline{\mathbf{C}}} - \bar{\mathrm{I}}_4 + 1)^2 - (\mathrm{I}_{\overline{\mathbf{C}}}^2 + \bar{\mathrm{I}}_4^2 - 2(\mathrm{II}_{\overline{\mathbf{C}}} + \bar{\mathrm{I}}_4) + 2(\bar{\mathrm{I}}_4^{-1}-1)\bar{\mathrm{I}}_5 + 1)\right) \\
&= \mathrm{II}_{\overline{\mathbf{C}}} + \mathrm{I}_{\overline{\mathbf{C}}}(1-\bar{\mathrm{I}}_4) + \bar{\mathrm{I}}_5(1-\bar{\mathrm{I}}_4^{-1}) \\
\mathrm{III}_{\mathbf{C}_\mathrm{r}} &= \det\mathbf{C}_\mathrm{r} = \det(\mathbf{F}_\mathrm{a}^{-\mathrm{T}}\,\overline{\mathbf{C}}\,\mathbf{F}_\mathrm{a}^{-1}) = \det\operatorname{tr}(\overline{\mathbf{C}}\,\mathbf{C}_\Theta^{-1}) = \det\overline{\mathbf{C}}\det\mathbf{C}_\Theta^{-1} = \det\left((\bar{\mathrm{I}}_4^{-1}-1)\mathbf{M}_0+\mathbf{1}\right) \\
&= \det\left((\bar{\mathrm{I}}_4^{-1}-1)\mathbf{M}_0\right) + \operatorname{cof}\left((\bar{\mathrm{I}}_4^{-1}-1)\mathbf{M}_0\right)\cdot\mathbf{1} + (\bar{\mathrm{I}}_4^{-1}-1)\mathbf{M}_0\cdot\operatorname{cof}(\mathbf{1}) + \det(\mathbf{1}) \\
&= (\bar{\mathrm{I}}_4^{-1}-1)^3\det\mathbf{M}_0 + (\bar{\mathrm{I}}_4^{-1}-1)^2\operatorname{cof}\mathbf{M}_0\cdot\mathbf{1} + (\bar{\mathrm{I}}_4^{-1}-1)\mathbf{M}_0\cdot\operatorname{cof}\mathbf{1} + \det\mathbf{1} \\
&= (\bar{\mathrm{I}}_4^{-1}-1)\mathbf{M}_0\cdot\mathbf{1} + 1 = (\bar{\mathrm{I}}_4^{-1}-1) + 1 \\
&= \bar{\mathrm{I}}_4^{-1}
\end{aligned}
$$

using

$$
\begin{aligned}
\operatorname{tr}\mathbf{C}_\mathrm{r}^2 &= \operatorname{tr}(\mathbf{F}_\mathrm{a}^{-\mathrm{T}}\,\overline{\mathbf{C}}\,\mathbf{F}_\mathrm{a}^{-1}\,\mathbf{F}_\mathrm{a}^{-\mathrm{T}}\,\overline{\mathbf{C}}\,\mathbf{F}_\mathrm{a}^{-1}) = \operatorname{tr}(\overline{\mathbf{C}}\,\underbrace{\mathbf{F}_\mathrm{a}^{-1}\,\mathbf{F}_\mathrm{a}^{-\mathrm{T}}}_{\mathbf{C}_\mathrm{a}^{-1}}\,\overline{\mathbf{C}}\,\underbrace{\mathbf{F}_\mathrm{a}^{-1}\,\mathbf{F}_\mathrm{a}^{-\mathrm{T}}}_{\mathbf{C}_\mathrm{a}^{-1}}) \\
&= \operatorname{tr}(\overline{\mathbf{C}}\,\mathbf{C}_\Theta^{-1}\,\overline{\mathbf{C}}\,\mathbf{C}_\Theta^{-1}) = \overline{\mathbf{C}}\,\mathbf{C}_\Theta^{-1}\cdot\mathbf{C}_\Theta^{-1}\,\overline{\mathbf{C}} = \overline{\mathbf{C}}\left((\bar{\mathrm{I}}_4^{-1}-1)\mathbf{M}_0+\mathbf{1}\right)\cdot\left((\bar{\mathrm{I}}_4^{-1}-1)\mathbf{M}_0+\mathbf{1}\right)\overline{\mathbf{C}} \\
&= \left((\bar{\mathrm{I}}_4^{-1}-1)\overline{\mathbf{C}}\mathbf{M}_0 + \overline{\mathbf{C}}\right)\cdot\left((\bar{\mathrm{I}}_4^{-1}-1)\mathbf{M}_0\overline{\mathbf{C}} + \overline{\mathbf{C}}\right) \\
&= (\bar{\mathrm{I}}_4^{-1}-1)^2\underbrace{\overline{\mathbf{C}}\mathbf{M}_0\cdot\mathbf{M}_0\overline{\mathbf{C}}}_{\bar{\mathrm{I}}_4^2} + (\bar{\mathrm{I}}_4^{-1}-1)(\underbrace{\overline{\mathbf{C}}\mathbf{M}_0\cdot\overline{\mathbf{C}}}_{\bar{\mathrm{I}}_5} + \underbrace{\overline{\mathbf{C}}\cdot\mathbf{M}_0\overline{\mathbf{C}}}_{\bar{\mathrm{I}}_5}) + \underbrace{\overline{\mathbf{C}}\cdot\overline{\mathbf{C}}}_{\operatorname{tr}\overline{\mathbf{C}}^2} \\
&= \bar{\mathrm{I}}_4^2(\bar{\mathrm{I}}_4^{-1}-1)^2 + 2\bar{\mathrm{I}}_5(\bar{\mathrm{I}}_4^{-1}-1) + \operatorname{tr}\overline{\mathbf{C}}^2 \\
&= \bar{\mathrm{I}}_4^2(\bar{\mathrm{I}}_4^{-2} - 2\bar{\mathrm{I}}_4^{-1} + 1) + 2\bar{\mathrm{I}}_5(\bar{\mathrm{I}}_4^{-1}-1) + \underbrace{\operatorname{tr}\overline{\mathbf{C}}^2 - \mathrm{I}_{\overline{\mathbf{C}}}^2}_{-2\mathrm{II}_{\overline{\mathbf{C}}}} + \mathrm{I}_{\overline{\mathbf{C}}}^2 \\
&= \mathrm{I}_{\overline{\mathbf{C}}}^2 + \bar{\mathrm{I}}_4^2 - 2(\mathrm{II}_{\overline{\mathbf{C}}} + \bar{\mathrm{I}}_4) + 2(\bar{\mathrm{I}}_4^{-1}-1)\bar{\mathrm{I}}_5 + 1
\end{aligned}
$$

to calculate the second invariant $\mathrm{II}_{\mathbf{C}_\mathrm{r}}$, with

$$
\begin{aligned}
\overline{\mathbf{C}}\mathbf{M}_0\cdot\mathbf{M}_0\overline{\mathbf{C}} &= \overline{\mathbf{F}}^{\mathrm{T}}\,\overline{\mathbf{F}}\,\mathbf{M}_0\cdot\mathbf{M}_0\,\overline{\mathbf{F}}^{\mathrm{T}}\,\overline{\mathbf{F}} = \overline{\mathbf{F}}\,\mathbf{M}_0\,\overline{\mathbf{F}}^{\mathrm{T}}\cdot\overline{\mathbf{F}}\,\mathbf{M}_0\,\overline{\mathbf{F}}^{\mathrm{T}} \\
&= (\bar{\mathrm{I}}_4\mathbf{M})\cot(\bar{\mathrm{I}}_4\mathbf{M}) = \bar{\mathrm{I}}_4^2\underbrace{\mathbf{M}\cdot\mathbf{M}}_{\mathbf{1}} = \bar{\mathrm{I}}_4^2 \\
\overline{\mathbf{C}}\mathbf{M}_0\cdot\overline{\mathbf{C}} &= \overline{\mathbf{C}}\cdot\mathbf{M}_0\overline{\mathbf{C}} = \overline{\mathbf{C}}^2\cdot\mathbf{M}_0 = \bar{\mathrm{I}}_5.
\end{aligned}
$$

A.3. Calculation of $\mathbf{C}_{\mathrm{a}}^{-1}$

The tensor $\mathbf{C}_{\mathrm{a}}$ is given by Eq.(3.29), i.e.,

$$\mathbf{C}_{\mathrm{a}} = (\bar{\lambda}_{\mathrm{a}}^2 - 1)\mathbf{M}_0 + \mathbf{1} = (\bar{\mathrm{I}}_4 - 1)\mathbf{M}_0 + \mathbf{1}$$

The inverse of $\mathbf{C}_{\mathrm{a}}$ is calculated by applying the Cayley-Hamilton Theorem, which states that if a square tensor is set in its own characteristic polynomial, the result is zero or, in other words, the tensor satisfies its own characteristic equation, see (Hartmann, 2003) and (Ogden, 1997). To this end, the characteristic polynomial of $\mathbf{C}_{\mathrm{a}}$ reads

$$-\mathbf{C}_{\mathrm{a}}^3 + \mathrm{I}_{\mathbf{C}_{\mathrm{a}}}\mathbf{C}_{\mathrm{a}}^2 - \mathrm{II}_{\mathbf{C}_{\mathrm{a}}}\mathbf{C}_{\mathrm{a}} + \mathrm{III}_{\mathbf{C}_{\mathrm{a}}}\mathbf{1} = \mathbf{0}, \tag{A.3.1}$$

leading to

$$\mathbf{C}_{\mathrm{a}}^{-1} = \frac{1}{\mathrm{III}_{\mathbf{C}_{\mathrm{a}}}}\left(\mathbf{C}_{\mathrm{a}}^2 - \mathrm{I}_{\mathbf{C}_{\mathrm{a}}}\mathbf{C}_{\mathrm{a}} + \mathrm{II}_{\mathbf{C}_{\mathrm{a}}}\mathbf{1}\right), \tag{A.3.2}$$

with

$$\begin{aligned}
\mathbf{C}_{\mathrm{a}}^2 &= \left((\bar{\mathrm{I}}_4 - 1)\mathbf{M}_0 + \mathbf{1}\right)\left((\bar{\mathrm{I}}_4 - 1)\mathbf{M}_0 + \mathbf{1}\right) \\
&= \left((\bar{\mathrm{I}}_4 - 1)^2 + 2(\bar{\mathrm{I}}_4 - 1)\right)\mathbf{M}_0 + \mathbf{1} \\
&= \left(\bar{\mathrm{I}}_4^2 - 2\bar{\mathrm{I}}_4 + 1 + 2\bar{\mathrm{I}}_4 - 2)\right)\mathbf{M}_0 + \mathbf{1} \\
&= (\bar{\mathrm{I}}_4^2 - 1)\mathbf{M}_0 + \mathbf{1}
\end{aligned}$$

and the three principal invariants of $\mathbf{C}_{\mathrm{a}}$ read

$$\begin{aligned}
\mathrm{I}_{\mathbf{C}_{\mathrm{a}}} &= \mathrm{tr}\,\mathbf{C}_{\mathrm{a}} &&= \bar{\mathrm{I}}_4 + 2 \\
\mathrm{II}_{\mathbf{C}_{\mathrm{a}}} &= \tfrac{1}{2}((\mathrm{tr}\,\mathbf{C}_{\mathrm{a}})^2 - \mathrm{tr}\,\mathbf{C}_{\mathrm{a}}^2) &&= 2\bar{\mathrm{I}}_4 + 1 \\
\mathrm{III}_{\mathbf{C}_{\mathrm{a}}} &= \det\mathbf{C}_{\mathrm{a}} &&= \bar{\mathrm{I}}_4,
\end{aligned}$$

see Eq.(3.30). Thus, inserting $\mathbf{C}_{\mathrm{a}}$, $\mathbf{C}_{\mathrm{a}}^2$ as well as the three invariants $\mathrm{I}_{\mathbf{C}_{\mathrm{a}}}$, $\mathrm{II}_{\mathbf{C}_{\mathrm{a}}}$ and $\mathrm{III}_{\mathbf{C}_{\mathrm{a}}}$ into Eq.(A.3.2), gives

$$\begin{aligned}
\mathbf{C}_{\mathrm{a}}^{-1} &= \frac{1}{\bar{\mathrm{I}}_4}\left((\bar{\mathrm{I}}_4^2 - 1)\mathbf{M}_0 + \mathbf{1} - (\bar{\mathrm{I}}_4 + 2)\left((\bar{\mathrm{I}}_4 - 1)\mathbf{M}_0 + \mathbf{1}\right) + (2\bar{\mathrm{I}}_4 + 1)\mathbf{1}\right) \\
&= \frac{1}{\bar{\mathrm{I}}_4}\left((\bar{\mathrm{I}}_4^2 - 1)\mathbf{M}_0 + \mathbf{1} - (\bar{\mathrm{I}}_4^2 + \bar{\mathrm{I}}_4 - 2)\mathbf{M}_0 - (\bar{\mathrm{I}}_4 + 2)\mathbf{1} + (2\bar{\mathrm{I}}_4 + 1)\mathbf{1}\right) \\
&= \frac{1}{\bar{\mathrm{I}}_4}\left((1 - \bar{\mathrm{I}}_4)\mathbf{M}_0 + \bar{\mathrm{I}}_4\mathbf{1}\right) \\
&= (\bar{\mathrm{I}}_4^{-1} - 1)\mathbf{M}_0 + \mathbf{1}.
\end{aligned} \tag{A.3.3}$$

A.4. Calculation of 2nd Piola-Kirchhoff Stress Tensor

The calculation of the 2nd Piola-Kirchhoff stress tensor, given in Eq.(3.48), requires the derivatives of the strain-energy functions in (3.47) with respect to the right Cauchy-Green tensor $\mathbf{C}$. The beginning is with the term $\partial\psi^{\text{vol}}(J,\mathrm{I}_4)/\partial\mathbf{C}$

$$\mathsf{D}_{\mathbf{C}}\,\psi^{\text{vol}}(J,\mathrm{I}_4)[\mathbf{H}] = \underbrace{\frac{1}{2}\left(\frac{\partial\psi^{\text{vol}}(J,\mathrm{I}_4)}{\partial J}J\mathbf{C}^{-1} + 2\frac{\partial\psi^{\text{vol}}(J,\mathrm{I}_4)}{\partial\mathrm{I}_4}\mathbf{M}_0\right)}_{\dfrac{\mathrm{d}\psi^{\text{vol}}(J,\mathrm{I}_4)}{\mathrm{d}\mathbf{C}}}\cdot\mathbf{H} = \tag{A.4.1}$$

$$= \frac{\mathrm{I}_4^{-1/2}}{2}(U'(J)J\mathbf{C}^{-1} - \psi^{\text{vol}}(J,\mathrm{I}_4)\mathbf{M}_0)\cdot\mathbf{H}$$

with

$$U'(J) = \frac{K}{10}(J^4 - J^{-6})$$

and

$$\frac{\partial\psi^{\text{vol}}(J,\mathrm{I}_4)}{\partial\mathrm{I}_4} = -\frac{1}{2}U(J)\mathrm{I}_4^{-3/2}.$$

In this case, the Gateaux-derivative is employed

$$\mathsf{D}\,f(x)[h] = \frac{\mathrm{d}}{\mathrm{d}s}\,f(x+sh)|_{s=0}\,.$$

The second expression results from the Gateaux-derivative of the function $v(\overline{\lambda}_{\mathsf{a}})$,

$$\mathsf{D}_{\mathbf{C}}\,v(\overline{\lambda}_{\mathsf{a}}(\overline{\mathbf{C}}(\mathbf{C})))[\mathbf{H}] = v'(\overline{\lambda}_{\mathsf{a}})\mathsf{D}_{\mathbf{C}}\,\overline{\lambda}_{\mathsf{a}}(\overline{\mathbf{C}}(\mathbf{C}))[\mathbf{H}].$$

Using definitions (3.23) and (3.7) requires the differential

$$\mathbf{H}_1 = \mathsf{D}_{\mathbf{C}}\,\overline{\mathbf{C}}(\mathbf{C})[\mathbf{H}] = \mathsf{D}_{\mathbf{C}}\,((\det\mathbf{C})^{-1/3}\mathbf{C})[\mathbf{H}] = (\det\mathbf{C})^{-1/3}\left[\mathcal{I} - \frac{1}{3}\mathbf{C}\otimes\mathbf{C}^{-1}\right]\mathbf{H} \tag{A.4.2}$$

with the fourth-order identity tensor

$$\mathcal{I} := [\mathbf{I}\otimes\mathbf{I}]^{T_{23}} = \delta_{ik}\delta_{jl}\boldsymbol{e}_i\otimes\boldsymbol{e}_j\otimes\boldsymbol{e}_k\otimes\boldsymbol{e}_l,$$

$\mathcal{I}\mathbf{A} = \mathbf{A}$. The transposition T_{23} indicates the exchange of the second and third index leading to the property

$$[\mathbf{A}\otimes\mathbf{B}]^{T_{23}}\,\mathbf{C} = \mathbf{A}\mathbf{C}\mathbf{B}^{\mathrm{T}},$$

see, for example, Hartmann (2002b) or Hartmann (2003). For

$$\mathsf{D}_{\mathbf{C}}\,\overline{\lambda}_{\mathsf{a}}(\overline{\mathbf{C}}(\mathbf{C}))[\mathbf{H}] = \mathsf{D}\,\overline{\lambda}_{\mathsf{a}}(\overline{\mathbf{C}})[\mathsf{D}_{\mathbf{C}}\,\overline{\mathbf{C}}(\mathbf{C})[\mathbf{H}]] = \mathsf{D}\,\overline{\lambda}_{\mathsf{a}}(\overline{\mathbf{C}})[\mathbf{H}_1]$$

with $\mathbf{H}_1$ of Eq.(A.4.2), the chain-rule is applied, see Bowen (1989). Based on Eq.(3.23), it follows

$$\begin{aligned}
\mathsf{D}\,\overline{\lambda}_{\mathrm{a}}(\overline{\mathbf{C}})[\mathbf{H}_1] &= \tfrac{1}{2}(\overline{\mathbf{C}}\cdot\mathbf{M}_0)^{-1/2}\mathbf{M}_0\cdot\mathbf{H}_1 = \\
&= \frac{\bar{\mathrm{I}}_4^{-1/2}}{2}\mathbf{M}_0\cdot(\det\mathbf{C})^{-1/3}\left[\mathcal{I}-\frac{1}{3}\mathbf{C}\otimes\mathbf{C}^{-1}\right]\mathbf{H} = \\
&= \frac{\bar{\mathrm{I}}_4^{-1/2}(\det\mathbf{C})^{-1/3}}{2}\left[\mathcal{I}-\frac{1}{3}\mathbf{C}^{-1}\otimes\mathbf{C}\right]\mathbf{M}_0\cdot\mathbf{H} = \\
&= \frac{\bar{\mathrm{I}}_4^{-1/2}(\det\mathbf{C})^{-1/3}}{2}\left(\mathbf{M}_0-\frac{\mathrm{I}_4}{3}\mathbf{C}^{-1}\right)\cdot\mathbf{H}.
\end{aligned}$$

The derivative accordingly reads

$$\begin{aligned}
\frac{\mathrm{d}v(\overline{\lambda}_{\mathrm{a}})}{\mathrm{d}\mathbf{C}} &= \tfrac{1}{2}v'(\overline{\lambda}_{\mathrm{a}})\bar{\mathrm{I}}_4^{-1/2}(\det\mathbf{C})^{-1/3}\left(\mathbf{M}_0-\frac{\mathrm{I}_4}{3}\mathbf{C}^{-1}\right) && \text{(A.4.3)}\\
&= \tfrac{1}{2}v'(\overline{\lambda}_{\mathrm{a}})\bar{\mathrm{I}}_4^{-1/2}(\det\mathbf{C})^{-1/3}\left(\mathbf{M}_0\mathbf{C}-\tfrac{1}{3}\mathrm{I}_4\mathbf{1}\right)\mathbf{C}^{-1}\\
&= \tfrac{1}{2}v'(\overline{\lambda}_{\mathrm{a}})\bar{\mathrm{I}}_4^{-1/2}\underbrace{\left(\mathbf{M}_0\overline{\mathbf{C}}-\tfrac{1}{3}\bar{\mathrm{I}}_4\mathbf{1}\right)}_{(\mathbf{M}_0\overline{\mathbf{C}})^{\mathrm{D}}}\mathbf{C}^{-1}\\
&= \tfrac{1}{2}v'(\overline{\lambda}_{\mathrm{a}})\bar{\mathrm{I}}_4^{-1/2}(\mathbf{M}_0\overline{\mathbf{C}})^{\mathrm{D}}\mathbf{C}^{-1} && \text{(A.4.4)}
\end{aligned}$$

The derivative of $w(\mathbf{C}_{\mathrm{r}})$ with respect to $\mathbf{C}$ is more complicated. Again the chain-rule is applied

$$\mathsf{D}_{\mathbf{C}}\,w(\mathbf{C}_{\mathrm{r}}(\overline{\mathbf{C}}(\mathbf{C})))[\mathbf{H}] = \mathsf{D}w(\mathbf{C}_{\mathrm{r}})\overbrace{[\mathsf{D}\mathbf{C}_{\mathrm{r}}(\overline{\mathbf{C}})\underbrace{[\mathsf{D}_{\mathbf{C}}\,\overline{\mathbf{C}}(\mathbf{C})[\mathbf{H}]]}_{\mathbf{H}_1}]}^{\mathbf{H}_2} \qquad \text{(A.4.5)}$$

with $\mathbf{H}_1$ given in Eq.(A.4.2). Using definition (3.35) leads to the differential

$$\begin{aligned}
\mathbf{H}_2 = \mathsf{D}_{\overline{\mathbf{C}}}\,\mathbf{C}_{\mathrm{r}}(\overline{\mathbf{C}})[\mathbf{H}_1] &= \mathbf{F}_{\mathrm{a}}^{-T}\mathbf{H}_1\mathbf{F}_{\mathrm{a}}^{-1} = \left[\mathbf{F}_{\mathrm{a}}^{-T}\otimes\mathbf{F}_{\mathrm{a}}^{-T}\right]^{T_{23}}\mathbf{H}_1 = \\
&= (\det\mathbf{C})^{-1/3}\left[\mathbf{F}_{\mathrm{a}}^{-T}\otimes\mathbf{F}_{\mathrm{a}}^{-T}\right]^{T_{23}}\left[\mathcal{I}-\frac{1}{3}\mathbf{C}\otimes\mathbf{C}^{-1}\right]\mathbf{H}.
\end{aligned}$$

Inserting this expression into Eq.(A.4.5), yields

$$\begin{aligned}
\mathsf{D}_{\mathbf{C}}\,w(\mathbf{C}_{\mathrm{r}}(\overline{\mathbf{C}}(\mathbf{C})))[\mathbf{H}] &= (\det\mathbf{C})^{-1/3}\frac{\mathrm{d}w}{\mathrm{d}\mathbf{C}_{\mathrm{r}}}\cdot\left[\mathbf{F}_{\mathrm{a}}^{-T}\otimes\mathbf{F}_{\mathrm{a}}^{-T}\right]^{T_{23}}\left[\bar{\mathrm{I}}_4-\frac{1}{3}\mathbf{C}\otimes\mathbf{C}^{-1}\right]\mathbf{H} = \\
&= (\det\mathbf{C})^{-1/3}\mathbf{F}_{\mathrm{a}}^{-1}\frac{\mathrm{d}w}{\mathrm{d}\mathbf{C}_{\mathrm{r}}}\mathbf{F}_{\mathrm{a}}^{-T}\cdot\left[\mathcal{I}-\frac{1}{3}\mathbf{C}\otimes\mathbf{C}^{-1}\right]\mathbf{H}. \qquad \text{(A.4.6)}
\end{aligned}$$

The term

$$\mathbf{F}_{\mathrm{a}}^{-1}\frac{\mathrm{d}w(\hat{\mathrm{I}}_{\mathbf{C}_{\mathrm{r}}})}{\mathrm{d}\mathbf{C}_{\mathrm{r}}}\mathbf{F}_{\mathrm{a}}^{-T}$$

is obviously the pull-back operation of a stress-tensor

$$\hat{\mathbf{S}} = \frac{\mathrm{d}w(\hat{\mathrm{I}}_{\mathbf{C}_\mathrm{r}})}{\mathrm{d}\mathbf{C}_\mathrm{r}},$$

which operates on the intermediate configuration $\hat{\mathcal{B}}$, see Fig. 3.2. For the strain-energy function (3.44), the derivative

$$\frac{\mathrm{d}w(\hat{\mathrm{I}}_{\mathbf{C}_\mathrm{r}})}{\mathrm{d}\mathbf{C}_\mathrm{r}} = \frac{\beta}{2}\mathbf{1}$$

is obtained, leading to

$$\begin{aligned}
\mathsf{D}_{\mathbf{C}}\, w(\mathbf{C}_\mathrm{r})[\mathbf{H}] &= w'(\hat{\mathrm{I}}_{\mathbf{C}_\mathrm{r}})(\det\mathbf{C})^{-1/3}\left(\mathbf{C}_\mathrm{a}^{-1} - \frac{1}{3}(\mathbf{C}\cdot\mathbf{C}_\mathrm{a}^{-1})\mathbf{C}^{-1}\right)\cdot\mathbf{H} = \\
&= w'(\hat{\mathrm{I}}_{\mathbf{C}_\mathrm{r}})(\det\mathbf{C})^{-1/3}\left((\overline{\lambda}_\mathrm{a}^{\,-2}-1)\mathbf{M}_0 + \mathbf{I} - \frac{1}{3}(\operatorname{tr}\mathbf{C} + \lambda_\mathrm{a}^2(\overline{\lambda}_\mathrm{a}^{\,-2}-1))\mathbf{C}^{-1}\right) = \\
&= w'(\hat{\mathrm{I}}_{\mathbf{C}_\mathrm{r}})\left((\det\mathbf{C})^{-1/3}((\bar{\mathrm{I}}_4^{-1}-1)\mathbf{M}_0 + \mathbf{I}) - \frac{1}{3}(\mathrm{I}_{\overline{\mathbf{C}}} - \bar{\mathrm{I}}_4 + 1)\mathbf{C}^{-1}\right) \\
&= w'(\hat{\mathrm{I}}_{\mathbf{C}_\mathrm{r}})\left((\bar{\mathrm{I}}_4^{-1}-1)\det\mathbf{C}^{-1/3}(\mathbf{M}_0\mathbf{C} - \tfrac{1}{3}\mathrm{I}_4\mathbf{1})\mathbf{C}^{-1} + \det\mathbf{C}^{-1/3}(\mathbf{C} - \tfrac{1}{3}\mathrm{I}_1\mathbf{1})\mathbf{C}^{-1}\right) \\
&= w'(\hat{\mathrm{I}}_{\mathbf{C}_\mathrm{r}})\left((\bar{\mathrm{I}}_4^{-1}-1)\underbrace{(\mathbf{M}_0\overline{\mathbf{C}} - \tfrac{1}{3}\bar{\mathrm{I}}_4\mathbf{1})}_{(\mathbf{M}_0\overline{\mathbf{C}})^{\mathrm{D}}}\mathbf{C}^{-1} + \underbrace{(\overline{\mathbf{C}} - \tfrac{1}{3}\mathrm{I}_{\overline{\mathbf{C}}}\mathbf{1})}_{\overline{\mathbf{C}}^{\mathrm{D}}}\mathbf{C}^{-1}\right) \\
&= w'(\hat{\mathrm{I}}_{\mathbf{C}_\mathrm{r}})\left((\bar{\mathrm{I}}_4^{-1}-1)(\mathbf{M}_0\overline{\mathbf{C}})^{\mathrm{D}}\mathbf{C}^{-1} + \overline{\mathbf{C}}^{\mathrm{D}}\mathbf{C}^{-1}\right) \\
&= w'(\hat{\mathrm{I}}_{\mathbf{C}_\mathrm{r}})\left((\bar{\mathrm{I}}_4^{-1}-1)\mathbf{M}_0\overline{\mathbf{C}} + \overline{\mathbf{C}}\right)^{\mathrm{D}}\mathbf{C}^{-1}
\end{aligned} \tag{A.4.7}$$

Of course, $\hat{\mathrm{I}}_{\mathbf{C}_\mathrm{r}}$ has to be substituted by Eq.(3.37a).

Eq.(A.4.6) uses the properties

$$\left[[\mathbf{A}\otimes\mathbf{B}]^{T_{23}}\right]^{\mathrm{T}} = \left[\mathbf{A}^T\otimes\mathbf{B}^T\right]^{T_{23}} \tag{A.4.8}$$

$$[\mathbf{A}\otimes\mathbf{B}]^{T_{23}}\,[\mathbf{C}\otimes\mathbf{D}]^{T_{23}} = [\mathbf{A}\mathbf{C}\otimes\mathbf{B}\mathbf{D}]^{T_{23}} \tag{A.4.9}$$

$$\mathbf{A}\cdot\mathcal{C}\mathbf{B} = \mathcal{C}^{\mathrm{T}}\mathbf{A}\cdot\mathbf{B} \tag{A.4.10}$$

with

$$\mathcal{C}^{\mathrm{T}} = c_{klij}\boldsymbol{e}_i\otimes\boldsymbol{e}_j\otimes\boldsymbol{e}_k\otimes\boldsymbol{e}_l.$$

Combining Eqns.(A.4.1), (A.4.3) and (A.4.7) leads to Eq.(3.48).

A.5. Tangent Operator

The fourth order tangent operator is expressed in relation to the reference configuration

$$\tilde{\mathcal{C}} := 2\frac{\mathrm{d}\tilde{\mathbf{T}}}{\mathrm{d}\mathbf{C}} = 4\frac{\partial^2\psi(\mathbf{C},\mathbf{M}_0)}{\partial\mathbf{C}\partial\mathbf{C}}. \tag{A.5.1}$$

Using the strain-energy function defined in Eq.(3.47), or the 2nd Piola-Kirchhoff stress tensor (3.48), the tangent operator $\tilde{\mathcal{C}}$ takes the following form

$$\tilde{\mathcal{C}} = \tilde{\mathcal{C}}_1 + \tilde{\mathcal{C}}_2 + \tilde{\mathcal{C}}_3 + \tilde{\mathcal{C}}_4 + \tilde{\mathcal{C}}_5$$

with

$$\begin{aligned}\tilde{\mathcal{C}}_1 = (\mathrm{I}_4^{-2}\,\overline{\lambda}_{\mathrm{a}}\left(-v'(\overline{\lambda}_{\mathrm{a}}) + \overline{\lambda}_{\mathrm{a}}\,v''(\overline{\lambda}_{\mathrm{a}})\right) + 4\,\mathrm{I}_4^{-2}\left(-w'(\hat{\mathrm{I}}_{\mathbf{C}_{\mathrm{r}}}) + w''(\hat{\mathrm{I}}_{\mathbf{C}_{\mathrm{r}}})\right)\\ + 4\,J^{-2/3}(J^{-2/3} - 2\,\mathrm{I}_4^{-1})\,w''(\hat{\mathrm{I}}_{\mathbf{C}_{\mathrm{r}}}) + 4\,\frac{\partial^2\psi^{\mathrm{vol}}}{\partial\mathrm{I}_4\partial\mathrm{I}_4})\,[\mathbf{M}_0\otimes\mathbf{M}_0]\end{aligned}$$

$$\begin{aligned}\tilde{\mathcal{C}}_2 = (\frac{1}{9}\,\overline{\lambda}_{\mathrm{a}}\left(v'(\overline{\lambda}_{\mathrm{a}}) + \overline{\lambda}_{\mathrm{a}}\,v''(\overline{\lambda}_{\mathrm{a}})\right) + \frac{4}{9}((\mathrm{I}_{\overline{\mathbf{C}}} - \mathrm{I}_4)\left(w'(\hat{\mathrm{I}}_{\mathbf{C}_{\mathrm{r}}}) + 2\,w''(\hat{\mathrm{I}}_{\mathbf{C}_{\mathrm{r}}})\right)\\ + (\mathrm{I}_{\overline{\mathbf{C}}}^2 + \bar{\mathrm{I}}_4^2 - 2\,\mathrm{I}_{\overline{\mathbf{C}}}\,\bar{\mathrm{I}}_4 + 3\,J^{-2/3}\,\mathrm{I}_{\overline{\mathbf{C}}} + 1)\,w''(\hat{\mathrm{I}}_{\mathbf{C}_{\mathrm{r}}})) + J\,(\frac{\partial\psi^{\mathrm{vol}}}{\partial J} + J\frac{\partial^2\psi^{\mathrm{vol}}}{\partial J\partial J}))\,[\mathbf{C}^{-1}\otimes\mathbf{C}^{-1}]\end{aligned}$$

$$\begin{aligned}\tilde{\mathcal{C}}_3 = (-\tfrac{1}{3}\,\mathrm{I}_4^{-1}\,\overline{\lambda}_{\mathrm{a}}\,(v'(\overline{\lambda}_{\mathrm{a}}) + \overline{\lambda}_{\mathrm{a}}\,v''(\overline{\lambda}_{\mathrm{a}})) + \frac{4}{3}(J^{-2/3}\left(w'(\hat{\mathrm{I}}_{\mathbf{C}_{\mathrm{r}}}) + 2\,w''(\hat{\mathrm{I}}_{\mathbf{C}_{\mathrm{r}}})\right)\\ + (J^{-2/3}\,(\mathrm{I}_{\overline{\mathbf{C}}} - \bar{\mathrm{I}}_4) - \mathrm{I}_4^{-1}(\mathrm{I}_1 + 1))\,w''(\hat{\mathrm{I}}_{\mathbf{C}_{\mathrm{r}}})))\,[\mathbf{M}_0\otimes\mathbf{C}^{-1} + \mathbf{C}^{-1}\otimes\mathbf{M}_0]\end{aligned}$$

$$\begin{aligned}\tilde{\mathcal{C}}_4 = 4\,J^{-2/3}\,(\mathrm{I}_4^{-1} - J^{-2/3})\,w''(\hat{\mathrm{I}}_{\mathbf{C}_{\mathrm{r}}})\,[\mathbf{M}_0\otimes\mathbf{1} + \mathbf{1}\otimes\mathbf{M}_0]\\ + \frac{4}{3}\,J^{-2/3}\,(-\mathrm{I}_{\overline{\mathbf{C}}} + \bar{\mathrm{I}}_4 - 2)\,w''(\hat{\mathrm{I}}_{\mathbf{C}_{\mathrm{r}}})\,[\mathbf{C}^{-1}\otimes\mathbf{1} + \mathbf{1}\otimes\mathbf{C}^{-1}]\end{aligned}$$

$$\tilde{\mathcal{C}}_5 = 4\,J^{-4/3}\,w''(\hat{\mathrm{I}}_{\mathbf{C}_{\mathrm{r}}})\,[\mathbf{1}\otimes\mathbf{1}] + (\tfrac{2}{3}\,\overline{\lambda}_{\mathrm{a}}\,v'(\overline{\lambda}_{\mathrm{a}}) + \frac{4}{3}\,\mathrm{I}_{\overline{\mathbf{C}}}\,w'(\hat{\mathrm{I}}_{\mathbf{C}_{\mathrm{r}}}) - 2J\,\frac{\partial\psi^{\mathrm{vol}}}{\partial J})\,[\mathbf{C}^{-1}\otimes\mathbf{C}^{-1}]^{T_{23}}$$

In the case of small strains, which is common with composite materials, the elasticity tensor $\tilde{\mathcal{C}}_0$ reads

$$\begin{aligned}\tilde{\mathcal{C}}_0 := \tilde{\mathcal{C}}|_{\mathbf{F}=\mathbf{I}} = 2(2\alpha-\beta)[\mathbf{M}_0\otimes\mathbf{M}_0] + \tfrac{2}{3}(-2\alpha+\beta)[\mathbf{M}_0\otimes\mathbf{1} + \mathbf{1}\otimes\mathbf{M}_0]\\ + \left(\frac{4}{9}(\alpha+\beta) + K\right)[\mathbf{1}\otimes\mathbf{1}] + 2\beta[\mathbf{1}\otimes\mathbf{1}]^{T_{23}}.\end{aligned}$$

For $\boldsymbol{a}_0 = \boldsymbol{e}_1$, $\tilde{\mathcal{C}}_0$ reads

$$\tilde{\mathcal{C}}_0 = \begin{bmatrix} \frac{1}{9}(16\alpha+14\beta)+K & \frac{1}{9}(-8\alpha+10\beta)+K & \frac{1}{9}(-8\alpha+10\beta)+K & 0 & 0 & 0 \\ \frac{1}{9}(-8\alpha+10\beta)+K & \frac{1}{9}(4\alpha+22\beta)+K & \frac{1}{9}(4\alpha+4\beta)+K & 0 & 0 & 0 \\ \frac{1}{9}(-8\alpha+10\beta)+K & \frac{1}{9}(4\alpha+4\beta)+K & \frac{1}{9}(4\alpha+22\beta)+K & 0 & 0 & 0 \\ 0 & 0 & 0 & 2\beta & 0 & 0 \\ 0 & 0 & 0 & 0 & 2\beta & 0 \\ 0 & 0 & 0 & 0 & 0 & 2\beta \end{bmatrix} \tag{A.5.2}$$

in the matrix representation, which is defined by five different coefficients being the number of coefficients required for the case of transverse isotropy, see Green and Zerna (1992).

A.6. Calculation of the Inverse of Thermal Part Of The Deformation Gradient $\mathbf{F}_\Theta^{-1}$

The thermal part of the deformation gradient tensor is defined in Eq.(4.8) as

$$\mathbf{F}_\Theta = (\zeta - \varphi)\mathbf{M}_0 + \varphi\mathbf{1}$$

Analogous to the procedure given in A.3, the inverse of $\mathbf{F}_\Theta$ is calculated by applying the Cayley-Hamilton Theorem. Thus, the characteristic polynomial of $\mathbf{F}_\Theta$ is given by

$$-\mathbf{F}_\Theta^3 + \mathrm{I}_{\mathbf{F}_\Theta}\mathbf{F}_\Theta^2 - \mathrm{II}_{\mathbf{F}_\Theta}\mathbf{F}_\Theta + \mathrm{III}_{\mathbf{F}_\Theta}\mathbf{1} = \mathbf{0}, \tag{A.6.1}$$

yielding,

$$\mathbf{F}_\Theta^{-1} = \frac{1}{\mathrm{III}_{\mathbf{F}_\Theta}}\left(\mathbf{F}_\Theta^2 - \mathrm{I}_{\mathbf{F}_\Theta}\mathbf{F}_\Theta + \mathrm{II}_{\mathbf{F}_\Theta}\mathbf{1}\right). \tag{A.6.2}$$

The first term in the parenthesis read

$$\begin{aligned} \mathbf{F}_\Theta^2 &= \left((\zeta-\varphi)\mathbf{M}_0 + \varphi\mathbf{1}\right)\left((\zeta-\varphi)\mathbf{M}_0 + \varphi\mathbf{1}\right) \\ &= \left((\zeta-\varphi)^2 + 2(\zeta-\varphi)\right)\mathbf{M}_0 + \varphi^2\mathbf{1} \\ &= (\zeta^2-\varphi^2)\mathbf{M}_0 + \varphi^2\mathbf{1}, \end{aligned}$$

and the three principal invariants of $\mathbf{F}_\Theta$ are

$$\begin{aligned} \mathrm{I}_{\mathbf{F}_\Theta} &= \mathrm{tr}\,\mathbf{F}_\Theta = \mathrm{tr}\left((\zeta-\varphi)\mathbf{M}_0 + \varphi\mathbf{1}\right) && = \zeta + 2\varphi \\ \mathrm{II}_{\mathbf{F}_\Theta} &= \tfrac{1}{2}\left((\mathrm{tr}\,\mathbf{F}_\Theta)^2 - \mathrm{tr}\,\mathbf{F}_\Theta^2\right) = \tfrac{1}{2}\left((\zeta+2\varphi)^2 - (\zeta^2+2\varphi^2)\right) && = 2\zeta\varphi - \varphi^2 \\ \mathrm{III}_{\mathbf{F}_\Theta} &= \det\mathbf{F}_\Theta = \det\left((\zeta-\varphi)\mathbf{M}_0 + \varphi\mathbf{1}\right) && = \zeta\varphi^2, \end{aligned} \tag{A.6.3}$$

where the third invariant $\mathrm{III}_{\mathbf{F}_\Theta}$ is calculated in (4.11), and

$$\begin{aligned} \mathrm{tr}\,\mathbf{F}_\Theta^2 &= \mathrm{tr}\left((\zeta^2-\varphi^2)\mathbf{M}_0 + \varphi^2\mathbf{1}\right) = (\zeta^2-\varphi^2)\,\mathrm{tr}\,\mathbf{M}_0 + \varphi^2\,\mathrm{tr}\,\mathbf{1} \\ &= (\zeta^2-\varphi^2) + 3\varphi^2 = \zeta^2 + 2\varphi^2 \end{aligned}$$

Inserting $\mathbf{F}_\Theta$, $\mathbf{F}_\Theta^2$ and the above three invariants ($\mathrm{I}_{\mathbf{F}_\Theta}, \mathrm{II}_{\mathbf{F}_\Theta}, \mathrm{III}_{\mathbf{F}_\Theta}$) into Eq.(A.6.2), yields

$$\begin{aligned}\mathbf{F}_\Theta^{-1} &= \frac{1}{\zeta\varphi^2}\left((\zeta^2-\varphi^2)\mathbf{M}_0 + \varphi^2\mathbf{1} - (\zeta+2\varphi)\left((\zeta-\varphi)\mathbf{M}_0 + \varphi\mathbf{1}\right) + (2\zeta\varphi-\varphi^2)\mathbf{1}\right)\\ &= \frac{1}{\zeta\varphi^2}\left((\varphi^2-\zeta\varphi)\mathbf{M}_0 + \zeta\varphi\mathbf{1}\right)\\ &= (\zeta^{-1}-\varphi^{-1})\mathbf{M}_0 + \varphi^{-1}\mathbf{1}. \end{aligned} \tag{A.6.4}$$

Furthermore, the inverse of the thermal left Cauchy-Green tensor, required in (4.21a) and (4.21b), can be calculated

$$\begin{aligned}\mathbf{B}_\Theta^{-1} &= \mathbf{F}_\Theta^{-\mathrm{T}}\,\mathbf{F}_\Theta^{-1}\\ &= \left((\zeta^{-1}-\varphi^{-1})\mathbf{M}_0 + \varphi^{-1}\mathbf{1}\right)\left((\zeta^{-1}-\varphi^{-1})\mathbf{M}_0 + \varphi^{-1}\mathbf{1}\right)\\ &= \left((\zeta^{-1}-\varphi^{-1})^2 + 2(\zeta^{-1}-\varphi^{-1})\right)\mathbf{M}_0 + \varphi^{-2}\mathbf{1}\\ &= (\zeta^{-2}-\varphi^{-2})\mathbf{M}_0 + \varphi^{-2}\mathbf{1}. \end{aligned} \tag{A.6.5}$$

The inverse of the thermal right Cauchy-Green tensor $\mathbf{C}_\Theta^{-1}$ is the transpose of $\mathbf{B}_\Theta^{-1}$, i.e.,

$$\begin{aligned}\mathbf{C}_\Theta^{-1} &= \mathbf{F}_\Theta^{-1}\,\mathbf{F}_\Theta^{-\mathrm{T}} = (\mathbf{B}_\Theta^{-1})^{\mathrm{T}} = \left((\zeta^{-2}-\varphi^{-2})\mathbf{M}_0 + \varphi^{-2}\mathbf{1}\right)^{\mathrm{T}}\\ &= (\zeta^{-2}-\varphi^{-2})\mathbf{M}_0 + \varphi^{-2}\mathbf{1}. \end{aligned} \tag{A.6.6}$$

A.7. Proof of the Identities Given in Eqs.(4.53a) and (4.53b)

The constitutive equation of the specific entropy, see (4.47), contains the two terms $\hat{\mathbf{S}}_\Theta \cdot \mathbf{C}_\mathrm{M}$ and $\hat{\mathbf{S}}_\Theta \cdot \mathbf{C}_\mathrm{M}\mathbf{M}_0$, which are rewritten as $\mathrm{tr}\,\mathbf{P}$ and $\mathbf{P}\cdot\mathbf{M}_0$ in Eqs.(4.53a) and (4.53b), respectively, with $\mathbf{P}$ as the Mandel stress tensor. Here, the proof of these two identities is presented. First of all, Eqs.(4.1) and (4.32) are recalled, i.e.,

$$\mathbf{F} = \mathbf{F}_\mathrm{M}\,\mathbf{F}_\Theta \Longrightarrow \mathbf{F}_\mathrm{M} = \mathbf{F}\,\mathbf{F}_\Theta^{-1}$$

and

$$\hat{\mathbf{S}}_\Theta = \mathbf{F}_\Theta\,\tilde{\mathbf{T}}\,\mathbf{F}_\Theta^{\mathrm{T}}$$

To this end, the first term $\hat{\mathbf{S}}_\Theta \cdot \mathbf{C}_\mathrm{M}$ can easily be proven

$$\begin{aligned}\hat{\mathbf{S}}_\Theta \cdot \mathbf{C}_\mathrm{M} &= \mathbf{F}_\Theta\,\tilde{\mathbf{T}}\,\mathbf{F}_\Theta^{\mathrm{T}} \cdot \mathbf{F}_\mathrm{M}^{\mathrm{T}}\,\mathbf{F}_\mathrm{M} = \tilde{\mathbf{T}} \cdot \mathbf{F}_\Theta^{\mathrm{T}}\,\mathbf{F}_\mathrm{M}^{\mathrm{T}}\,\mathbf{F}_\mathrm{M}\,\mathbf{F}_\Theta = \tilde{\mathbf{T}} \cdot (\mathbf{F}_\mathrm{M}\,\mathbf{F}_\Theta)^{\mathrm{T}}\,(\mathbf{F}_\mathrm{M}\,\mathbf{F}_\Theta)\\ &= \tilde{\mathbf{T}} \cdot \mathbf{F}^{\mathrm{T}}\,\mathbf{F} = \tilde{\mathbf{T}} \cdot \mathbf{C} = \mathbf{C}\tilde{\mathbf{T}} \cdot \mathbf{1} = \mathbf{P} \cdot \mathbf{1} = \mathrm{tr}\,\mathbf{P}. \end{aligned} \tag{A.7.1}$$

Similarly, the second term $\hat{\mathbf{S}}_\Theta \cdot \mathbf{C}_\mathrm{M}\mathbf{M}_0$ is reformulated as

$$\begin{aligned}\hat{\mathbf{S}}_\Theta \cdot \mathbf{C}_\mathrm{M}\mathbf{M}_0 &= \mathbf{F}_\Theta\, \tilde{\mathbf{T}}\, \mathbf{F}_\Theta^\mathrm{T} \cdot \mathbf{F}_\mathrm{M}^\mathrm{T}\, \mathbf{F}_\mathrm{M}\, \mathbf{M}_0 = \mathbf{F}_\Theta\, \tilde{\mathbf{T}}\, \mathbf{F}_\Theta^\mathrm{T} \cdot (\mathbf{F}\, \mathbf{F}_\Theta^{-1})^\mathrm{T}\, (\mathbf{F}\, \mathbf{F}_\Theta^{-1})\, \mathbf{M}_0 \\ &= \mathbf{F}_\Theta\, \tilde{\mathbf{T}}\, \mathbf{F}_\Theta^\mathrm{T} \cdot \mathbf{F}_\Theta^\mathrm{T}\, \mathbf{F}^\mathrm{T}\, \mathbf{F}\, \mathbf{F}_\Theta^{-1} = \tilde{\mathbf{T}} \cdot \underbrace{\mathbf{F}_\Theta^\mathrm{T}\, \mathbf{F}_\Theta^{-\mathrm{T}}}_{\mathbf{1}} \underbrace{\mathbf{F}^\mathrm{T}\, \mathbf{F}}_{\mathbf{C}} \underbrace{\mathbf{F}_\Theta^{-1}\, \mathbf{M}_0\, \mathbf{F}_\Theta}_{\mathbf{M}_0} \\ &= \tilde{\mathbf{T}} \cdot \mathbf{C}\mathbf{M}_0 = \mathbf{C}\, \tilde{\mathbf{T}} \cdot \mathbf{M}_0 = \mathbf{C}\, \tilde{\mathbf{T}} \cdot\, \mathbf{M}_0 = \mathbf{P} \cdot \mathbf{M}_0, \end{aligned} \tag{A.7.2}$$

where

$$\begin{aligned}\mathbf{F}_\Theta^{-1}\mathbf{M}_0\mathbf{F}_\Theta &= \big((\zeta^{-1} - \varphi^{-1})\mathbf{M}_0 + \varphi^{-1}\mathbf{1}\big)\, \mathbf{M}_0\, ((\zeta - \varphi)\mathbf{M}_0 + \varphi\mathbf{1}) \\ &= \big((\zeta - \varphi)(\zeta^{-1} - \varphi^{-1}) + \varphi^{-1}(\zeta - \varphi) + \varphi(\zeta^{-1} - \varphi^{-1}) + 1\big)\, \mathbf{M}_0 \\ &= \mathbf{M}_0, \end{aligned} \tag{A.7.3}$$

in which the definitions of $\mathbf{F}_\Theta$ and $\mathbf{F}_\Theta^{-1}$ given in Eqs.(4.8) and (A.6.4) are employed.

A.8. Calculation of the Mechanical Unimodular Left Cauchy-Green Tensor $\overline{\mathbf{B}}_\mathrm{M}$

As shown in Eq.(4.62), the mechnaical unimodular left Cauchy-Green tensor $\overline{\mathbf{B}}_\mathrm{M}$ can be represented in term of the total unimodular left Cauchy-Green tensor $\overline{\mathbf{B}}$ and the structural tensor $\mathbf{M}$. This formulation is explained in the following. The Unimodular mechanical tensor is defined as

$$\overline{\mathbf{B}}_\mathrm{M} = J_\mathrm{M}^{-2/3}\, \mathbf{B}_\mathrm{M} \tag{A.8.1}$$

with

$$\begin{aligned}\mathbf{B}_\mathrm{M} &= \mathbf{F}_\mathrm{M}\, \mathbf{F}_\mathrm{M}^\mathrm{T} = \mathbf{F}\, \mathbf{F}_\Theta^{-1}\, \mathbf{F}_\Theta^{-\mathrm{T}}\, \mathbf{F}^\mathrm{T} = \mathbf{F}\, \mathbf{C}_\Theta^{-1}\, \mathbf{F}^\mathrm{T} = \mathbf{F}\, \big((\zeta^{-2} - \varphi^{-2})\mathbf{M}_0 + \varphi^{-2}\mathbf{1}\big)\, \mathbf{F}^\mathrm{T} \\ &= (\zeta^{-2} - \varphi^{-2})\, \mathbf{F}\, \mathbf{M}_0\, \mathbf{F}^\mathrm{T} + \varphi^{-2}\mathbf{F}\, \mathbf{1}\, \mathbf{F}^\mathrm{T} = (\zeta^{-2} - \varphi^{-2})\, \mathbf{F}\boldsymbol{m}_0 \otimes \mathbf{F}\boldsymbol{m}_0 + \varphi^{-2}\mathbf{F}\, \mathbf{F}^\mathrm{T} \\ &= (\zeta^{-2} - \varphi^{-2})\, \zeta^2\lambda_\mathrm{M}^2\, \boldsymbol{m} \otimes \boldsymbol{m} + \varphi^{-2}\, \mathbf{B} = (1 - \frac{\zeta^2}{\varphi^2})\, \lambda_\mathrm{M}^2\, \boldsymbol{m} \otimes \boldsymbol{m} + \varphi^{-2}\, \mathbf{B}, \\ &= \lambda_\mathrm{M}^2\, (1 - \frac{\zeta^2}{\varphi^2})\, \mathbf{M} + \frac{1}{\varphi^2}\, \mathbf{B}, \end{aligned} \tag{A.8.2}$$

in which, $\mathbf{C}_\Theta^{-1}$ from (A.6.6) is inserted, and use of the property

$$\mathbf{F}\, \mathbf{M}_0\, \mathbf{F}^\mathrm{T} = \mathbf{F}\, (\boldsymbol{m}_0 \otimes \boldsymbol{m}_0)\, \mathbf{F}^\mathrm{T} = \mathbf{F}\boldsymbol{m}_0 \otimes \mathbf{F}\boldsymbol{m}_0 = \zeta^2\lambda_\mathrm{M}^2\, \boldsymbol{m} \otimes \boldsymbol{m},$$

is made, where $\mathbf{F}\boldsymbol{m}_0 = \zeta\lambda_{\mathrm{M}}\boldsymbol{m}$ is given by (4.5). Substituting the determinant of the mechanical deformation J_{M} given in (4.13) and the final result of (A.8.2) into (A.8.1) yields

$$\begin{aligned}
\overline{\mathbf{B}}_{\mathrm{M}} &= J_M^{-2/3}\,\lambda_{\mathrm{M}}^2\,(1-\frac{\zeta^2}{\varphi^2})\,\mathbf{M} + \varphi^{-2}\,(\zeta\varphi^2)^{2/3} J^{-2/3}\,\mathbf{B} \\
&= \overline{\lambda}_{\mathrm{M}}{}^2\,(1-\frac{\zeta^2}{\varphi^2})\,\mathbf{M} + \frac{\zeta^{2/3}}{\varphi^{2/3}} J^{-2/3}\,\mathbf{B} \\
&= \overline{\lambda}_{\mathrm{M}}{}^2\,(1-\eta^2)\,\mathbf{M} + \eta^{2/3}\,\overline{\mathbf{B}} \\
&= \eta^{-2/3}\,\overline{\lambda}_{\mathrm{a}}^2\,(1-\eta^2)\,\mathbf{M} + \eta^{2/3}\,\overline{\mathbf{B}} \\
&= \eta^{2/3}\left(\overline{\lambda}_{\mathrm{a}}^2(\eta^{-2}-1)\mathbf{M} + \overline{\mathbf{B}}\right), \qquad \text{(A.8.3)}
\end{aligned}$$

where $\overline{\lambda}_{\mathrm{M}} = \eta^{-2/3}\,\overline{\lambda}_{\mathrm{a}}^2$ is inserted, see Eq.(4.38c).

A.9. Some Results of Cook's Membrane Example

Table A.1.: Displacements of point A at time $t = 0.5\,\mathrm{sec}$ and $t = 1\,\mathrm{sec}$.

	$t = 0.5$ sec.				$t = 1$ sec.			
p-Level	x-X	y-Y	z-Z	displ.	x-X	y-Y	z-Z	displ.
1	-2.8337	4.0	-0.6329	4.9102	-6.0518	8.0	-1.4806	10.140
3	-7.7669	4.0	12.644	15.354	-17.027	8.0	17.046	25.387
5	-7.2815	4.0	-9.5665	12.667	-14.858	8.0	-12.154	20.796
7	-7.1776	4.0	-8.9838	12.161	-14.851	8.0	-10.591	19.918
9	-7.1464	4.0	-8.8675	12.057	-14.765	8.0	-10.495	19.803
10	-7.1447	4.0	-8.8655	12.055	-14.750	8.0	-10.502	19.795

Table A.2.: Displacements of point B at time $t = 0.5\,\mathrm{sec}$ and $t = 1\,\mathrm{sec}$.

	$t = 0.5$ sec.				$t = 1$ sec.			
p-Level	x-X	y-Y	z-Z	displ.	x-X	y-Y	z-Z	displ.
1	-1.2381	1.2719	-0.0825	1.7769	-2.5368	2.5743	-0.0927	3.6154
3	-0.5958	0.2538	-1.1193	1.2929	-1.3893	0.7299	-0.2573	3.6154
5	-3.2772	0.3823	-7.5841	8.2707	-8.4010	0.4833	-12.851	15.361
7	-3.2938	0.3764	-7.4312	8.1371	-8.4353	0.5579	-12.525	15.111
9	-3.2966	0.3769	-7.4035	8.1130	-8.4707	0.6185	-12.299	14.947
10	-3.2968	0.3771	-7.4040	8.1136	-8.4802	0.6334	-12.249	14.912

B. List of Symbols

$\mathcal{B}$	Material body
$\mathcal{P}$	Material point
$\mathbb{E}^3$	Euclidean space
$\mathcal{K}$	Configuration of a material body
$\boldsymbol{\mathcal{R}}$	Reference configuration of a material body
$\boldsymbol{\chi}_t$	Current configuration of a material body
$\boldsymbol{X}$	Number triplets of a material point in the reference configuration
$\boldsymbol{x}$	Number triplets of a material point in the current configuration
$\boldsymbol{\chi}$	Deformation function represent the motion of a material body
t	Time
$\boldsymbol{C}(\xi)$	A smooth curve in reference configuration
$\boldsymbol{c}(\xi)$	A smooth curve in current configuration
$\mathbf{F}$	Deformation gradient tensor
$\mathrm{d}\boldsymbol{X}$	Material line element in reference configuration
$\mathrm{d}\boldsymbol{x}$	Material line element in current configuration
Grad	Gradient of a vector field in material representation
grad	Gradient of a vector field in spatial representation
$\det$	Determinant of a tensor field
J	Determinant of the deformation gradient tensor $\mathbf{F}$
$\boldsymbol{u}$	Displacement vector
$\mathbf{1}$	Identity second-order tensor
$(\bullet)^{\mathrm{T}}$	Transpose of a tensor field $(\bullet)$
$\mathrm{d}\boldsymbol{A}$	Material surface element in reference configuration
$\mathrm{d}\boldsymbol{a}$	Material surface element in current configuration
$\mathrm{d}V$	Material volume element in reference configuration
$\mathrm{d}v$	Material volume element in current configuration
cof	Cofactor of a tensor field
$\boldsymbol{v}$	Velocity of a material line element
$\boldsymbol{a}$	Acceleration of a material line element
$\mathbf{L}$	Spatial velocity gradient tensor
$\mathbf{D}$	Strain-rate tensor
$\mathbf{W}$	Spin tensor
$\dot{(\bullet)}$	Time derivative $\mathrm{d}(\bullet)/\mathrm{d}t$
$\mathbf{U}$	Right stretch tensor
$\mathbf{V}$	Left stretch tensor

$\mathbf{R}$	Rotation tensor
$\mathbf{C}$	Right Cauchy-Green tensor
$\mathbf{B}$	Left Cauchy-Green tensor
$\mathbf{E}$	Green strain tensor
$\mathbf{A}$	Almansi strain tensor
$\boldsymbol{n}$	Normal unit vector in current configuration
$\boldsymbol{t}$	Cauchy stress vector
$\mathbf{T}$	Cauchy stress tensor
$\boldsymbol{n}_{\mathrm{R}}$	Normal unit vector in reference configuration
$\boldsymbol{t}_{\mathrm{R}}$	Piola-Kirchhoff stress vector
$\mathbf{T}_{\mathrm{R}}$	First Piola-Kirchhoff stress vector
$\boldsymbol{f}$	Body force vector
$\tilde{\mathbf{T}}$	Second Piola-Kirchhoff stress tensor
L_i	Stress power
$(\,\cdot\,)$	Scalar product
m	Mass of a material body
ϱ	Mass density of a material body in current configuration
ϱ_{R}	Mass densities of a material body in reference current
$\boldsymbol{J}$	Linear momentum
$\boldsymbol{F}$	Resulting force
div	Divergence in spatial representation
Div	Divergence in material representation
$\boldsymbol{D}_{\mathrm{C}}$	Angular momentum
$\boldsymbol{M}_{\mathrm{C}}$	Resultant moment
$\boldsymbol{c}$	A positioning vector
$\overset{3}{\boldsymbol{\epsilon}}$	Third order permutation tensor
K	Kinetic energy
E	Internal energy
L_e	Mechanical work
Q	Heat supply
e	Specific internal energy per unit mass
$\boldsymbol{q}$	Heat flux vector in spatial representation
r	Volume-distributed heat supply
q	Heat flux
$\boldsymbol{q}_{\mathrm{R}}$	Heat flux vector in material representation
S	Entropy
s	Specific entropy per unit mass
H	Entropy supply
$\boldsymbol{\Sigma}$	Entropy flux vector
σ	Volume-distributed entropy supply
Γ	Entropy production
γ	Specific entropy production per unit mass

Θ	Absolute temperature
δ	Internal dissipation
Ψ	Specific strain-energy per unit mass
$\mathfrak{S}$	Functional
$\mathcal{Q}$	Material particle
$\boldsymbol{\chi}_\tau$	Motion of a material particle at time τ
$\mathfrak{U}$	Group of material points
$\mathbf{Q}$	Orthogonal tensor
$(\bullet)^*$	Quantity associated with an orthogonal transformation
$\mathcal{G}$	Symmetry group
Φ	Scalar-valued function
$\boldsymbol{\Phi}$	Tensor-valued function
$\mathrm{O}(3)$	Orthogonal group
$\mathrm{SO}(3)$	Proper orthogonal group
$\boldsymbol{m}_0$	Unit vector defines the preferred direction in the reference configuration
I_1	First principal invariant of $\mathbf{C}$
I_2	Second principal invariant of $\mathbf{C}$
I_3	Third principal invariant of $\mathbf{C}$
$\mathrm{tr}(\bullet)$	Trace of a tensor field
$\mathbf{M}_0$	Structural tensor
$(\otimes)$	Dyadic product
adj	Adjugate of a tensor field
$\mathrm{I}_4, \mathrm{I}_5$	Two invariant arise from anisotropy
$\hat{\mathbf{F}}$	Volume-changing (volumetric) deformation gradient
$\overline{\mathbf{F}}$	Volume-preserving (isochoric) deformation gradient
$\overline{\mathbf{C}}$	Unimodular right Cauchy-Green strain tensor
$\mathrm{I}_{\overline{\mathbf{C}}}$	First principal invariant of $\overline{\mathbf{C}}$
$\mathrm{II}_{\overline{\mathbf{C}}}$	Second principal invariant of $\overline{\mathbf{C}}$
U	Volumetric part of a strain-energy function
$\hat{\psi}^{\mathrm{i}}, \overline{\psi}^{\,\mathrm{i}}$	Isotropic part of a strain-energy function
$\tilde{\psi}^{\mathrm{t}}, \overline{\psi}^{\,\mathrm{t}}$	Anisotropic part of a strain-energy function
$\bar{\mathrm{I}}_4, \bar{\mathrm{I}}_5$	Two unimodular invariants arise from anisotropy
Λ_0	Length of a material line element in material representation
Λ	Length of a material line element in spatial representation
$\boldsymbol{m}$	Unit vector defines the preferred direction in the current configuration
λ_{a}	Stretch of the bulk material along the preferred direction
$\mathbf{F}_{\mathrm{a}}$	Deformation gradient tensor contains only the deformation along the preferred direction
$\mathbf{F}_{\mathrm{r}}$	Deformation gradient tensor contains all the remaining deformations
$\hat{\mathcal{B}}$	Intermediate configuration
$\hat{\boldsymbol{m}}$	Unit vector defines the preferred direction in the intermediate configuration
$\overline{\lambda}_{\mathrm{a}}$	Isochoric stretch of the bulk material along the preferred direction
$\boldsymbol{E}_1, \boldsymbol{E}_2, \boldsymbol{E}_3$	Base vectors of Cartesian coordinates relative to the reference configuration

$\hat{\boldsymbol{e}}_1, \hat{\boldsymbol{e}}_2, \hat{\boldsymbol{e}}_3$	Base vectors of Cartesian coordinates relative to the intermediate configuration
$\boldsymbol{e}_1, \boldsymbol{e}_2, \boldsymbol{e}_3$	Base vectors of Cartesian coordinates relative to the current configuration
$\mathbf{C}_{\mathrm{a}}$	Strain tensor contains only the deformation along the preferred direction
$\mathrm{I}_{\mathbf{C}_{\mathrm{a}}}, \mathrm{II}_{\mathbf{C}_{\mathrm{a}}}, \mathrm{III}_{\mathbf{C}_{\mathrm{a}}}$	Principal invariants of $\mathbf{C}_{\mathrm{a}}$
$\hat{\mathrm{I}}_{\mathbf{C}_{\mathrm{a}}}, \hat{\mathrm{II}}_{\mathbf{C}_{\mathrm{a}}}, \hat{\mathrm{III}}_{\mathbf{C}_{\mathrm{a}}}$	Basic invariants of $\mathbf{C}_{\mathrm{a}}$
$\mathbf{C}_{\mathrm{r}}$	Strain tensor contains all the remaining deformations
$\mathrm{I}_{\mathbf{C}_{\mathrm{r}}}, \mathrm{II}_{\mathbf{C}_{\mathrm{r}}}, \mathrm{III}_{\mathbf{C}_{\mathrm{r}}}$	Principal invariants of $\mathbf{C}_{\mathrm{r}}$
$\hat{\mathrm{I}}_{\mathbf{C}_{\mathrm{r}}}, \hat{\mathrm{II}}_{\mathbf{C}_{\mathrm{r}}}, \hat{\mathrm{III}}_{\mathbf{C}_{\mathrm{r}}}$	Basic invariants of $\mathbf{C}_{\mathrm{r}}$
$\psi_{\mathrm{a}}^{\mathrm{isc}}, v$	Strain-energy functions associated with the deformation along the preferred direction
$\psi_{\mathrm{r}}^{\mathrm{isc}}, w$	Strain-energy functions associated with the remaining deformations
ψ^{vol}	Modified volumetric strain-energy function
K, α, β	Material parameters
$\tilde{\mathbf{T}}_{\mathrm{vol}}$	Volumetric part of second Piola-Kirchhoff stress tensor
$\tilde{\mathbf{T}}_{\mathrm{isc}}$	Isochoric part of second Piola-Kirchhoff stress tensor
$\mathbf{T}_{\mathrm{vol}}$	Volumetric part of Cauchy stress tensor
$\mathbf{T}_{\mathrm{isc}}$	isochoric part of Cauchy stress tensor
$(\bullet)^{\mathrm{D}}$	Deviatoric of a tensor field $(\bullet)$
$\overline{\mathbf{B}}$	Unimodular left Cauchy-Green strain tensor
$\mathbf{B}_{\mathrm{r}}$	The left Cauchy-Green tensor of the remaining part
$\tilde{\mathcal{C}}$	Tangent operator
$\sigma_{i,j}$	i, j component of Cauchy stress ($i, j = 1, 2, 3$)
P_{ij}	i, j component of 1st Piola-Kirchhoff stress ($i, j = 1, 2, 3$)
κ	Shear stretch
$\mathbf{F}_{\Theta}$	Thermal part of the deformation gradient tensor $\mathbf{F}$
$\mathbf{F}_{\mathrm{M}}$	Mechanical part of the deformation gradient tensor $\mathbf{F}$
$\hat{\mathbf{F}}_{\mathrm{M}}$	Volumetric part of $\mathbf{F}_{\mathrm{M}}$
$\overline{\mathbf{F}}_{\mathrm{M}}$	Isochoric part of $\mathbf{F}_{\mathrm{M}}$
$\mathbf{F}_{\mathrm{M}}^{a}$	Part of $\overline{\mathbf{F}}_{\mathrm{M}}$ constrained along the preferred direction
$\mathbf{F}_{\mathrm{M}}^{r}$	Part of $\overline{\mathbf{F}}_{\mathrm{M}}$ contains all remaining deformations
λ_{M}	Mechanical stretch along the preferred direction
ζ	Thermal stretch along the preferred direction
φ	Thermal stretch normal to the preferred direction
α_a	Thermal expansion coefficient along the preferred direction
α_n	Thermal expansion coefficient normal to the preferred direction
Θ_0	Reference temperature
ϑ	Temperature difference
J_{Θ}	Determinant of the thermal deformation gradient $\mathbf{F}_{\Theta}$
J_{M}	Determinant of the mechanical deformation gradient $\mathbf{F}_{\mathrm{M}}$
$\mathbf{E}_{\Theta}$	Thermal Gree strain tensor
$\mathbf{C}_{\Theta}$	Thermal right Cauchy-Green strain tensor
$\mathbf{E}_{\mathrm{M}}$	Mechanical Green strain tensor
$\hat{\boldsymbol{\gamma}}$	Total strain tensor in the intermediate configuration

$\hat{\boldsymbol{\gamma}}_{\Theta}$	Thermal strain tensor in the intermediate configuration
$\hat{\boldsymbol{\gamma}}_{\mathrm{M}}$	Mechanical strain tensor in the intermediate configuration
$\mathbf{C}_{\mathrm{M}}$	Mechanical right Cauchy-Green strain tensor
$\mathbf{B}_{\Theta}$	Thermal left Cauchy-Green strain tensor
$\mathbf{A}_{\Theta}$	Thermal Almansi strain tensor
$\mathbf{A}$	Mechanical Almansi strain tensor
ζ'	Derivative of the ζ with respect to temperature Θ
φ'	Derivative of the φ with respect to temperature Θ
$\mathbf{L}_{\Theta}$	Thermal spatial velocity gradient tensor
$\mathbf{D}_{\Theta}$	Thermal strain-rate tensor
$\mathbf{W}_{\Theta}$	Thermal spin tensor
$\overset{\triangle}{\hat{\boldsymbol{\gamma}}}$	Total Oldroyd strain-rate tensor in the intermediate configuration
$\overset{\triangle}{\hat{\boldsymbol{\gamma}}}_{\Theta}$	Thermal Oldroyd strain-rate tensor in the intermediate configuration
$\overset{\triangle}{\hat{\boldsymbol{\gamma}}}_{\mathrm{M}}$	Mechanical Oldroyd strain-rate tensor in the intermediate configuration
$\overset{\triangle}{\mathbf{A}}$	Total Oldroyd strain-rate tensor in the current configuration
$\overset{\triangle}{\mathbf{A}}_{\Theta}$	Thermal Oldroyd strain-rate tensor in the current configuration
$\overset{\triangle}{\mathbf{A}}_{\mathrm{M}}$	Mechanical Oldroyd strain-rate tensor in the current configuration
ψ_{Θ}	Thermal strain-energy function
ψ_{M}	Mechanical strain-energy function
$\overline{\lambda}_{\mathrm{M}}$	Isochoric mechanical stretch along the preferred direction
$\mathrm{I}_{4\mathrm{M}}, \bar{\mathrm{I}}_{4\mathrm{M}}$	Invariants arise from anisotropy
$\mathrm{I}^{\mathrm{r}}_{\mathrm{M}}$	First principal invariant of $\mathbf{C}^{\mathrm{r}}_{\mathrm{M}}$
I_{M}	First principal invariant of $\mathbf{C}_{\mathrm{M}}$
η	Ratio of thermal stretch
p	Stress power
$\hat{\mathbf{S}}_{\Theta}$	Kirchhoff-type stress tensor relative to the intermediate configuration
$\mathbf{S}$	Kirchhoff stress tensor
$\mathbf{P}$	Mandel stress tensor
$\hat{\mathbf{S}}^{\mathrm{vol}}_{\Theta}$	Volumetric part of $\hat{\mathbf{S}}_{\Theta}$
$\hat{\mathbf{S}}^{\mathrm{isc}}_{\Theta}$	Isochoric part of $\hat{\mathbf{S}}_{\Theta}$
$\overline{\mathbf{B}}_{\mathrm{M}}$	Unimodular mechanical left Cauchy-Green tensor
κ_c	Thermal conductivity
$\boldsymbol{\kappa}_{\mathbf{C}}$	Thermal conductivity tensor in spatial representation
κ_a	Thermal conductivity along the preferred direction
κ_n	Thermal conductivity normal to the preferred direction
$\boldsymbol{\kappa}_{\mathbf{R}}$	Thermal conductivity tensor in material representation
c_{p}	Heat capacity
d	Thermoelastic coupling
$c_{\mathrm{p}0}$	Heat capacity at $\Theta = \Theta_0$

$\ln$	Natural logarithm
$\partial\mathcal{B}$	Surface of the material body $\mathcal{B}$
$\partial\mathcal{B}_R$	Surface of the material body in material representation
$\partial\mathcal{B}_C$	Surface of the material body in spatial representation
$\partial_{\mathrm{u}}\mathcal{B}$	Boundary with prescribed displacement
$\partial_{\Theta}\,\mathcal{B}$	Boundary with prescribed temperature
t_{i}	Starting time of a process
t_{e}	End time of a process
$\partial_{\mathrm{s}}\mathcal{B}$	Boundary with prescribed stress
$\partial_{\mathrm{q}}\mathcal{B}$	Boundary with prescribed heat flux
$\partial_{\mathrm{u}}\mathcal{B}_R$	Boundary with prescribed displacement in material representation
$\partial_{\Theta}\,\mathcal{B}_R$	Boundary with prescribed temperature in material representation
$\partial_{\mathrm{s}}\mathcal{B}_R$	Boundary with prescribed stress in material representation
$\partial_{\mathrm{q}}\mathcal{B}_R$	Boundary with prescribed heat flux in material representation
$\boldsymbol{\mathcal{S}}_{u,t}$	Set of displacement trial functions
$\mathcal{S}_{\theta,t}$	Set of temperature trial functions
$\boldsymbol{\mathcal{V}}_u$	Set of displacement test functions
$\mathcal{V}_\theta$	Set of temperature test functions
$\delta\boldsymbol{u}$	Virtual displacement
$\delta\Theta$	Virtual temperature
$\boldsymbol{u}^h$	Approximated displacement of a material body
$\boldsymbol{N}_{\mathrm{ad}}$	Matrix containing all shape functions for the displacement field
$\boldsymbol{N}_{\mathrm{d}}$	Matrix containing shape functions for the unknown displacement coefficients
$\overline{\boldsymbol{N}}_{\mathrm{d}}$	Matrix containing shape functions for the prescribed displacement coefficients
$\delta\boldsymbol{u}^h$	Approximated virtual displacement
Θ^h	Approximated absolute temperature
$\boldsymbol{N}_{\mathrm{a}\Theta}$	Matrix containing all shape functions for the temperature field
$\boldsymbol{N}_{\Theta}$	Matrix containing shape functions for the unknown temperature coefficients
$\overline{\boldsymbol{N}}_{\Theta}$	Matrix containing shape functions for the prescribed temperature coefficients
$\delta\Theta^h$	Approximated virtual temperature
$\boldsymbol{u}_{\mathrm{a}}$	Column matrix contains all coefficients of the displacement field
$\boldsymbol{\Theta}_{\mathrm{a}}$	Column matrix contains all coefficients of the temperature field
$\boldsymbol{u}$	Column matrix contains all unknown coefficients of the displacement field
$\overline{\boldsymbol{u}}$	Column matrix contains all prescribed coefficients of the displacement field
$\boldsymbol{\Theta}$	Column matrix contains all unknown coefficients of the temperature field
$\overline{\boldsymbol{\Theta}}$	Column matrix contains all prescribed coefficients of the temperature field
ϵ	A small parameter $0 < \epsilon \ll 1$
t_{n+1}	Current time step
t_n	Previous time step
Δt	Step size
$\boldsymbol{u}_{n+1}$	Displacement column matrix at time step t_{n+1}
$\boldsymbol{u}_n$	Displacement column matrix at time step t_n

$\boldsymbol{\Theta}_{n+1}$	Temperature column matrix at time step t_{n+1}
$\boldsymbol{\Theta}_n$	Temperature column matrix at time step t_n
$\boldsymbol{G}$	A system of non-linear equations
$\boldsymbol{y}$	A vector of unknowns
N	Number of time steps
n	Time step
s	Number of time stages
i	Time stage
m	Iteration index
ϵ_u	Relative error in displacements
ϵ_T	Relative error in stresses
u_k	Components of displacement of a discretization under investigation, $k = 1, 2, 3$
$u_{\text{ex}k}$	Components of displacement of reference solution, $k = 1, 2, 3$
t_k	Components of stress of a discretization under investigation, $k = 1, \ldots, 6$
$t_{\text{ex}k}$	Components of stress of a the reference solution, $k = 1, \ldots, 6$
n_{evp}	Number of evaluation points of the background grid
ϵ_Θ	Error in temperature
$\mathcal{I}$	Fourth-order identity tensor
$\tilde{\mathcal{C}}_0$	Elasticity tensor for the case of small deformations
BVP	Boundary value problem
IBVP	Initial-boundary value problem
DAE	Differential-algebraic equation
NRM	Newton-Raphson method
DIRK	Diagonal implicit Runge-Kutta method
FEM	Finite element method
p-FEM	p-Version finite element method
h-FEM	h-Version finite element method
DOF	Degree of freedom
RMSE	Root mean square error

Bibliography

Al-Kinani, R., Hartmann, S., and Netz, T. (2012). Anisotropic finite strain hyperelasticity based on the multiplicative decomposition of the deformation gradient. *Proceedings in Apllied Mathematics and Mechanics*, 12:295–296.

Al-Kinani, R., Hartmann, S., and Netz, T. (2014). Transversal isotropy based on a multiplicative decomposition of the deformation gradient within p-version finite elements. *ZAMM Zeitschrift für Angewandte Mathematik und Mechanik*, pages 1–20.

Alexander, R. (1977). Diagonally implicit Runge-Kutta methods for stiff O.D.E.'s. *SIAM Journal on Numerical Analysis*, 14:1006–1021.

Almeida, E. S. and Spilker, R. L. (1998). Finite elements formulations for hyperelastic transversely isotropic biphasic soft tissues. *Computer Methods of Applied Mechanics and Engineering*, 151:513–538.

Annaidh, A. N., Destrade, M., Gilchrist, M. D., and Murphy, J. G. (2013). Deficiencies in numerical models of anisotropic nonlinearly elastic materials. *Biomech Model Mechanobiol*, 12:781–791.

Babuŝka, I. and Suri, M. (1992a). Locking effects in the finite element approximation of elasticity problems. *Numerische Mathematik*, 62:439–463.

Babuŝka, I. and Suri, M. (1992b). On locking and robustness in the finite elemnt method. *SIAM Journal on Numerical Analysis*, 29:1261–1293.

Balzani, D., Neff, P., Schröder, J., and Holzapfel, G. A. (2006). A polyconvex framework for soft biological tissues. adjustment to experimental data. *International Journal of Solids and Structures*, 43:6052–6070.

Bowen, R. M. (1989). *Introduction to Continuum Mechanics for Engineers*. Plenum Press, New York.

Brenan, K. E., Campbell, S. L., and Petzold, L. R. (1996). *Numerical Solution of Initial-Value Problems in Differential-Algebraic Equations*. Society for Industrial and Applied Mathematics, Philadelphia.

Bronzino, J. D. (2006). *Biomedical Engineering Fundamentals*. Taylor & Francis, Boca Raton, Florida.

Brown, L. W. and Smith, L. M. (2011). A simple transversely isotropic hyperelstic constitutive model suitable for finite element analysis of fiber reinforced elastomers. *Journal of Engineering Materials and Technology*, 133:1–13.

Calvo, B., Pena, E., Martins, P., Mascarenhas, T., Doblare, M., Natal Jorge, R. M., and Ferreira, A. (2009). On modelling damage process in vaginal tissue. *Journal of Biomechanics*, 42:642–651.

Calvo, B., Ramirez, A., Alonso, A., Grasa, J., Stoeras, F., Osta, R., and Munoz, M. J. (2010). Passive nonlinear elastic behavior of skeletal muscle: Experimental results and model formulation. *Journal of Biomechanics*, 43:318–325.

Cecen, V., Tavman, I. H., Kok, M., and Aydogdu, Y. (2009). Epoxy- and polyester- based composites reinforced with glass, carbon and aramid fabrics: Measurement of heat capacity and thermal conductivity of composites by differential scannin claorimetry. *Polymer Composites*, 30(2):1299–1311.

Chadwick, P. (1974). Thermo-mechanics of rubberlike materials. *Philosophical Transactions of the Royal Socity of London, Series A, Mathematical and Physical Sciences*, 276:371–403.

Chadwick, P. (1999). *Continuum Mechanics: Concise Theory and Problems*. Dover Publications, New York.

Ciarletta, P., Izzo, I., Micera, S., and Tendick, F. (2011). Stiffening by fiber reinforcement in soft materials: A hyperelastic theory at large strains and its application. *Journal of the Mechanical Behavior of Biomedical Materials*, 4:1359–1368.

Criscione, J. C., Douglas, A. S., and Hunter, W. C. (2001). Physically based strain invariants set for materials exhibiting transversely isotropic behavior. *Journal of Mechanics and Physics of Solids*, 49:871–891.

Darijani, H. and Naghdabadi, R. (2013). Kinematics and kinetics modeling of thermoelastic continua based on the multiplicative decomposition of the deformation gradient. *International Journal of Engineering Science*, 62:56–69.

Deuflhard, P. (2006). *Newton Methods for Nonlinear Problems: Affine Invariance and Adaptive Algorithms*. Springer-Verlag, Berlin Heidelberg.

Diani, J., Brieu, M., Vacherand, J. M., and Rezgui, A. (2003). Directional model for anisotropic hyperelastic rubber-like materials. *Journal of Physics. IV France*, 105:281–288.

Diani, J., Brieu, M., Vacherand, J. M., and Rezgui, A. (2004). Directional model for isotropic and anisotropic hyperelastic rubber-like materials. *Mechanics of Materials*, 36:313–321.

Diebels, S., Ebinger, T., and Steep, H. (2005). An anisotropic damage model of foams on the basis of a micromechanical description. *JOURNAL OF MATERIALS SCIENCE*, 40:5919–5924.

Diebels, S., Ellsiepen, P., and Ehlers, W. (1999). Error-controlled runge-kutta time integration of a visoplastic hybrid two phases model. *Technische Mechanik*, 19:19–27.

Düster, A. (2001). *High order finite elements for three-dimensional, thin-walled nonlinear continua*. Dissertation, Lehrstuhl für Bauinformatik, Fakultät für Bauingenieur- und Vermessungswesen, Technische Universität München.

Düster, A., Hartmann, S., and Rank, E. (2003). p-FEM applied to finite isotropic hyperelastic bodies. *Computer Methods in Applied Mechanics and Engineering*, 192:5147–5166.

Düster, A., Rank, E., Diebels, S., Ebinger, T., and Steeb, H. (2005). Second order homogenization method based on higher order finite elements. *Proceedings in Applied Mathematics and Mechanics*, 5:391–392.

Ebbing, V. (2010). *Desig of polyconvex energy functions for all anisotropy classes*. Dissertation, Fakultät für Ingenieurwissenschaften, Abteilung Bauwissenschaften der Universität Duisburg-Essen, Institut für Mechanik, Bericht Nr. 8.

Ehret, A. E. and Itskov, M. (2007). A polyconvex hyperelastic model for fiber-reinforced materials in application to soft tissues. *Journal of Materials Science*, 42:8853–8863.

Ellsiepen, P. and Hartmann, S. (2001). Remarks on the interpretation of current non-linear finite-element-analyses as differential-algebraic equations. *International Journal for Numerical Methods in Engineering*, 51:679–707.

Eringen, A. C. (1980). *Mechanics of Continua*. Robert E. Krieger Publishing Company, New York.

Flory, P. J. (1961). Thermodynamic relations for high elastic materials. *Transaction of the Faraday Society*, 57:829–838.

Gear, C. W. (1971). The simultaneous numerical solution of differential-algebraic equations. *IEEE Transactions on Circuit Theory*, TC-18:89–95.

Green, A. E. and Zerna, W. (1992). *Theoretical Elasticity*. Dover Publications, INC., New York.

Guo, Z. Y. and Caner, F. C. (2010). Mechanical behavior of transversely isotropic porous neo-hookeansolids. *International Journal of Applied Mechanics*, 2:11–39.

Guo, Z. Y., Peng, X. Q., and Moran, B. (2006). A composites-based hyperelastic constitutive model for soft tissue with application to the human annulus fibrosus. *Journal of the Mechanics and Physics of Solids*, 54:1952–1971.

Guo, Z. Y., Peng, X. Q., and Moran, B. (2007). Mechanical responce of neo-hookean fiber reinforced incompressible nonlinearly elastic solids. *International Journal of Solids and Structures*, 44:1949–1969.

Guo, Z. Y., Peng, X. Q., and Moran, B. (2008). On constitutive modelling of porous neo-hookean composites. *Journal of the Mechanics and Physics of Solids*, 56:2338–2357.

Gurtin, M. E., Fried, E., and Anand, L. (2011). *The Mechanics and Thermodynamics of Continua*. Cambridge, New York.

Hairer, E., Norsett, S. P., and Wanner, G. (2008). *Solving Ordinary Differential Equations I: Nonstiff Problems*. Springer-Verlag, Berlin Heidelberg, second revised edition edition.

Hairer, E. and Wanner, G. (2002). *Solving Ordinary Differential Equations II: Stiff and Differential-Algebraic Problems*. Springer-Verlag, Berlin Heidelberg, second edition edition.

Halliday, D., Resnick, R., and Walker, J. (2001). *Fundamentals of physics*. Wiley, New York, sixth edition edition.

Hamkar, A.-W. (2013). *Eine iterationfreie Finite-Elemente Methode im Rahmen der finiten Thermoviskoelastizität*. Dissertation, Berichte des Instituts für Technische Mechanik 1.

Hamkar, A.-W. and Hartmann, S. (2012). Theoretical and numerical aspects in weak-compressible finite strain thermo-elasticity. *Journal of Theoretical and Applied Mechanics*, 50:3–22.

Hartmann, S. (2001). Runge-kutta-type integration schemes for inelastic constitutive equations. *COMMAS Summer School on Computational Mechanics and Materials and Structures, University of Stuttgart*.

Hartmann, S. (2002a). Computation in finite-strain viscoelasticity: finite elements based on the interpretation as differential-algabric equations. *Computer Methods in Applied Mechanics and Engineering*, 191:1439–1470.

Hartmann, S. (2002b). Computation in finite strain viscoelasticity: finite elements based on the interpretation as differential-algebraic equations. *Computer Methods in Applied Mechanics and Engineering*, 191(13-14):1439–1470.

Hartmann, S. (2003). *Finite-Elemente Berechnung inelastischer Kontinua. Interpretation als Algebro-Differentialgleichungssysteme*. Habilitation, University of Kassel, Institute of Mechanics. Report No. 1/2003.

Hartmann, S. (2004). Newton- vs. multilevel-newton method in the fem. *Proceedings in Applied Mathematics and Mechanics*, 4:318–319.

Hartmann, S. (2005). A remark on the application of the Newton-Raphson method in non-linear finite element analysis. *Computational Mechanics*, 36(2):100–116.

Hartmann, S. (2006a). TASA-FEM: Ein Finite-Elemente-Programm für raum- und zeitadaptive gekoppelte Strukturberechnungen. Technical Report 1/2006, Institute of Mechanics, University of Kassel, Kassel, Germany.

Hartmann, S. (2006b). A thermodynamically consistent constitutive model for polyoxymethylene: experiments, material modeling and computation. *Archive of Applied Mechanics*, 76:349–366.

Hartmann, S. (2010). The class of Simo & Pister-type hyperelasticity relations. Technical Report Series Fac3-10-02, Faculty of Mathematics/Computer Science and Mechanical Engineering, Clausthal University of Technology (Germany).

Hartmann, S. (2012). Comparison of the multiplicative decompositions $\mathbf{F} = \mathbf{F}_\Theta\mathbf{F}_\mathrm{M}$ and $\mathbf{F} = \mathbf{F}_\mathrm{M}\mathbf{F}_\Theta$ in finite strain thermo-elasticity. *Technical Report Series, Faculty of Mathematics/Computer Science and Mechanical Engineering, Clausthal University of Technology (Germany)*, Fac3-12-01.

Hartmann, S. and Bier, W. (2008). High-order time integration applied to metal powder plasticity. *International Journal of Plasticity*, 24(1):17–54.

Hartmann, S. and Neff, P. (2003). Polyconvexity of generalized polynomial-type hyperelastic strain energy functions for near-incompressibility. *International Journal of Solids and Structures*, 40(11):2767–2791.

Hartmann, S., Quint, K. J., and Arnold, M. (2008). On plastic incompressibility within time-adaptive finite elements combined with projection techniques. *Computer Methods in Applied Mechanics and Engineering*, 198:178–193.

Hartmann, S. and Rothe, S. (2013). A rigorous application of the method of vertical lines to coupled systems in finite element analysis. *Recent Developments in the Numerics*, 120:161–175.

Haupt, P. (1985). On the concept of an intermediate configuration and its application to a representation of viscoelastic-plastic material behavior. *International Journal of Plasticity*, 1:303–316.

Haupt, P. (2002). *Continuum Mechanics and Theory of Materials*. Springer, Berlin, second edition edition.

Haupt, P. and Tsakmakis, C. (1989). On the application of dual variables in continuum mechanics. *Journal of Continuum Mechanics and Thermodynamics*, 1:165–196.

Heimes, T. (2005). *Finite Thermoinelastizität*. Number 709 in Fortschrittsberichte, Reihe 5, Grund- und Werkstoffe/Kunststoffe. VDI-Verlag, Düsseldorf.

Heisserer, U., Hartmann, S., Düster, A., and Yosibash, Z. (2008). On volumetric locking-free behavior of p-version finite elements under finite deformations. *Communications in Numerical Methods in Engineering*, 24:1019–1032.

Helfenstein, J., Jabareen, M., Mazza, E., and Govindjee, S. (2010). On non-physical response in models for fiber-reinforced hyperelastic materials. *International Journal of Solids and Structures*, 47:2056–2061.

Holbery, J. and Houston, D. (2006). Natural-fiber-reinforced polymer composites in automotiv applications. *JOM: the Journal of the Minerals, Metals and Materials Society*, 58:80–86.

Holzapfel, G. and Ogden, R. (2010). Constitutive modelling of arterials. *Proceedings of the Royal Society of London A*, 466:1551–1597.

Holzapfel, G. A. (2000). *Nonlinear Solid Mechanics*. Wiley & Sons, Chichester.

Holzapfel, G. A., Gasser, T. C., and Ogden, R. W. (2000). A new constitutive framework for arterial wall mechanics and a comparative study of material models. *Journal of Elasticity*, 61:1–48.

Huang, X., Ren, J. S., and Yuan, X. G. (2011). Experiment modeling of the finite thermo-hyperelasticity for fiber-reinforced rubber composites. *Advances in Heterogeneous Material Sciences*, pages 568–571.

Hutter, K. and Jöhnk, K. (2004). *Continuum Methods of Physical Modeling*. Springer, Berlin.

Hyndman, R. J. and Koehler, A. B. (2006). Another look at measures of forecast accuracy. *International Journal of Forecasting*, 22:679–688.

Itskov, M. (2009). *Tensor Algebra and Tensor Analysis for Engineers*. Springer-Verlag, Berlin Heidelberg, second edition edition.

Itskov, M. and Aksel, N. (2004). A constitutive model or orthotropic elasto-plasticity at large deformatiom. *Archive of Applied Mechanics*, 74:75–91.

Itskov, M., Ehret, A. E., and Mavrilas, D. (2006). A polyconvex anisotropic strain-energy function for soft collagenous tissues. *Biomechanics and Modeling in Mechanobiology*, 5:17–26.

Johlitz, M., Diebels, S., and Possart, W. (2012). Investigation of the thermoviscoelastic material behaviour of adhesive bonds close to the glass transition temperature. *Archive of Applied Mechanics*, 82:1089–1102.

Johlitz, M., Scharding, D., Diebels, S., Retka, J., and Lion, A. (2010). Modelling of thermo-viscoelastic material behavior of polyurethane close to the glass transition temperature. *Zeitschrift für Angewandte Mathematik und Mechanik*, 90:387–398.

Kambouchev, N., Fernandez, J., and Radovitzky, R. (2007). A polyconvex model for materials with cubic symmetry. *Modeling and Simulation in Materials Science and Engineering*, 15:451–467.

Kambouchev, N., Radovitzky, R., and Fernandez, J. (2006). Anisotropic materials which can be modeled by polyconvex strain energy functions. *47th AIAA/ASME/ASCE/ASC Structures, Structural Dynamics, and Materials Conference*, AIAA 2006-2250:1–6.

Krämer, S., Rothe, S., and Hartmann, S. (2013). Homogeneous stress-strain state computed by 3D-stress algorithms of FE-codes. Application to material parameters identification. *Engineering with Computers (accepted for publication)*, 1-29.

Kunkel, P. and Mehrmann, V. (2006). *Differential-Algebraic Equations: Analysis and Numerical Solution*. European Mathematical Society, Zürich.

Latorre, M. and Montans, F. J. (2012). Spline-based hyperelasticity for transversely isotropic incompressible materials. *"Proceedings of the Eleventh International Conference on Computational Structures Technology", Civil-Comp Press, Stirlingshire, Scotland*, Paper 260.

Latorre, M. and Montans, F. J. (2013). Extension of the sussman-bathe spline-based hyperelastic model to incompressible transversely isotropic materials. *Computers and Structures*, 122:13–26.

Limons, D. S. (2013). *A Student's Guide to Entropy*. Cambridge University Press, New York.

Lion, A. (2000). *Thermomechanik von Elastomeren. Experimente und Materialtheorie*. Habilitation, Institute of Mechanics, University of Kassel. Report No. 1/2000.

Lu, J. and Zhang, L. (2005). Physically motivated invariant formulation for transversely isotropic hyperelasticity. *Internatioal Journal of Solids and Structures*, 42:6015–6031.

Lu, S. and Pister, K. (1975). Decomposition of deformation and representation of the free energy function for isotropic thermoelastic solids. *International Journal of Slids and Structures*, 11:927–934.

Lubarda, V. A. (2004). Constitutive theories based on the multiplicative decomposition of deformation gradient: Thermoelasticity, elastoplasticity, and biomechanics. *Applied Mechanics Review*, 57:95–108.

Malvern, L. E. (1969). *Introduction to the Mechanics of a Continuous Medium*. Prentice-Hall, New Jersey.

Mark, J. E. (2007). *Physical properties of polymers Handbook*. Springer, Cincinnati.

Markert, B., Ehlers, W., and Karajan, N. (2005). A general polyconvex strain-energy function for fiber-reinforced materials. *Proceedings in Applied Mathematics and Mechanics PAMM*, 5:245–246.

Marsden, J. E. and Hughes, T. J. R. (1994). *Mathematical Foundations of Elasticity*. Dover Publications, New York.

Mićunović, M. (1982). Thermo-elasticity of idial fiber-reinforced materials. *Journal of Technical Physics*, 23:59–67.

Miehe, C. (1995). Entropic thermoelasticity at finite strains. aspects of the formulation and numerical implementation. *Computer Methods in Applied Mechanics and Engineering*, 120:243–269.

Netz, T. (2013). *High-order space and time disretization scheme applied to problems of finite thermo-viscoelasticity*. Dissertation, Berichte des Instituts für Technische Mechanik 3.

Netz, T., Düster, A., and Hartmann, S. (2013a). High-order finite elements compared to low-order mixed element formulations. *Journal of Applied Mathematics and Mechanics*, 93:163 – 176.

Netz, T., Hamkar, A.-W., and Hartmann, S. (2013b). High-order quasi-static finite element computations in space and time with application to finite strain viscoelasticity. *Computers and Mathematics with Applications*, 66:441 – 459.

Noll, W. (1995). On material frame-indifference. *Department of Mathematical Science. Paper 580. http://repository.cmu.edu/math/580*.

Odegrad, G. M., Haut Donahue, T. L., Morrow, D. A., and Kaufman, K. R. (2008). Constitutive modeling of skeletal muscle tissue with an explicit strain-energy function. *Journal of Biomechanical Engineering*, 130:1–9.

Ogden, R. W. (1997). *Non-Linear Elastic Deformations*. Dover Publications, New York.

Pena, E., Martins, P., Mascarenhas, T., Jorge, R., Ferreira, A., Doblare, M., and Calvo, B. (2011). Mechanical characterization of the softening behavior of human vaginal tissue. *Journal of the Mechanical Behavior of Biomedical Materials*, 4:275–283.

Petzold, L. (1982). Differential/algebraic equations are not odeś. *Journal on Scientific Computing*, 3:367–384.

Qiu, G. Y. and Pence, T. J. (1997). Remarks on the behavior of simple directionally reinforced incompressible nonlinearly elastic solids. *Journal of Elasticity*, 49:1–30.

Quint, K. J. (2012). *Thermomechanically coupled processes for functionally graded materials: experiments, modeling and finite element analysis using high-order DIRK-methods*. Dissertation, Berichte des Instituts für Technische Mechanik 2.

Rothe, S., Hamkar, A.-W., Quint, K. J., and Hartmann, S. (2012). Comparison of diagonal-implicit, linear-implicit and half-explicit runge-kutta methods in non-linear finite element analyses. *Archive of Applied Mechanics*, 82:1057–1074.

Rubin, M. B. and Jabareen, M. (2008). Physically based invariants for nonlinear elastic orthotropic solids. *Journal of Elasticity*, 90:1–18.

Rüter, M. and Stein, E. (2000). Analysis, finite element computation and error estimation in transversely isotropic nearly incompressible finite elasticity. *Computer Methods in Applied Mechanics and Engineering*, 190:519–541.

Sansour, C. (2008). On the physical assumptions underlying the volumetric-isochoric split and the case of anisotropy. *European Journal of Mechanics - A/Solids*, 27:28–39.

Schmitt, J. and Diebels, S. (2005). Experimentelle untersuchung zum anisotropen verhalten eines polypropylen-schaums. *Proceedings in Applied Mathematics and Mechanics*, 5:517–518.

Schröder, J. and Neff, P. (2003). Invariant formulation of hyperelasticity transverse isotropy based on polyconvex free energy functions. *International Journal of Solids and Structures*, 40:401–445.

Schröder, J., Neff, P., and Balzani, D. (2005). A variational approach for materially stable anisotropic hyperelasticity. *International Journal of Solids and Structures*, 42:4352–4371.

Schröder, J., Neff, P., and Ebbing, V. (2008). Anisotropic polyconvex energies on the basis of crystallographic motivated structural tensors. *Journal of the Mechanics and Physics of Solids*, 56:3486–3506.

Simo, J. C. and Pister, K. S. (1984). Remarks on rate constitutive equations for finite deformation problems: Computational implications. *Computer Methods in Applied Mechanics and Engineering*, 46:201–215.

Spencer, A. J. M. (1971). *Theory of Invariants*. In Eringen, A. C., editor. Continuum Physics, New York: Academic Press, p.240-253.

Spencer, A. J. M. (1984). *Continuum Theory of the Mechanics of Fiber-Reinforced Composites*. Springer, Wien - New York.

Steigmann, D. J. (2003). Frame-invariant polyconvex strain energy functions for some anisotropic solids. *Mathematics and Mechanics of Solids*, 8:497–506.

Stojanovic, R. (1969). On the stress relation in non-linear thermoelasticity. *International Journal of Non-Linear Mechanics*, 4:217–233.

Stojanovic, R., Djuric, S., and Vujosevic, L. (1964). On finite thermal deformations. *Arch. Mech. Stosow.*, 16:103–108.

Sussman, T. and Bathe, K.-J. (2009). A model of incompressible isotropic hyperelstic material behavior using spline interpolations of tension-compression test data. *Communications in Numerical Methods in Engineering*, 25:53–63.

Szabo, B. and Babuska, I. (1991). *Finite Element Analysis*. John Wiley & Sons, Canada.

Tadmor, E. B., Miller, R. E., and Elliott, R. S. (2012). *Continuum Mechanics and Thermodynamics: From Fundamentals Concepts to Governing Equations*. Cambridge, Cambridge.

Tang, C. Y., Zhang, G., and Tsui, C. P. (2009). A 3d skeletal muscle model coupled with active contraction of muscle fibers and hyperelastic behavior. *Journal of Biomechanics*, 42:865–872.

Truesdell, C. and Noll, W. (2004). *The Non-Linear Field Theories of Mechanics*. Springer, Berlin, third edition edition.

Vujosevic, L. and Lubarda, V. A. (2002). Finite-strain thermoelasticity based on multiplicative decomposition of deformation gradient. *Theoritical and Applied Mechanics*, 28-29:379–399.

Weiss, J. A., Maker, B. N., and Govindjee, S. (1996). Finite element implementation of incompressible, transversely isotropic hyperelasticity. *Computer Methods in Applied Mechanics and Engineering*, 135:107–128.

Yosibash, Z., Hartmann, S., Heisserer, U., Düster, A., and Rank, E. (2007). Axisymmetric pressure boundary loading for finite deformation analysis using p-FEM. *Computer Methods in Applied Mechanics and Engineering*, 196:1261–1277.

Yosibash, Z. and Priel, E. (2011). p-fems for hyperelastic anisotropic nearly incompressible materials under finite deformations with applications to arteries simulation. *International Journal for Numerical Methods in Engineering*, 88:1152–1174.

Yosibash, Z., Weiss, D., and Hartmann, S. (2014). High-order fems for thermo-hyperelasticity at finite strains. *Computers and Mathematics with Applications*, 67:477–496.

Zhang, Z. (2010). *Thermo-mechanical behavior of polymer composites exposed to fire*. Dissertation, Faculty of the Virginia Polytechnic Institute and State University, Blacksburg, Virginia.

Zienkiewicz, O. C., Taylor, R. T., and Zhu, J. Z. (2005). *Finite Element Method: Its Basis & Fundamentals*. Elsevier Butterworth-Heinemann, Burlington.

Curriculum Vitae

Personal Data

Name	Raad Al-Kinani
Date of Birth	19.06.1982
Place of Birth	Baghdad
Nationality	Iraqi
E-mail	raad.al-kinani@gmx.de

Education

2001 – 2004	B.Sc. Mechanical Engineering, Al-Nahrain University, Baghdad, Iraq
2004 – 2007	M.Sc. Mechanical Engineering, Al-Nahrain University, Baghdad, Iraq

Employment

Jun. 2006 – Jun. 2010	Assistant Lecturer, Department of Engineering Projects, Al-Nahrain University, Baghdad, Iraq
Since Oct. 2010	Research Assistant, Institute of Applied Mechanics, Clausthal University of Technology, Clausthal-Zellerfeld, Germany